ABSTRACT

Title of Document: REDUCTIONS IN ESTROGENIC FUNCTION LEAD TO METABOLIC DYSFUNCTION IN ADIPOSE TISSUE AND SKELETAL MUSCLE.

Lindsay Wohlers

Directed By: Assistant Professor Espen E. Spangenburg, Ph.D., Kinesiology

This dissertation research is comprised of three studies which investigated the effects of reduced ovarian hormones induced by surgical ovariectomy (OVX) on metabolic parameters in adipose tissue and skeletal muscle. Reduced ovarian function is associated with changes in body composition that result in increased risk for development of the metabolic syndrome and cardiovascular disease. It is hypothesized that ovarian hormones protect women from the development of metabolic disease by significantly influencing the metabolic phenotype of adipose tissue and skeletal muscle. Study #1 examined the efficacy of voluntary wheel running or 17β-estradiol supplementation as interventions to ameliorate the detrimental effects of OVX on adipose tissue. OVX resulted in significant increases in visceral fat mass and basal lipolysis that 17β-estradiol delivery completely attenuated compared to the control (SHAM) mice. Wheel running in the OVX mice completely attenuated increased circulating glucose levels and partially attenuated increased visceral fat mass, but failed to prevent changes in lipolytic function.

Study #2 determined that cellular regulation of lipolysis in visceral adipose tissue during an acute exercise bout was impaired in the OVX compared to the SHAM group. In the final study, it was determined that adipose tissue expansion following OVX was mediated by adipocyte hypertrophy as measured by significant increases in adipocyte size. Using a novel co-culture approach containing isolated single skeletal muscle fibers and adult adipocytes the interactive effects of OVX and adipocyte exposure on skeletal muscle metabolic function were investigated. Both control and co-cultured skeletal muscle fibers from OVX animals displayed impaired insulin-stimulated glucose uptake coupled with impaired insulin signaling compared to SHAM fibers. Co-culture with adipocytes attenuated insulin-stimulated glucose uptake in SHAM fibers when adipocytes were of visceral, but not subcutaneous origin and this effect was independent of intramuscular lipid content. Collectively, these studies provide unique insight into cellular alterations in metabolic regulation that may contribute to metabolic diseases such as insulin resistance in women when ovarian hormone levels are reduced.

REDUCTIONS IN ESTROGENIC FUNCTION LEAD TO METABOLIC
DYSFUNCTION IN ADIPOSE TISSUE AND SKELETAL MUSCLE.

By

Lindsay Michelle Wohlers

Dissertation submitted to the Faculty of the Graduate School of the
University of Maryland, College Park, in partial fulfillment
of the requirements for the degree of
Doctor of Philosophy
2012

Advisory Committee:
Assistant Professor Espen E. Spangenburg, Chair
Professor James M. Hagberg
Assistant Professor Eva R. Chin
Assistant Professor Richard M. Lovering
Associate Professor Brian J. Bequette, Dean's Representative

Acknowledgements

There are multiple people I would like to thank who have had major influences on my academic career and life as a whole. First and foremost I would like to thank my parents who instilled in me the value of hard work and who have been incredible role models throughout my life. It is their love and support of me in all endeavors that has made reaching this major milestone in my life possible. I would also like to thank my sister Erin for her support along the way and for being the best friend I could ever ask for in a sibling.

I would like to thank my advisor Dr. Espen Spangenburg for all of his guidance throughout the past five years. Espen, I have learned so much from you and am grateful for everything you have taught me. Thank you for working with me in the lab and teaching me when I came to Maryland without any real lab experience. Thank you for helping me learn to write and think like a scientist. And lastly, thank you Espen for not only helping me to grow and evolve as a scientist, but also as a person.

Also, I would like to thank my committee members for their scientific input and advice which helped shape my dissertation work. I would like to thank Dr. Eva Chin for countless conversations providing experimental and scientific advice. Also, I thank you Eva for offering support, insight, and perspective in multiple aspects of life. I thank Dr. James Hagberg for his role as a teacher, committee member, and mentor throughout the course of both my master's and Ph.D programs. Dr. Richard Lovering is thanked for his assistance with laboratory techniques, use of equipment, and support of my work as a graduate student. I would like to thank Dr. Brian Bequette for taking the time to serve as my Dean's Representative, as well as for experimental assistance and insight.

I thank Andy Ludlow for his love and support in everything that I do, for helping me scientifically the past five years, and for being my best friend and companion in life.

Thank you to my lab mates Katie Jackson and Ana Valencia who have been great friends both in and out of school, your company and friendship has been immensely helpful in getting to this point. I would also like to thank all members of the exercise physiology "super lab" past and present who have been an important component of my life as a graduate student. In particular I would like to thank Dr.'s Erik Hanson and Sarah Witkowski for their help, advice, and friendship.

Table of Contents

List of Tables

List of Figures

Chapter 1: Introduction and Specific Aims

Introduction

Insulin resistance, type 2 diabetes, and cardiovascular disease are directly related to an increase in fat mass (i.e. adiposity) (69, 78, 80). Both the type of adipose tissue expansion and the location of excess fat storage (visceral versus subcutaneous) play roles in determining the health consequences of increased adiposity. In females where ovarian function is disrupted, such as age-induced menopause or when oophorectomy is done for clinical reasons, changes in fat storage occur that are associated with increased risk for the development of obesity-related conditions (125, 237). Specifically, there is increased fat storage in the visceral region, which is of particular concern due to the contribution of visceral fat to the onset of metabolic disease. In addition, changes in adipocyte function (i.e. increased basal lipolysis) occur that facilitate storage of ectopic fat in other tissues, such as skeletal muscle and liver (296, 297).

In skeletal muscle, the presence of ectopic fat (i.e. excess lipid in the storage form of triacylglycerol) is associated with cellular dysfunction, impairing processes such as insulin-stimulated glucose uptake. Based on the association between increased adiposity and the risk for diseases such as type 2 diabetes, it would be logical to hypothesize that there may be interaction between fat and skeletal muscle which mediates this relationship. Indeed, ectopic fat deposition in skeletal muscle results in "lipotoxicity" which is likely the result of increased lipid intermediates and is associated with skeletal muscle insulin resistance (160, 162). While an association between ectopic fat deposition and insulin resistance has been demonstrated in humans and animal models, the mechanisms which link changes in adipocyte characteristics to decreased insulin

signaling in skeletal muscle remain unknown. This gap in our understanding of the relationship between adiposity and the skeletal muscle response to insulin are of particular importance based on the absence of a widely accepted treatment for women experiencing reduced ovarian function. We have previously shown that ovariectomy (OVX) results in elevated basal lipolysis (297), impaired stimulated lipolytic function (296), and increased adipocyte size; however, the relationship between these adipocyte alterations and skeletal muscle insulin resistance has not yet been determined in the OVX model. By elucidating the mechanisms which link adipocyte function to metabolic function in skeletal muscle when ovarian hormones are reduced, it may be possible to develop a new intervention for the large subset of at-risk females. Therefore, the overall aim of this dissertation research was to determine the impact of ovariectomy on adipocyte function and metabolic properties of skeletal muscle fibers. To this end, four studies were conducted utilizing the ovariectomized (OVX) mouse model of ovarian hormone reduction. The OVX model was selected since it is possible to perform the surgery at a young age, thereby removing the confounding effects of aging on tissue metabolism. The first two published studies examined lipolytic alteration in adipose tissue under basal and stimulated conditions. The third unpublished study examined the time course of alterations in adipocyte size, number, and storage depot under conditions of reduced ovarian function. The adipocyte data from the third study will be combined with the data from the final study for a third publication. Based on the findings of the first three studies, the final study was conducted in which a novel co-culture system was developed that allowed for mature adipocytes and isolated adult skeletal muscle fibers to be placed in the same culture media. This co-culture approach allow for both cell types to be

exposed to circulating factors without any physical interaction. Insulin signaling and glucose uptake were measured to determine the effect of adipocyte co-culture on the skeletal muscle response to insulin. Collectively, the results of all of these four studies have shed light on the impact of ovarian hormone reduction on the metabolic interaction between skeletal muscle and adipocyte function, as well as how cross-talk between the two cell types may contribute to changes in skeletal muscle insulin responsiveness. This research is of particular importance given the increased risk, and absence of a treatment, for obesity-related conditions such as insulin resistance and type 2 diabetes, in females where ovarian function is compromised.

Specific Aims

Specific Aim 1: To determine the effect of ovarian hormone status on basal adipose tissue lipolytic activity in female mice.

The purpose of Study #1 was to characterize the effects of ovariectomy, 17β-estradiol supplementation, and voluntary wheel running intervention on visceral adipose tissue lipolysis in female mice. Under basal conditions in a healthy individual, lipolytic breakdown of fat stores is relatively low; however, in pathological states such as obesity, elevation of basal lipolysis often occurs (89, 223). We found greater visceral adipose tissue mass, as well as elevated basal levels of serum non-esterified fatty acids (NEFA's), glycerol, and blood glucose in OVX animals compared to SHAM. In addition, adipose tissue content of the key lipolytic proteins adipose triglyceride lipase (ATGL) and perilipin (PLIN1) were observed to increase and decrease, respectively. The loss of PLIN1 and enhanced activation of ATGL would contribute to increased basal lipolysis in

OVX mice in that under basal conditions PLIN1 protects the lipid droplet from unstimulated lipolytic attack by ATGL and hormone sensitive lipase (HSL). At the whole body level, the increased basal lipolysis would have detrimental consequences for peripheral insulin sensitivity as a result of elevated circulating NEFA contributing to increased ectopic fat deposition in liver and skeletal muscle. Thus, a reduction in ovarian hormone levels appeared to result in altered protein content of lipolytic regulators, in particular higher ATGL and lower PLIN1, contributing to increased adipose tissue lipolysis under basal conditions that would be predicted to contribute to peripheral insulin resistance. However, this hypothesis remains untested at this time.

Specific Aim 2: To determine the effect of ovarian hormone status on stimulated adipose tissue lipolytic activity in female mice.

The findings of Study #1 demonstrated that basal lipolysis was significantly higher in OVX mice compared to SHAM due to loss of cellular control of key regulators of lipolytic function. Further, the data from Study #1 suggested that OVX mice would also exhibit impaired stimulated lipolytic function compared to SHAM mice. Thus, Study #2 was conducted to determine whether OVX also impacted lipolysis in female mice under physiologically stimulated conditions (i.e. acute exercise). As in Study #1, OVX animals were found to have greater omental/mesenteric (i.e. visceral) fat mass, as well as higher ATGL protein content and lower PLIN1 protein content in fat compared to SHAM animals. Further, in a sedentary state, OVX animals exhibited higher serum glycerol and blood glucose levels than their SHAM counterparts. In response to an acute bout of treadmill running, a physiological activator of lipolysis, OVX animals exhibited

impaired lipolytic activation compared to control animals, as an exercise-induced increase in glycerol levels was detected in the SHAM animals only. In addition, acute exercise resulted in increased HSL Ser660 phosphorylation in only the SHAM group, demonstrating impairment of a critical step in the regulation of lipolytic breakdown of fat stores in OVX animals. Studies #1 and #2 clearly demonstrated that OVX results in increased basal adipose tissue lipolytic activity which would result in chronic exposure of peripheral tissue to NEFA. This repetitive exposure of skeletal muscle to NEFA would be expected to result in the deposition of ectopic fat and thus increase the risk for developing peripheral lipotoxicity and subsequently insulin resistance.

Specific Aim 3: To determine the mechanism and time course of visceral (i.e. omental) and inguinal (i.e. subcutaneous) adipose tissue expansion following ovariectomy.

Changes in lipolytic function are often tightly correlated with changes in adipocyte size (84, 207). For instance, in conditions where adipocyte size is increased to a significant extent, such as in the obese state, basal lipolytic activity concurrently increases because the fat cells have reached the upper limit of storage capacity (147). This increase in adipocyte lipolytic activity results in elevated circulating NEFA and glycerol levels, increasing the likelihood of peripheral ectopic fat deposition which could contribute to the development of insulin resistance (84, 124, 182, 207). On the other hand, when increases in fat storage are mediated by an increase in adipocyte number, lipolytic activity is not altered and the metabolic consequences (i.e. development of insulin resistance) of increased adiposity are attenuated or eliminated completely (147).

In addition to the mechanism which drives an increase in fat mass (i.e. increased adipocyte size or increased adipocyte number), the location of excess fat storage plays a role in the physiological consequences of increased adiposity. When fat is stored in inguinal (i.e. subcutaneous) depots, health consequences are minimal compared to storage in omental (i.e. visceral) depots, in part due to the greater adipocyte lipolytic activity of omental adipocytes (123, 302). Therefore, we sought to determine the manner by which adipose tissue expansion occurs in female mice following OVX in both omental and inguinal adipose tissue. A limited number of studies have found increased adipocyte size in the OVX model, however they have only measured changes at a single time-point where adipose tissue mass is already significantly elevated (i.e. 12 weeks after OVX) in one anatomical fat pad (68, 228, 263). We sought to determine the time-course of changes in adipocyte size/number at 2, 4, and 8 weeks after the surgical ovariectomy procedure. We found progressive increases in adipocyte size in both the omental and inguinal depots from the OVX animals compared to SHAM animals. Adipocyte size peaked at the 8 week time-point where omental and inguinal adipose tissue masses in OVX animals were significantly greater than SHAM animals. Interestingly, our data indicated that OVX adipose tissue expansion was the result of increased adipocyte size without a change in cell number. These data provided crucial information for designing the experiments necessary to address Specific Aim 4.

Specific Aim 4: To determine the effect of ovarian hormone-induced changes in adipocyte lipolytic status and secretory profile on the skeletal muscle response to insulin stimulation.

The results of the studies comprising Specific Aims 1-3 culminated in a fourth study which was designed to determine whether OVX-induced alterations in adipocyte function contribute to skeletal muscle insulin resistance. In conditions such as obesity and type 2 diabetes, impaired insulin signaling in skeletal muscle is frequently observed (16, 32, 100). Since skeletal muscle is the primary tissue responsible for 75-80% of total glucose disposal, impairment in the insulin signaling pathway in this tissue significantly contributes to insulin resistance at the whole body level (64, 246). In addition to skeletal muscle, there are depot-specific effects of adipose tissue expansion on whole body insulin sensitivity, with inguinal fat storage promoting increased insulin sensitivity and omental fat storage contributing to impaired insulin sensitivity (88, 123, 147, 155). The underlying contributions of obesity are complex and the effects on skeletal muscle are poorly understood because it is often impossible to determine the direct effects of the adipocyte on skeletal muscle due to the numerous other physiological disarrangements that result from obesity. It is well documented that following ovarian hormone reduction, females undergo alterations in fat storage and are at a substantially increased risk for developing insulin resistance and type 2 diabetes (102, 121, 155). Therefore, Study #4 sought to determine if there was a direct relationship between adiposity and the development of insulin resistance in skeletal muscle.

To this end, a novel co-culture system was utilized with isolated primary adult skeletal muscle fibers, omental adipocytes, and inguinal adipocytes from both OVX and

SHAM animals. Specific co-culture combinations of skeletal muscle fibers and adipocytes were employed to test the effects of both OVX and adipocyte co-culture on skeletal muscle insulin responsiveness.

We hypothesized:

1) OVX fibers would display an inherent defect in the skeletal muscle response to insulin that was independent of adipocyte exposure.

2) The upregulation of basal lipolytic activity in OVX adipocytes compared to SHAM would be associated with impaired OVX skeletal muscle insulin responsiveness following co-culture.

3) Omental adipocyte exposure would impair skeletal muscle insulin responsiveness to a greater extent than inguinal adipocyte exposure.

In obese and insulin resistant states, an impaired skeletal muscle response to insulin results in altered skeletal muscle substrate metabolism. For example, in obese and type 2 diabetic individuals, lipid infiltration into skeletal muscle results in reduced capacity for skeletal muscle glucose uptake and oxidation (34, 144). Therefore, lipid content and skeletal muscle glucose uptake were measured in a second set of SHAM and OVX skeletal muscle fibers following adipocyte co-culture.

We hypothesized:

1) OVX muscle fibers would exhibit higher lipid content without adipocyte co-culture than SHAM muscle fibers.

2) Lipid content in skeletal muscle fibers would be greater following co-culture with OVX adipocytes than following co-culture with SHAM adipocytes.

3) Co-culture with omental adipocytes would result in greater skeletal muscle lipid content than co-culture with inguinal adipocytes.

Exploratory Aim: To identify factors secreted from omental and inguinal adipose tissue of SHAM and OVX animals that may contribute to alterations in insulin signaling.

Altered adipocyte secretory profiles have been documented under various conditions, such as obesity, and may have a significant impact on skeletal muscle insulin resistance and the onset of diabetes (34, 144). Further, the secretory profile of adipocytes appears to be depot-specific, with the factors released from inguinal adipocytes facilitating insulin sensitivity to a greater degree than factors released from omental adipocytes (81, 216, 226). Therefore, the analysis of factors secreted from inguinal and omental adipose tissue provides useful insight into potential differences in insulin responsiveness observed in the co-culture model. For example, numerous adipokines have been indentified which are thought to impact insulin signaling in peripheral tissue (81, 216, 226). Thus, we measured levels of specific cytokines which are known to be released from adipocytes and may potentially impact insulin signaling in skeletal muscle. **We hypothesized that altered adipokine secretion may provide a mechanism by which ovarian hormone reduction contributes to increased prevalence of insulin resistance in females.**

Chapter 2: Review of Literature

The purpose of this review of literature is to examine the role of ovarian hormone status in the development of visceral adiposity, peripheral insulin resistance and the metabolic syndrome.

Obesity and Insulin Resistance:

The prevalence of obesity in America has reached new heights in recent years. Not one state has achieved the Healthy People 2010 goals of a 15% obesity rate for adults and a 5% obesity rate for children, instead obesity rates have continued to rise (4). Corresponding to this obesity epidemic is a parallel increase in the prevalence of obesity-related conditions, which has proven costly, with $147 billion spent annually on the treatment of obesity-related diseases (187). Further, each obese individual costs health insurance companies an additional $1,429 per year for medical treatment compared to an individual of normal weight (187). One of the most common complications associated with the onset of obesity is peripheral insulin resistance (1). Peripheral insulin resistance is preventable, but often leads to type 2 diabetes when the appropriate dietary and lifestyle modifications are not taken, contributing to higher mortality in obese individuals (50, 176). Therefore, it is not surprising that the national pattern of obesity prevalence looks remarkably similar to the pattern for diabetes prevalence (See Figure 1 below).

Obesity

Diagnosed Diabetes
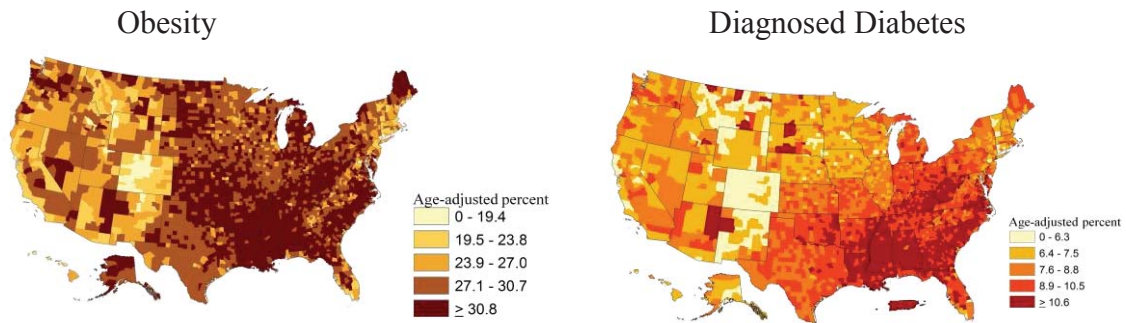
Figure 1. Obesity and diagnosed diabetes prevalence in the United States. CDC, 2010 (2, 3).

Although, excess caloric consumption and a sedentary lifestyle are thought to be the major contributors to obesity, certain hormonal imbalances can also result in increased adiposity. For example, women who are experiencing a reduction in ovarian hormone levels or estrogen signaling function are at increased risk for developing visceral adiposity.

In females, ovarian hormone reduction occurs in response to naturally occurring menopause, as well as in response to surgical hysterectomy which can be accompanied by elective removal of the ovaries, however, generally results in premature 'aging' of the ovary.   In addition, females undergoing treatment for estrogen-positive cancers experience similar side effects that are visible with reduced ovarian function (66, 67). The resulting visceral adipose tissue expansion that occurs in women with any of these conditions results in increased risk for development of the metabolic syndrome and cardiovascular disease.

In normal cycling females, multiple hormones are released from the ovaries which exert their effects on peripheral tissue. The ovarian hormones released in the largest quantity are progesterone and estrogens, with 17β-estradiol the most abundant and

biologically active isoform of estrogen released from the ovaries. Estrogens play an important role in regulation of numerous physiological processes, including the menstrual cycle, the development of female secondary sex characteristics, and bone growth to name a few (186). In addition, follicle stimulating hormone (FSH) released from the anterior pituitary is critical to hormone release from the ovary. During the menstrual cycle, FSH both facilitates the release of an ovum from the ovary, as well as stimulates the ovarian follicles to release estrogens. Thus, in women there is a dynamic hormonal regulatory process that controls the menstrual cycle, which is regulated by a number of circulating hormones that can originate from different endocrine tissues.

The menstrual cycle in females is regulated by hormones released from the ovaries, as well as hormones which are released from other tissues which act upon the ovaries. The menstrual cycle, which is necessary for reproduction, is regulated by multiple hormones, with estrogens playing a particularly important role. The menstrual cycle consists of three phases: the follicular phase, ovulation, and the luteal phase. The typical human menstrual cycle is 28 days long, with day one defined as the onset of menses. During the menstrual cycle, levels of estradiol, progesterone, FSH, and luteinizing hormone (LH) fluctuate in order for ovulation and menstruation to occur (124) (See Figure 2 below). The follicular phase is characterized by a small rise in FSH and a low concentration of estrogens and progesterone. The follicular phase allows for the development of a primary follicle that is necessary for ovulation. As the follicular phase progresses, FSH stimulates release of estrogens from the ovarian follicle. A large increase in estrogens, as well as a spike in FSH and LH levels, marks ovulation, the phase where the fully-developed dominant follicle is released from the ovary. Although FSH

12

stimulates the development of multiple primary follicles, only one follicle, termed the dominant follicle, is released with each menstrual cycle. The surge in LH at the time of ovulation stimulates formation of the corpus luteum from the granulosa and theca cells of the ovary and marks the transition to the luteal phase. During the luteal phase, progesterone levels rise, as increased expression of LH receptors on the corpus luteum stimulates LH-induced progesterone secretion. In the absence of fertilization, the corpus luteum undergoes atresia as a result of reduced FSH and LH levels in the luteal phase. Further, at the end of the luteal phase estrogens and progesterone levels drop. The decline in estrogens and progesterone results in a rise in FSH secretion, and the next menstrual cycle begins.
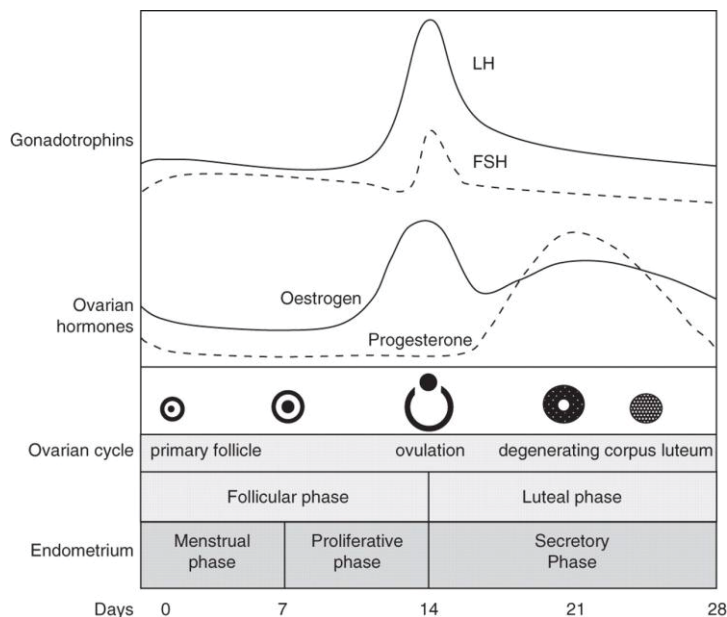
Figure 2. Regulation of the menstrual cycle. From Peacock et al., 2010 (214). LH = luteinizing hormone, FSH = follicle stimulating hormone.

Following the reproductive years, the onset of menopause marks the end of menstrual cycling and the transition into reproductive senescence. In human

females, the onset of menopause occurs at an average age of 51 years (277); thus, females spend ~40% of their lives in reproductive senescence. Therefore, understanding physiological and metabolic changes that occur during the onset of reproductive senescence is critical to women's health. For example, following the onset of menopause, females are at increased risk for the development of metabolic and cardiovascular diseases (41, 206, 210, 293). As a result, a large subset of the female population is at increased disease risk based on ovarian hormone status. With the completion of the Women's Health Initiative, no widely accepted treatment exists to prevent the onset of these diseases in post-menopausal women, thus further research into the role of ovarian hormones in metabolic regulation is necessary.

The onset of menopause occurs due to ovarian follicle depletion (293). The number of follicles, or eggs, is determined at birth, with each menstrual cycle resulting in follicular recruitment and subsequent reduction in total follicle number. Once a female reaches mid-life, the follicles remaining are fewer in number and the viability of the follicles is reduced. Importantly, follicles are responsible for most of the estrogens secreted in the body. Thus, atresia of follicles during the menopausal transition results in a decrease in circulating estrogens and an increase in FSH secretion, which occurs as a compensatory feedback mechanism in response to the diminishing follicular pool (293). In addition, levels of the androgen androstenedione and the hormone inhibin decrease as a result of changes in the ovaries and uterine lining. Secretion of FSH is inhibited by inhibin, therefore the post-menopausal drop in inhibin is an additional trigger for the rise in FSH (149). Androstenedione is a precursor to the formation of estrogens, thus the decline in androstenedione contributes to the reduced levels of estrogens in post-

menopausal women (189). Together, all of these hormonal changes in women following menopause provide evidence as to the difficulty of establishing mechanisms which explain the key contributing factors to increased disease risk.

In addition to menopause, other clinical conditions result in altered levels or function of circulating hormones in women. For example, following oophorectomy, which may be performed alone, or accompanied by hysterectomy, women experience hormonal alterations similar to post-menopausal females. Removal of the ovarian tissue results in reduced circulating estrogens and inhibin, as well as increased FSH levels, similar to the changes observed in natural menopause (203). However, due to the complete removal of ovarian tissue, the decline in androstenedione levels is greater in women who undergo oophorectomy compared to natural menopause, as the post-menopausal ovary still secretes androgens (170).

In females, disruption of ovarian hormone function can also occur in response to treatment of estrogen-positive breast cancers (66, 67). Many of the methods used to treat estrogen-positive breast carcinomas involve the use of substances which antagonize estrogen receptors (ER's) and thus interfere with the ability of circulating estrogens to promote growth of the tumor cells (37). While breast cancer treatment involves disruption of ER's and menopause results in a decrease in the level of circulating estrogens, both mechanisms for disruption of the ovarian hormone signaling axis result in similar changes in tissue function that increase the risk for metabolic disease (37, 41).

These changes in circulating hormone levels and/or function following ovarian disruption in females impact multiple physiological processes and have implications for the development of metabolic disease. In particular, a common link

between natural menopause, oophorectomy, and estrogen-positive breast cancer treatment is an increase in visceral fat mass (41, 125). This increase in visceral fat mass is coupled with an increased risk for the development of metabolic disease (41, 132). Further, in women experiencing reduced ovarian hormone levels there are intrinsic changes in skeletal muscle and liver function due to reduced exposure to estrogens, resulting in increased prevalence of insulin resistance (35). While the outward physiological changes that occur in females following ovarian hormone reduction have been well documented, many of the cellular mechanisms which regulate these changes in skeletal muscle, adipose and hepatic tissue remain to be elucidated.

In order to further investigate the impact of reduced ovarian hormone levels on tissue function, a variety of animal models have been developed. Multiple animal models of reproductive failure have been developed to date, with five primary animal models currently utilized in the study of ovarian hormone dysruption. These models are the follitropin receptor knock out (FORKO), 4-vinylcyclohexene diepoxide injection (VCD), aromatase knock out (ArKO), estrogen receptor knock out (ERKO), and surgical ovariectomy (OVX). In general, the models of ovarian hormone reduction fall into two categories, ovary intact, which includes the FORKO, ERKO, ArKO, and VCD models and surgically altered, of which bi-lateral OVX is the most common model.

FORKO animals are a genetic model of ovarian hormone reduction in which the animals lack the receptor for FSH (56, 58-61). In the FORKO animals, whole body knock out of the FSH receptor is accomplished by homologous recombination (71). Elevated FSH levels are observed in FORKO mice due to the lack of a negative feedback mechanism that is regulated by the FSH receptors (56). In the FORKO animals, absence

of the FSH receptor prevents the development of mature follicles, resulting in reduced secretion of estrogens. The increase in FSH levels mimics what is observed in post-menopausal women (293). Homozygous FORKO animals display ovarian hormone abnormalities at birth, with low levels of estrogens, slightly elevated androgen levels, and elevated FSH levels which are similar to those observed in post-menopausal females (17). However, unlike humans, FORKO homozygous mice are in a state of reproductive senescence at birth, being acyclic and infertile, a condition that is similar to primary amenorrhea in humans. Further, FORKO homozygotes have reduced oocyte numbers at birth, suggesting reproductive developmental abnormalities exist (17, 60, 71). In both natural and surgical-induced menopause in females, a portion of the life span is still associated with fertility and general reproductive health. The FORKO mice do not ever experience menstrual cycling and therefore the observed phenotypic changes may not exactly parallel human females (17, 60, 71). Further, prior to menopause, females exhibit a perimenopausal phase where hormonal levels fluctuate for a period of time prior to complete cessation of menstrual cycling and true menopause. Since the FORKO mice are born acyclic, this phase is never observed (17). Therefore, the FORKO homozygote may be a good model for primary amenorrhea, a fairly rare condition in humans, and is a good model for studying the effects of low levels of ovarian hormones with the effects of age removed, however it does not translate very well to surgical or natural menopause.

On the other hand, the FORKO heterozygotes more closely resemble human menopause and have been termed "menopausal" mice (23). The heterozygotes are born without apparent reproductive abnormalities, and do not exhibit the developmental defects in oocyte production observed in the homozygous animals (56). Similar to

humans, the heterozygotes are fertile for the beginning of their lives; however, by 6-8 months of age an inability to conceive occurs, with almost all females becoming acyclic by 12 months of age (61). The infertility occurs due to a progressive and steep decline in oocyte number which is preceded by a reduction in FSH receptor content on the ovaries. Following cessation of the cycle, obesity is observed in heterozygotes, with a ~25% increase in body weight and an increase in fat mass. Further, the changes in hormone levels are similar to those observed in post-menopausal females. FSH levels are elevated at 7 months, and continue to increase until 12 months of age (59). Estradiol levels are normal in 3 month old mice; however, by 7 months of age serum estradiol and progesterone levels are reduced by 50-60%. Testosterone levels are elevated by 7 months (58, 61), and inhibin levels, which are used as a marker of ovarian aging and reflect a reduction in follicular number, are reduced by 12 months (58). Also, aging in the FORKO heterozygote results in structural abnormalities of the reproductive tract, such as the development of cysts when androgen synthesis increases due to elevated LH levels (58, 60). The FORKO heterozygotes experience development of metabolic dysfunction and symptoms of reproductive aging similar to what is observed in menopausal females (57, 62). Another positive aspect of this model is the mechanism which drives the reproductive senescence. In both the FORKO heterozygote (61) and human females (293), it is follicular depletion that results in changes in ovarian hormone levels. The FORKO mice represent a genetic model of reproductive failure, with the heterozygotes exhibiting hormonal and structural changes similar to menopausal females. While similarities exist between the FORKO heterozygote and post-menopausal females, it is important to note that the physiological alterations leading up to menopause in women

18

occur mid-life, while the genetic mutation which results in the reproductive phenotype of the FORKO animal is present during development. Thus, it is possible that developmental changes in these animals may contribute to the observed phenotype.

In order to address the need for a perimenopausal period to mimic human menopause, a method for chemical induction of menopause in mice was developed. Injection of a chemical called 4-vinylcyclohexene diepoxide (VCD), which is produced during the manufacture of rubber products, results in reproductive aging in animals. A connection between environmental VCD exposure and development of reproductive abnormalities led to further investigation on the effects of VCD. To study reproductive aging, VCD is given by an intraperitoneal injection for ~15 consecutive days. Similar to human menopause, VCD results in atresia of follicles, with primary and primordial follicles being affected first, followed by atresia of the larger, estrogen-secreting mature follicles (280). Unlike other models, which result in either abrupt or developmental changes in circulating hormones, the process of VCD-induced menopause is gradual, as it takes time for follicles to be depleted. Therefore, the use of VCD creates a period which mimics perimenopause in humans, where hormone levels fluctuate prior to the complete depletion of follicles and entry into reproductive senescence. Since the ovaries remain intact in VCD animals, changes in androgen levels, in addition to levels of the estrogens and FSH, parallel changes observed in humans. The ratio of estrogens to androgens in mice treated with VCD closely resembles the ratio in post-menopausal females (6). Cyclic disruption becomes apparent in some mice ~58 days following VCD injections, with most mice becoming acyclic by day 75. While VCD is a toxic chemical, the low doses used in recent studies to induce reproductive failure do not appear to result in

abnormalities in other organs, such as the liver, pancreas, or spleen. However, when high doses of VCD are used, or the length of exposure is long, such as 2 years, there is an increased occurrence of liver disease and other detrimental effects (9, 191, 198). The use of VCD to induce menopause allows application of the treatment to multiple different animals models (i.e. different species, different disease models, etc.). Further, since the hormonal changes parallel those in humans, it may be easier to extrapolate findings in mice following VCD treatment to human menopause. This model may not be as applicable for surgically-induced menopause in humans, since hormonal fluctuations occur. While studies have suggested that low doses of VCD are specific to follicular atresia and do not result in negative consequences in other organ systems, the use of an industrial chemical still calls into question the potential for other systemic alterations that may confound the changes observed due to reproductive senescence.

Further, the importance of estrogens in metabolic regulation is supported by the detrimental effects of aromatase knock out (ArKO) in both male and female mice. Aromatase catalyzes the final step in the synthesis of estrogens from cholesterol and is located in ovarian, placental, testicular, brain, skin, and adipose tissues (247). When aromatase is knocked out in a mouse model, the absence of endogenous synthesis of estrogens contributes to the development of obesity and insulin resistance. ArKO mice lack the ability to produce estrogens and also exhibit elevated FSH levels similar to what is observed in females with ovarian dysfunction (29). Female ArKO mice present with elevated body weight and fat pad mass compared to control mice that is apparent at three months of age (138). In male ArKO mice, gonadal fat mass is significantly greater than that of control mice at 3 months, however, a significant increase in total body weight is

not observed until one year of age (138). The elevated fat mass in both male and female mice is mediated by increased adipocyte size, and completely attenuated by 17β-estradiol supplementation (138). Further, the expansion of adipose tissue is not a result of increased food intake, as ArKO mice do not become hyperphagic, rather they exhibit reduced spontaneous physical activity (138). Similar to ovary compromised females, both female (138) and male ArKO (138, 267) mice develop insulin resistance. Thus, the ArKO mouse recapitulates the changes in estrogens and FSH, adipose tissue expansion, and onset of insulin resistance observed in females with reduced ovarian hormone levels. However, as with the FORKO model, the possibility of developmental effects from genetic manipulation should be considered.

Use of the estrogen receptor knock out (ER-KO) animal model has also provided critical evidence concerning the contribution of estrogen signaling to overall organ function. The estrogen receptor has two major isoforms, ERα and ERβ. The effect of estrogen signaling through these receptors is impacted by tissue specific distribution of ERα and ERβ. Specifically, mRNA expression of ERβ is highest in the ovary and prostate, with lower expression found in bladder lung, ovary, brain, uterus, and testis (161). On the other hand, ERα is highly expressed in epididymis, testis, pituitary, uterus, kidney, and adrenal tissue (161). While both isoforms are expressed in skeletal muscle and adipose tissue, ERα plays the dominant role in the regulation of skeletal muscle (18) and adipose tissue (72) metabolic function, thus this section will focus on the whole body ERα-knock out (ERα-KO) model. In the ERα-KO mouse, alterations occur in both females and males that demonstrate the importance of estrogenic function on metabolic regulation. For example, in the ERα-KO mouse, adipose tissue mass and

adipocyte size are significantly greater than control mice in both sexes (118). The phenotype is more severe in male mice, with a greater elevation in adipose tissue mass compared to their wild-type male controls relative to the difference observed in female mice. As with human females experiencing ovarian hormone dysfunction, the changes in adipose tissue mass and body weight in the ERα-KO model are due to reduced activity levels, rather than hyperphagia (118, 224). In both sexes, the elevated adipose tissue mass is associated with reduced insulin sensitivity (118), providing support for the importance of estrogen signaling in the prevention of peripheral insulin resistance. Specifically, in ERα-KO mice insulin signaling is impaired in skeletal muscle, and insulin resistance is observed in hepatic tissue, which exhibits impaired suppression of glucose production in response to insulin (224). Further, ERα-KO mice display lower whole body energy expenditure than control mice, as well as markers of impaired skeletal muscle fatty acid oxidation (224). Overall, research utilizing the ERα-KO model has provided important insight into the role of estrogen signaling on whole body and skeletal muscle metabolism. However, 17β-estradiol levels are elevated in ERα-KO animals, as opposed to the dramatic reduction observed in menopausal females (224). While the ERα-KO mouse resembles the mechanism of ovarian hormone disruption observed in estrogen-positive breast cancer treatment, where estrogen receptor antagonism occurs, it does not parallel the ovarian hormone changes observed in natural or surgically-induced menopause.

While multiple models of ovarian hormone disruption exist, the most commonly used animal model is bi-lateral ovariectomy. OVX can be performed at any age; therefore OVX of young animals provides a model where the effects of the

aging process may be removed from the effects of ovarian hormone reduction. In terms of hormonal changes, levels of circulating estrogens are significantly reduced (by ~70%; (248)) similar to post-menopausal females and females following surgically-induced menopause. OVX animals also have elevated FSH levels, as is observed during natural menopause (5). However, OVX animals do not undergo a perimenopausal phase where hormonal levels fluctuate; the increase in FSH and decline in estradiol occur sharply following the removal of the ovaries (43). OVX results in reduced inhibin levels (5), a hormone which prevents release of FSH (185), thus contributing to the increase in FSH levels observed in both OVX animals and human females (5, 293). In terms of hormonal levels, the OVX mice are fairly similar to post-menopausal females, with an increase in FSH and reduction in estradiol and inhibin. However, OVX results in a sharper decline in androstenedione levels than observed in post-menopausal women who retain ovarian tissue (170, 299). Additionally, species-specific responses must be considered when using the OVX model. In rats, OVX results in hyperphagia (295), while food intake is not increased by OVX in mice (31, 228, 295). This difference in food intake between OVX rats and mice should be carefully considered when selecting a model for investigation of metabolic changes following ovarian hormone reduction. While changes in food intake following OVX differ between mice and rats, both animal models experience an increase in adiposity similar to what is observed in ovary compromised females (68, 168, 169, 296, 297). As a whole, the OVX mouse presents with similar hormonal and metabolic changes to those observed in women and is thus a good model for studying the response to ovarian hormone reduction.

When examining similarities and differences between these animal models of ovarian hormone reduction, it stands out that all five exhibit the same visceral adipose tissue expansion that is observed in women with reduced ovarian hormone levels or function. While advantages and disadvantages exist for each animal model, each has provided important mechanistic insight into alterations which occur in response to ovarian hormone disruption. In particular, the development of insulin resistance and visceral adiposity in all of these models makes them useful for studying the mechanisms which link ovarian hormone reduction to the onset of the metabolic syndrome in women.

In both diet-induced obesity and in obesity resulting from reduced ovarian function, changes in adipose tissue result in increased risk for the development of insulin resistance. At the tissue level, skeletal muscle and adipose tissue play important roles in the development of insulin resistance in the obese state. The next section will provide a detailed description of skeletal muscle and adipose tissue metabolism, as well as how changes in ovarian hormone levels impact both tissues.

Skeletal muscle comprises a large percentage of total body mass, and significantly contributes to whole body metabolic activity. At rest, variation in energy expenditure between individuals has been largely accounted for by differences in skeletal muscle mass (311). Further, acute exercise results in an even greater contribution of skeletal muscle to whole body metabolism, as evidenced by increased oxygen delivery to the active skeletal muscle relative to other tissues (171). Based on the contribution of skeletal muscle to energy expenditure both at rest and during exercise, it is clear that skeletal muscle plays an important role in whole body metabolism. Therefore, it is not

surprising that skeletal muscle metabolic dysfunction has significant implications for metabolic disease and the development of insulin resistance.

Skeletal muscle accounts for ~80% of postprandial glucose uptake and is therefore critical to the regulation of circulating glucose levels. Skeletal muscle insulin resistance is a major risk factor for type 2 diabetes due to the large percentage of glucose disposal it is responsible for in the body (65). In insulin-sensitive individuals, the release of insulin following a meal results in a corresponding uptake of blood glucose by skeletal muscle. Skeletal muscle glucose uptake is regulated by an intricate cell signaling pathway that is initiated in response to elevated levels of circulating insulin (See Figure 3 below). In the post-prandial state, the binding of insulin to the insulin receptor (IR) initiates a phosphorylation cascade that begins with autophosphorylation of the IR on multiple tyrosine residues. Subsequently, the activated IR phosphorylates the family of insulin receptor substrates (IRS-1/IRS-2) on multiple tyrosine residues which facilitate their activation. Once activated, IRS recruits phosphoinositide 3-kinase (PI3K), activating PI3K upon binding to the p85 regulatory subunit (15). Next, PI3K phosphorylates Akt on the regulatory Ser473 and Thr308 residues, both of which are required for maximal Akt activity (7). Phosphorylation of the downstream targets of Akt, TBC1D1 and TBC1D4 (aka AS160), facilitates the translocation of GLUT4 (the primary glucose transporter in skeletal muscle; (286, 309)) to the plasma membrane for uptake of circulating glucose. Further, AS160 is critical for GLUT4 vesicle fusion to the plasma membrane, with mutation of AS160 on the N-terminal phosphotyrosine binding domain resulting in impaired membrane fusion of GLUT4 in response to insulin (156). Together, this coordinated activation of signaling molecules results in the translocation and fusion

of GLUT4 to the plasma membrane, facilitating insulin-stimulated glucose uptake. Upon entry into the cell, glucose must be phosphorylated to glucose-6-phosphate (G-6-P), a step which is catalyzed by the enzyme hexokinase (HK). Once inside the muscle cell, G-6-P may either be metabolized, or stored within the muscle cell in its storage form of glycogen. The storage of glucose as glycogen is regulated by the activation state of glycogen synthase kinase-3β (GSK-3β). In the basal state, GSK-3β inhibits glycogen synthase (GS), the enzyme which catalyzes the addition of glucose to a glycogen chain. In response to insulin signaling in the post-prandial state, Akt inactivates GSK-3β by phosphorylation on the Ser9 residue subsequently removing inhibition on GS and encouraging the storage of glucose as glycogen (265). Failure of insulin signaling at any of these steps may result in the development of insulin resistance and eventually the onset of type 2 diabetes.
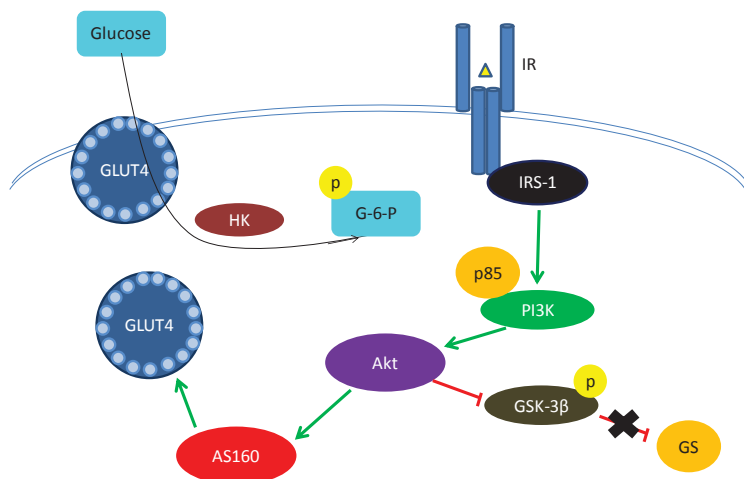
**Figure 3. Insulin signaling in skeletal muscle.** IR = insulin receptor, IRS-1 = insulin receptor substrate-1, PI3K = phosphoinositide 3-kinase, GSK-3β = glycogen synthase kinase-3β, GLUT4 = glucose transporter 4, HK = hexokinase, G-6-P = glucose-6-phosphate.

In the obese state, alterations in skeletal muscle lipid content and metabolic regulation occur that contribute to the onset of insulin resistance. In both obese

humans and animal models of obesity, intramuscular triglyceride (IMTG) content is elevated (117, 140, 197). This increase in IMTG in the obese state has been implicated in the path from obesity to insulin resistance.

Multiple theories have been put forth to explain how increased circulating lipid and IMTG in the obese state contribute to the development of insulin resistance. First, the glucose-fatty acid cycle was described by Philip Randle and colleagues in 1963, a mechanism by which oxidation of fatty acid (FA) inhibits the oxidation of glucose (221). This concept provided a link between the regulation of adipose tissue and skeletal muscle metabolism, whereby increased FA oxidation in skeletal muscle as a result of excess FA supply from adipose tissue inhibits skeletal muscle oxidation of glucose (See Figure 4 below). Specifically, they postulated FA oxidation impairs glucose utilization via two different mechanisms. First, the increase in cytoplasmic citrate in response to FA oxidation results in inhibition of phosphofructokinase, which in turn results in increased G-6-P concentration. The increase in G-6-P inhibits HK, subsequently resulting in impaired glucose uptake. In addition, increased FA oxidation results in elevated intracellular acetyl-CoA levels, which activates pyruvate dehydrogenase kinase (PDK). PDK inhibits pyruvate dehydrogenase, attenuating pyruvate oxidation and contributing to the impaired glucose utilization in response to increased FA oxidation. Thus, in the obese state, increased circulating FA levels contribute to elevated skeletal muscle FA oxidation that inhibits glucose uptake and utilization, contributing to the onset of type 2 diabetes (221). While the glucose-fatty acid cycle as originally proposed has been challenged, and is certainly more complicated than described in 1963, it provided a starting point for understanding

the interplay between oxidation of FAs and glucose and their role in the etiology of obesity-induced insulin resistance.
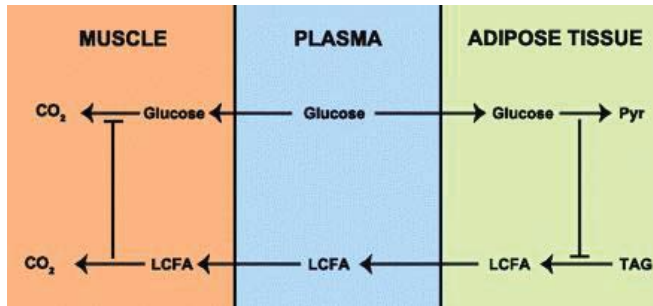
Figure 4. Overview of the "glucose-fatty acid cycle." From Hue and Taegtmeyer, 2009 (127).

More recently, the concept of "lipotoxicity" has been put forth as a mechanism driving the development of insulin resistance in the obese state. Lipotoxicity refers to the detrimental effects of excess FA storage in tissues other than adipose, such as the pancreas, liver, and skeletal muscle. In these tissues, the storage of excess FA as triacylglycerol (TAG) is often referred to as ectopic lipid, and in skeletal muscle can also be specifically termed intramuscular triglyceride (IMTG) or intramyocellular lipid (IMCL). First described in 1995 in pancreatic β-cells of Zucker obese rats, elevated lipid content in pancreatic islets corresponded with hypersecretion of insulin which was followed by the development of diabetes (279). Further, even in normal weight individuals without diabetes, lipid content of skeletal muscle is inversely related to insulin sensitivity (160). However, recent evidence suggests that IMTG is not inherently lipotoxic; rather lipid-induced mitochondrial dysfunction which contributes to the build-up of other lipid-based products is responsible for the relationship between IMTG and insulin resistance. Evidence that IMTG is not causal of insulin resistance

comes from the athlete's paradox, whereby elevated IMTG content in obese individuals is accompanied by insulin resistance, while exercise-trained individuals with elevated IMTG are highly insulin sensitive (98). In the exercise-trained state, increased IMTG content is coupled with upregulation of machinery for both β-oxidation and oxidative phosphorylation of FA via mitochondrial biogenesis (98). However, in obese individuals, ectopic lipid deposition in skeletal muscle often contributes to increased capacity for FA β-oxidation, but is not accompanied by the mitochondrial adaptations necessary for complete oxidation of FAs (158) (Review: (201)). The reduced capacity for FA oxidation results in rerouting of FAs down other metabolic pathways, such as DAG and ceramide synthesis (131, 174). Build-up of DAG and ceramide has been implicated in the onset of insulin resistance in skeletal muscle by interfering with insulin signal transduction (236). For instance, ceramide may inhibit phosphorylation of Akt (45), while DAG may activate protein kinase C (PKC) and nuclear factor kappa B (NF-κB) signaling, both of which interfere with IRS-1 activation (45, 131), thus impairing glucose uptake and contributing to the onset of obesity-induced insulin resistance.

Women experiencing reduced ovarian hormone levels experience alterations in skeletal muscle metabolism that contribute to increased risk for insulin resistance. As discussed above, the increase in ectopic fat in sedentary individuals contributes to impaired insulin sensitivity since the capacity for complete FA oxidation does not increase to meet FA availability and may result in increased DAG and ceramide content (49, 75, 154) (Reviews: (199, 287)). While little evidence of increased IMTG content in ovarian hormone compromised females exists, OVX of mice results in

29

increased lipid content of skeletal muscle, which may contribute to insulin resistance without adequate upregulation of complete FA oxidation (175). Further, the impact of IMTG deposition on skeletal muscle insulin signaling in ovarian hormone compromised females may be intensified by a reduction in physical activity levels that is observed in both humans (183) and animal models (228). This reduction in physical activity may further exacerbate the imbalance between β-oxidation and complete FA oxidation, as in the sedentary state upregulation of Krebs cycle and electron transport chain (ETC) proteins does not occur. Thus, increased IMTG and reduced physical activity levels may contribute to the onset of insulin resistance in women following a reduction in ovarian hormones.

Studies conducted in the OVX mouse model have provided further insight into potential links between ovarian hormone reduction and the onset of insulin resistance. Multiple studies have reported reduced whole body glucose uptake in OVX animals (212, 225, 233). As skeletal muscle is responsible for ~75-80% of glucose uptake in the post-prandial state, it is no surprise that skeletal muscle metabolic properties have therefore been investigated in the OVX model. While some studies report reduced glucose uptake at the skeletal muscle level following OVX, not all are in agreement. Hansen et al. found no impairment in basal or insulin-stimulated 2-deoxy-D-[1,2-3H]glucose (2-[3H]DG) (2-DG) uptake in soleus or epitrochlearis muscles from OVX rats (115). However, other studies have shown reduced glucose uptake by soleus and EDL muscle following OVX (220, 233). These opposing findings may be in part due to the length of time following removal of the ovaries at which skeletal muscle analysis

occurred, with the Hansen et al. study examining muscle after only 5 weeks of OVX, and the other studies waiting until the 12 week time-point.

Furthermore, many investigations of OVX-mediated alterations in skeletal muscle metabolic gene expression have been conducted, reporting changes in proteins of the insulin-signaling pathway, as well as β-oxidation, oxidative phosphorylation, and lipogenesis in response to OVX. In a study by Beckett et al., OVX rats were reported to have reduced activity of enzymes involved in glycogen synthesis (glycogen synthase) and the Krebs cycle (citrate synthase) in the vastus medialis muscle after only 16 days of ovariectomy, suggesting OVX may impact both glucose disposal and oxidative metabolism in skeletal muscle (22). Others have reported reduced insulin-stimulated tyrosine phosphorylation of both the insulin receptor and IRS-1, as well as reduced Akt phosphorylation (Ser473) in the skeletal muscle of rats following OVX, all of which correspond to reduced insulin-stimulated glucose transport (220). It is currently unclear whether a reduction in GLUT4 content following OVX may contribute to impaired skeletal muscle glucose uptake, with some studies showing a decrease in GLUT4 content (233), and others showing no change (115, 212). However, it is possible that impaired insulin-stimulated glucose uptake in OVX muscle may be due to a failure of GLUT4 translocation to the plasma membrane, rather than a reduction in GLUT4 content (225). In addition to alteration of glucose uptake, OVX may also result in upregulation of lipogenic enzyme protein content in skeletal muscle. Particularly, D'Eon et al. report that treatment of OVX animals with 17β-estradiol reduces mRNA expression of specific lipogenic enzymes in skeletal muscle and hypothesize that the observed upregulation of PPARδ and its downstream targets by 17β-estradiol may

partition FAs toward oxidation and away from storage (68). At the whole body level, the balance between carbohydrate and fat oxidation in female mice, as indicated by the respiratory exchange ratio (RER), fluctuates over the course of the estrous cycle, indicating a role for ovarian hormones in the regulation of substrate oxidation (95). Further, multiple studies have reported altered AMP-activated protein kinase (AMPK) activation in response to OVX and/or 17β-estradiol supplementation, yet another mechanism by which ovarian hormones may impact skeletal muscle metabolism (68, 298). Lastly, 17β-estradiol treatment of OVX rats increases enzymes of β-oxidation and FA oxidation, with skeletal muscle mRNA expression of pyruvate dehydrogenase kinase 4 (PDK4) and carnitine palmitoyltransferase I (CPT I) increased by 15 days of 17β-estradiol treatment compared to untreated OVX rats (39).   It is possible that these alterations in lipid regulation in OVX animals may eventually result in increased lipid deposition and lipotoxicity in skeletal muscle, thus contributing to the onset of insulin resistance.

Based on the current literature in both humans and animals models, it is clear that ovarian hormones significantly impact skeletal muscle metabolism. However, much of the evidence for this interaction is based on mRNA data, with only a few studies reporting functional alterations in skeletal muscle metabolic enzymes in response to changes in ovarian hormones. In order to fully elucidate a regulatory role for ovarian hormones in skeletal muscle metabolism additional studies must be conducted to investigate this relationship at a functional level. Thus, further investigation into the role of ovarian hormones in skeletal muscle glucose disposal is necessary considering the

large percentage of the female population at risk for peripheral insulin resistance due to ovarian hormone status.

While skeletal muscle accounts for a large percentage of metabolic activity, adipose tissue also plays an important role in the regulation of energy balance within the body. The primary function of adipose tissue is to store FA in the form of TAG. However, the notion of adipose tissue as an inert organ for TAG storage has been challenged by the recent classification of adipose tissue as an endocrine organ. Adipose tissue TAG storage occurs though either TAG esterification following uptake of circulating FAs, or through *de novo* lipogenesis of carbohydrate precursors. The catabolic process, TAG lipolysis, results in the breakdown of stored TAG to release FAs in response to circulating factors and metabolic demand. <u>Importantly, in conditions such as obesity and ovarian hormone reduction, dysregulation of these processes in adipose tissue may contribute to the onset of insulin resistance and the metabolic syndrome.</u>

The primary mechanism by which adipose tissue stores FA is known as triacylglycerol esterification. The storage form of FAs is TAG, which requires the addition of three FAs to a glycerol backbone. These FAs may either come from the diet, or from the process of lipogenesis, which will be discussed below. Within these tissues, TAG is found in lipid droplets, which serve as storage pools for FAs. The lipid droplets either expand or shrink in response to dietary factors and/or metabolic demand. The coordination of TAG esterification is complex, requiring a multistep process of coordinated enzyme activity (For review: (51)). The committed and rate-limiting step in the synthesis of TAG via the glycerol phosphate pathway is catalyzed by glycerol-sn-3-

phosphate acyltransferase (GPAT), which acylates glycerol-3-phosphate with the help of FA-CoA to produce lysophosphatidate (LPA). The expression of GPAT is highest in tissues with the greatest capacity for TAG storage, particularly adipose tissue, liver, and soleus muscle (177). Further, GPAT expression and activity is highly sensitive to dietary factors. For example, in rats 48 hours of fasting results in a 30-50% decrease in adipose tissue and liver GPAT protein content, and subsequent refeeding increases GPAT activity and expression to levels which surpass the basal state basal by 30-60% (177). Following the formation of LPA, another FA-CoA, and the enzyme acylglycerol-P acyltransferase (AGPAT) catalyze the formation of phosphatidate (PA). Next, phosphatidic acid phosphohydrolase (PAP) converts PA to diacylglycerol (DAG). Additionally, DAG formation may occur through the monoacylglycerol (MAG) pathway, in which a FA-CoA is added to MAG via activity of an enzyme called monoacylglycerol transferase (MGAT). At this point the pathways converge, and DAG may either commit to phospholipid synthesis, or to TAG synthesis. The formation of TAG from DAG is catalyzed by diacylglycerol acyltransferase (DGAT), which has two isoforms, DGAT1 and DGAT2, with the final TAG product being stored in intracellular lipid droplets (For review: (51)).

Another mechanism which may contribute to stored TAG content is lipogenesis, the process of synthesizing FAs from glucose precursors. True *de novo* lipogenesis occurs in mammary, hepatic, and adipose tissues (122). Lipogenesis was previously thought to play a minor role in human metabolism, with only a small portion of the FAs in the adipose tissue TAG pool attributable to lipogenesis. Recently, Strawford et al. reported ~20% of the subcutaneous adipose tissue FAs stored in TAG to

be produced by lipogenesis in healthy, weight stable individuals (262). Lipogenic activity is stimulated by insulin release in response to elevated blood glucose levels. Therefore, a high carbohydrate diet is a powerful stimulus for increased lipogenic activity. In response to insulin, adipocytes take up glucose with the aid of the GLUT4 transporter. Once glucose enters the cell, it is immediately converted to G-6-P by HK and travels through glycolysis, where it can be converted to acetyl CoA. An enzyme called acetyl CoA carboxylase-1 (ACC-1), the rate limiting enzyme of lipogenesis, converts acetyl CoA to malonyl CoA. Fatty acid synthase (FAS) can then bind malonyl CoA on the acyl carrier protein (ACP) motif. Next, through a series of four enzymatic reactions there is a subsequent addition of another three carbon malonyl CoA to the growing carbon chain attached to FAS. The carbon chain is completed when a 16 carbon palmitic acid is formed and the new FA undergoes hydrolysis to release it from the ACP on FAS. After release, the FA produced by *de novo* lipogenesis may be esterified and added to the TAG storage pool within the adipocyte. Lipogenesis is primarily regulated by circulating glucose and insulin levels, as well as the activity of GLUT4, ACC and FAS, ultimately playing a role in the storage of TAG in adipose tissue.

The development of the obese state due to nutrient excess may result in the upregulation of both TAG esterification and lipogenesis, with an increase in circulating FA and ectopic fat deposition contributing to the onset of insulin resistance.

The catabolic breakdown of stored TAG is known as lipolysis, or TAG hydrolysis. The regulation of lipolysis is complex in that it is dependent upon the levels of multiple circulating factors, as well as the coordinated activity of multiple lipases. The

primary storage site for TAG is in adipose tissue; however, smaller stores are also located in skeletal muscle and liver. When stimulated, these TAG stores may be broken down, resulting in the release of FAs and glycerol. Serum glycerol is typically used as a circulating indicator of lipolytic activity rather than FAs (30, 111, 128, 129, 137, 181, 238). Glycerol released from adipose and skeletal muscle lipolysis must enter the bloodstream because these tissues do not contain glycerol kinase to re-utilize the glycerol. However, it is possible for FAs within adipose tissue or skeletal muscle to be re-esterified, thus circulating levels of FA may not accurately reflect lipolytic activity.

The primary circulating factors which regulate lipolytic activity are insulin and catecholamines (epinephrine and norepinephrine). Catecholamines are important regulators of lipolytic activity both at rest and under conditions of lipolytic stimulation. The catecholamines bind to adrenergic receptors, of which there are two types: α-adrenergic receptors, which are inhibitory to lipolysis (163), and β-adrenergic receptors, which are stimulatory (36). The ratio of α- to β-adrenergic receptors in adipocytes plays a major role in the regulation of adipose tissue lipolytic activity and varies by adipose tissue depot. For instance, subcutaneous adipocytes contain a greater number of α-adrenergic receptors relative to β-adrenergic receptors, while in omental adipose tissue the number of β-adrenergic receptors equals, or is slightly greater than, the number of α-adrenergic receptors (190). This difference in the balance between stimulatory and inhibitory adrenergic receptors results in elevated lipolytic activity in omental adipose tissue relative to subcutaneous adipose tissue (11). In addition, differences in catecholamine sensitivity of the two adrenergic receptor types impacts lipolytic regulation. In omental adipocytes, epinephrine promotes lipolytic activity regardless of

the concentration (24, 190). However, in subcutaneous adipocytes, low concentrations of epinephrine are anti-lipolytic, while higher doses facilitate lipolytic activity (24, 190). These depot-specific effects may thus be due to differences in α-adrenergic receptor responsiveness observed between subcutaneous and omental adipocytes.

When catecholamines bind to β-adrenergic receptors, they activate a stimulatory G protein that is coupled to the receptor. The G protein in turn activates adenylate cyclase (AC), which catalyzes the production of cAMP from ATP. Next, cAMP activates protein kinase A (PKA), which phosphorylates multiple lipases that regulate lipolytic breakdown of TAG stores. Further, PKA phosphorylates the lipid droplet coat protein perilipin. Under basal conditions, perilipin protects TAG stores, preventing unstimulated lipolytic breakdown. However, under stimulated conditions, perilipin facilitates lipolysis by undergoing a conformational change that allows hormone sensitive lipase (HSL) access to the lipid droplet. Therefore, perilipin has both a role to protect the lipid stores under basal conditions, and to facilitate lipolysis under stimulated conditions (268). HSL is also phosphorylated by PKA, and translocates to the lipid droplet following phosphorylation. HSL was long believed to be the rate-limiting enzyme in lipolysis, however, knock out of HSL does not reduce lipolytic rate or TAG levels to a large extent either *in vivo* (112, 209, 285) or *in vitro* (208). This led to the discovery of another enzyme, adipose triglyceride lipase (ATGL) which is now believed to be the rate-limiting enzyme of lipolysis (133, 282, 308). ATGL catalyzes the breakdown of TAG to DAG, releasing one FA. HSL breaks down DAG to monoacylglycerol (MAG), releasing a second FA. Lastly, monoglyceride lipase (MGL) breaks MAG into glycerol and a FA (See Figure 5 below). Therefore, the regulation of lipolysis is dependent upon the

coordination of multiple lipases to release glycerol and FAs, a process which is stimulated by the action of catecholamines. The primary inhibitor of lipolytic activity is insulin. Insulin inhibits lipolytic activity by activating phosphodiesterase, which breaks down cAMP and terminates transmission of adrenergic signaling. Overall, the regulation of lipolysis is dependent upon the levels of circulating insulin and catecholamines, which influence the activity of the lipases regulating lipolysis at a cellular level.
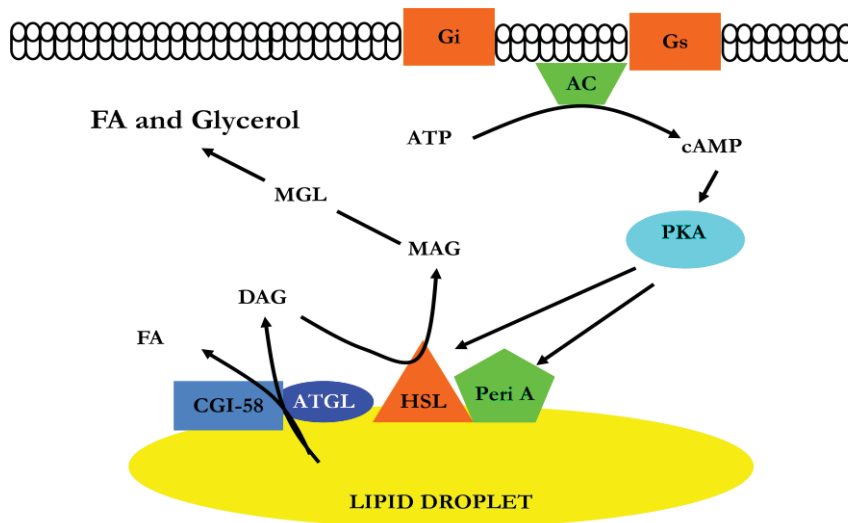
Figure 5. Cellular regulation of lipolysis. (Adapted from: (28)). Gi = inhibitory G protein, Gs = stimulatory G protein, AC = adenylate cyclase, PKA = protein kinase A, Peri A = PLIN1 (Perilipin), HSL = hormone sensitive lipase, ATGL = adipose triglyceride lipase, CGI-58 = comparative gene identification-58, DAG = diacylglycerol, MAG = monoacylglycerol, MGL = monoglyceride lipase, FA = fatty acid.

Obesity-induced alterations in TAG storage and breakdown, and the metabolic consequences of these changes, are dependent upon a multitude of factors. In particular, alterations in adipose tissue distribution and adipocyte phenotype play roles in the pathological consequences of obesity on skeletal muscle, and subsequently on the development of whole body insulin resistance.

The location of fat storage plays an important role in determining whether or not an increase in adiposity will contribute to the onset of obesity-related conditions. Recent findings have suggested that metabolic disease risk is lower when excess fat is stored in subcutaneous (i.e. inguinal) adipose tissue (13), with multiple studies demonstrating little change in peripheral insulin sensitivity with increased subcutaneous fat storage (99, 130). However, excess storage of lipid in the visceral (i.e. omental) region significantly contributes to the development of obesity-related conditions such as insulin resistance (205, 219, 284). In post-menopausal females, a tendency to store fat in the abdominal region, primarily as visceral fat, has been associated with increased prevalence of the metabolic syndrome as compared to women who store more fat in the lower body, where fat is stored in subcutaneous depots (155). Overall, the presence of visceral (central) adiposity has been widely recognized as an independent risk factor for the metabolic syndrome, coronary heart disease, and insulin resistance in multiple populations.

In addition to the location of fat storage, the mechanism responsible for expansion of adipose tissue mass, either an increase in adipocyte size or an increase in adipocyte number, plays a critical role in defining the phenotype of the fat pad and the subsequent risk for metabolic disease. In particular, adipose tissue expansion due to an increase in adipocyte size is correlated with increased risk of obesity-related conditions in that large adipocytes are thought to promote insulin resistance due to their contribution to mechanisms involved in lipotoxicity and/or inflammation-induced insulin resistance (84, 207). For example, both the *ob/ob* mouse model of obesity and the insulin receptor 2 knock-out mouse (IRS2-/-) develop visceral obesity that is associated with an

increase in adipocyte size (266). In contrast, adipose tissue expansion due to an increase in adipocyte number is often associated with enhanced insulin sensitivity which appears to be due to the greater number of small adipocytes. For example, when adiponectin overexpression is induced in the *ob/ob* mouse, a commonly used genetic model of obesity, the diabetic phenotype of the *ob/ob* mouse is completely attenuated in spite of increased body weight and total fat mass (147). These improvements are largely attributable to both the preferential storage of fat in subcutaneous adipose tissue depots rather than visceral depots, as well as to the expansion of adipose tissue via an increase in adipocyte number rather than an increase in adipocyte size (147). Adipocyte hyperplasia results in a greater number of small adipocytes which are capable of storing excess circulating lipid, thus alleviating any circulating lipid burden on the individual. Further evidence is also found in humans where obesity is not always associated with insulin resistance (207) in that obese individuals with subcutaneous adipose tissue expansion mediated by adipocyte hyperplasia are more insulin sensitive than those with visceral obesity mediated by adipocyte hypertrophy.

It is therefore of concern that the most visible change associated with ovarian dysfunction in women is a significant increase in visceral fat. The link between estrogens and body composition has been demonstrated in both human and animal models (68, 169, 210, 245). Significant increases in visceral fat mass have been attributed to decreased levels of estrogens in post-menopausal females (164, 168, 169, 222, 245). Further, the increase in visceral fat mass in females during and after the menopausal transition is independent of the increase in visceral fat mass observed due to aging alone. In the SWAN cohort, women were monitored for a 4 year period, with some

women becoming menopausal in this time and others not undergoing the menopausal transition. This allowed for age matching of pre- and post-menopausal females. In this cohort, the females who went through menopause during the study increased visceral fat mass to a greater extent than the age-matched females who did not become menopausal, indicating an age-independent effect of ovarian hormone levels on visceral fat mass (132). In females, estrogens promote the deposition of fat in the hip and thigh region, known as gynoid distribution, rather than in the visceral region, which is characteristic of males and termed android distribution (178). In females with intact ovarian function, activity of adipose tissue lipoprotein lipase (LPL) in the gluteal region is elevated compared to LPL activity in the visceral region (271). LPL catalyzes the release of FAs from circulating TAG and very low density lipoprotein (VLDL), which may then be taken up by adipocytes and esterified back to TAG for storage in lipid droplets. When ovarian hormones are reduced, this regional difference in LPL activity in females is eliminated and may be a contributing factor to the increase in visceral fat storage. Also, the increase in testosterone relative to estrogens in post-menopausal females may contribute to the alteration in fat distribution (132). The androgen receptor is expressed highly in preadipocytes in the visceral region and may promote fat storage in the visceral region preferentially to the subcutaneous depots (73, 74). In the SWAN cohort, a significant association was determined between free testosterone levels and visceral fat mass (132). Many studies have demonstrated an increased risk of cardiovascular and metabolic diseases associated with visceral fat accumulation (40, 205). Thus, as estrogens contribute to gynoid fat accumulation, females with intact ovarian function are

at decreased risk for cardiovascular disease and the metabolic syndrome compared to their male, and ovary compromised female counterparts (40, 104).

   In addition, all of the animal models discussed above have been used to study changes in adipose tissue following ovarian hormone reduction. These animals exhibit increased adiposity, as well as a shift in adipose tissue distribution, with a dramatic increase in fat storage in the visceral region (56, 62, 68, 138, 280, 295-297). This visceral fat storage in the OVX, VCD, FORKO, ERα-KO, and ArKO mice results in metabolic dysfunction that qualitatively resembles the metabolic syndrome observed in females with ovarian hormone disruption (56, 62, 68, 138, 280, 295-297). Further, adipose tissue expansion in the OVX model is mediated by an increase in adipocyte size, which may contribute to the onset of ectopic lipid deposition and peripheral insulin resistance (68). Additionally, it is possible that the elevated basal lipolysis observed as a result of altered adipose tissue lipase expression in OVX mice (297) may facilitate ectopic lipid deposition in skeletal muscle. As described above, this ectopic lipid deposition may contribute to skeletal muscle insulin resistance in sedentary individuals due to multiple mechanisms (i.e. lipid intermediates, PKC signaling, etc.).

   Collectively, the changes in adipose tissue observed in humans and animal models clearly demonstrate a link between ovarian hormone reduction, changes in adipose tissue, and the onset of peripheral insulin resistance. However, while the physiological changes in adipose that occur in females following ovarian hormone reduction have been well documented, further research is necessary to elucidate many of the cellular mechanisms which link these alterations to the onset of insulin resistance and other metabolic diseases.

The discovery of leptin in 1994 dramatically changed the understanding of skeletal muscle and adipose tissue roles in metabolic regulation and resulted in a new field of study focusing on adipose tissue and skeletal muscle cross-talk. Leptin was found to be secreted from adipocytes and exert peripheral effects in both the hypothalamus and in skeletal muscle. This discovery dramatically changed the notion of adipose tissue as an inert storage depot and led to the elucidation of multiple factors secreted from adipose tissue, now termed adipokines (See Figure 6 below). In the hypothalamus, leptin acts to control food intake, acting as a satiety signal (47). In skeletal muscle, leptin plays a role in controlling energy expenditure (249). Importantly, leptin can regulate lipid oxidation and lipid storage in skeletal muscle, making it an attractive target for the study of skeletal muscle metabolism. Specifically, leptin has been reported to promote oxidation over storage of fat in skeletal muscle (202). In addition, leptin may increase skeletal muscle glucose uptake (200). Together, leptin promotes insulin sensitivity, both via an increase in glucose uptake and also by prevention of ectopic lipid deposition in skeletal muscle.

In addition to leptin, adiponectin is also positively associated with insulin sensitivity. Leptin and adiponectin are unique among the currently identified adipokines in that they are positively associated with insulin sensitivity, whereas the other adipokines are negatively associated with insulin sensitivity. Adiponectin was classified as an adipokine after it was determined to be secreted primarily by adipocytes and have receptors in peripheral tissues. The adiponectin receptors AdipoR1 and AdipoR2 are located primarily in skeletal muscle and liver, respectively (25). Similar to leptin, adiponectin was observed to exert insulin-sensitizing effects on skeletal muscle via

activation of AMPK (33, 274). In animals where adiponectin is overexpressed, insulin sensitivity and skeletal muscle glucose disposal are high (12). When adiponectin is knocked out in a mouse model, the animals develop insulin insensitivity and have impaired clearance of FA from circulation (301). Further, when the transgenic mouse overexpressing adiponectin is crossed with the obese, insulin resistant *ob/ob* mouse, there is an improvement in insulin sensitivity in spite of increased body weight compared to the *ob/ob* mouse alone (147). The thiazolidinedione (TZD) class of drugs, which are often used for treatment of type 2 diabetes, activate PPAR-γ and also increase adiponectin expression in adipose tissue and adiponectin levels in circulation (114, 275), improving insulin resistance. This once again supports a role for adiponectin in promoting insulin sensitivity. It is clear that the release of adiponectin from adipose tissue exerts peripheral effects on skeletal muscle; therefore adiponectin is a good example of an adipose tissue endocrine factor.

Unlike adiponectin and leptin, many other adipokines exert negative effects on peripheral insulin sensitivity. The most well-characterized of these factors is tumor necrosis factor alpha (TNF-α). TNF-α is secreted from adipocytes, however, much of the TNF-α in circulation comes from macrophages which infiltrate adipose tissue in disease states such as obesity. TNF-α inhibits skeletal muscle insulin sensitivity by interfering with the insulin signaling pathway. In particular, TNF-α promotes serine (inhibitory) phosphorylation of IRS-1 (139, 240) as well as inhibition of Akt and AS160 phosphorylation (179, 218, 259). Genetic ablation of TNF-α in mice results in attenuation of high fat diet-induced insulin resistance (229), suggesting TNF-α to be a critical mediator of insulin resistance observed in diseased states. In lean individuals,

adiponectin serves to inhibit TNF-α secretion from macrophages (303). However, in the obese state, adiponectin is reduced, and macrophage infiltration is increased, both of which result in increased TNF-α release from adipose tissue and subsequent impairment in skeletal muscle insulin signaling (21).

IL-6 is an extremely controversial endocrine factor, with studies reporting both a negative effect on insulin sensitivity and a positive effect on insulin sensitivity (94, 145, 291). IL-6 may be secreted from skeletal muscle as a myokine, or from adipose tissue as an adipokine. Under resting conditions, relatively low levels of IL-6 are present in circulation, with adipose tissue accounting for ~10-35% of this circulating IL-6 (195). When released as a myokine in response to acute exercise, IL-6 has beneficial effects, such as to help to maintain blood glucose levels via facilitation of hepatic gluconeogenesis (119, 143). However, in the sedentary state elevated circulating levels of IL-6 are associated with insulin resistance (145, 283). Based on these divergent findings, it has been suggested that an acute increase in IL-6, such as in response to exercise, is insulin-sensitizing, while chronic low grade exposure, such as in the inflammatory state of obesity, has negative effects on insulin sensitivity (136, 151, 152). Circulating IL-6 levels are elevated in obese compared to lean individuals (20). Additionally, adipose tissue and circulating levels of IL-6 are reduced by weight loss, thus implicating adipose tissue in mediating the increased IL-6 levels in the obese state (20). IL-6 inhibits insulin signal transduction in hepatocytes and skeletal muscle cells, suggesting a mechanistic role for IL-6 in the development of insulin resistance in peripheral tissues (148, 242). Together, the current evidence suggests that chronically

elevated IL-6 of adipose tissue origin may contribute to the onset of insulin resistance in the obese state (136, 151, 152).

In addition, the expansion of adipose tissue results in increased release of another adipokine, monocyte chemoattractant protein-1 (MCP-1), which recruits macrophages into adipose tissue. When adipose tissue expansion occurs, an increase in cell size without a parallel increase in adipose tissue blood flow may result in hypoxic conditions, which leads to adipocyte cell death. Macrophages are often observed clustered around the sites of cell death, forming "crown-like" structures. Therefore, through both cell death and release of MCP-1, the obese state results in increased macrophage recruitment to adipose tissue and a state of chronic low-grade inflammation due to inflammatory factors secreted from the macrophages. Further, MCP-1 has recently been reported to negatively impact insulin signaling in skeletal muscle, suggesting that its role as an endocrine factor should be further investigated (139, 240).

Many other adipokines have been identified, such as retinol binding protein 4 (RBP4), visfatin, resistin, etc. These adipokines are increased in the obese and insulin resistant states; however, mechanisms of action or direct roles in disease pathologies are unknown. In the case of resistin, animal models have linked the adipokine to insulin signaling defects, however, resistin was later found to be expressed only in trace amounts in humans. Based on the endocrine effects of leptin, adiponectin, MCP-1, IL-6, and TNF-α on skeletal muscle, the further study of adipokines and their roles in health and disease is warranted.
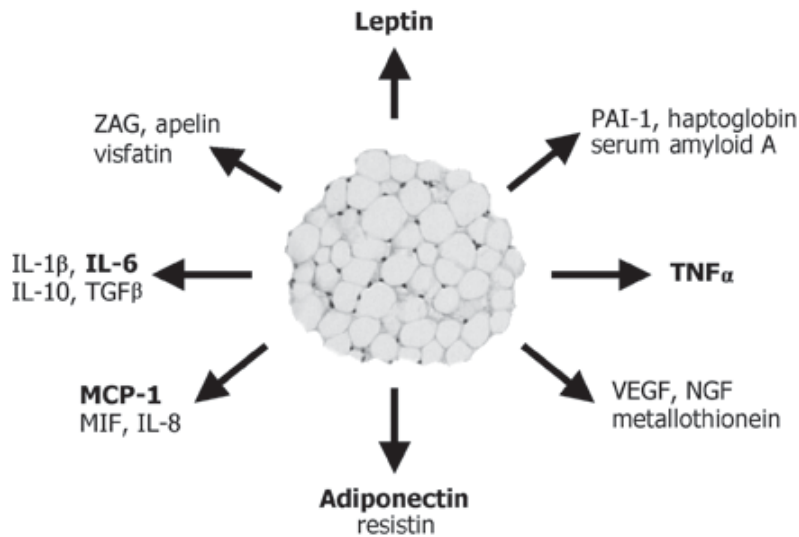
Figure 6. Some of the major adipokines released from white adipose tissue. Trayhurn et al. 2006 (276).

While little evidence exists, it appears that in response to ovarian hormone reduction both in females and in OVX mice, changes in adipokine levels occur which may be related to the development of insulin resistance. Studies have reported higher leptin levels in post-menopausal women compared to pre-menopausal women (46, 173, 244). However, this elevation in circulating leptin appears to be mediated by the larger fat mass observed in post-menopausal women, as the difference in leptin levels between pre- and post-menopausal females is not significant when controlling for fat mass (244). Further, changes in adiponectin in women are controversial, however some studies have reported an increase in adiponectin in post-menopausal compared to pre-menopausal women (173). In opposition to leptin, adiponectin levels in post-menopausal women are inversely related to adipose tissue mass (173). Findings are divergent on the impact of OVX on circulating adiponectin and leptin levels, with some studies showing no change (14) and others report a decrease following OVX (68). Together, these

findings suggest that adipokine levels are in some way altered by ovarian hormone status. However, the relative contribution of ovarian hormone levels versus increased adipose tissue mass on adipokine levels in post-menopausal women remains to be determined. Due to the relationship between adipokines and insulin resistance, as well as the increased prevalence of insulin resistance in ovary compromised females, further investigation into ovarian hormone-induced changes in adipokines is necessary.

The research on adipokines to date clearly demonstrates interaction between adipose tissue and skeletal is possible due to the endocrine capacity of adipose tissue. Further, changes observed in adipokine secretion and function in the obese and diabetic states point to a mechanistic role for these factors in the etiology of disease.

As discussed above, one such population that is at significantly increased risk for diseases such as the metabolic syndrome, cardiovascular disease, and insulin resistance is ovarian hormone compromised females. Unfortunately, following the Women's Health Initiative, no treatment is clinically accepted to prevent the physiological changes in women experiencing ovarian hormone dysfunction that result in increased disease risk. Thus, while a vast amount of information has been elucidated in regards to the impact of ovarian hormones on metabolic function, much work remains such that a treatment may be developed for this at-risk population.

It is clear that skeletal muscle and adipose tissue play significant roles in the path to insulin resistance in both obesity and ovarian hormone reduction. Further, the evolving field of adipose tissue and skeletal muscle cross-talk provides a new angle for the study of these tissues and their impact on metabolic disease. Multiple studies have demonstrated that ovarian hormones have a significant impact on metabolic

function, both at the whole body and tissue levels. However, whether the onset of insulin resistance in ovary compromised females is due to direct effects of ovarian hormones on skeletal muscle, or is downstream of changes in adipose tissue remains to be elucidated. Therefore, we have studied OVX-induced metabolic changes in adipose tissue and skeletal muscle, as well as investigated the interaction between primary cells from these two tissues. The elucidation of skeletal muscle and adipocyte metabolic properties that are sensitive to ovarian hormone status in both ovary intact and OVX animals may eventually contribute to development of a treatment for ovary compromised females.

Chapter 3: 17β-Estradiol Supplementation Attenuates Ovariectomy-Induced Increases in ATGL Signaling and Reduced Perilipin Expression in Visceral Adipose Tissue.

The following article was published in the Journal of Cellular Biochemistry (110:420-427, 2010).

17β-estradiol supplementation attenuates ovariectomy-induced increases in ATGL signaling and reduced perilipin expression in visceral adipose tissue.

Lindsay M. Wohlers[1] and Espen E. Spangenburg[1*]

[1] University of Maryland, School of Public Health, Department of Kinesiology, College Park, MD 21045

Running title: Adipose tissue signaling in ovariectomized mice

*Corresponding Author:

Espen E. Spangenburg, Ph. D.
University of Maryland
Department of Kinesiology
College Park, MD 21045
1-301-405-2483 (office)
1-301-405-5578 (fax)
espen@umd.edu

Abstract:

Adipocytes from post-menopausal females have high basal lipolytic rates compared to pre-menopausal women, which contributes to increased risk of developing dyslipidemia. The purpose of this study was to delineate the cellular mechanisms affecting adipose tissue function in the ovariectomized (OVX) mouse and determine if physical activity or estrogen supplementation alter any detected changes. Female C57/Bl6 mice were placed into SHAM, OVX sedentary (OVX), OVX exercise (OVX-Ex), and OVX sedentary + 17β-estradiol (OVX+E_2) groups. Visceral fat mass, glycerol, and NEFA levels were significantly higher in OVX mice compared to SHAM animals, but they were not elevated in the E_2 treated animals. Voluntary running failed to change circulating levels of glycerol or NEFA in OVX mice, but did partially attenuate the increase in visceral fat mass. ATGL protein content was significantly elevated in visceral fat from OVX and OVX-Ex groups compared to SHAM, while ATGL-CGI-58 interaction was significantly higher in OVX than SHAM and OVX+E_2 mice. No significant differences in HSL phosphorylation were detected between groups, however ERK1/2 phosphorylation was significantly elevated in the OVX mice. To determine if ERK1/2 function was critical for the increased glycerol levels, visceral fat was treated with MEK inhibitor PD98059, with no differences in glycerol release detected. Perilipin protein content was decreased significantly in OVX and OVX-Ex mice compared to SHAM. Thus, these data suggest that increased ATGL signaling and reduced perilipin protein content may contribute to increased rates of TAG hydrolysis in OVX mice, which are attenuated with E_2 treatment, but not by exercise.

Key Words: menopause, lipid, hormone sensitive lipase, adipocyte

Introduction:

It is well documented that as women transition into menopause, those who do not take hormone replacement therapy (HRT) demonstrate disproportionate increases in lipid storage with an apparent decline in lipid utilization (83). Loss of ovarian function also leads to an increase in visceral fat mass, which concurrently results in an increased lipolytic rate (76, 210, 237). The link between ovarian hormones and alterations in metabolism has been demonstrated in both human and animal models (68, 169, 210, 245). The enhanced lipolytic rate is particularly problematic because it may contribute to the development of peripheral insulin resistance and ectopic lipid deposition in the liver, both of which have been observed in animals with reduced ovarian function (211, 233). These conditions result in an increased risk for developing cardiovascular disease (CVD) or other lipid-based conditions (41, 231). In addition to ectopic lipid deposition in liver tissue, a high level of circulating lipid places the individual at increased risk for ectopic fat deposition in skeletal muscle (97). Furthermore, post-menopausal women are at increased risk for developing CVD and insulin resistance. Therefore, it is critical to understand mechanisms which are affecting metabolic function in post-menopausal women.

Triacylglycerols (TAG) are stored and utilized as energy substrates primarily by adipose tissue and skeletal muscle, respectively. To oxidize free fatty acids (FFA), the FFA must be liberated from the TAG through enzymatic-regulated hydrolysis of the stored TAG. Although hormone sensitive lipase (HSL) was long believed to be the rate-limiting lipase, several recent studies have demonstrated the importance of adipose triglyceride lipase (ATGL) to lipolysis (83, 288, 290). ATGL, also known as desnutrin,

was found to catalyze the first step in lipid hydrolysis, breaking TAG down to diacyglycerol (DAG) and releasing a FFA (282, 308). HSL subsequently cleaves another FFA, converting DAG to monoacylglycerol (MAG). The final step of lipid hydrolysis is catalyzed by monoacylglyceride lipase (MGL), which breaks down MAG to glycerol and FFA's, which are then released into systemic circulation (86). Thus, elucidating the mechanisms regulating ATGL and HSL activity is a critical step towards understanding lipid metabolism.

The complete activation of ATGL is thought to be regulated by protein-protein interaction and/or by phosphorylation, albeit very little is known about regulation of ATGL through phosphorylation (28). A number of potential phosphorylation sites have been suggested for ATGL, but at this time none have been documented to be necessary for complete lipase activity (308). For example, ATGL contains an ERK1/2 specific phosphorylation motif, suggesting that ATGL may be sensitive to changes in MAPK activation, although this has never been measured (19). However, it is well known that complete ATGL activation is dependent upon interaction with comparative gene identification-58 (CGI-58) (167). CGI-58, also known as abhydrolase domain containing 5, plays a critical role in the autosomal recessive disease Chanarin-Dorfman syndrome, which is characterized by excessive TAG accumulation in various tissues (77).

Unlike ATGL, the cellular regulation of HSL is well understood. HSL is phosphorylated at five different serine residues (Ser563, Ser565, Ser600, Ser659, and Ser660) (289). Activation of protein kinase A (PKA) results in increased phosphorylation of serine sites 563, 659, and 660 (8), all of which lead to increased HSL

activity. Also, ERK1/2 can phosphorylate HSL at Ser600, enhancing HSL activity (108). Conversely, phosphorylation of Ser565 by AMPK appears to reduce HSL activity (93).

Alterations in the expression of adipose tissue lipases have been demonstrated with obesity (68), however the effects of reduced ovarian function on ATGL and HSL signaling is unknown. There are reasons to suspect that changes in ATGL and HSL function may occur in post-menopausal females. For example, cells isolated from adipose tissue of post-menopausal women exhibit increased lipolytic rates independent of adipocyte cell size or body fat percentage (68, 206). These data suggest that the increased rates of lipolysis observed in post-menopausal women cannot be explained solely by changes in adipose tissue size. Unfortunately, very little evidence is available documenting changes in cellular signals that regulate lipolysis following a decline in ovarian function.

Thus, the purpose of this investigation was two-fold: first to determine if cellular mechanisms that regulate lipid droplet function are increased in mice after surgically-induced menopause and second to determine if voluntary wheel running effectively prevents increases in both visceral fat accumulation and circulating lipid in a manner similar to 17β-estradiol supplementation in OVX mice. The goal of the second component of these experiments was to determine if physical activity can be as effective as 17 β-estradiol supplementation in attenuating the negative changes following OVX in female mice.

Methods:

Animals: Thirty-two 8-week old C57/BL6 (Harlan) female mice were divided into four groups (SHAM, OVX, OVX-Ex, OVX+E$_2$). One group of mice (n=12) underwent a bi-lateral ovariectomy (OVX), a frequently used animal model of menopause (142). Our lab has previously shown that this model decreases the levels of circulating estrogens by 70% within 48 hours (248). Further, previous research has shown that surgical removal of the ovaries from mice does not resulting in changes in feed patterns (31, 228). A second group (n=5) was subjected to a SHAM surgery where they were anesthetized, but did not undergo ovariectomy. The third group (n=5) consisted of ovariectomized mice which underwent a second surgery one week after ovariectomy where exogenous estrogen was introduced via implantation of a subcutaneous time-release pellet (Innovative Research, Sarasota, FL). This pellet results in the animals receiving ~40pg/mL of 17β-estradiol per day, which is similar to levels found in the mouse during estrous (196).

Mice were given ad libitum access to water and standard rodent chow (Purina Laboratory Rodent Diet 5001: 23% protein, 4.5% fat, 6% fiber) and were housed in a temperature-controlled room on a 12h light/dark cycle. The exercise training group (OVX-Ex) was placed in cages with voluntary running wheels, while the sedentary groups were placed in standard mouse cages. Running activity was monitored for eight weeks with a photocell counter interfaced with a computer through customized software (Layfayette Instruments, Layfayette, IN). The eight-week time point was chosen because in preliminary experiments we found that large increases in visceral fat pad mass (i.e. parametrial fat depots) were detected at this point (data not shown). After eight weeks all animals were sacrificed, tissue was collected and snap frozen in liquid nitrogen, and then

stored at -80°C. Mice were removed from the wheel cages 24 hours prior to sacrifice to account for acute effects of exercise, followed by the removal of food 4-5 hours prior to sacrifice. All aspects of this study were approved by the University of Maryland Institutional Animal Care & Use Committee (IACUC) Review Board.

Western Blotting of Adipose Tissue: Western blotting was performed on visceral adipose tissue (i.e. parametrial fat depots). Fat was homogenized in Mueller buffer (50 mM Hepes (pH 7.4), 0.1% Triton –X100, 4 mM EGTA, 10 mM EDTA, 15 mM $Na_4P_2O_7H_2O$, 100 mM β-glycerophosphate, 25 mM NaF, 50 μg/mL leupeptin, 50 μg/mL pepstatin, 40 μg/mL aprotinin, 5 mM Na_3VO_4, and 0.1% NP-40) using a mechanical homogenizer, then centrifuged for 10 minutes at 4°C and 13,000 rpm. The supernatant between the fat cake and the pellet was removed using a syringe and placed into a separate tube, which was spun once more under the same conditions and the supernatant was again removed. Protein concentrations were determined on the supernatant using the BCA protein assay. Equal amounts of total protein (75μg) were resolved on 10% SDS-PAGE gels and transferred to PVDF membranes as previously described (254, 298). Blots were visualized with Ponceau S (Sigma Chemical) to confirm equal loading of the lanes and then blocked with 5% nonfat dry milk in Tris-buffered saline with 0.1% Tween (TBS-T). Membranes were probed with antibodies obtained from Cell Signaling (unless indicated) for p-ERK1/2 (Thr 202/Tyr 204; 1:2000), total ERK1/2 (1:2000), total ATGL (1:1000), p-AMPK (Thr172; 1:1000), p-HSL565 (1:1000), p-HSL660 (1:1000), total HSL (1:2000) (kind gift of Dr. F.B. Kraemer, Stanford University), or Perilipin (1:200, Santa Cruz) in a buffer of 5% BSA in TBS-T on a rocker at 4ºC overnight. Following incubation with the primary antibody, membranes were washed in TBS-T (3 x 5 min) and then incubated for

1 hour with horseradish peroxidase (HRP)-conjugated rabbit secondary antibody (1:1000) in 5% nonfat dry milk in TBS-T. Next, membranes were washed in TBS-T (1 x 10 min, 3 x 5 min), followed by enhanced chemiluminescence reagent (ECL) (Pierce, Rockford, Ill). Membranes were visualized with a chemilumiscence imager (Syngene, Frederick, Md) and quantified with Image J software (NIH Bethesda, MD).

Immunoprecipitation: Two-hundred and fifty µg of total protein was combined with ATGL antibody (1:100 dilution) and rocked overnight at 4ºC. A 25 µL aliquot of protein A-Sepharose (EZview Red Protein A Affinity Gel Beads, Sigma, St. Louis, MO) was washed repeatedly in Mueller buffer without protease inhibitors. After the last wash, the samples containing the protein and antibody complex were added to the tubes containing the protein A-Sepharose pellets. Samples were gently mixed and then rocked for 1 hour at 4 ºC. After rocking for 1 hour, samples were centrifuged at 13,000 rpm at 4 ºC for 5 minutes. The supernatant was removed and the pellet was re-suspended in 1 mL of Mueller buffer, followed by another spin of 13,000 rpm at 4 ºC for 5 minutes (repeated 3x). Following the last wash, the supernatant was removed and the pellet was re-suspended in 30 µL of 4X sample loading buffer, boiled for 5 minutes, and centrifuged briefly. Samples were loaded onto 10% SDS-PAGE gels and transferred to PVDF membranes as previously described (254, 298). Blots were then blocked with 5% nonfat dry milk in Tris-buffered saline with TBS-T. Membranes were probed with an antibody for CGI-58 as previously described (264) (1:25,000, kind gift from Dr. Dawn Brasaemle, Rutgers University) or an antibody specific for serine phosphorylation (1:1000, Millipore). Westerns protocol was the same as described above.   The membranes were

stripped and re-probed for total ATGL as described above. All quantified data were normalized to total ATGL expression.

NEFA and Glycerol levels: Non-esterified fatty acids (NEFA) were measured in mouse serum using a colorimetric assay (Wako Diagnostics, Richmond, VA). Glycerol levels were determined in mouse serum or media using a free glycerol determination kit (Sigma, St. Louis, MO).

Isolated Organ Bath Experiments: In a second set of animals (SHAM n=5; OVX n=5), organ bath experiments were performed on visceral adipose tissue (i.e. parametrial fat depots). The adipose tissue was carefully dissected and placed in an organ bath containing oxygenated media (95% O_2; 5% CO_2). After 30 minutes, half of the adipose tissue and 1 mL of the media was removed and frozen for glycerol analysis. The remaining adipose tissue was washed with media and then exposed to fresh media containing MEK inhibitor PD98059 (30μM) for another 30 minutes. The tissue was frozen and 1 mL of media was preserved for glycerol analysis. All glycerol measurements from the bath assay were normalized to the total protein content from the isolated adipose tissue.

Statistical Analysis: All data are expressed as means ± SEM. Statistical significance was determined using t-tests with Sigma Stat statistical analysis software (Systat Software Inc., San Jose, CA). A p-value of <0.05 was considered significant.

Results:

Anatomical characteristics:

The body weight of sedentary OVX animals was significantly greater than the SHAM animals by 9.8%, however, no differences were detected in absolute liver, heart, or skeletal muscle mass (Table 1). The visceral fat mass in the sedentary OVX group was significantly greater than all other groups by ~300% (Figure 1). The visceral fat mass of OVX-Ex mice was significantly lower than sedentary OVX mice, however, still significantly greater than the SHAM group ($p<0.05$). When fat mass was normalized to body weight, only the sedentary OVX mice differed significantly from the SHAM mice ($p<0.05$). OVX mice with voluntary wheel access ran 2448.80 ± 157.85 m/day, which is consistent with previously published data (103). Supplementation with 17β-estradiol prevented any increase in visceral fat mass of the OVX animals when compared to the SHAM animals.

NEFA and glycerol levels:

Average fasted non-esterified fatty acid (NEFA) and glycerol levels are summarized in Table 2. NEFA was significantly elevated in the OVX and OVX+Ex groups compared to the SHAM and OVX+E_2 groups. Glycerol levels were significantly elevated in the sedentary OVX mice as compared to SHAM mice, with no other differences detected between groups. However, glycerol levels of the OVX+Ex group were elevated and reached levels close to statistical significance when compared to the SHAM group ($p=0.06$).

ATGL protein content and interaction with CGI-58:

To understand the effect of ovarian hormones on cellular signaling in visceral adipose tissue, we measured indices of ATGL and HSL activation. Total ATGL protein content was elevated in OVX and OVX+Ex mice as compared to SHAM (Figure 2), while OVX+E_2 mice were not significantly different from SHAM mice. Using immunoprecipitation assays we found increased ATGL-CGI-58 interaction in the OVX and OVX+Ex mice compared to SHAM. OVX+E_2 mice exhibited levels of ATGL-CGI-58 interaction that were significantly lower than the OVX mice and not different from the SHAM mice (Figure 3). Further, no differences in total serine phosphorylation of immunoprecipated ATGL were found between any groups (data not shown).

HSL protein content and phosphorylation:

Next, we sought to determine if changes in HSL activation were detectable in visceral fat isolated from these animals (Figure 4A). Minimal phosphorylation was detected, with no quantitative differences in phosphorylation of HSL at Ser659/660, a site which is phosphorylated by PKA (Figure 4B; quantitative data not shown). We detected minor alterations in AMPK phosphorylation (Thr172) in visceral fat; however, these differences did not correlate to changes in HSL565 phosphorylation (Figure 4B; quantitative data not shown). This suggests that the Ser565 site on HSL may be phosphorylated by something other than AMPK (93).

Alterations in ERK1/2 protein content:

A previous investigation has documented that ERK1/2 phosphorylates HSL at Ser600 and results in a significant increase in HSL activity (252). In our samples, significant differences were detected between the sedentary SHAM and OVX mice, as

well as between the sedentary OVX and OVX+ E_2 mice in normalized ERK1 (Figure 5).

Significant differences were also detected between the SHAM and sedentary OVX mice, as well as between the SHAM and OVX+ E_2 mice in normalized ERK2 (Figure 5). In spite of differences in ERK1/2 activation, it is not possible to determine if HSL phosphorylation was different at serine residue 600 since there are no available antibodies to measure phosphorylation changes at this site.

Glycerol levels and ERK1/2 protein content with MAPK inhibitor application:

Thus, to determine if activation of ERK1/2 is critical for increased glycerol release by the adipose tissue of the OVX animals, we isolated visceral adipose tissue from SHAM and OVX animals for organ bath experiments. The adipose tissue was divided and placed in oxygenated media. To achieve pre-drug treatment values, the tissue was incubated for 30 minutes, after which a portion of the adipose tissue and media was removed and frozen. The remaining adipose tissue was exposed to fresh media supplemented with the MEK inhibitor PD98059 (30µM). Glycerol levels were significantly elevated in the media that was incubated with visceral adipose tissue from the OVX mice compared to the media that incubated visceral adipose tissue from the SHAM mice (Figure 6). However, application of PD98059 did not decrease glycerol levels in either group (Figure 6), even though the concentration of PD98059 was sufficient to reduce ERK1/2 phosphorylation (Figure 6).

Perilipin protein content:

Perilipin plays a critical role in lipolysis by regulating lipase function at the lipid droplet (243). Perilipin protein content was significantly decreased in the OVX and OVX+Ex groups compared to SHAM. Animals supplemented with 17β-estradiol had

significantly greater perilipin protein content compared to OVX and OVX+Ex animals. However, perilipin protein content was still significantly lower in the OVX+E$_2$ group than in the SHAM group (Figure 7).

Discussion:

The decline in ovarian hormone levels during menopause has been associated with changes in body fat and body composition (76, 210, 230, 237), and results in increased basal (i.e non-stimulated) lipolysis (83). The data presented here demonstrate that reduced ovarian function in OVX mice results in significant elevation of serum glycerol, NEFA, and visceral (i.e. parameterial) fat mass compared to SHAM mice. Thus, qualitatively the OVX mice present with similar metabolic changes as described previously in post-menopausal women (237). Further, it appears that increased glycerol and NEFA levels in the OVX animals compared to SHAM coincides with increased ATGL-CGI-58 interaction and reduced perilipin protein content in the visceral fat. These changes were attenuated with 17β-estradiol supplementation, but not with voluntary wheel running. Surprisingly, minimal differences in HSL phosphorylation were detected between groups. In spite of increases in ERK1/2 phosphorylation in the OVX animals, it does not appear that increases in ERK1/2 contribute to the increased glycerol release by the adipose tissue.

Similar to previous studies (90, 134), we found 17β-estradiol supplementation prevented the increases in visceral fat mass, glycerol and NEFA in OVX mice. D'Eon et al. found increased levels of serum FFA following fasting in OVX mice (68), which were successfully attenuated with 17β-estradiol supplementation. However, no SHAM group was presented in their data making it unclear how the FFA values compared to untreated mice. Further, our data agree with D'Eon et al. who found increased glycerol release in fat isolated from OVX mice compared to 17β-estradiol supplemented OVX mice. Also, in line with other studies, fat mass accumulation was attenuated in OVX mice

supplemented with 17β-estradiol (106, 192, 215, 245). Providing the OVX mice with voluntary running wheels resulted in significant attenuation of the increase in visceral fat mass, but the distances that the OVX mice ran were not significant enough to prevent the changes in serum NEFA or glycerol levels. It should be noted that normal female mice will run an average of 5-7km/day (data not shown), thus in agreement with other labs, the OVX mice ran significantly less distance (103). Supplementation with 17β-estradiol partially returns voluntary running activity, with mice running on average 4-6km/day (data not shown). It is unclear if these changes in adipose tissue function would be attenuated or abolished if the OVX mice were running a greater distance. Based on these data 17β-estradiol appears to have a more potent effect than voluntary activity on the cellular signaling mechanisms in the visceral fat of OVX mice.

At a cellular level, TAG hydrolysis is regulated by several lipases, most notably ATGL and HSL, which combined account for more than 95% of TG hydrolase activity in white adipose tissue (239). Total ATGL protein content was elevated in adipose tissue of OVX animals and attenuated in animals supplemented with 17β-estradiol, but not with voluntary exercise. The inability of voluntary exercise to affect total ATGL protein content agrees with Huisman et al. who found no change in adipose tissue ATGL protein content in mice following an endurance training protocol (128). Previous publications have suggested ATGL can be phosphorylated at several serine residues (308), however we found no differences between any groups in total serine phosphorylation of ATGL. Full activation of ATGL is dependent upon interaction with another protein, CGI-58 (167). We found that the OVX animals demonstrated a significant increase in ATGL-CGI-58 interaction, which was associated with increases in serum glycerol and NEFA

levels. As has been shown in cell culture studies, this interaction of ATGL and CGI-58 appears to be a critical link contributing to increases in basal lipolysis of TG (239). The increase in ATGL-CGI-58 interaction in the OVX mice was not attenuated by exercise, but was reduced by 17β-estradiol supplementation, corresponding with the changes in glycerol and NEFA levels.

Perilipin is the major protein associated with the lipid droplet in adipocytes and plays a critical role in the regulation of metabolic function of the adipose tissue by controlling lipase access to the TAGs in the lipid droplet of the adipocyte (243). Perilipin null mice have constitutively high lipolytic rates with little activation of HSL in the adipose tissue, confirming a protective role for perilipin in adipocytes (234). The phenotype of the perilipin null mice is remarkably similar to the OVX mice. Here, the OVX and OVX+Ex mice, which exhibit increased serum levels of glycerol and NEFA, also express significantly lower perilipin protein content in the adipose tissue, suggesting that loss of perilipin in the adipose tissue of these mice is associated with increased TAG breakdown. In addition, voluntary exercise did not prevent the decrease in perilipin protein content in the visceral adipose tissue, while 17β-estradiol supplementation did attenuate the decrease. Previous research indicates that voluntary exercise does not change perilipin protein content in the mesenteric fat pad (44), however 17β-estradiol supplementation does prevent the loss of perilipin (68).

Following the breakdown of TAG to DAG by ATGL, HSL continues the process of lipolysis, breaking DAG to MAG. We found little difference between our groups in HSL phosphorylation at the Ser565 or Ser559/660 residues, suggesting that HSL is not contributing to differences in circulating NEFA and glycerol levels in the OVX mice.

This result was also seen in the perilipin null mice, where very little activation of HSL was detected even though increased rates of glycerol release were detected from the adipose tissue (234). Further, we found differences in AMPK phosphorylation did not correspond with differences in HSL565 (Figure 4B), suggesting that a factor other than AMPK is altering the phosphorylation status of Ser565 in the visceral fat from our animals. Previous studies have shown that ERK1/2 also enhances HSL activity (108, 126) by phosphorylating HSL at Ser600, and subsequently enhancing lipolysis (253). ERK1/2 phosphorylation was significantly elevated in sedentary OVX animals, suggesting activation of ERK1/2 may increase TAG hydrolysis. As expected, PD98059 decreased phosphorylation of ERK1/2, however, glycerol levels in the solution remained equivalent to those of the non-treated media. Therefore, in the OVX mice, activation of ERK1/2 is not responsible for the increased glycerol levels.

Estrogen has been shown to have an effect on adipocyte size, with estrogen treatment resulting in decreased adipocyte diameter (68). It is possible that changes in adipocyte cell size in the visceral fat of the OVX mice may play contribute to the observed changes in protein content, however previous data have suggested that increased rates of lipolysis detected in post-menopausal women are not related to adipocyte cell size (206). Further studies will be conducted to determine if changes in fat cell size are occurring and contributing to the observed alterations in lipolytic protein content.

The data presented here demonstrate for the first time that changes in signaling proteins which regulate TAG hydrolysis occur with the loss of ovarian function. Specifically, there was increased interaction of ATGL-CGI-58 and reduced perilipin

protein content in the visceral fat of OVX mice. These findings provide cellular evidence as to why glycerol and NEFA levels are elevated in female mice following ovariectomy, and further suggest that low levels of physical activity may not effectively prevent these changes.   However, this should not be misconstrued that physical activity is not beneficial when ovarian hormone levels are decreased. It is well documented that endurance exercise training results in enhanced lipid oxidation by peripheral tissues and thus even though exercise failed to attenuate the increased lipolysis in these mice it is likely that various peripheral organs (i.e. skeletal muscle) gained an improved ability to oxidize the excess lipid.   The data presented here provide support that 17β-estradiol supplementation may be beneficial when ovarian hormone levels are low, such as in female mice following ovariectomy, and suggest that further studies on the role of estradiol are necessary and critical. Clearly, our understanding of the effects of estradiol supplementation when ovarian hormones decline is poor and more mechanistic studies must be conducted.

Acknowledgements:

Tables:

Table 3.1. *Anatomical characteristics for SHAM, OVX, OVX+Ex, and OVX+E$_2$ groups.*

	Body Weight (g)	**Fat Mass (g)**	**Fat Mass/Body Weight**	**Liver (g)**	**Heart (g)**	**TA (g)**	**Quad (g)**
SHAM	22.94 ± 0.57	0.27 ± 0.06	0.011 ± 0.002	0.904 ± 0.06	0.102 ± 0.002	0.039 ± 0.0005	0.148 ± 0.005
OVX Sed	25.20 ± 0.96*	0.83 ± 0.14*	0.03 ± 0.005*	0.940 ± 0.07	0.105 ± 0.007	0.037 ± 0.0009	0.149 ± 0.009
OVX Ex	23.85±0.53	0.46 ± 0.09*	0.02 ± 0.003	0.939 ± 0.06	0.106 ± 0.002	0.036 ± 0.001	0.142 ± 0.007
OVX+E$_2$	23.72±0.43	0.27 ± 0.07	0.01 ± 0.003	1.025 ± 0.05	0.104 ± 0.004	0.04 ± 0.003	0.150 ± 0.004

Values are presented as means ± SEM.
* Indicates significantly different from SHAM group ($p < 0.05$)

Table 3.2. *Fasted glycerol and NEFA levels from SHAM, OVX, OVX+Ex, and OVX+E$_2$ groups.*

	SHAM	OVX	OVX + Ex	OVX + E$_2$
Glycerol (mg/ml)	304.43 ± 23.61	467.33 ± 52.00 *	484.25 ± 102.78 #	373.45 ± 51.50
NEFA (mmol/L)	0.424 ± 0.0057	0.649 ± 0.0101*	0.555 ± 0.0133*	0.411 ± 0.0088
Glucose (mg/dl)	188.5 ± 14.48	221.42 ± 9.09 *	176.42 ± 19.40 $	177.1 ± 20.07 $

Values are presented as means ± SEM.
* Indicates significantly different from SHAM and OVX+E$_2$ groups (p<0.05).
$ Indicates significantly different from OVX group (p<0.05).
# Indicates compared to SHAM (p=0.06).

Figures:

Figure 3.1

Figure 3.1. Ovariectomy increased total ATGL protein content in the visceral fat pad, but 17β-estradiol supplementation prevented the increase. Example blots of ATGL are shown beneath the graph.
* Indicates significantly different from SHAM (p<0.05).

Figure 3.2
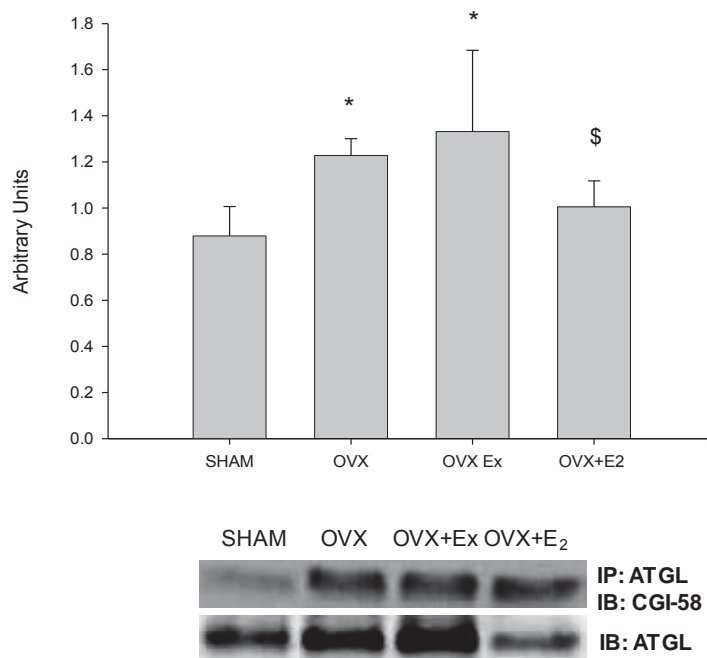
Figure 3.2. ATGL-CGI-58 interaction was elevated in OVX mice, but this increase was attenuated in OVX+E$_2$ mice. The blot was stripped and re-probed for ATGL. All CGI-58 data were normalized to ATGL protein content. Example blots of CGI-58 and ATGL are shown beneath the graph.
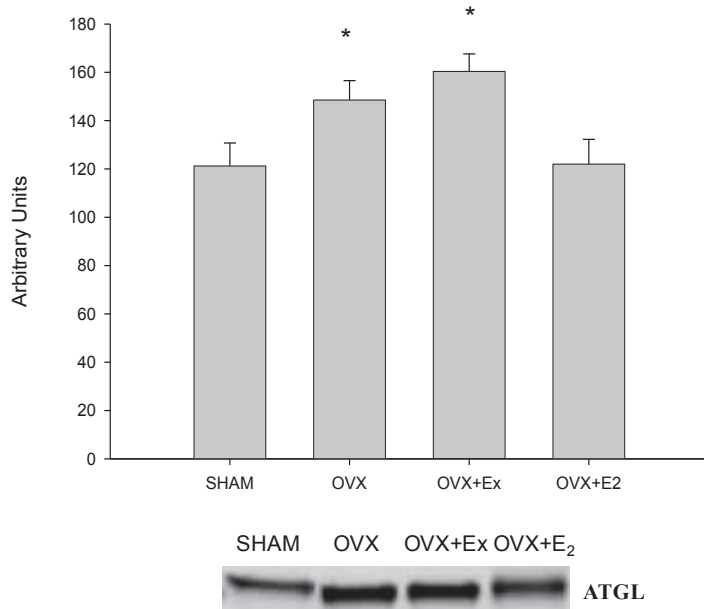* Indicates significantly different from SHAM ($p<0.05$). $ Indicates significantly different from OVX ($p<0.05$).

Figure 3.3
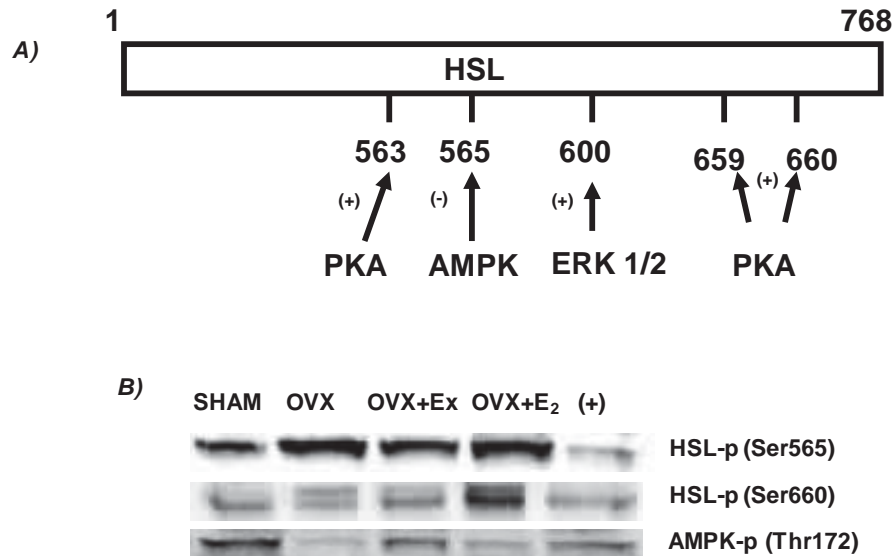
Figure 3.3 (A-B). Ovariectomy had little effect on HSL phosphorylation in visceral fat at the Ser565 or Ser600 residues**.**
A) Regulation of HSL.
(+) indicates activation via phosphorylation. (-) indicates inactivation via phosphorylation (adapted from (289))
B) No changes were detected in HSL565 or HSL660 phosphorylation in any sample**.**

Figure 3.4
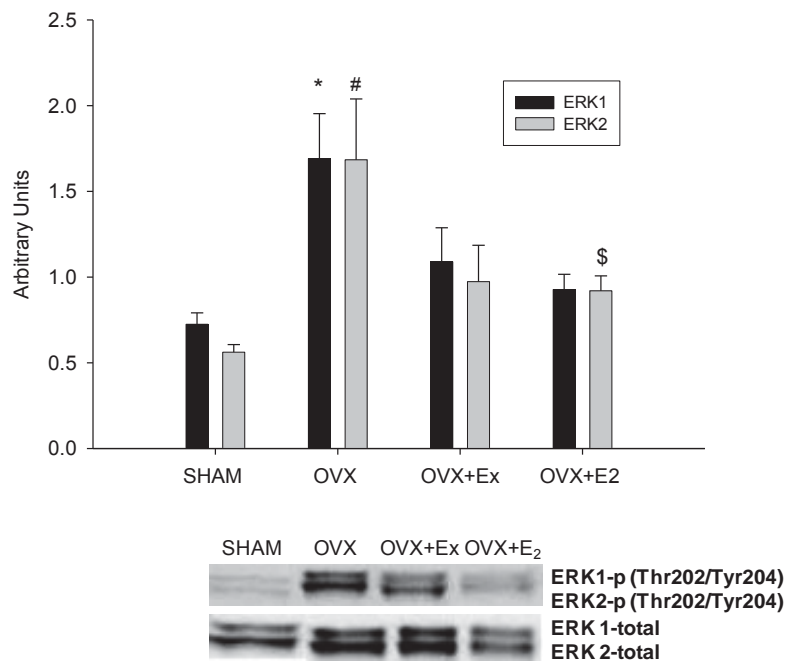
Figure 3.4. Normalized phosphorylation of ERK1/2 was elevated in OVX mice and attenuated by both voluntary wheel running and 17β-estradiol supplementation. Example blots of ERK1/2 are shown beneath the graph.
* Indicates significantly different from all other groups ($p < 0.05$). [#] Indicates significantly different from SHAM ($p < 0.05$). [$] Indicates significantly different from OVX ($p < 0.05$).

Figure 3.5
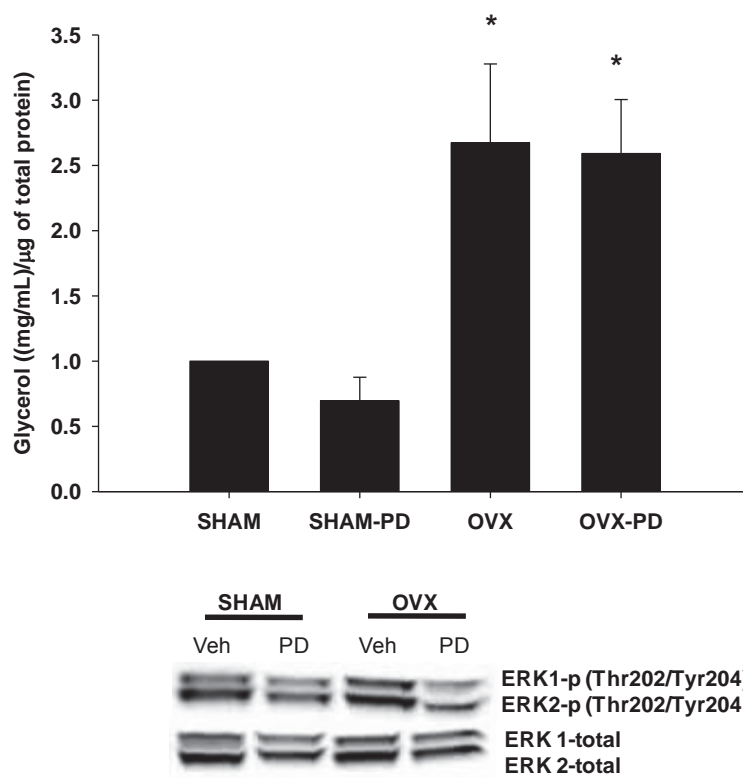
Figure 3.5. Pharmacological inhibition of ERK1/2 by MEK inhibitor PD98059 did not reduce levels of glycerol released from the visceral adipose tissue isolated from OVX mice. Example blots of ERK1/2 are shown beneath the graph.
* Indicates significantly different from SHAM and SHAM-PD (p<0.05).

Figure 3.6
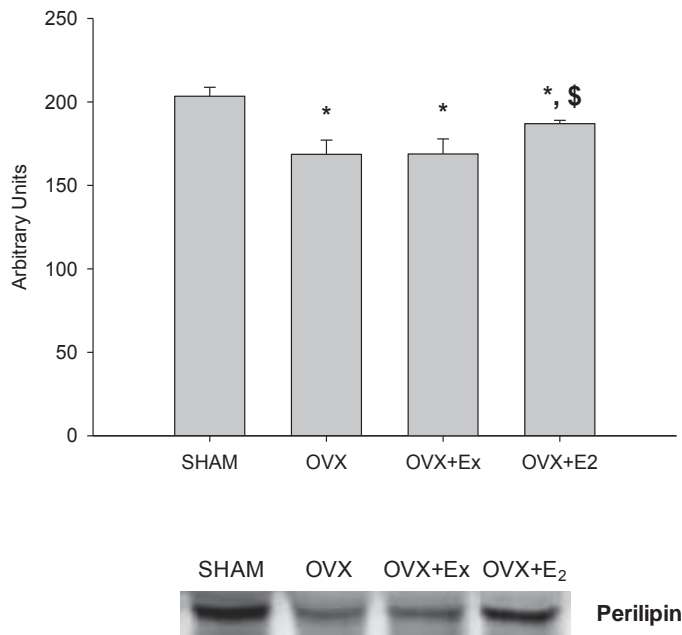
Figure 3.6. Perilipin protein content was decreased in OVX and OVX-Ex animals and partially restored in OVX+E$_2$ mice. Example blots of total perilipin are shown beneath the graph.

* Indicates significantly different from SHAM (p<0.05). $^{\$}$ Indicates significantly different from OVX (p<0.05).

Chapter 4: Lipolytic Signaling in Response to Acute Exercise is Altered in Female Mice Following Ovariectomy

The following article was published in the Journal of Cellular Biochemistry (112:3675-3684, 2011).

Lipolytic signaling in response to acute exercise is altered in female mice following ovariectomy.

Lindsay M. Wohlers, Kathryn C. Jackson, and Espen E. Spangenburg*

University of Maryland, School of Public Health, Department of Kinesiology, College Park, MD 21045

Running title: Lipolytic signaling in fat following ovariectomy
Key Words: Lipid; Adipose; Adipose Triglyceride Lipase; Lipolysis; PLIN; Female sex steroids

*Corresponding Author:
Espen E. Spangenburg, Ph.D.
University of Maryland
School of Public Health
Department of Kinesiology
College Park, MD 21045
1-301-405-2483 (office)
1-301-405-5578 (fax)
espen@umd.edu

Abbreviations List:

ABHD5 = Abhydrolase domain containing 5
ADRP/ADFP = Adipose differentiation related protein
ATGL = Adipose triglyceride lipase
CGI-58 = Comparative gene identification 58
Cont = Control
DAG = Diacylglycerol
Ex = Exercised
FFA = Free fatty acid
FA = Fatty acid
HSL = Hormone sensitive lipase
LD = Lipid droplet
MAG = Monoacylglycerol
MGL = Monoglyceride lipase
NEFA = Non-esterified fatty acid
O/M = Omental/mesenteric
OVX = Ovariectomy
PKA = Protein kinase A
PLIN = Perilipin
TAG = triglyceride

Abstract:

Impaired ovarian function alters lipid metabolism, ultimately resulting in increased visceral fat mass. Currently, we have a poor understanding of alterations in signaling events regulating lipolysis after ovarian function declines. The purpose of this study was to determine if cellular mechanisms regulating lipolysis are altered in mice after ovariectomy (OVX) and if OVX mice exhibit impaired lipolytic signaling when stimulated by acute exercise. SHAM and OVX mice were divided into two groups: control (SHAM cont; OVX cont) or acute treadmill exercise (SHAM ex; OVX ex). The omental/mesenteric (O/M) fat mass of all OVX mice was significantly greater than the SHAM mice. Serum glycerol and blood glucose levels were significantly elevated in OVX cont compared to SHAM cont. Treadmill exercise increased serum glycerol levels only in SHAM mice, with no exercise-induced change detected in OVX mice. NEFA levels were significantly elevated by acute exercise in the SHAM and OVX groups. In O/M fat from both OVX groups there were significant increases in cytosolic ATGL and PLIN2 in the fat cake fraction with concurrent reductions in PLIN1 in the fat cake compared to SHAM. Further, exercise induced significant increases in HSL Ser660 phosphorylation in SHAM mice, but not OVX mice. This suggests that reduced ovarian function has significant effects on critical lipolytic cell signaling mechanisms in O/M adipose tissue.

Introduction:

The prevalence of obesity-related conditions, such as the metabolic syndrome, has increased dramatically in recent years. Android, or centripetal (i.e. visceral) obesity, is of particular concern due to its high correlation with the development of obesity-related conditions. While expansion of subcutaneous adipose tissue depots may be metabolically favorable (147), studies have linked visceral fat accumulation to increased incidence rates of type 2 diabetes, cardiovascular disease, and risk of myocardial infarction in both men and women (304). In females, fat storage in subcutaneous adipose tissue depots is favored over visceral fat storage when ovarian function is normal (204). However, an increase in visceral fat mass is observed when female sex steroid function is disrupted, such as following menopause, hysterectomy, or breast cancer treatment (125, 237). For example, post-menopausal women have a 60% chance of developing metabolic syndrome, while in age-matched pre-menopausal women the risk is only 20-30% (213). However, little is known regarding the mechanisms by which ovarian hormones impact metabolic function of adipose tissue.

Adipose tissue mass is controlled by a balance between storage of triglyceride (TAG) and breakdown of TAG via lipolysis. When lipolysis is activated, such as during an acute bout of moderate intensity exercise or during starvation, free fatty acids (FFAs), the breakdown products of TAG, become key energy substrates for peripheral tissues. However, in certain circumstances it is possible to detect high levels of circulating FFAs at rest and it has been suggested that the FFAs may contribute to increases in ectopic fat storage. For example, we and others have shown that ovarian hormone status in females impacts basal lipolytic function, with a reduction in circulating female sex steroids

resulting in elevated levels of circulating glycerol (68, 297). Further, we have previously demonstrated an increase in unstimulated glycerol release from isolated adipose tissue of OVX mice compared to SHAM mice (297). In addition, other studies have also reported an increase in circulating glycerol in female mice following ovariectomy (68). One would expect that metabolic abnormalities in adipose tissue during diminished female sex steroid function could increase the risk for type 2 diabetes or cardiovascular disease (304). Indeed, adipocytes isolated from OVX animals exhibit impaired *in vitro* lipolytic responses to catecholamine stimulation, which are reversed with 17β-estradiol supplementation (68). Together, these findings support a role for female sex steroids in the metabolic regulation of adipose tissue.

Complete catabolic breakdown of TAG is enzymatically regulated. First, adipose triglyceride lipase (ATGL), also known as desnutrin and encoded by the gene PNPLA2, catalyzes the conversion of TAG to diacylglycerol (DAG), releasing one FA (282, 308). Next, hormone sensitive lipase (HSL) cleaves off a second FA, resulting in the breakdown of DAG to monoacylglycerol (MAG). The last step in lipolysis is performed by monoglycerol lipase (MGL), which separates the final FA from the glycerol backbone (86). The acute regulatory mechanism of ATGL is still relatively unknown, however interaction with a protein known as comparative gene identification-58 (CGI-58), which is encoded by the gene abhydrolase domain containing 5 (ABHD5), is critical for activation of ATGL (167). Unlike ATGL, the regulation of HSL has been well elucidated. Multiple phosphorylation sites on HSL exist which serve either to activate or inhibit HSL activity. Further, complete activation of HSL is dependent upon translocation from the cytosol to the lipid droplet (LD), which is the site of TAG storage.

Beta adrenergic stimulation results in protein kinase A (PKA)-induced phosphorylation of HSL at serine 563, 659, and 660 (in rodents) residues, all of which activate HSL, promote translocation of HSL, and enhance lipolysis by 2-3 fold (8). In isolated rat adipocytes, mutational analysis has determined that phosphorylation of Ser659 and Ser660 is necessary for lipolytic activation in response to isoproternol stimulation (8). In addition, the ability of HSL to interact with the LD is dependent upon PKA-phosphorylation of perilipin (PLIN1), which undergoes a conformational change leaving the LD exposed for access by HSL (194). PLIN1 is a member of the PLIN gene family and is found to exclusively localize to surfaces of intracellular lipid storage droplets. In this manner, PLIN1 serves two roles: first to protect the LD from unstimulated lipolytic breakdown, and secondly to enhance stimulated lipolysis (243). Further, PLIN1 interacts with the ATGL co-activator CGI-58, releasing CGI-58 to bind to ATGL when lipolytic activity is stimulated (264). In the PLIN1 null mouse, adipose tissue mass is severely reduced due to constitutively active lipolytic function, demonstrating the importance of PLIN1 in lipolytic regulation (234).

Thus, although numerous seminal investigations have shed valuable light defining how these lipases are critical in the regulation of both basal and stimulated lipolysis, we still have a poor understanding of how these mechanisms are activated in various conditions in which metabolic function of adipose tissue is disrupted. Using the ovariectomized (OVX) mouse model we previously found sedentary animals exhibit increased circulating levels of glycerol compared to SHAM mice, which suggests female sex steroids may affect protein regulators of lipolytic function (297). Unfortunately, the study left unanswered questions that are critically important to defining the regulation of

cellular lipolytic responses in the OVX animals. Specifically, we did not determine *in vivo* if stimulated glycerol release would be impaired in the OVX mice, nor could we account for the cellular location of these lipolytic proteins. Thus, the purpose of the present study was to determine if physiological activation (i.e. acute exercise bout) of lipolysis would be reduced in the OVX model due to low PLIN1 content. We hypothesized that PLIN1 content would be reduced in OVX compared to SHAM animals resulting in a lower corresponding release of glycerol in response to acute exercise in the OVX mice. Further, a second purpose was to determine if impairments in stimulated glycerol release in the OVX model were due to alterations in the cellular location of critical lipolytic proteins or due to changes in the composition of PLIN proteins found in the fat cake fraction. For this aim, we hypothesized that OVX mice would exhibit altered localization events of key lipolytic proteins and/or potential changes in PLIN protein content compared to the SHAM mice.

Methods:

ANIMALS Twenty-seven 8-week-old C57/BL6 (Harlan) female mice were divided into two groups, SHAM and surgical ovariectomy (OVX). The OVX mice (n=14) underwent a bi-lateral ovariectomy, a frequently used method to disrupt the female sex steroid signaling axis (142). Our lab has previously shown that this model decreases the levels of circulating estrogens by 70% within 48h (248) and we also find substantial reductions in uterine weight (~80%; unpublished data) in this model. Further, previous research has shown that surgical removal of the ovaries from mice does not result in changes in feeding patterns (31, 228, 295). The SHAM group (n=13) was subjected to a SHAM surgery where they were anesthetized, but did not undergo ovariectomy. Mice were given ad libitum access to water and standard rodent chow (Purina Laboratory Rodent Diet 5001: 23% protein, 4.5% fat, 6% fiber) and were housed in a temperature-controlled room on a 12 h light/dark cycle. Mice were kept in standard cages for 8 weeks, at which point an acute bout of exercise was performed by half of the mice in each group (n=14). Mice did not undergo exercise training; however, an acclimation period was included prior to acute exercise testing in order to familiarize the animals with the treadmill. Both groups underwent treadmill acclimation in order to keep the environmental stimuli as equal as possible across groups in the period prior to testing and sacrifice. To acclimate the mice to the treadmill, mice were exposed to treadmill running for 6 days, beginning with 10 mins at 10m/min and 5% incline, and gradually increasing the running duration and speed each day until by day 6 they were running for 35 minutes (5 mins at 25m/min followed by 20 mins at 28m/min, then 5 mins at 20m/min). For the acute about of exercise, mice ran on the treadmill at 26 m/min with a 5º incline until refusal to run,

which was determined by continuous sitting (>1 min) on the shock pad. There was no difference in total run time between the SHAM and OVX animals. Other studies of exercise-induced lipolysis have employed treadmill running protocols which closely resemble the protocol employed in this investigation (238). Therefore, our treadmill running protocol was selected based on the ability to induce lipolysis in adipose tissue and ensuring that both groups were able to complete the bout of exercise. Immediately following the acute exercise bout, animals were sacrificed, tissues were collected and snap frozen in liquid nitrogen, and then stored at -80° C. The control animals (n=13) were exposed to the initial acclimation period to ensure the same exposure to the treadmill. On the day of the acute treadmill test the control groups were not subjected to treadmill running but were still placed in the treadmill in a stationary fashion with an active shock pad for a duration equivalent to the exercise groups. All aspects of this study were approved by the University of Maryland Institutional Animal Care & Use Committee (IACUC) Review Board.

ISOLATION OF PROTEIN FROM ADIPOSE TISSUE The omental/mesenteric fat was homogenized on ice using a protocol to separate the cytosolic and fat cake (i.e. proteins associated with the LDs) fractions using previously described methods with some slight modifications (48, 79). It should be noted that this procedure was used to first demonstrate translocation of HSL from the cytosolic region to the LD (79). Fat was homogenized in Mueller buffer (50 mM HEPES (pH 7.4), 4 mM EGTA, 10 mM EDTA, 15 mM $Na_4P_2O_7H_2O$, 100 mM β-glycerophosphate, 25 mM NaF, 5 mM Na_3VO_4, and 1 protease inhibitor tablet/10 ml (Roche, Indianapolis, IN)), then centrifuged for 15 minutes at 4°C and 13,000g. The supernatant (cytosolic fraction) between the fat cake and the

pellet was removed using a syringe and placed into a separate tube. A second buffer (50 mM HEPES (pH 7.4), 4 mM EGTA, 10 mM EDTA, 15 mM $Na_4P_2O_7H_2O$, 100 mM β-glycerophosphate, 25 mM NaF, 5 mM Na_3VO_4, 0.05g SDS, 0.01% Triton X, and 1 protease inhibitor tablet/10 ml) was added to the pellet, which was heavily vortexed and then centrifuged for 15 minutes at 4°C and 13,000g. The middle layer (fat cake fraction) was again drawn off and placed in a fresh tube. Previous investigations have eloquently shown that this fractionation technique can be used to determine the cellular location of critical regulators of lipolytic function (48, 79). Specifically, the fat cake fraction contains proteins which are localized to the surface of lipid storage droplets, while the cytosolic fraction contains the proteins located in the cytosol (107). Protein concentrations were determined on the cytosolic and fat cake fractions using the BCA protein assay. To confirm proper isolation of the fractions, western blotting for ERK1/2 (cytosolic specific (307)) and PLIN1 (LD specific (107)) was performed. We found ERK1/2 protein content was contained in the cytosolic fraction and PLIN1 protein content was strictly observed in the fat cake fraction (see Figure 1).

WESTERN BLOTTING OF ADIPOSE TISSUE Equal amounts of total protein (50 μg) were resolved on 6% SDS–PAGE gels and transferred to PVDF membranes as previously described (254, 297, 298). Blots were visualized with Ponceau S (Sigma Chemical) to confirm equal loading of the lanes (data not shown) and then blocked with 3% nonfat dry milk in Tris-buffered saline with 0.1% Tween (TBS-T). In addition, in a secondary fashion, gels were run and stained with Coomassie blue to demonstrate equal loading of the samples (see Figure 2). Membranes were probed with antibodies for ATGL (Cell Signaling; 1:1,000), PLIN1 (perilipin) (Cell Signaling; 1:500), CGI-58 (kind gift from

Dr. Dawn Brasaemle, Rutgers University; 1:25,000), or PLIN2 (ADRP) (Novus Biologicals; 1:1000) in a buffer of 1-5% BSA in TBS-T on a rocker at 4°C overnight. Following incubation with the primary antibody, membranes were washed in TBS-T (3 x 5 min) and then incubated for 1 hr with horseradish peroxidase (HRP)-conjugated rabbit secondary antibody (1:1,000) in 3% nonfat dry milk in TBS-T. Next, membranes were washed in TBS-T (1 x 10 min, 3 x 5 min), followed by enhanced chemiluminescence reagent (ECL) (Pierce, Rockford, IL). Membranes were visualized with a chemiluminescence imager (Syngene, Frederick, MD) and quantified with Image J software (NIH, Bethesda, MD).

BLOOD AND SERUM MEASURES Non-esterified fatty acids (NEFA's) were measured in serum using a colorimetric assay (Wako Diagnostics, Richmond, VA). Glycerol levels were determined in serum using a free glycerol determination kit (Sigma–Aldrich, St. Louis, MO). Glucose levels in blood were measured using a glucometer (LifeScan, Milpitas, CA). Insulin levels were measured in serum using an ELISA kit (Millipore, Billerica, MA).

STATISTICAL ANALYSIS All data are expressed as means ± SEM. Statistical significance was determined using t-tests with Sigma Stat statistical analysis software (Systat Software, Inc., San Jose, CA). T-tests were chosen for statistical analysis due to the *a priori* derived specific and directional hypotheses. Specifically, the purpose of these experiments was to determine if known lipolytic mechanisms in adipose tissue failed to respond to a bout of exercise in the OVX mice. A P-value of ≤ 0.05 was considered significant.

Results:

ANATOMICAL CHARACTERISTICS No significant differences in body weights were detected between the SHAM and OVX groups. Previously, we have found a small significant difference of ~9% and here we saw a non-significant difference of ~4% (297). However, O/M fat mass was significantly greater in both the control OVX (referred to as cont in tables/figures) and acute exercised OVX (referred to as ex in tables/figures) groups compared to the control SHAM and acute exercised SHAM groups. When fat mass was normalized to body weight there were significant elevations in both groups of OVX mice compared to the SHAM mice. No significant differences in other tissue weights (i.e. heart, liver, skeletal muscle) were detected (data not shown). No significant difference in total run time was observed between the exercised OVX and SHAM groups (Table 1A).

BLOOD/SERUM ANALYSES In line with our previously published data (297), serum glycerol levels were significantly elevated in control OVX mice compared to control SHAM mice (Table 1B). Here, an acute bout of exercise was performed to physiologically stimulate lipolysis in the SHAM and OVX mice, with increases in serum glycerol and NEFA acting as surrogate indicators of lipolytic activation. Glycerol levels were significantly elevated in control OVX mice compared to control SHAM mice. When compared to the control group, there was a non-significant 14% (28% when normalized to O/M fat mass) increase in glycerol levels in response to exercise in the OVX animals and a significant 34% (41% when normalized to O/M fat mass) increase in the SHAM animals. No significant difference in serum NEFA levels was detected between control SHAM and OVX mice (Table 1B). In contrast, the acute exercise bout

resulted in significant elevations in serum NEFA levels in both SHAM and OVX groups when compared to their control counterparts, with no differences detected across groups in response to exercise. When compared to the control group, there was a 95% (119% when normalized to O/M fat mass) increase in NEFA levels in response to exercise in the OVX animals and a 34% (41% when normalized to O/M fat mass) increase in the SHAM animals. The finding of an exercise-induced increase in NEFA levels without an increase in glycerol levels in the OVX mice was surprising; however, this may be the result of a reduction in futile cycling. Blood glucose levels were significantly elevated in the control OVX mice compared to the control SHAM mice (Table 1B). The acute bout of exercise resulted in significant reductions in blood glucose in both the SHAM and OVX mice, with no difference observed between the two groups. No differences in insulin levels were detected between any groups (Table 1B).

PROTEIN CONTENT IN O/M ADIPOSE TISSUE

ATGL In a previous study, we detected elevations in ATGL protein content in total cell lysates isolated from the visceral adipose tissue of OVX animals. The elevation in ATGL coincided with elevated levels of circulating glycerol (297). Further, recent data have suggested that ATGL is a critical mediator of exercise-induced lipolysis (128). Thus we sought to expand our previous findings to determine if ATGL distribution between the cytosolic and fat cake fraction was altered in the OVX mice and to investigate whether an acute bout of exercise would alter the location of ATGL in SHAM or OVX mice. In agreement with our previous data, ATGL protein content was significantly elevated in the cytosolic fraction in both groups of OVX mice compared to control SHAM mice. The

92

exercised SHAM mice had significantly greater cytosolic ATGL protein content than the control SHAM mice, however, no effect of acute exercise on ATGL protein content was observed in OVX mice (Figure 2A). In addition, to determine if localization of ATGL was altered between groups we calculated the percent of total ATGL that was present in each fraction. However, we did not find any significant differences between groups (Figure 2B).

CGI-58 CGI-58 is a known regulator of ATGL through direct protein interaction, enhancing activation of ATGL (167). Therefore, we measured CGI-58 protein content to determine whether the capacity for ATGL activation is altered by acute exercise or by ovariectomy. As expected, CGI-58 protein content was primarily found in the fat cake fraction compared to the cytosolic fraction in all groups, with no between group differences detected. Thus, loss of ovarian function or performance of an acute exercise bout did not alter CGI-58 protein content in O/M adipose tissue (Figure 3 A). In addition, to determine if localization of CGI-58 was altered between groups we calculated the percent of total CGI-58 that was present in each fraction. However, we did not find any significant differences between groups (Figure 3B).

HSL Ser660 In the mouse, induction of HSL-mediated lipolysis is dependent upon phosphorylation of Ser660, thus to determine if HSL was associated with the increased levels of circulating glycerol we used a phosphorylation site specific antibody for HSL. In O/M adipose tissue, we found elevated levels of HSL Ser660 phosphorylation in the cytosolic fraction of exercised SHAM mice compared to control SHAM mice (Figure 4A). In the SHAM mice, the increase in HSL660 phosphorylation in the fat cake fraction of exercised mice did not reach statistical significance (p=0.08). However, we found no

changes in HSL Ser660 phosphorylation in the control OVX mice nor did we observe a response to acute exercise (Figure 4A).

PLIN1 PLIN1 is exclusively localized to the lipid storage droplet and plays an important role in the regulation of basal and stimulated lipolysis (105). We have previously shown PLIN1 protein content in a total cell lysate to be reduced in O/M adipose tissue of mice following ovariectomy (297). In the present study, we sought to determine if PLIN1 protein content/localization in the fat cake fraction is altered in the OVX mice or by an acute exercise bout. Since PLIN1 was not detected in the cytosolic fraction (Figure 1) only the fat cake fraction is shown. Confirming our previous findings, PLIN1 protein content in the fat cake fraction was significantly reduced in both OVX groups compared to the SHAM mice. The acute exercise bout did not result in alterations in PLIN1 protein content in SHAM or OVX mice (Figure 5).

PLIN2 (also known as adipose differentiation-related protein (ADRP/ADFP) Genetic ablation of PLIN1 results in a significant upregulation of PLIN2 protein content on the LD (269). However, the upregulation of PLIN2 does not confer the LD the same protection from lipolytic degradation, nor does PLIN2 act as an effective means for enhancing stimulated lipolysis (269). In our model, we observed both an elevation in resting circulating glycerol and a decrease in PLIN1 protein content in OVX mice, therefore we hypothesized that PLIN2 may be replacing PLIN1 on the LD. In both OVX groups, there was a significant increase in PLIN2 protein content in the fat cake fraction compared to the SHAM groups. No effect of acute exercise on PLIN2 protein content was observed in SHAM or OVX groups (Figure 6).

Discussion:

Here we demonstrate that in the OVX mice there are significant alterations in critical cellular regulators of lipolytic function in O/M adipose tissue when compared to SHAM mice. As with our own and others previous findings (68, 297), we observed an increased in O/M fat mass in the OVX mice. The elevated fat mass in the OVX mice was coupled with increased circulating glycerol and glucose levels under control conditions, with no differences in insulin levels observed. An acute bout of exercise resulted in significantly higher glycerol levels in exercised SHAM mice compared to control SHAM mice, however, no significant effect of exercise on glycerol levels was observed in OVX mice. This suggests that the OVX mice cannot further enhance the release of glycerol from the adipose tissue during this exercise bout. In both SHAM and OVX mice, an acute bout of exercise resulted in quantitatively similar reductions in blood glucose levels compared to control counterparts, indicating an equivalent response from the two different groups of mice. Cytosolic ATGL protein content was elevated in control and exercised OVX mice compared to control SHAM mice. However, there was no increase in ATGL protein content in the fat cake fraction in response to exercise in either group. There was significantly more of the phosphorylated form of HSL (Ser660) in the cytosolic fraction of exercised SHAM mice compared to control SHAM mice. However, no increase in HSL Ser660 phosphorylation was observed in OVX mice in response to acute exercise. Lastly, PLIN1 protein content in the fat cake fraction was reduced, while PLIN2 protein content in the fat cake fraction was elevated, in OVX mice compared to SHAM mice. These data demonstrate that signaling mechanisms that regulate basal and

stimulated lipolytic function are impaired in OVX mice compared to SHAM mice, suggesting a critical role for female sex steroids in the regulation of lipolytic function.

We, and multiple other investigators, have previously reported increases in visceral fat mass coupled with elevations in basal circulating glycerol, and glucose levels in OVX mice (68, 297). These metabolic changes qualitatively resemble changes reported in post-menopausal women who are not taking hormone replacement therapy (210). The elevation in circulating glycerol levels in the control OVX mice suggests that lipolysis is elevated even under resting conditions. A similar finding has been confirmed in adipocytes from humans (206). In addition, multiple other studies have reported estrogens to reduce adipose tissue lipolytic function in females (272, 281). In particular, a reduction in ovarian hormones results in increased basal lipolytic rate in adipocytes isolated from human omental adipose tissue (272). The acute bout of exercise resulted in a smaller, non-significant increase in glycerol levels in the OVX mice compared to the SHAM mice. Further, NEFA levels were elevated in both the OVX and SHAM mice in response to acute exercise, with a greater percent increase compared to the control group in the OVX mice. Due to the observed alterations in serum glycerol and NEFA levels, we explored potential alterations in localization of key lipolytic proteins in the SHAM and OVX mice.

In adipose tissue, 95% of all lipolytic activity is controlled by the lipases HSL and ATGL (239). When ATGL is genetically ablated in the mouse model, total TAG hydrolase activity in white adipose tissue is reduced by 82% (111), while in contrast overexpression of ATGL in adipocytes results in increased basal and beta-adrenergic stimulated lipolysis (308). In our study we found increased ATGL protein content in the

cytosolic fraction of O/M adipose tissue from OVX mice, which may explain the elevated basal glycerol levels in the OVX mice. While the increase in glycerol release without an increase in HSL phosphorylation may seem counterintuitive, multiple studies have demonstrated that glycerol release can occur when ATGL is overexpressed (308), or when HSL expression is absent. Specifically, Rydén et al. found inhibition of HSL attenuates, but does not prevent, increases in glycerol release from stimulated adipocytes (232). In addition, unstimulated glycerol release is also elevated under conditions of PLIN1 ablation (305), suggesting that the combination of increased ATGL and decreased PLIN1 is a potential contributor to the increased serum glycerol values in the control OVX animals. During the acute exercise bout, we did not find a large increase in serum glycerol values in the OVX animals compared to the SHAM animals. This could potentially be explained by the low levels of HSL phosphorylation in the OVX mice coupled with the low PLIN1 content since both HSL and PLIN1 work synergistically to increase lipolytic rate. Alternatively, the reduced glycerol response in the OVX animals during the exercise bout may have been a result of increased glycerol kinase activity, which would prevent the release of glycerol into circulation. Glycerol kinase was originally thought to be absent from adipose tissue, however multiple studies have demonstrated an increase in glycerol kinase to occur in the obese state in animal models as well as in humans (42, 260, 270). Albeit, at this time there is no evidence to indicate if glycerol kinase is elevated in the OVX model and this needs to be tested. Finally, ATGL also has acylglycerol transacylase activity (133), and can play a role in the formation of TAG and DAG, thus contributing to futile cycling between TAG storage and breakdown. It is possible that we are detecting indices of futile cycling in the OVX mice. Potentially,

97

this may have been observed when NEFA levels increased in the OVX mice in response to acute exercise without a substantial increase in serum glycerol levels. This suggests that higher serum NEFA values may not be derived from an increase in lipolytic rate. Thus, perhaps the exercise bout in the OVX mice reduced the acylglycerol transacylase activity of ATGL thereby releasing fatty acids that may have undergone re-esterification under the control conditions. While we do not have a measure to directly indicate futile cycling, our findings may suggest that under conditions where adipose tissue lipolysis is stimulated (i.e. exercise), there is a decrease in re-esterification in OVX mice and thus a reduction in futile cycling. The dual role of ATGL in lipolysis and TAG formation may explain how the OVX animals demonstrated increases in fat mass in spite of what appears to be an elevation in basal lipolytic rate. We are currently conducting further detailed studies in order to elucidate the effects of reduced female sex steroids and acute exercise on ATGL function as well as the potential role of futile cycling in the regulation of adipose tissue function by female sex steroids.

The increase in ATGL in the OVX mice is in line with observations in humans (258). At the mRNA level, Watt et al. reported an increase in ATGL in visceral fat from obese post-menopausal females and obese males. Further, Watt et al. did not detect a change in mRNA or protein content of CGI-58, an activator of ATGL, which is in agreement with our findings (258). We did not detect significant changes in ATGL protein content in the fat cake fraction in either SHAM or OVX mice in response to the acute bout of exercise. However, this is in agreement with other observations which have also shown that ATGL localization to the LD is unaffected by isoproternol stimulation, with the greatest proportion of ATGL protein residing in the cytoplasm (308). Thus, at

this time it is clear that our understanding of ATGL function needs to be further clarified in future studies.

HSL phosphorylation at the Ser660 site, the primary regulatory site for activation (8), results in HSL translocation from the cytosol to the LD where it may contribute to lipolytic breakdown of stored TAG (289).   We found elevated levels of the phosphorylated form of HSL (Ser660) in the cytosolic fraction (p=0.08 in the fat cake fraction) from SHAM mice in response to the acute exercise bout.   In contrast, no significant change in HSL Ser660 phosphorylation was detected in OVX mice in response to acute exercise.   No difference in HSL phosphorylation (Ser660) was observed between SHAM and OVX mice under basal conditions, suggesting that HSL is not responsible for the elevated serum glycerol levels in the OVX mice.   However, the failure to increase HSL Ser660 phosphorylation may partially explain the inability of the OVX mice to significantly increase glycerol release in response to an acute bout of exercise.   In adipocytes isolated from OVX mice and OVX mice supplemented with 17β-estradiol, D'Eon et al. showed no difference in total HSL between groups and suggested that changes in HSL content were not responsible for the increased catecholamine stimulated lipolysis in the mice supplemented with 17β-estradiol (68).   However, they did not measure HSL phosphorylation status or localization of HSL, which is critical to examining HSL activity.   Our observation in OVX mice of an inability to increase HSL Ser660 phosphorylation in response to an acute bout of exercise suggests that dysfunction of upstream regulators of HSL play a role in altered lipolytic activation in adipose tissue when female sex steroids are reduced.

Lipolytic regulation is multi-faceted with important regulatory steps defined by proteins that coat the LD's within adipocytes. PLIN1 is the primary LD associated protein involved in the regulation of adipocyte lipolysis (243). In the fat cake fraction isolated from the OVX mice, we found significant reductions in PLIN1 protein content and elevated PLIN2 protein content in O/M adipose tissue compared to the SHAM mice. These changes in PLIN1 and PLIN2 protein content in the OVX mice would have substantial effects on the regulation of lipolytic function. For example, the reduction in PLIN1 protein content may explain the lack of HSL response in OVX mice following the acute exercise bout. In adipocytes, the presence of PLIN1 on the LD has been shown to be critical for HSL translocation to the LD in order to promote catecholamine stimulated lipolytic activity (194). Thus, in the OVX mice where PLIN1 content is significantly reduced, activation and translocation of HSL may be impaired as a result. Other studies have demonstrated an effect of female sex steroids on lipolytic function. For example, reduced adipocyte PLIN1 content in OVX mice corresponds to impaired *ex vivo* catecholamine activated lipolysis, suggesting reduced lipolytic function in adipose tissue following OVX (68). Our data extend the findings of D'Eon et al by demonstrating that reduced female sex steroid levels also impair lipolysis when activated *in vivo* by a physiological stimuli (i.e. exercise). Although under most circumstances very little, if any, PLIN2 is found in mature adipocytes, there are suggestions that during states of increased FFA flux there is elevated content of PLIN2 associated with the LD's (26). Further, alternative explanation for PLIN2 appearing in the fat cake may be that PLIN2 can displace PLIN1 under conditions of extended lipolytic activation resulting in PLIN2 associating with LD's formed during re-esterification of the FAs (109). Further, an

increase in PLIN2 expression is observed in the PLIN1 knockout mouse, suggesting that PLIN2 may be upregulated in circumstances where PLIN1 is reduced (269). Even though PLIN2 is not typically found in mature adipocytes, due to the unique metabolic phenotype of the OVX mouse there appears to be a plausible explanation for the increased PLIN2 protein content.

LIMITATIONS One limitation to our findings is that adipocyte lipolysis was not directly measured. However, circulating glycerol levels are often used as an indicator of lipolysis (111, 128, 129, 137, 181, 238), and coupled with the findings of D'Eon et al (68) and our own (297) which demonstrate increased basal glycerol release from adipose tissue isolated from OVX animals, it does appear that unstimulated lipolysis appears to be elevated in the OVX animal. Another limitation to our study comes from the fractionation technique used to separate cytosolic and lipid droplet (fat cake) proteins. We chose to use this technique in hopes of capturing the localization of ATGL and HSL in our animals. Although isolation of the adipocytes from each group would have been ideal, staining of primary adipocytes is extremely difficult due to the large size of the LD, resulting in very little visible cytoplasmic volume (188). In addition, we were concerned that the adipocyte isolation process might result in movement of the proteins independent of the effects induced by exercise. Finally, we measured our targets in protein isolated from whole adipose tissue rather than from isolated adipocytes. Since CGI-58 and PLIN2 have been detected in the stromal vascular fraction of adipose tissue, we cannot be completely certain that some of the protein signal was not coming from cells other than the adipocytes themselves.

As summarized in Figure 7, the data presented here provide novel evidence that a reduction in female sex steroids results in impairment of stimulated lipolytic signaling and alterations in PLIN protein content in O/M adipose tissue. Using a physiological stimulus (acute exercise) to activate lipolysis, we determined that exercise fails to further elevate circulating levels of glycerol, which appears to be a result of dysfunctional lipolytic signaling. These data suggest that significant reductions in female sex steroid levels not only alter lipid partitioning, but also compromise key lipolytic functions in the adipose tissue. Thus, it is imperative that we begin to critically examine the role of sex steroids in the regulation of adipose tissue dynamics to allow for the development of a treatment to prevent metabolic disorders in females experiencing reduced ovarian function.

Acknowledgements:

Tables:

Table 4.1 (A/B). OVX mice exhibit significant differences in anatomic and metabolic parameters when compared to the SHAM mice. (N=6-7/group)

A	Body Weight (BW)	O/M Fat Mass (FM)	FM/BW	Run Time (min)
SHAM cont	22.92±0.50	0.278±0.017	0.012±0.0008	
SHAM ex	22.47±0.69	0.264±0.024	0.012±0.0008	36.5±4.3
OVX cont	23.42±0.52	0.710±0.061*	0.030±0.002*	
OVX ex	23.60±0.50	0.632±0.084*	0.026±0.003*	38.8±9.99

* Indicates significantly different from SHAM cont

B	Glycerol (mg/ml)	NEFA (mmol/L)	Glucose (mg/dl)	Insulin (ng/ml)
SHAM cont	309.22±14.02	0.664 ±0.066	137.17±3.36	0.627±0.230
SHAM ex	424.34±43.80 *	0.887±0.068*	111.29±7.92*	0.634±0.244
OVX cont	390.69±37.33 *	0.513±0.085	152.57±7.30*	0.460±0.219
OVX ex	417.88±21.07 *	$1.003\pm0.101^{\$}$	$100.71\pm7.84^{\$}$	0.390±0.089

* Indicates significantly different from SHAM cont
$ Indicates significantly different from OVX cont (P<0.05).

Figures:

Figure 4.1
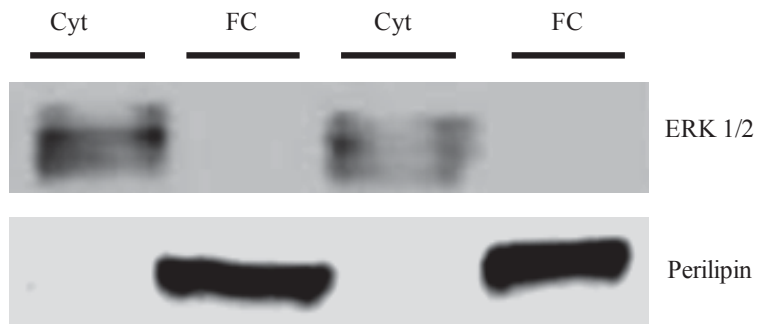
Figure 4.1. Determination of appropriate isolation of cytosolic and fat cake fractions from O/M adipose tissue. The expression of total ERK1/2, a cytosolic protein, appears only in the cytosolic fraction (Cyt), while PLIN1, which is known to be localized to the LD, appears only in the fat cake (FC) fraction.

Figure 4.2

A)

B)
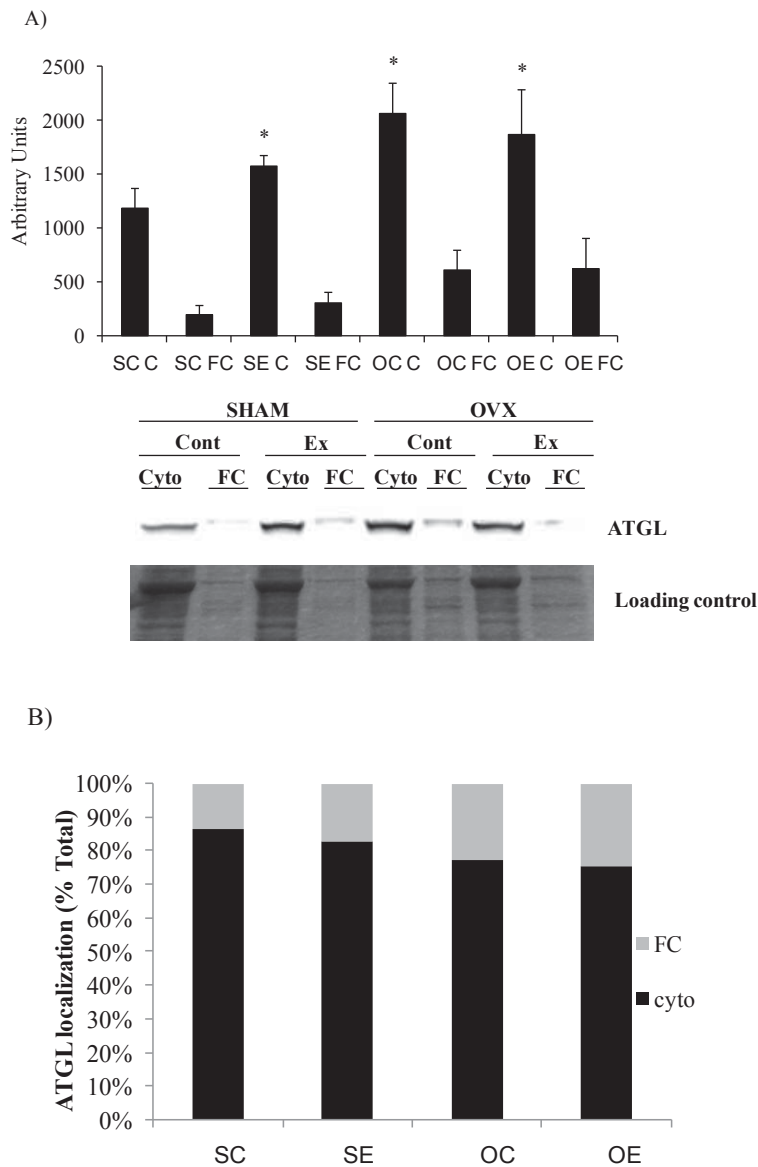
Figure 4.2 (A-B). ATGL protein content is upregulated in the cytosolic fraction from O/M adipose tissue, but not the fat cake fraction, in OVX animals compared to SHAM animals.

(A) ATGL protein content in different fractions isolated from O/M adipose tissue from control and acute exercised SHAM and OVX mice. Abbreviations for x-axis are as followed and consistently displayed on all of the remaining figures: SC C= sham control cytosolic fraction, SC FC = sham control fat cake fraction, SE C = sham exercised cytosolic fraction, SE FC = sham exercised fat cake fraction, OC C = OVX control cytosolic fraction, OC FC = OVX control fat cake fraction, OE C = OVX exercised

cytosolic fraction, OE FC = OVX exercised fat cake fraction. A representative ATGL blot is shown below the graph. In addition, in this figure a coomassie stained gel is depicted to demonstrate equal loading of the samples from each group. N=5/group
*Indicates significantly different from SC C (P<0.05).
(B) ATGL percent localization to the cytosolic and fat cake fractions. Within each bar, the grey area indicates ATGL localization to the fat cake fraction and the black area indicates localization to the cytosolic fraction. Abbreviations for x-axis are as followed and consistently displayed on all of the remaining figures: SC = SHAM control, SE = SHAM exercised, OC = OVX control, OE = OVX exercised.

Figure 4.3

A)

B)
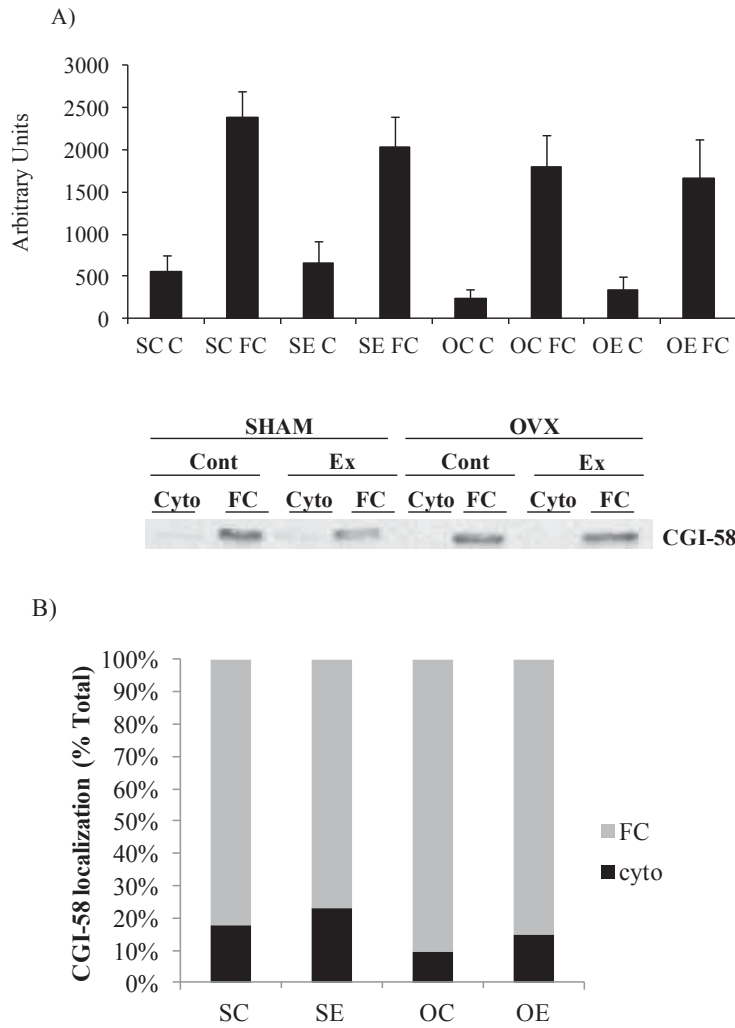
Figure 4.3 (A-B). CGI-58 protein is mostly contained in the FC fraction and does not differ between SHAM and OVX animals.

(A) CGI-58 protein content in O/M adipose tissue from control and acute exercised SHAM and OVX groups. A representative CGI-58 blot is shown below the graph. N=5/group

(B) CGI-58 percent localization to the cytosolic and fat cake fractions. Within each bar, the grey area indicates CGI-58 localization to the fat cake fraction and the black area indicates localization to the cytosolic fraction.

Figure 4.4
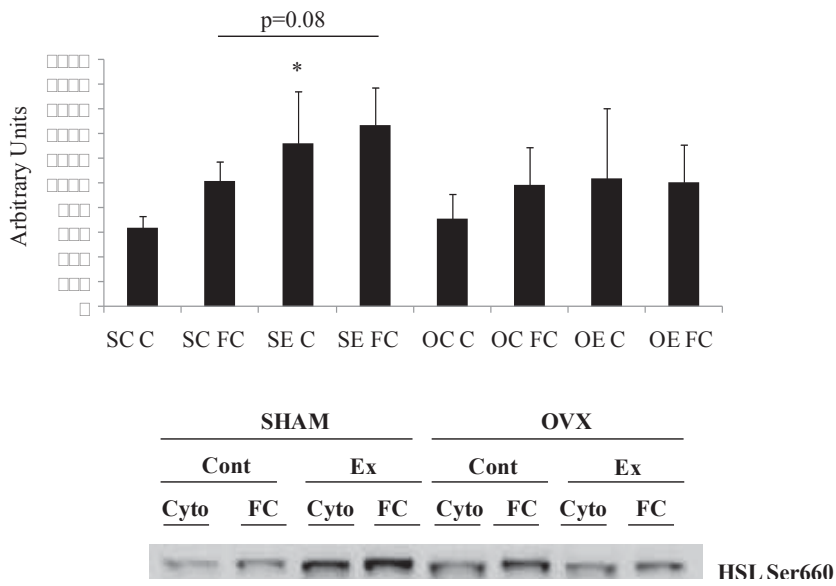
Figure 4.4. Phosphorylation of HSL (Ser660) in the cytosolic fractions from O/M adipose tissue is upregulated in response to acute exercise only in the SHAM animals and not the OVX animals. A representative HSL Ser 660 blot is shown below the graph. N=4/group

*Indicates significantly different from SC C (P<0.05).

Figure 4.5
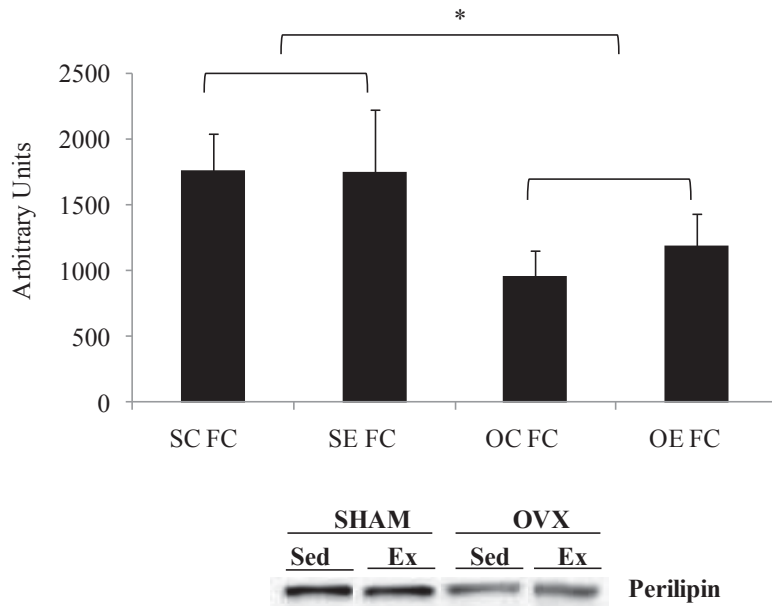
Figure 4.5. PLIN1 protein content in O/M adipose tissue is significantly reduced in OVX animals compared to SHAM animals. Since PLIN1 is localized to the LD and was not detected in the cytosolic fraction, only the fat cake fraction is shown. A representative PLIN1 blot is shown below the graph. N=5/group
*Indicates significantly different from SC FC and SE FC (P<0.05).

Figure 4.6
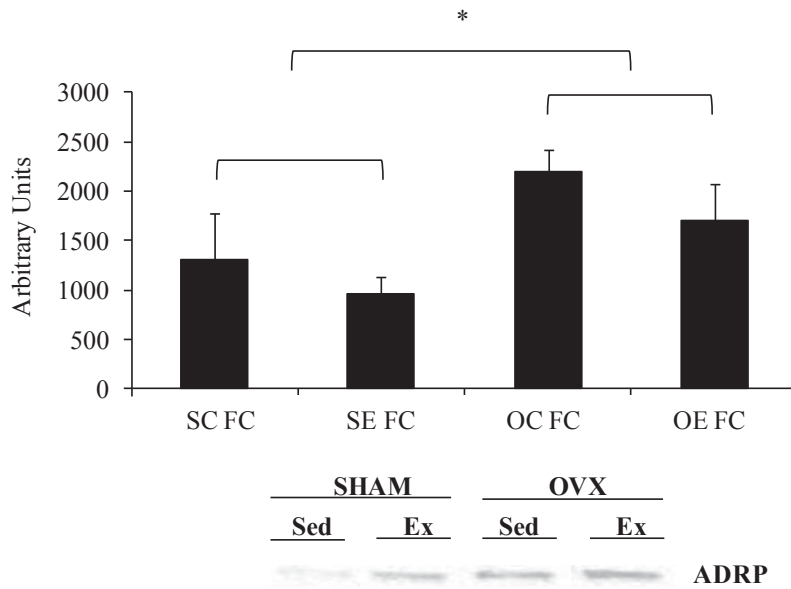
Figure 4.6. ADRP protein content is significantly elevated in O/M adipose tissue of OVX animals compared to SHAM animals. Since PLIN2 is localized to the LD and was not detected in the cytosolic fraction, only the fat cake fraction is shown. A representative PLIN2 blot is shown below the graph. N=5/group
*Indicates significantly different from SC FC and SE FC (P<0.05).

Figure 4.7
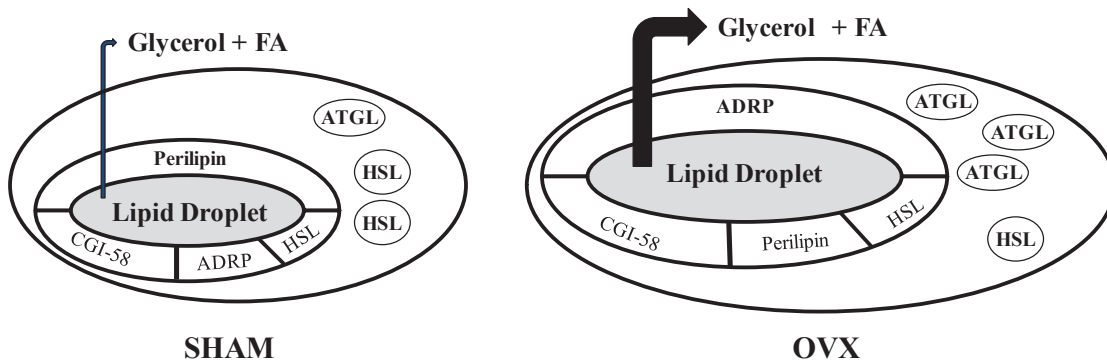
Figure 4.7. Summary of lipolytic protein content in adipose tissue from SHAM and OVX mice. OVX mice exhibit a reduction in PLIN1 protein content and an increase in ADRP protein content on the lipid droplet. Further, an increase in cytosolic ATGL protein content is observed in animals following ovariectomy.

Chapter 5: Skeletal muscle lipid deposition in response to ovariectomy or omental adipocyte co-culture is coupled with impaired insulin signaling and insulin-induced glucose uptake.

The following is a manuscript in preparation based on my final dissertation work.

Skeletal muscle lipid deposition in response to ovariectomy or omental adipocyte co-culture is coupled with impaired insulin signaling and insulin-induced glucose uptake.

Lindsay M. Wohlers, Brittany L. Powers, Eva R. Chin, and Espen E. Spangenburg

University of Maryland, School of Public Health, Department of Kinesiology, College Park, MD 21045

*Corresponding Author:
Espen E. Spangenburg, Ph.D.
University of Maryland
School of Public Health
Department of Kinesiology
College Park, MD 21045
1-301-405-2483 (office)
1-301-405-5578 (fax)
espen@umd.edu

Abstract

There is a known relationship between adiposity and insulin resistance, with increasing fat mass resulting in a greater propensity for the development of peripheral insulin resistance due to the development of tissue-specific lipotoxicity. Ovarian hormone reduction results in increased adiposity and skeletal muscle insulin resistance, but at this time the cellular relationship between these tissues remains poorly defined. The purpose of this study was to examine the impact of isolated adipocytes co-cultured with single skeletal muscle fibers collected from control (SHAM) and ovariectomized (OVX) mice on insulin responsiveness. SHAM and OVX primary adipocytes from both omental and inguinal adipose depots were isolated and co-cultured with primary skeletal muscle fibers for 24 hours. OVX skeletal muscle fibers displayed greater lipid content, impaired insulin signaling, and lower insulin-induced glucose uptake compared to SHAM fibers. Skeletal muscle fiber lipid content was greater in SHAM fibers following co-culture than in control SHAM fibers, and this lipid deposition was coupled with impaired insulin-induced glucose uptake when adipocytes were of omental, but not inguinal origin. Co-culture of OVX fibers with omental adipocytes resulted in higher lipid content, but no further reduction in insulin-stimulated glucose uptake compared to OVX control fibers. Together, OVX control fibers and SHAM fibers following omental adipocyte co-culture displayed impaired insulin signaling and glucose uptake, as well as elevated skeletal muscle fiber lipid content. These results demonstrate depot-specific effects of adipocyte exposure on skeletal muscle glucose uptake and further implicate a role for lipotoxicity in the pathogenesis of insulin resistance when ovarian hormones are reduced.

Introduction:

Insulin resistance, type 2 diabetes, and cardiovascular disease are directly related to an increase in fat mass (i.e. adiposity) (69, 78, 80). Both the type of adipose tissue expansion and the location of excess fat storage (visceral versus subcutaneous) play roles in determining the health consequences of increased adiposity. In females where ovarian function is disrupted due to age-induced menopause or clinically-used oophorectomy, there are changes in fat storage that are associated with increased risk for the development of obesity-related conditions (125, 237). Specifically, there is increased fat storage in the visceral region, which is associated with increased risk of developing the metabolic syndrome. In addition, changes in peripheral tissue function occur that facilitate increased prevalence of metabolic disease occur under these conditions (296, 297).

The location of fat storage strongly influences whether excess adiposity is pathological, with increases in omental (i.e. visceral) fat storage associated with more negative health consequences than increases in inguinal (i.e. subcutaneous) fat storage. Elevated omental fat mass has been associated with insulin resistance independent of total body weight, demonstrating the importance of body fat distribution in determining metabolic health (219). In addition, omental adipose tissue is more lipolytically active than inguinal (113, 123, 284), which contributes to elevated circulating fatty acid levels and may result in ectopic fat storage in liver and skeletal muscle. Further, the composition of fatty acids stored may vary by adipose tissue depot, with studies of obese subjects reporting elevated saturated fatty acids in omental adipose tissue compared to inguinal (91, 92). In response to changes in lipolytic activity, depot-specific fatty acid

storage may impact the composition of fatty acids in circulation, ultimately having differential effects on peripheral tissues. Lastly, the depot-specific release of endocrine factors, termed "adipokines" may potentially link adipose tissue to other peripheral organs and impact the risk for obesity-related conditions. For instance, more of the insulin-sensitizing adipokines adiponectin and leptin are released from inguinal adipose tissue than from omental adipose tissue. In addition, omental adipose tissue secretes more pro-inflammatory cytokines than inguinal adipose tissue, particularly in the obese state (217, 292). Together, these differentially secreted adipokines and inflammatory cytokines play a major role in the pathological outcomes of adipose tissue expansion, particularly in the development of peripheral insulin resistance.

In addition to the location of fat storage, the mechanism responsible for expansion of adipose tissue mass, either an increase in adipocyte size or an increase in adipocyte number, plays a critical role in the physiological phenotype of the fat pad and the subsequent risk for metabolic disease. In particular, adipose tissue expansion due to an increase in adipocyte size is correlated with increased risk of obesity-related conditions in that large adipocytes are thought to promote insulin resistance due to their contribution to mechanisms involved in lipotoxicity and/or inflammation-induced insulin resistance (84, 207). In contrast, adipose tissue expansion due to an increase in adipocyte number is often associated with enhanced insulin sensitivity, which appears to be due to the greater number of small adipocytes (52). Further evidence is also found in humans where obesity is not always associated with peripheral insulin resistance (207), with adipocyte size and adipose tissue distribution playing important roles in the relationship between obesity and insulin resistance. For example, several studies have reported a subset of

obese individuals who are termed metabolically healthy, with reduced ectopic lipid deposition, inguinal adipose tissue expansion, and smaller adipocytes compared to their obese, insulin-resistant counterparts (207, 257). Importantly, omental adipocyte size has a strong correlation with peripheral insulin resistance, while this correlation does exist for inguinal adipocyte size (207).

In sedentary individuals, the presence of ectopic fat in skeletal muscle (i.e. excess lipid in the storage form of triacylglycerol) results in tissue dysfunction, impairing processes such as insulin-stimulated glucose uptake (154, 158). Skeletal muscle accounts for ~80% of post prandial glucose uptake, therefore, reduced insulin-stimulated glucose uptake by skeletal muscle is a major factor contributing to insulin resistance (63, 65). Based on the association between increased adiposity and the risk for diseases such as type 2 diabetes, it would be logical to hypothesize that there may be interaction between adipose tissue and skeletal muscle which mediates this relationship. Indeed, ectopic fat deposition in skeletal muscle results in "lipotoxicity," which is likely the result of increased lipid products/intermediates and is associated with skeletal muscle insulin resistance (160, 162). While an association between ectopic fat deposition and insulin resistance has been demonstrated in humans and animal models, the mechanisms which link changes in adipocyte characteristics to impaired insulin action in skeletal muscle remain unknown.

This gap in our understanding of the relationship between adiposity and the skeletal muscle response to insulin are of particular importance based on the absence of a widely accepted treatment for women experiencing reduced ovarian function, a group which is at increased risk for insulin resistance and type 2 diabetes. We have previously

shown that OVX results in elevated basal lipolysis (297), impaired stimulated lipolytic function (296), and increased lipid storage in skeletal muscle; however, the relationship between these adipocyte alterations and skeletal muscle insulin resistance has not yet been directly addressed. To this end, we utilized a novel co-culture system, in which primary adipocytes and isolated skeletal muscle fibers were placed in close proximity. We hypothesized that fibers from OVX animals would exhibit greater lipid content and impaired insulin signaling and glucose uptake compared to SHAM fibers. In response to co-culture, we hypothesized that exposure of either SHAM or OVX skeletal muscle fibers to omental adipocytes would result in greater lipid deposition and further impairment of skeletal muscle insulin signaling and glucose uptake compared to inguinal adipocyte exposure. By elucidating the mechanisms which link adipocyte function to the regulation of skeletal muscle metabolism it may be possible to develop new interventions for ovarian hormone compromised women who at increased risk for metabolic diseases.

Methods:

Animals: Three sets of SHAM and ovariectomized (OVX) mice were utilized for this study. For all three sets, the OVX mice underwent a bi-lateral ovariectomy, a frequently used method to disrupt the female sex steroid signaling axis (142). Our lab has previously shown that this model decreases the levels of circulating estrogens by ~70% within 48h (248) and we also find substantial reductions in uterine weight (~80%; unpublished data). Further, previous research has shown that surgical removal of the ovaries from mice does not result in changes in feeding patterns (31, 228, 295). The SHAM group was subjected to a SHAM surgery where they were anesthetized, but did not undergo ovariectomy. Mice were given ad libitum access to water and standard rodent chow (Purina Laboratory Rodent Diet 5001: 23% protein, 4.5% fat, 6% fiber) and were housed in a temperature-controlled room on a 12 h light/dark cycle. The first set of mice was used to determine the time-course and depot-specific changes in adipocyte size and adipocyte number in female mice following OVX (N=9 SHAM; N=9 OVX). Groups of mice were sacrificed and adipocytes were isolated following 2, 4, and 8 weeks of housing in standard cages. The second set of animals was used for skeletal muscle fiber and adipocyte co-culture, subsequent insulin stimulation/western immunoblotting experiments, and glycerol/NEFA analysis of co-culture media (N=10 SHAM; N=10 OVX). The third set of mice was used for skeletal muscle fiber and adipocyte co-culture followed by BODIPY/DAPI staining and 2-NBDG experiments, as well as for cytokine analysis of co-culture media (N=5 SHAM; N=5 OVX). All aspects of this study were approved by the University of Maryland Institutional Animal Care & Use Committee (IACUC) Review Board.

Adipocyte Isolation: Primary adipocytes were isolated from omental and inguinal adipose tissue according to the Rodbell technique with slight modifications (227). Freshly prepared Kreb's Ringer Buffer (KRB, pH 7.4) (24.6 mM $NaHCO_3$, 1.1 mM KH_2PO_4, 130.2 mM NaCl, 4.7 mM KCl, 2.54 mM $MgSO_4$, 3.27 mM $CaCl_2$, 5 mM dextrose, 0.02 µM adenosine, and 4 mg/ml BSA) was equilibrated by bubbling with 95% O_2/5% CO_2 for 10 minutes. Adipose tissue was removed and rinsed with KRB, then placed in a conical tube with 1 mL KRB plus 10 µL of liberase blendzyme (Roche Applied Science, Indianapolis, IN) per gram of tissue. The conical tube containing the adipose tissue was then incubated in a shaking water bath at 37 C and 80 rpm for 45-60 minutes or until adipose tissue was fully digested. Following digestion, fat was strained through 250 µm mesh, rinsed with KRB, and then left to sit until adipocytes had floated to the top of the solution. The buffer below the adipocytes was removed using a syringe connected to medical tubing. Fresh KRB buffer was added to the cells, and the KRB was removed again once the cells had floated. This washing process was completed three times. Finally, the cells were left suspended in ~2 mL of KRB and an aliquot was removed for adipocyte size determination.

Adipocyte Size and Number: Approximately 20 µL of the adipocyte suspension was placed on a glass slide within a ring of vacuum grease. Two separate aliquots of the adipocyte suspension were used for imaging each sample. The adipocytes were imaged under a standard light microscope at 10X magnification then Image J software was used to measure adipocyte diameter (NIH Bethesda, MD). The distribution of adipocyte sizes in each sample was determined and graphed by counting the number of cells in 10 µm increments from 30 µm to >100 µm. A minimum of 300 adipocytes per sample from

each animal were measured for cell size determination. Adipocyte number was calculated using the average values for adipocyte size according to previously described methods (27, 228, 235). Briefly, the calculation was made from the fat pad weight divided by the average adipocyte volume times the known value for adipocyte density.

Adipocyte BODIPY Staining: After the aliquots of cells were removed for size determination, the remaining cells were incubated in 5 mL of KRB with 10 uL of BODIPY 493/503 (1 μg/mL in DMSO) for 15 minutes. KRB buffer below the cells was removed with a syringe and surgical tubing and 3 rinses were performed as described above. Adipocytes were suspended in 2 mL of KRB buffer and approximately 10 μL of the cell suspension was removed and placed on a glass slide for imaging. Cells were imaged using a Nikon Eclipse Ti-U fluorescent microscope (Nikon Instruments, Melville, NY).

Skeletal Muscle Fiber Isolation: Intact skeletal muscle fibers were isolated from the flexor digitorium brevis (FDB) muscle according to previously described techniques (184, 255). Briefly, surgically excised FDB muscles were incubated in dissociation media (DM) containing DMEM, 1% penn/strep, and 2% FBS. FDB muscles were placed in a 40 mm dish with 3 mL of DM plus 100 μl of liberase blendzyme (2.5 mg/mL stock; Roche Applied Science, Indianapolis, IN) and then in an incubator (37°C, 5% CO_2) for 2 hours. Following the 2 hour incubation, muscles were placed in a new 40 mm dish with fresh co-culture media (DMEM + 1% pen/strep, 2% FBS, 0.5% BSA, and 2 mmol/L L-carnitine) and triturated with a 1 mL pipette to dissociate the muscle into single FDB myofibers. Following the trituration process, fibers were plated onto extra-cellular matrix- (ECM; Sigma Aldrich, St. Louis, MO) coated 6 well plates such that each well

contained a total of 3 ml of co-culture media plus fibers. Fibers were incubated for 2 hours to allow adherence to the ECM before beginning the co-culture experiment.

Co-culture: Adipocytes were isolated as described above with one slight modification. Adenosine was not added to the KRB buffer to prevent external inhibition of adipocyte lipolysis. Adipocytes and skeletal muscle fibers were co-cultured such that both cell types were exposed to the same media, but could not physically interact with each other. Fibers were placed into 6 well plates as described above and adipocytes were placed in co-culture inserts which sat inside each well of the plate (Millipore, Billerica, MA). The base of the co-culture wells containing the adipocytes consisted of a permeable membrane with a pore size of 0.4 μm. This pore size allowed for circulating factors released from either cell type to pass through, but prevented cellular constituents from moving between the two compartments. The co-culture combinations consisted of SHAM skeletal muscle fibers without adipocytes, OVX skeletal muscle fibers without adipocytes, SHAM skeletal muscle fibers with SHAM omental adipocytes, OVX skeletal muscle fibers with OVX omental adipocytes, SHAM skeletal muscle fibers with SHAM inguinal adipocytes, and OVX skeletal muscle fibers with OVX inguinal adipocytes.

Adipocyte number for a set volume of packed adipocytes was determined with a hemacytometer in order to ensure that each co-culture well received the same number of adipocytes. For each sample, 5 μL of packed adipocytes was mixed with 15 μL of KRB buffer. The resulting cell suspension was placed on a hemacytometer (Hausser Scientific, Horsham, PA). The number of cells in the four corner squares, along with the center square, was counted and the number of adipocytes per 5 μL of packed cells was calculated. The resulting value was used to calculate the volume of packed adipocytes to

be added such that each well of fibers was co-cultured with 300,000 adipocytes. From preliminary experiments, 300,000 adipocytes was chosen based on glycerol and NEFA release in the media not exceeding levels we have previously measured in mouse serum (296, 297). The appropriate volume of packed adipocytes was added to the co-culture wells after the fibers were allowed to adhere to the ECM for 2 hours. Adipocytes and skeletal muscle fibers were co-cultured for 24 hours.

Insulin stimulation: Following the overnight co-culture, co-culture inserts containing the adipocytes were removed from the 6-well plates. Next, 1.5 mL of media was removed from each well and discarded, followed by the addition of 1.5 mL of serum-free DMEM. This process was repeated three times in order to place the fibers in serum-free media without exposing them to ambient air. Fibers were returned to the incubator for a 5 hour period of serum-starvation. After 5 hours, one well from each condition (no adipocytes, omental adipocyte co-culture, inguinal adipocyte co-culture) was stimulated with insulin, with the other well from each condition serving as an unstimulated (basal) control. First, 1.5 mL of media was removed from each well and discarded, with the unstimulated wells receiving 1.5 mL of fresh serum-free DMEM. The remaining three wells received 1.5 mL of DMEM plus insulin such that a final insulin concentration of 50 nM was attained. The 50 nM concentration was chosen based on values reported in the literature (165, 166, 259), as well as on preliminary data collected using different concentrations of insulin to stimulate C2C12 myotubes and skeletal muscle fibers. At a 50 nM concentration, it was possible to detect increases in Akt phosphorylation (Ser473) via Western immunoblotting and a 100 nM dose did not result in greater Akt phosphorylation than the 50 nM dose (data not shown). Fibers were returned to the incubator and allowed to sit for 30 minutes

prior to isolation of protein for subsequent Western immunoblotting. The 30 minute insulin stimulation was chosen based on the literature, in which maximal GLUT4 translocation in skeletal muscle has been observed after 20-30 minutes of insulin exposure (172), as well as on preliminary experiments where phosphorylation of insulin signaling targets was reduced following a 60 minute stimulation period compared to 30 minutes (data not shown).

Protein Isolation: Following the co-culture and insulin stimulation, protein was isolated from the skeletal muscle fibers in order to determine phosphorylation status and total content of proteins involved in the insulin signaling response. Immediately after insulin stimulation, media was removed and 300 µL of ice cold Mueller buffer (0.1% Triton – X100, 4 mM EGTA, 10 mM EDTA, 15 mM $Na_4P_2O_7H_2O$, 100 mM β-glycerophosphate, 25 mM NaF, 5 mM Na_3VO_4 and 1 protease inhibitor tablet/10 mL (Roche, Indianapolis, IN)) was placed into the well with the fibers. A cell scraper was used to detach fibers from the extracellular matrix, after which the Mueller buffer containing the fibers was drawn off and placed in a 1.5 mL microcentrifuge tube and put on ice. A plastic dounce (Kimble & Kontes, Vernon Hills, IL) was used to homogenize fibers in the 1.5 mL microcentrifuge tubes while on ice for ~1 minute. To improve cellular fractionation, tubes containing the fibers were placed in a -80C freezer overnight, after which samples were thawed on ice, then vortexed and rocked at $4^{o}C$ for one hour, with additional vortexing every 15 minutes. After rocking, samples were vortexed and placed at -80 C until further analysis.

Protein Assay: Protein concentration was determined for each sample according to the BCA protein assay method (Thermo Fischer Scientific, Rockford, IL).

Western Blotting: Following determination of protein concentration, equal amounts of total protein were resolved on either 10% or 4-15% SDS-PAGE criterion gels (Biorad, Hercules, CA) according to previously published methods (296-298). Membranes were probed with antibodies for p-Akt (Ser473), total Akt, p-p38 (Thr180/Tyr182), total p38, p-GSK-3β (Ser9), total GSK-3β, HKII, GAPDH (Cell Signaling, Danvers, MA) and GLUT4 (Abcam, Cambridge, MA). Images were quantified with Image J software (NIH, Bethesda, MD) and all phosphorylated targets were normalized to their respective total protein (i.e. p-Akt normalized to total Akt). In addition, total protein gels were run and stained with Oriole fluorescent protein stain (Biorad, Hercules, CA). HKII and GLUT4 were normalized to myosin as previously described (187).

Glycerol and NEFA: Media samples were collected after 1 and 24 hours of co-culture. Glycerol and NEFA levels in the media were measured from these samples according to commercially available kits. Glycerol levels were measured using a free glycerol determination kit from Sigma (Sigma Aldrich, St. Louis, MO) and NEFA was measured using a kit from Wako Diagnostics (Wako Diagnostics, Richmond, VA).

Glucose Uptake: Glucose uptake was measured using the fluorescent D-glucose analog 2-[N-(7-nitrobenz-2-oxa-1,3-diazol-4-yl)amino]-2-deoxy-d-glucose (2-NBDG) (Invitrogen, Grand Island, NY). 2-NBDG has been successfully used as an alternative to radio labeled 2 deoxyglucose (2-DOG) in the measurement of glucose uptake in multiple cell types (116, 166, 300, 310). The experiments conducted for optimization of 2-NBDG uptake in skeletal muscle fibers are included in the appendices (See Appendix 1). For this set of experiments, fibers were placed in 6-well plates without ECM, and co-culture was conducted as described above. Following the 24-hour co-culture period, adipocytes

were removed, and 600 µL aliquots of media plus fibers were plated into ECM coated wells of a 24 well plate, resulting in 8 wells per co-culture condition. Fibers were allowed to adhere for 1 hour, after which they were placed into serum free DMEM for a serum starvation period of 5 hours. Following serum starvation, fibers were rinsed 3X with Kreb's Ringer buffer (135 mM NaCl, 10 mM $NaHCO_3$, 5 mM KCl, 3 mM $CaCl_2$, 2 mM $MgSO_4$, 1.2 mM NaH_2PO_4) until all media was removed from the wells (without exposing fibers to ambient air). For each co-culture condition, half of the wells (N=4) underwent a 30 minute pretreatment with 50 nM insulin, while the other half served as the unstimulated (basal) wells. During these 30 minutes, the plate was returned to the incubator. After the 30 minute pretreatment, all wells were treated with 50 µM 2-NBDG for 30 minutes, with the insulin treated wells receiving 50 nM insulin treatment along with the 2-NBDG. During the 2-NBDG treatment, the plate was covered in foil and underwent gentle agitation at room temperature. After 2-NBDG treatment, fresh Ringer buffer was used to wash the wells (without exposing fibers to ambient air) 3X until no excesses 2-NBDG remained. After rinsing, all Ringer buffer was removed and 100 µL of ice cold cell lysis buffer (40 mM KCl, 20 mM Tris-base, 1% NP-40; pH 7.4) was added to each well. The plate was again covered in foil and gently agitated for 10 minutes, at which point wells were scraped and isolated lysates were placed into a black 96 well plate. The 2-NBDG fluorescence was measured on a BioTek Synergy plate reader (BioTek, Winooski, VT) at an excitation wavelength of 438 nm and emission wavelength of 535 nm. An aliquot of the cell lysate was removed and run on an SDS-PAGE gel, followed by incubation with Oriole fluorescent protein stain (Biorad, Hercules, CA). The gel was visualized under UV light using a Kodak EDAC290 imaging system (Eastman

Kodak, Rochester, NY) and the myosin band was quantified using Image J software (NIH, Bethesda, MD) to normalize the 2-NBDG fluorescent signal from each well.

Skeletal Muscle Fiber Staining: Fluorescent staining of the skeletal muscle fibers was conducted according to previously published techniques (255) using two different dyes. BODIPY 493/503 was used in order to determine the neutral lipid content of the fibers (Invitrogen, Cambridge, MA). In addition, 4,6-diamidino-2-phenylindole (DAPI) was used to label nuclei (Invitrogen, Cambridge, MA). First, following the 24 hour co-culture period, a 200 μL aliquot of fibers was placed onto an ECM coated well of a 6 well glass bottom plate for each condition (MatTek, Ashland, MA). Fibers were allowed to adhere for 1 hour, after which wells were rinsed with Ringer buffer to remove all media. After rinsing, cells were incubated with Ringer buffer containing BODIPY 493/503 and DAPI at concentrations of 1:1000, and 1:5000, respectively for 30 minutes. After 30 minutes, the dyes were removed by rinsing fibers 3X with fresh Ringer buffer. Fibers were imaged using a Zeiss AxioObserver Z1 fluorescent microscope with both 20X at 40X long distance objective lenses (Carl Zeiss MicroImaging, Jena, Germany). A total of 5 fibers per co-culture condition were imaged for all animals. Z-stacking was performed for all images such that it was possible to look at the fluorescent distribution throughout the fiber. A 20X surface image and an image 6 μm deep were used for quantification of each fiber. For each image, BODIPY 493/503 signal was quantified at three different points per fiber using Image J software (NIH, Bethesda, MD). No differences BODIPY 493/503 signal were detected between surface and 6 μm sections, therefore the two were averaged for the final data analysis.

<u>Cytokine/Adipokine Analysis of Media</u>: Measurement of IL-10, IL-6, MCP-1, TNFα, adiponectin and leptin was conducted by the Cytokine Core Laboratory at the University of Maryland Baltimore using a Luminex Multianalyte System. Samples were measured in duplicate and on the same plate within targets. IL-10, IL-6, MCP-1, and TNFα were all measured on one plate, while adiponectin and leptin were measured on a separate plate. To start, 200 uL of assay buffer was added per well of a 96 well filter plate (Millipore, Billerica, MA). After 10 minutes of shaking, the plate was vacuumed and 25 uL of assay buffer was added to each well, followed by 25 uL of standard/sample. Next, 25 uL of a mixture containing the appropriate cytokine (1:50 dilution) conjugated to beads was added to the wells and the plate was placed on a shaker at 4 C overnight. The following day, the plate was vacuumed and 200 uL of wash buffer was added to each well. The wash buffer was vacuumed off, and the washes were repeated two more times. Following the last vacuum of wash buffer, 25 uL of detection antibody was added to each well and the plate was then placed back on the shaker for 30 minutes. After the 30 minutes, three more rounds of washing were performed, followed by the addition of 150 uL of Sheath Fluid to each well. The plate was read using a Luminex 100 plate reader and Softmax Pro Software, and then the data was calculated using BioRad software (Biorad, Hercules, CA).

<u>Statistics:</u> Statistical analysis was conducted using a two way analysis of variance (ANOVA), a one way ANOVA, or t-tests where appropriate. In all cases, Student-Newman Keuls was used post-hoc to control for multiple comparisons. All analyses were completed with Sigma Stat statistical software (Systat Software, Inc., San Jose, CA). Statistical significance was accepted at an alpha level of $p \leq 0.05$.

Results:

Anatomical Characteristics: Following 8 weeks of ovariectomy, the body weight of the OVX animals was significantly greater than the SHAM group (Table 1). No differences in absolute heart or liver mass were detected between groups. However, when normalized to body weight, heart mass was significantly lower in the OVX animals compared to the SHAM animals (Table 1). The mass of the omental and inguinal adipose tissue was significantly greater in the OVX animals compared to the SHAM animals. In addition, while no differences were detected between the omental and inguinal adipose tissue masses in the SHAM animals, omental fat mass was significantly greater than inguinal fat mass in OVX animals (Figure 1).

Adipocyte Size: The paracrine action of adipose tissue is influenced by the number and size of the adipocytes contained within each depot. Although it is well recognized that OVX results in increased visceral fat mass, there is little documentation concerning changes in individual adipocyte size and/or number after the OVX surgery. Thus, changes in adipocyte size and number were investigated in omental and inguinal adipose tissue from SHAM and OVX mice at 2, 4, and 8 weeks after OVX and SHAM surgeries.

Omental: Average omental adipocyte size was found to be significantly greater in OVX animals compared to SHAM animals 8 weeks following OVX surgery (Figure S1A). At the 2 and 4-week post-ovariectomy time-points, the average omental adipocyte size was not different between SHAM and OVX animals (Figure S1A). However, when adipocyte size was plotted as a frequency histogram (Figure 2A-B), the data revealed a rightward shift in the distribution of adipocytes from OVX animals, indicating an increasing percentage of cells with a large diameter. In contrast, there was no change in the omental

adipocyte size distribution in the SHAM animals across all time-points (Figure 2A). The shift to the right in the OVX animals was already apparent at the 2 week post-OVX time-point, with the rightward shift becoming more pronounced after 4 and 8 weeks (Figure 2B). No differences in omental adipocyte number were detected between SHAM and OVX animals at any time-point (Figure S2A).

Inguinal: Average inguinal adipocyte size was significantly greater in the OVX animals compared to the SHAM animals at both the 4 and 8 week time-points (Figure S1B). At the 2 week time-point, no difference in average inguinal adipocyte size was observed between SHAM and OVX animals. When adipocyte size was plotted as a frequency histogram (Figure 2D-E), the data revealed a rightward shift in the distribution of adipocytes from OVX animals. In contrast, there was relatively little change in the inguinal adipocyte size distribution in the SHAM animals across all time-points (Figure 2D). The shift to the right in the OVX animals was apparent at the 4 and 8 week time-points (Figure 2E). No differences in inguinal adipocyte number were detected between SHAM and OVX animals at any time-point (Figure S2B).

Co-culture media analysis: In order to assess the levels of glycerol and fatty acids that the skeletal muscle fibers were exposed to media was collected after 1 hour and 24 hours of co-culture. To determine the relative amount that was specifically derived from the cultured adipocytes, glycerol and NEFA values from the control media that was cultured with skeletal muscle fibers only were subtracted from the glycerol and NEFA values from the co-culture conditions.

Glycerol: For both SHAM and OVX omental and inguinal adipocytes, 24 hours of co-culture resulted in glycerol levels that were significantly elevated compared to the 1 hour

time-point. At the 1 hour time-point, OVX inguinal glycerol levels were significantly lower than OVX omental, with the same tendency observed for SHAM co-culture. Further, both SHAM and OVX inguinal glycerol levels were undetectable at the 1 hour time-point. After 24 hours, OVX omental co-culture resulted in significantly greater glycerol levels than OVX inguinal co-culture. The same tendency was observed for SHAM omental co-culture compared to SHAM inguinal co-culture, however, this difference did not reach statistical significance ($p = 0.06$) (Table 2).

NEFA: NEFA levels following inguinal, but not omental, co-culture were markedly elevated in media from OVX compared to SHAM after 24 hours. At the 1 hour time-point, NEFA levels were undetectable in SHAM omental and inguinal media, with levels still undetectable in the SHAM omental media after 24 hours. While no significant differences were detected between SHAM and OVX at the 1 hour time-point, there was a tendency for 1 hour OVX omental NEFA to be greater than SHAM omental ($p = 0.09$). Another tendency was observed for 24 hour OVX inguinal NEFA levels to be greater than OVX omental ($p = 0.1$) (Table 2).

Lipid Content: The lipid content of skeletal muscle fibers was assessed using the fluorescent dye BODIPY 493/503, which stains all stored neutral lipids (255). In the control fibers, lipid content was 57% greater in the OVX group compared to SHAM, which was statistically significant (Figure 4A). Co-culture of SHAM skeletal muscle fibers with omental or inguinal adipocytes resulted in significantly higher lipid content compared to the control condition (Figure 4B). Co-culture of OVX skeletal muscle fibers with omental adipocytes resulted in significantly greater lipid content than OVX control fibers. Further, the elevated fiber lipid content following OVX omental co-culture was

185% greater than the fiber lipid content following SHAM omental co-culture. In response to inguinal adipocyte co-culture, OVX fibers displayed significantly greater lipid content than OVX control fibers. Interestingly, unlike SHAM co-culture, OVX omental co-culture resulted in significantly greater skeletal muscle fiber lipid content than inguinal co-culture (Figure 4D).

Glucose uptake: Glucose uptake in skeletal muscle fibers was assessed using the fluorescent glucose analog 2-NBDG, which has been used successfully to measure glucose uptake in multiple cell lines as an alternative to 2-deoxyglucose (116, 166, 300, 310). In the control fibers, 2-NBDG uptake in OVX fibers in the basal state was significantly greater than that of SHAM fibers. In response to 50 nM insulin stimulation, SHAM control fibers displayed significantly greater 2-NBDG uptake compared to the basal state while OVX fibers did not demonstrate any response to insulin (Figure 5A). Co-culture with adipocytes isolated from the omental region completely prevented insulin-induced 2-NBDG uptake in the SHAM skeletal muscle fibers. In addition, there was a tendency for insulin-induced 2-NBDG uptake following omental co-culture to be lower than insulin-induced 2-NBDG uptake in control fibers ($p = 0.078$). However, in SHAM skeletal muscle fibers co-cultured with inguinal adipocytes, the greater uptake of 2-NBDG in response to insulin was preserved. There was another tendency for higher insulin-induced 2-NBDG uptake following inguinal co-culture compared to insulin-induced 2-NBDG uptake following omental co-culture in SHAM fibers ($p = 0.076$) (Figure 5B). In control fibers from OVX animals, 2-NBDG uptake in skeletal muscle fibers exposed to insulin was not greater than the basal uptake of 2-NBDG, indicating a failure of the muscle fibers to respond to insulin. Neither omental nor inguinal adipocyte

co-culture had a significant impact on basal or insulin-induced 2-NBDG uptake (Figure 5C).

Western Immunoblotting of skeletal muscle fibers: In OVX skeletal muscle fibers, and in SHAM fibers following omental adipocyte co-culture, insulin-induced uptake of 2-NBDG was lower than that observed in SHAM control fibers. In order to assess the impact of OVX and adipocyte co-culture on the insulin signaling pathway, multiple signaling proteins were assessed using western immunoblotting.

Akt phosphorylation (Ser473). Phosphorylation of Akt is a critical step in insulin stimulated GLUT4 translocation (96), with phosphorylation on the Ser473 site required for complete activation of Akt (251). In response to insulin, Akt activation results in subsequent phosphorylation of downstream targets, such as AS160, to facilitate GLUT4 translocation (159) and GSK-3β to promote glycogen storage (53). Exposure to 50 nM insulin for 30 minutes resulted in significantly greater Akt phosphorylation (Ser473) compared to the basal condition in SHAM control fibers. Significantly greater Akt phosphorylation (Ser473) was also observed in response to insulin in the OVX fibers; however, the magnitude of the difference between basal and insulin-stimulated Akt phosphorylation was significantly attenuated by 58% compared to SHAM fibers (Figure 6A). In SHAM fibers, the insulin-induced phosphorylation of Akt was preserved following omental and inguinal co-culture, however, the magnitude of the response was blunted in both co-culture conditions compared to SHAM control fibers (Figure 6B). In OVX fibers, insulin-induced Akt phosphorylation was preserved in both omental and inguinal adipocyte co-culture conditions. As opposed to the SHAM fibers,

phosphorylation of Akt in response to insulin was not lower in the fibers exposed to adipocyte co-culture than in the OVX control fibers (Figure 6C).

GSK-3β. GSK-3β acts as a negative regulator of glycogen synthesis by inhibiting the activity of glycogen synthase (GS). In response to insulin, phosphorylation on the Ser9 residue inhibits GSK-3β activity, thus removing inhibition on GS and facilitating the synthesis of glycogen (265). In both SHAM and OVX control fibers, fibers exposed to insulin displayed significantly greater phosphorylation of GSK-3β (Ser9) than basal fibers (Figure 7A). In SHAM fibers co-cultured with either omental or inguinal adipocytes, there was a tendency greater phosphorylation of GSK-3β in insulin-stimulated fibers compared to unstimulated fibers (p = 0.07). However, while the response to insulin was still intact in the SHAM fibers, there was a tendency for the magnitude of insulin-stimulated GSK-3β phosphorylation to be lower following inguinal co-culture compared to control (p = 0.07) (Figure 7B). In OVX control fibers and fibers co-cultured with omental adipocytes, GSK-3β phosphorylation was higher in insulin-stimulated than in unstimulated fibers. OVX inguinal adipocyte co-culture completely blunted insulin-induced GSK-3β phosphorylation and was significantly lower than both the control and omental co-culture conditions (Figure 7C).

GLUT4. In skeletal muscle, the primary transporter for glucose uptake is GLUT4 (309). Upon stimulation, GLUT4 translocates to the plasma membrane where it facilitates glucose uptake into the cell. No difference in GLUT4 protein content was detected between SHAM and OVX control fibers (Figure 8A). In SHAM skeletal muscle fibers, there was no effect of adipocyte co-culture on GLUT4 protein content (Figure 8B). The

same was observed for OVX skeletal muscle fibers, with no differences in GLUT4 content detected between conditions (Figure 8C).

HKII. Hexokinase (HK) catalyzes the conversion of glucose to glucose-6-phosphate upon glucose entry into the cell. Multiple isoforms of HK exist, with HKII the primary isoform detected in skeletal muscle (110, 141). No difference in HKII content was detected between SHAM and OVX control skeletal muscle fibers (Figure 9A). In fibers isolated from SHAM animals, neither omental nor inguinal adipocyte co-culture resulted in a change in HKII protein content compared to control fibers (Figure 9B). However, in fibers from OVX animals, both omental and inguinal co-cultured fibers displayed lower HKII protein content compared to control (Figure 9C).

p38. p38 is a member of the family of mitogen activated protein kinases (MAPK), which are responsive to various stress stimuli. In the insulin signaling pathway, activation of p38 may increase serine phosphorylation of IRS-1, resulting in inhibition of insulin signaling transduction (10, 70). In the basal state, OVX control fibers exhibited a tendency for greater p38 phosphorylation (Thr180/Tyr182) compared to SHAM control fibers ($p = 0.07$), however, no difference was observed in the insulin-stimulated state (Figure 10A). Following co-culture with omental or inguinal adipocytes, SHAM fibers exhibited a tendency for higher basal p38 phosphorylation than control fibers ($p = 0.07$) (Figure 10B). In OVX fibers, no differences in p-38 phosphorylation were observed in the co-culture groups compared to control (Figure 10C).

Cytokine Analysis of Media: In order to assess the release of cytokines from cells in the co-culture system, IL-6, MCP-1, IP-10, TNF-α, adiponectin, and leptin were measured in co-culture media after 24 hours. These factors were selected due to their reported roles to

facilitate or inhibit insulin signaling. Adiponectin concentration was significantly higher in SHAM omental and SHAM inguinal co-culture compared to SHAM control, as well as in OVX omental and OVX inguinal co-culture compared to control. However, no differences were observed between omental and inguinal co-culture, or between SHAM and OVX. No differences were detected in MCP-1 concentrations between any conditions. Further, no significant differences were detected between conditions for IL-6; however, there was a tendency for OVX omental co-culture to be greater than OVX control (p=0.06). The concentrations of IP-10, TNF-α, and leptin were below the range of detection (Table 5.3).

2-NBDG Correlation: Plotting of the insulin-induced increase in 2-NBDG uptake for control fibers against the insulin-induced increase in 2-NBDG uptake in fibers following omental adipocyte co-culture revealed a moderate negative correlation ($R^2 = 0.67$). This relationship demonstrates that the more insulin-responsive the control fibers from an animal are, the more detrimental the response to co-culture with omental adipocytes.

Discussion

Here we have demonstrated that compared to SHAM animals, OVX animals exhibit greater intramuscular lipid content and impaired insulin-induced glucose uptake in isolated single muscle fibers from skeletal muscle of adult female mice. An inherent deficit in insulin-induced phosphorylation of Akt (Ser473) was observed in OVX fibers compared to SHAM, as well as a tendency for higher basal phosphorylation of p38 (Thr180/Tyr182). Further, utilizing a novel co-culture model, exposure of the skeletal muscle fibers from OVX animals to omental or inguinal adipocytes isolated from the same OVX animals did not further exacerbate the decrement in insulin-induced glucose uptake. Both SHAM omental and inguinal adipocyte co-culture resulted in greater skeletal muscle fiber lipid content and reductions in insulin signaling compared to SHAM control fibers, however, only omental co-culture impaired insulin-induced glucose uptake. In addition, SHAM skeletal muscle fiber co-culture with both omental and inguinal adipocytes resulted in lower insulin-induced Akt phosphorylation and a tendency for higher basal p38 phosphorylation compared to SHAM control fibers. In OVX skeletal muscle fibers, inguinal adipocyte co-culture impaired insulin-induced GSK-3β phosphorylation (Ser9), while both omental and inguinal co-culture lowered HKII protein content compared to OVX control fibers. Lastly, adiponectin concentrations were elevated to a similar degree in both omental and adipocyte co-culture media from SHAM and OVX animals compared to control media from fibers alone, while no significant differences in MCP-1 or IL-6 were detected between any conditions. These data suggest a critical role for ovarian hormones in the regulation of skeletal muscle insulin action, as

well as provide insight into the effect of adipocyte exposure on insulin action in skeletal muscle.

When ovarian hormones are reduced, alterations in body composition and body fat distribution occur, placing females at an increased risk for the development of obesity-related conditions such as insulin resistance. Following ovariectomy in mice, we observed a higher body weight compared to SHAM mice, which in part was mediated by greater adipose tissue mass (Table 1). These data are in agreement with previous reports from our lab and that of others (68, 228, 296, 297). Further, there was a disproportionate elevation in omental fat mass relative to inguinal fat mass, indicating that OVX results in a shift in overall adipose tissue distribution (Figure 1). This accumulation of omental adipose tissue is also observed in human females experiencing reduced ovarian function (41, 125) which is of particular concern given the relationship between omental adiposity and the onset of the metabolic syndrome, insulin resistance, and cardiovascular disease (40).

In OVX animals, we found the expansion of both omental and inguinal adipose tissue to be mediated by adipocyte hypertrophy (Figure 2 A-F), with adipocyte size becoming significantly greater than SHAM eight weeks following surgery. As a point of reference, while adipocytes from OVX animals were significantly larger than SHAM adipocytes at the eight-week time-point they were not as large as adipocytes in the *ob/ob* genetic mouse model of obesity, and in obesity induced by a high-fat diet. For example, Libinaki et al. report average epididymal adipocyte diameter of 138 μm in mice following 32 weeks of high-fat feeding, and an average diameter of 127 μm in *ob/ob* mice (180). In contrast, on a standard chow diet, we observed an average omental

adipocyte diameter of 81 μm and inguinal adipocyte diameter of 65 μm in OVX mice at the eight week time-point. Others have reported adipocyte hypertrophy in the OVX model; however, these studies only investigated adipocyte size at a single time-point after ovary removal, and have not measured hypertrophy in the omental depot (68, 228). As omental fat mass is a significant component of the relationship between adiposity and metabolic disease in post-menopausal women (155), investigation of this depot in the OVX model is of critical importance. Thus, our findings provide novel insight into the impact of OVX on the time-course of adipocyte hypertrophy following OVX and on the impact of OVX on specific fat depots. Regardless, visceral adipose tissue expansion via adipocyte hypertrophy is more likely to result in insulin resistance than adipose tissue expansion mediated by increased adipocyte number, which may be insulin-sensitizing (147). We found no evidence for changes in adipocyte number in OVX mice compared to SHAM (Figure S2 A/B). It has been proposed that large amounts of adipocyte hypertrophy result in fatty acid overflow and ectopic lipid deposition in skeletal muscle and liver as adipocytes reach their maximal storage capacity (278). Our previously published data found greater fatty acid release from visceral adipose tissue from OVX animals compared to SHAM animals, suggesting a possible overflow effect (297). Thus, our finding of omental and inguinal adipocyte hypertrophy in OVX mice provides critical evidence towards identifying mechanisms to help explain the increased risk for development of insulin resistance in the OVX animals.

In order to further investigate the relationship between OVX-mediated alterations in adipocyte function and the onset of insulin resistance in skeletal muscle, we developed a novel co-culture system whereby primary adipocytes and primary skeletal muscle fibers

were placed in the same culture well. Specifically, isolated primary skeletal muscle fibers were adhered to the bottom of culture plates, while primary adult adipocytes were floated in the same wells but within co-culture inserts. These inserts contained a permeable membrane with a 0.4 μm pore size, thus allowing for exchange of circulating factors between the two cell types, but preventing physical interaction. To assess the lipolytic state within the co-culture system, media levels of glycerol and NEFA were measured. The glycerol and NEFA concentrations from the OVX co-culture suggested incomplete lipolysis was occurring, as demonstrated by a five fold greater concentration of NEFA relative to glycerol compared to SHAM animals (Table 2). The potential for incomplete adipocyte lipolysis in the OVX co-culture condition is supported by our previous data in which we found that OVX animals display elevated adipose triglyceride lipase content, which catalyzes release of the first fatty acid in triglyceride lipolysis, without a change in hormone sensitive lipase, which catalyzes the second step of lipolysis (308). Further, differences in glycerol and NEFA from omental and inguinal co-culture point to depot-specific lipid regulation of adipocytes. Specifically, after 24 hours of co-culture, glycerol levels were higher in OVX omental than inguinal co-culture media, with the same tendency observed for SHAM (p=0.06). This observation is in-line with other studies which have found elevated lipolytic rate in omental adipocytes compared to inguinal adipocytes (123). While some studies have reported elevated basal lipolytic rate in omental adipocytes from post-menopausal females compared to pre-menopausal females (272), we did not observe a significant difference in glycerol between SHAM and OVX co-culture media at the 24 hour time-point. It is clear that the lipolytic state of the co-culture system is impacted both by ovarian hormone status and by adipocyte depot

141

of origin. However, due to the potential for NEFA to be either re-esterified by adipocytes, or to be taken up and by the skeletal muscle fibers, NEFA levels alone do not provide a clear indication of lipolytic dynamics across co-culture conditions.

In order to assess the lipid content of skeletal muscle fibers we stained them with a fluorescent dye specific for neutral lipid. Lipid content was significantly greater in control skeletal muscle fibers from OVX animals than from SHAM (Figure 4A). The higher lipid content in control fibers from OVX animals compared to SHAM is in-line with unpublished observations from our laboratory and has recently been reported by another group (135), suggesting ovarian hormone reduction impacts ectopic lipid deposition in skeletal muscle. Both omental and inguinal co-culture of SHAM fibers resulted in similar skeletal muscle fiber lipid content that was significantly greater than that of SHAM control fibers (Figure 4B). Thus, in SHAM co-culture, the statistically equivalent NEFA levels observed following omental and inguinal co-culture was paralleled by similar muscle fiber lipid content. However in OVX, muscle fiber lipid content was significantly greater following omental co-culture compared to the control and inguinal co-culture conditions (Figure 4C). As NEFA levels were significantly elevated in OVX inguinal media, but lipid content was not elevated to the same degree, for unknown reasons it appears OVX fibers did not readily take up and store fatty acids from inguinal adipocytes compared to omental. Studies have reported depot-specific differences in fatty acid composition that may be altered in the obese state (91, 92). In particular, obese individuals present with elevated saturated fatty acids in omental adipose tissue compared to inguinal (91, 92). Therefore it is possible that the inguinal adipocytes from OVX animals release a specific fatty acid species that is not efficiently

taken up by the skeletal muscle fibers compared to other species of fatty acids that may be released from omental adipocytes. Together, these findings demonstrate that both OVX and adipocyte co-culture result in skeletal muscle fiber lipid deposition, which is of particular concern due to the relationship between skeletal muscle lipid content and insulin resistance in the sedentary state.

Excess skeletal muscle lipid deposition in the sedentary state has been shown to impair insulin signal transduction and facilitate the onset of insulin resistance. Thus, we sought to determine if direct exposure of OVX skeletal muscle fibers or SHAM fibers to adipocyte co-culture conditions resulted in impaired insulin-induced glucose uptake. In fibers from SHAM animals, insulin stimulation significantly increased glucose uptake in control fibers, but this response was significantly impaired in control fibers from OVX animals. Our finding of lower insulin-induced glucose uptake in skeletal muscle fibers from OVX mice is in-line with other studies reporting reduced glucose uptake in whole skeletal muscle of OVX animals compared to ovary intact controls (220, 233). Interestingly, glucose uptake in the basal state was higher in skeletal muscle fibers from OVX animals than from SHAM animals. In the OVX model, others have reported no difference in basal glucose uptake compared to SHAM animals (115); while in the ob/ob model of obesity basal skeletal muscle glucose uptake is reduced compared to control animals (54). As serum starvation has been reported to reduce basal rates of glucose transport into muscle (150), it is possible that the higher basal glucose uptake in OVX fibers compared to SHAM reflects and inability to metabolically adapt to changes in substrate availability. In SHAM skeletal muscle fibers, omental adipocyte co-culture blunted the increase in insulin-induced glucose uptake. In the control OVX skeletal

143

muscle fibers, and SHAM fibers following omental adipocyte co-culture, the impaired insulin-induced glucose uptake was associated with elevated muscle fiber lipid content. Currently, two prevailing hypotheses exist for explaining lipid-mediated impairment of skeletal muscle glucose uptake in response to insulin. The Randle hypothesis (Glucose-Fatty Acid Cycle) postulates that increased fatty acid oxidation in response to elevated fatty acid exposure impairs glucose flux through glycolysis resulting in attenuated glucose uptake (221). In addition and more recently, the theory of lipotoxicity suggests that impaired capacity for fatty acid oxidation results in the accumulation of lipid products such as diacylglycerol (DAG) and ceramide (131, 174), which can impair insulin-induced glucose uptake in skeletal muscle by interfering with insulin signal transduction (45, 131). With the exception of the SHAM inguinal co-culture, the data in this study demonstrate reductions in insulin-induced glucose uptake in the muscle fibers when lipid storage is high which suggests that lipotoxicity is a potential contributor. In support of this in the OVX model, others have shown reduced activity of mitochondrial enzymes in skeletal muscle of OVX animals (22, 38), and additionally we have observed impaired mitochondrial oxygen consumption in skeletal muscle fibers of OVX mice compared to SHAM (unpublished data). These impairments in lipid substrate metabolism may lead to rerouting of fatty acids toward DAG and ceramide synthesis (131, 174). Therefore, it is possible that skeletal muscle lipid deposition in the OVX state impairs insulin signaling due elevated fatty acid availability that is not matched by fatty acid oxidation capacity, resulting in lipotoxicity. However, we can only speculate that lipotoxicity may be occurring in the OVX fibers, as we do not have data on DAG and ceramide content. It appears that reduced capacity for fatty acid oxidation by OVX mice

144

is mediated by reduced estrogen levels since D'Eon et al. reported 17β-estradiol treatment of OVX mice resulted in select upregulation of genes associated with fat oxidation (68). In contrast to the other conditions, SHAM fibers co-cultured with inguinal adipocytes did not exhibit impaired insulin-induced glucose uptake in spite of intramuscular lipid content equivalent to SHAM fibers following omental co-culture. This suggests that in the metabolically healthy SHAM condition, lipid content alone was not enough to predict skeletal muscle insulin resistance, an observation that is supported by findings reporting the presence of high skeletal muscle lipid content in both insulin-sensitive exercise-trained and insulin-resistant obese individuals (98, 199). It is possible that differences in the species of fatty acids released from omental versus inguinal adipocytes impacted the outcome of co-culture on skeletal muscle glucose uptake. For example, when skeletal muscle is exposed to saturated fatty acids, the biosynthesis of DAG and ceramide is elevated compared to muscle exposed to mono- and poly-unsaturated fatty acid exposure (174), therefore greater saturated fatty acid content of omental compared to inguinal adipocytes could be responsible for the divergent insulin responses in co-cultured SHAM fibers. Further, in fibers from OVX animals no effect of co-culture on glucose uptake was observed. Thus, fibers from the OVX animals display inherent insulin resistance, and may have adapted to the elevated levels of NEFA exposure *in vivo* such that no additional impairment is observed in response to adipocyte co-culture.

Based on the alterations in glucose uptake observed in SHAM and OVX fibers, we investigated the phosphorylation status of key regulators of insulin-induced glucose uptake in skeletal muscle. In response to insulin stimulation, Akt is phosphorylated by

PI3K at the Ser473 and Thr308 residues, both of which are critical for maximal Akt activity and insulin-stimulated glucose uptake via GLUT4 translocation (7). In control OVX fibers, the magnitude of Akt phosphorylation (Ser473) in response to insulin was reduced compared to SHAM fibers. This corresponds with the observations for insulin-induced glucose uptake, with impairment in control OVX fibers compared to control SHAM fibers. It is also in agreement with others reporting reduced insulin-stimulated Akt phosphorylation and glucose uptake in OVX skeletal muscle (220). In SHAM fibers, insulin-induced Akt phosphorylation (Ser473) was lower following omental and inguinal co-culture compared to SHAM control. As hypothesized, SHAM omental co-culture resulted in impaired insulin-stimulated Akt phosphorylation coupled with attenuated glucose uptake. Interestingly, insulin-induced glucose uptake was not lower following SHAM inguinal co-culture compared to SHAM control in spite of impaired insulin-induced phosphorylation of Akt in the SHAM inguinal co-culture condition. Thus, it is possible that inguinal adipocyte exposure results in activation of an alternate insulin-sensitive pathway in SHAM skeletal muscle fibers, or perhaps a pathway completely independent of insulin. For example, activation of AMP-activated protein kinase (AMPK) is critical in mediating contraction-induced glucose uptake via phosphorylation of AS160 or TBC1D1/TBC1D4, which is also downstream of Akt and ultimately facilitates GLUT4 translocation to the plasma membrane (For review: (294)). Precedence exists for activation of AMPK independent of muscle contraction with recent reports demonstrating AMPK activation by the insulin-sensitizing adipokines adiponectin and leptin (33, 193). Thus, it is possible that adipokines released in greater quantities from inguinal SHAM adipose tissue (i.e. adiponectin, leptin) mediated the insulin

146

response via activation of AMPK, potentially facilitating GLUT4 translocation and glucose uptake downstream of Akt. However, we found no differences in adiponectin concentrations across conditions and leptin was undetectable in the co-culture media, suggesting that these adipokines were not mediating the depot-specific differences observed in SHAM co-culture. In OVX muscle fibers, the impaired Akt phosphorylation in response to insulin is likely mediated by skeletal muscle lipid deposition, however it is unclear what factors contribute to the depot-specific disconnect between Akt phosphorylation and glucose uptake following SHAM co-culture.

Another insulin-sensitive signaling protein, glycogen synthase kinase-3β (GSK-3β), which sits downstream of Akt and plays an important role in the cellular fate of glucose was examined. In response to insulin stimulation, GSK-3β is phosphorylated on the Ser9 residue by Akt, removing cellular inhibition of glycogen synthase and facilitating glycogen storage (265). In our study, ovarian hormone reduction did not impact GSK-3β phosphorylation (Ser9), as basal and insulin-stimulated phosphorylation was similar between OVX and SHAM control fibers. Following inguinal, but not omental adipocyte co-culture, OVX fibers displayed lower insulin-induced GSK-3β phosphorylation than control fibers. This same tendency was observed in SHAM inguinal co-culture, however it did not reach statistical significance (p=0.07). Others have shown reduced, GSK-3β phosphorylation in skeletal muscle when exposed to excess circulating lipid. Specifically, intralipid infusion in rats results in impaired insulin-stimulated GSK-3β phosphorylation in quadriceps muscle (85). As glucose may either be stored or metabolized upon uptake, it is possible that co-culture impacted the fate of glucose in a depot-specific fashion; however, further investigation is necessary to

147

determine the impact of co-culture on the cellular metabolism of glucose in skeletal muscle fibers.

In addition to the regulation of glycogen storage, phosphorylation of downstream substrates of Akt in response to insulin results in GLUT4 translocation to the plasma membrane, facilitating the uptake of circulating glucose (286). Here we have found no effect of either OVX or of adipocyte co-culture on the protein content of GLUT4. Some studies have reported reduced GLUT4 protein content in OVX skeletal muscle (233), while others have found no effect of OVX (115, 212). Reduced skeletal muscle GLUT4 translocation in rats following ovary removal has been reported by Rincon et al. (225), thus it is possible that impaired GLUT4 translocation, rather than total protein content, may explain alterations in glucose uptake in OVX fibers and in SHAM fibers following omental adipocyte co-culture. Therefore, measurement of total GLUT4 content is a limitation to our study, and future investigation of GLUT4 translocation should be performed to fully elucidate the impact of both OVX and adipocyte co-culture on glucose uptake.

In addition to GLUT4, HKII, the primary isoform in muscle, plays an important role in skeletal muscle glucose uptake, phosphorylating glucose to glucose-6-phosphate upon entry into the cell. The Randle hypothesis (Glucose-Fatty Acid Cycle) postulates that increased fatty acid oxidation in response to elevated fatty acid exposure impairs glucose flux through glycolysis by reducing hexokinase and/or phosphofructokinase function resulting in attenuated glucose uptake (221). We found reduced HKII protein content in OVX fibers following co-culture with both omental and inguinal adipocytes, but no effect of OVX alone, or of adipocyte co-culture on SHAM fibers. This finding is

148

likely important since heterozygous ablation of HKII in mice suppresses whole body insulin action and insulin-stimulated skeletal muscle glucose uptake (87). Further, in both obese and type 2 diabetic states, skeletal muscle expression of HKII is reduced in humans (55). In another co-culture model, reduced HKII mRNA expression in primary myotubes following adipocyte co-culture has also been reported (157). Interestingly, we only found significantly lower HKII protein content in OVX co-culture condition, suggesting a differential effect between SHAM and OVX. This difference in the HKII response to co-culture could be dictated by differential fatty acid release from the OVX adipocytes or increased skeletal muscle susceptibility to co-culture in the OVX group. Others have shown that long chain fatty acid acyl-CoA exposure impairs HKII activity in skeletal muscle. Specifically, exposure of human skeletal muscle to palmitoyl-CoA resulted in a 75% reduction in HKII activity compared to control (273). Further, in cardiac muscle, long chain acyl-CoA's are inhibitory to HK activity, while medium chain acyl-CoA's activate HK (261), providing support for adipocyte fatty acid composition to play a role in the outcome of co-culture on HKII. The lower HK protein content in OVX fibers following co-culture compared to OVX control would implicate the Randle hypothesis in mediating lipid-induced insulin resistance. In addition, a key part of the Randle hypothesis is the intracellular elevation in citrate levels which is the result of increased fat oxidation (221). We have observed higher citrate levels in OVX skeletal muscle compared to SHAM skeletal muscle (unpublished data), which would potentially support the Randle Cycle in the OVX animals. However, in our hands under OVX control conditions we have not observed increased lipid oxidation, thus it is likely that the Randle cycle may only be visible under the co-culture conditions. However, in spite of

149

the lower HKII protein content, we did not observe lower insulin-induced glucose uptake in OVX fibers following co-culture compared to OVX control fibers. It is possible that a co-culture period of greater than 24 hours would have impaired glucose uptake in OVX co-cultured fibers compared to OVX control fibers. At this time, additional evidence would be necessary to confirm if the Randle hypothesis of lipid-induced insulin resistance is present in the OVX co-culture model. Regardless, it is clear based on the OVX-dependent response of co-culture system that it is important to take into account changes in both ovarian hormones and adipocyte phenotype in the study of lipid-mediated insulin resistance in women.

In addition to changes in content of insulin signaling targets, activation of multiple signaling pathways in the obese state may impair insulin signal transduction. The MAPK family member p38 is a stress activated kinase with a role in signal transduction for multiple processes such as apoptosis, differentiation, proliferation, gene expression, and a more recently described role in insulin signaling (250, 306). The role of p38 in insulin signaling is controversial, with some studies reporting a positive role for p38 activity in insulin-stimulated glucose uptake (250), and others suggesting p38 activity to be inhibitory to insulin signal transduction (120). We found a tendency for elevated p38 phosphorylation (Thr180/Tyr182) in control fibers from OVX animals compared to SHAM animals ($p=0.07$). In contrast, the only other study which has investigated phosphorylation of p38 in the OVX model reported no difference in basal p38 phosphorylation between SHAM and OVX in soleus muscle (220). Further, there was a tendency for p38 phosphorylation to be higher in SHAM fibers following omental and inguinal co-culture than in SHAM control fibers ($p=0.07$), thus pointing to an effect

150

of co-culture on activation of p38. In support for this hypothesis, two novel adipokines, chemerin and pigment epithelium derived factor, have recently been reported to activate p38 in cultured primary human skeletal muscle cells (82, 241). In OVX control and co-cultured fibers, as well as in SHAM co-cultured fibers, the tendency for greater p38 phosphorylation was mirrored by higher muscle fiber lipid content compared to SHAM control. The potential for lipid to activate p38 is supported by the finding that lipid infusion in mice results in increased p38 phosphorylation in skeletal muscle that is coupled with skeletal muscle insulin resistance (146). In addition, with the exception of SHAM inguinal co-culture, insulin-induced glucose uptake was impaired in all conditions which exhibited a tendency for elevated p38 phosphorylation. This relationship is in-line with studies reporting elevation of p38 phosphorylation in skeletal muscle of type 2 diabetic individuals (153) and playing an inhibitory role in the regulation of insulin signaling (120). According to the theory of lipotoxicity, when skeletal muscle fiber lipid content is elevated, p38 activation may impair insulin signal transduction via IRS-1 serine phosphorylation (120). OVX control skeletal muscle fibers had impaired insulin-induced glucose uptake and a tendency for greater p38 phosphorylation compared to SHAM control fibers, which may implicate lipotoxicity in the reduced insulin responsiveness in the OVX model. Our findings demonstrate that alterations in skeletal muscle lipid content in response to OVX and to adipocyte co-culture of SHAM fibers are associated with elevated phosphorylation of p38 in the basal state, and subsequently may contribute to impaired insulin-induced glucose uptake.

Together, many of our findings suggest that the *in vitro* effects of skeletal muscle adipocyte exposure are dependent upon the *in vivo* environment from which they were

derived. For example, in control OVX fibers, insulin-induced glucose uptake was reduced compared to SHAM, and co-culture did not result in further reduction. Thus, it is possible that glucose uptake impairment in the control OVX fibers was already maximal due to the elevated skeletal muscle lipid content resulting from high levels of circulating fatty acid exposure *in vivo*. Following OVX omental co-culture, skeletal muscle fiber lipid content was significantly higher than both OVX control fibers and OVX fibers which were exposed to inguinal adipocytes; however, no differences in insulin-induced glucose uptake were observed between these conditions. While this would suggest further lipotoxicity is not occurring in the OVX fibers in response to co-culture we can't rule out the possibility that 24 hours was not a long enough duration for adipocytes to impair insulin-induced skeletal muscle fiber glucose uptake in the OVX condition, and that co-culture for a longer period of time may further impair glucose uptake in OVX fibers. Further, it is possible that a factor other than lipid may be contributing to impaired skeletal muscle insulin responsiveness in the OVX fibers. The potential influence of the *in vivo* environment on the effects of co-culture is supported by the relationship between insulin-induced glucose uptake in control fibers and insulin-induced glucose uptake following co-culture (Figure 10). In both OVX and SHAM mice, animals with control fibers having the greatest insulin-induced glucose uptake exhibited the largest attenuation in insulin-induced glucose uptake in response to omental adipocyte co-culture and vice versa.

Taken together, OVX results in skeletal muscle lipid deposition and impaired insulin responsiveness, suggesting a role for lipotoxicity in mediating the onset of insulin resistance when ovarian hormones are reduced. Based on studies utilizing ARKO and

ERKO knock out mice, as well as *in vivo* stimulation of the estrogen receptor, there is evidence that reduced estrogens may be the link between ovarian dysfunction and skeletal muscle insulin resistance (101, 118, 138, 267). However, since OVX results in multiple hormonal changes (i.e. FSH, inhibin, androstenedione, etc.) we can't rule out the contribution of other circulating factors to impaired insulin responsiveness in our model. In addition to the findings in OVX fibers, the effects of omental adipocyte co-culture on SHAM fibers also implicate ectopic lipid deposition in the development of insulin resistance. Further elucidation of the interaction between ovarian hormones, adiposity, and the skeletal muscle response to insulin is crucial considering the increased prevalence of insulin resistance and type 2 diabetes and the absence of a widely accepted treatment for females with reduced ovarian function.

Tables:

Table 5.1. Eight weeks following ovariectomy, OVX mice exhibit a significant increase in total body weight, but no change in absolute heart or liver mass. Relative to body weight, heart mass is significantly reduced in OVX animals. N = 15/group.

	SHAM (N = 15)	OVX (N = 15)
Body Weight (g)	22.18 ± 0.44	25.33 ± 0.57*
Heart (g)	0.129 ± 0.003	0.125 ± 0.003
Liver (g)	1.02 ± 0.04	1.03 ± 0.07
Heart/Body Weight	0.0058 ± 0.00016	0.00495 ± 0.00013*
Liver/Body Weight	0.0458 ± 0.0013	0.0408 ± 0.0033

Data are presented as means ± SEM.
* Indicates significantly different from SHAM ($p \leq 0.05$).

Table 5.2. Glycerol and NEFA levels from co-culture media after 1 and 24 hours.
All values are presented as the difference from the respective control condition. N = 10 per group.

	Glycerol (µg/mL)		NEFA (mmol/L)	
	1 hour	24 hours	1 hour	24 hours
SHAM omental	20.69 ± 10.36	72.17 ± 13.08 *	UD	UD
SHAM inguinal	UD	40.36 ± 15.78 *	UD	1.1E-05 ± 0.01
OVX omental	21.2 ± 14.18	85.41 ± 13.53 *	0.02 ± 0.01	0.009 ± 0.008
OVX inguinal	UD $	41.08 ± 12.57 * $	0.021 ± 0.01	0.041 ± 0.01 # ^

UD = undetectable
* Indicates significantly different from respective 1 hour value.
$ Indicates significantly different from respective OVX omental time point ($p \leq 0.05$).
# Indicates significantly different from both 1 and 24 hour SHAM omental.
^ Indicates significantly different from both 1 and 24 hour SHAM inguinal ($p \leq 0.05$).

**Table 5.3. Cytokine concentrations in media following 24 hours of co-culture (pg/mL).** N = 5/group.

	SHAM Control	SHAM Omental	SHAM Inguinal	OVX Control	OVX Omental	OVX Inguinal
IL-6	354.7 ± 183.1	507.4 ± 168.1	495.4 ± 127.0	268.1 ± 130.3	748.8 ± 261.6	459.9 ± 168.7
MCP-1	2875.7 ± 479.2	2571.2 ± 364.0	2506.6 ± 112.4	2628.0 ± 837.2	2339.3 ± 278.8	2238.42 ± 223.5
Adipo	463.3 ± 35.8	2165.5 ± 196.6 *	1691.0 ± 240.2 *	416.4 ± 14.6	2260.7 ± 280.8 *	1981.5 ± 314.3 *
IP-10	UD					
TNF-α	UD					
Leptin	UD					

UD = undetectable; Adipo = Adiponectin
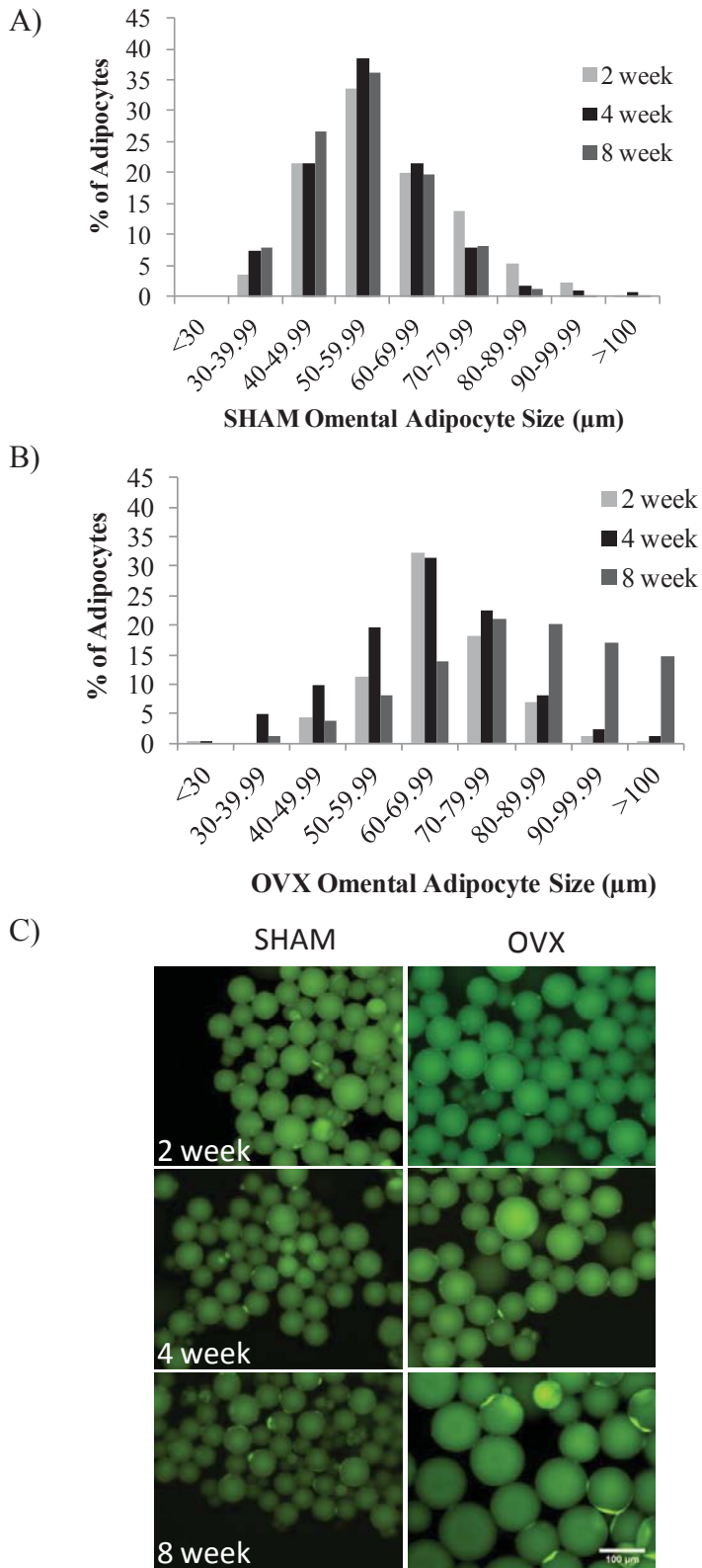* Indicates significantly different from respective control

Figure 5.1
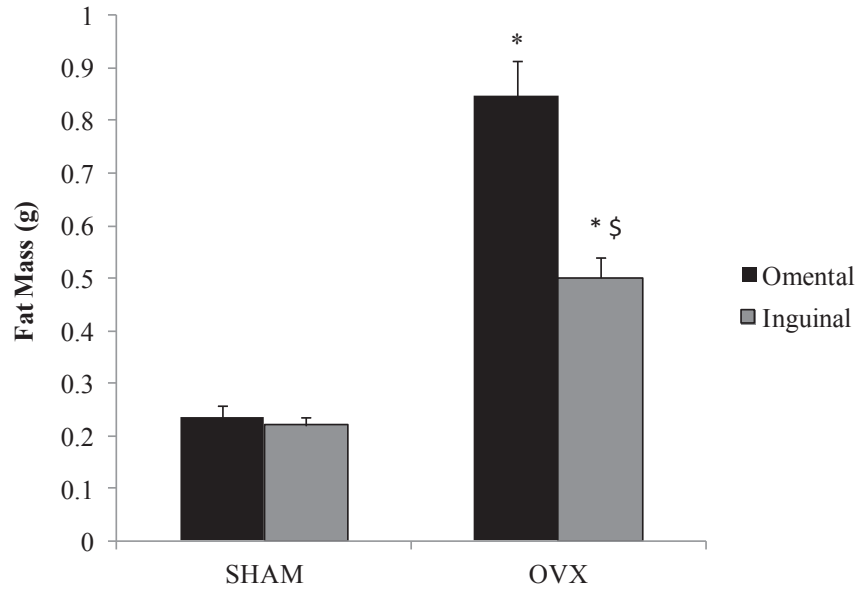
Figure 5.1: Both omental and inguinal fat mass are elevated in OVX mice eight weeks following surgery, with the omental fat mass increasing to a greater extent than the inguinal fat mass. Black bars indicate omental fat, grey bars indicate inguinal fat mass. N = 15/group.
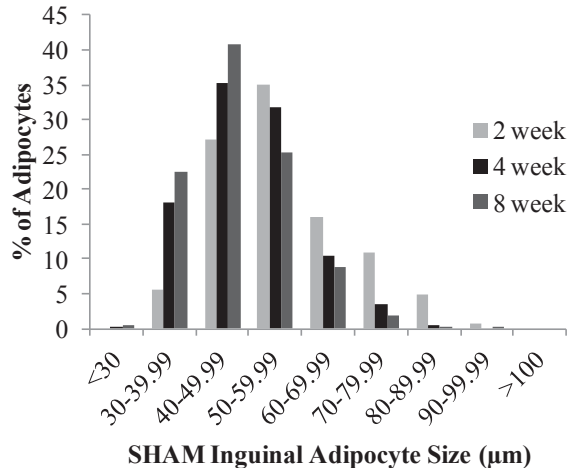* Indicates significantly different from SHAM.
$ Indicates significantly different from OVX omental (p $\leq$ 0.05).

Figure 5.2

A)

SHAM Omental Adipocyte Size (µm)

B)

OVX Omental Adipocyte Size (µm)

C)

D)

% of Adipocytes

2 week
4 week
8 week

<30 30-39.99 40-49.99 50-59.99 60-69.99 70-79.99 80-89.99 90-99.99 >100

SHAM Inguinal Adipocyte Size (μm)

E)

% of Adipocytes

2 week
4 week
8 week

<30 30-39.99 40-49.99 50-59.99 60-69.99 70-79.99 80-89.99 90-99.99 >100

OVX Inguinal Adipocyte Size (μm)

F)

SHAM   OVX

2 week

4 week

8 week

100 μm
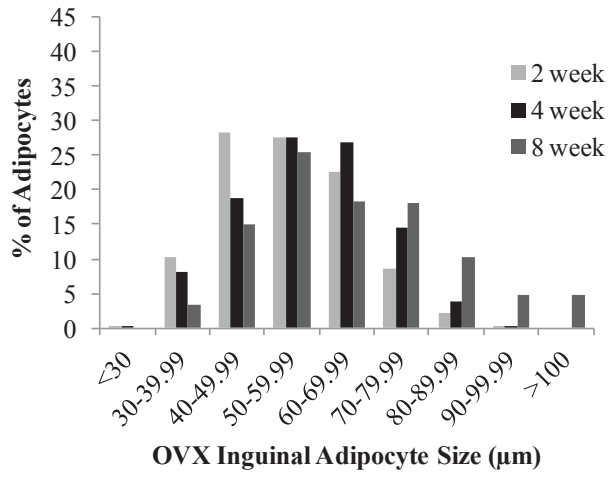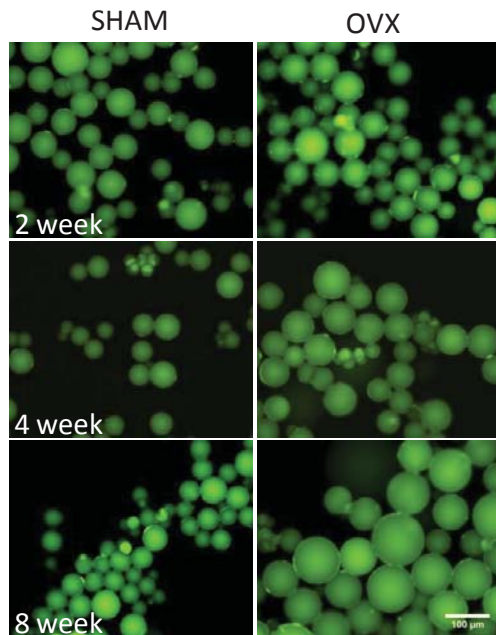
Figure 5.2 (A-F): OVX mice exhibit a rightward shift of both omental and inguinal adipocyte size distribution, indicating a greater number of large adipocytes compared to SHAM mice. Light grey bars represent the 2 week mice, dark grey bars represent the 4 week mice, and black bars represent the 8 week mice.

(A) Omental adipocyte size distribution for SHAM mice at the 2, 4 and 8 week time-points.

(B) Omental adipocyte size distribution for OVX mice at the 2, 4 and 8 week time-points.

(C) Isolated SHAM and OVX omental adipocytes stained with Bodipy 493/503 at the 2, 4, and 8 week time-points.

(D) Inguinal adipocyte size distribution for SHAM mice at the 2, 4 and 8 week time-points.

(E) Inguinal adipocyte size distribution for OVX mice at the 2, 4 and 8 week time-points.
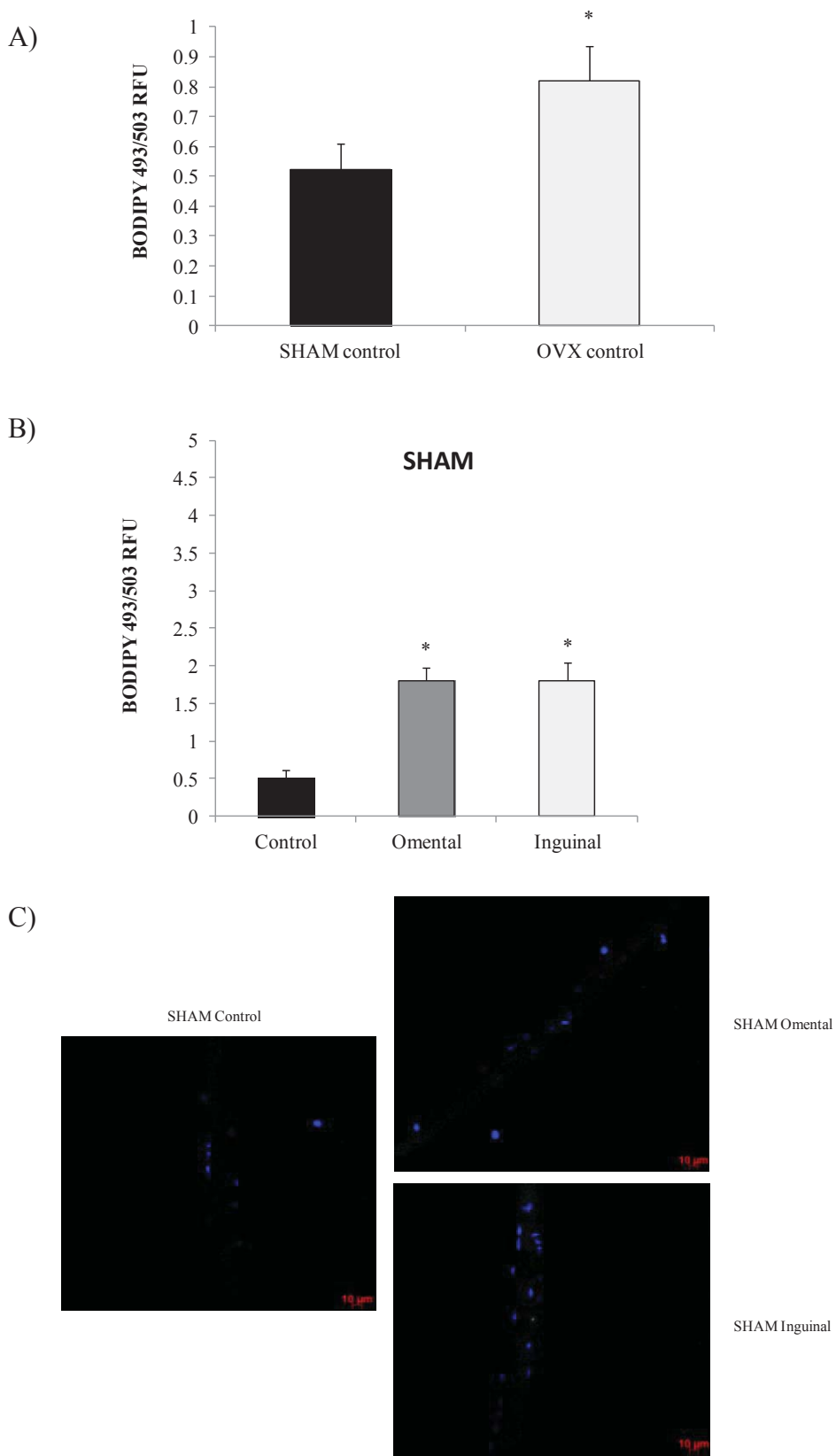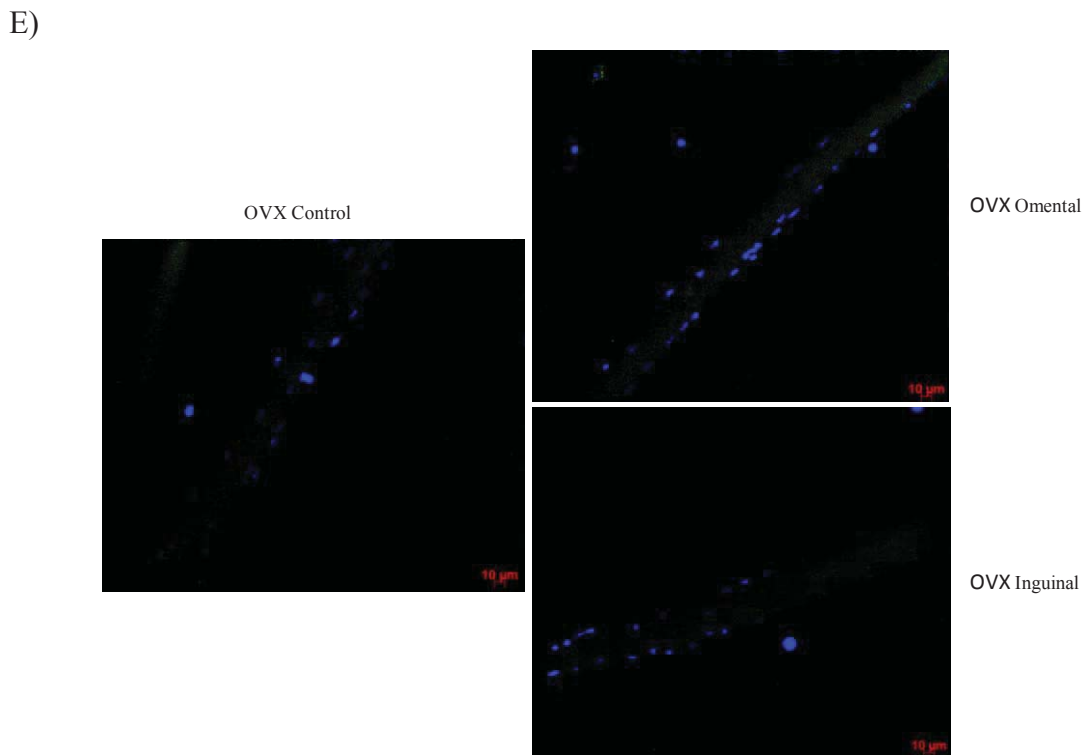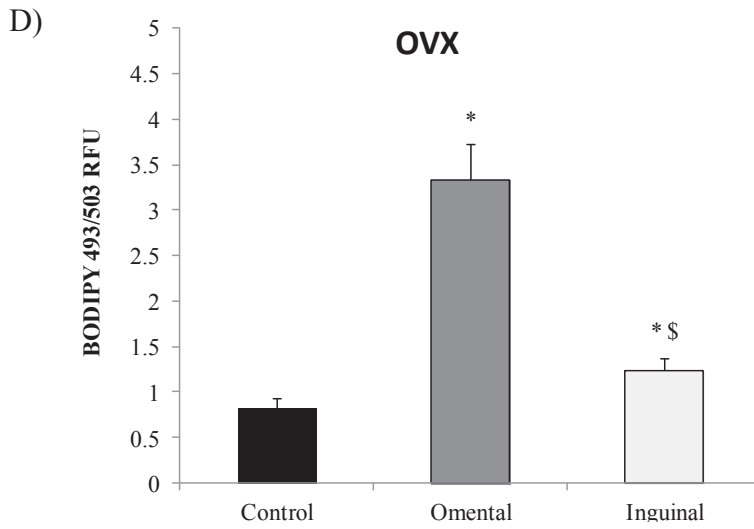
(F) Isolated SHAM and OVX inguinal adipocytes stained with Bodipy 493/503 at the 2, 4, and 8 week time-points.

Figure 5.3

A)

B)

C)

Figure 5.3 (A-E): BODIPY 493/503 stain for neutral lipid content of skeletal muscle fibers. Data are presented as relative fluorescence units (RFU). Both surface and center (6μm deep) slices were quantified, with no differences in staining between the two. Therefore, the surface and center slices were pooled in the data presented above. N = 25 fibers/group (5 fibers/animal for each condition).

(A) Skeletal muscle fiber BODIPY 493/503 fluorescence was elevated in control fibers from OVX animals compared to SHAM control fibers.

* Indicates significantly different from SHAM control ($p \leq 0.05$).

(B) Bodipy fluorescence in SHAM skeletal muscle fibers is elevated in response to both omental and inguinal adipocyte co-culture to a similar extent.

* Indicates significantly different from control ($p \leq 0.05$).

(C) Representative images of BODIPY 493/503 in SHAM skeletal muscle fibers. Images shown are maximum intensity projections (MIPs) obtained from z-stacks of the fibers. In the images, BODIPY appears as green and DAPI nuclear stain appears blue.

(D) Bodipy fluorescence in OVX skeletal muscle fibers is elevated in response to omental, but not inguinal co-culture.

* Indicates significantly different from OVX control.

$ Indicates significantly different from OVX omental ($p \leq 0.05$).

(E) Representative images of BODIPY 493/503 in OVX skeletal muscle fibers. Images shown are maximum intensity projections (MIPs) obtained from z-stacks of the fibers. In the images, BODIPY appears as green and DAPI nuclear stain appears blue.
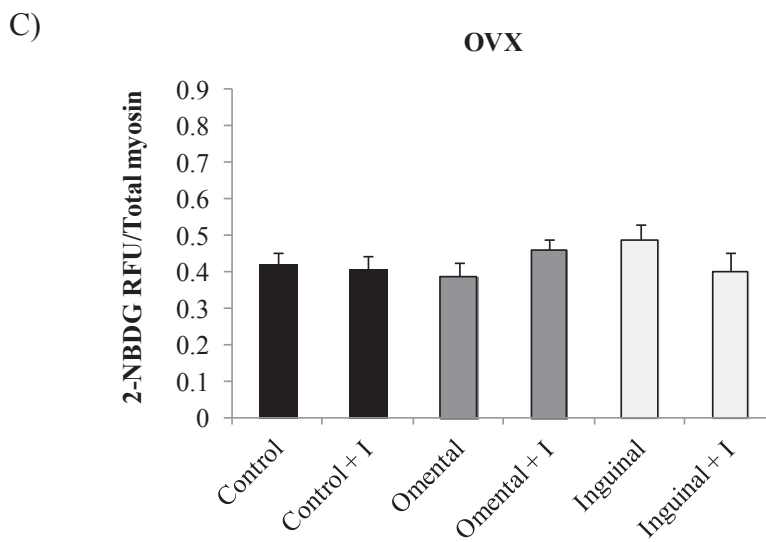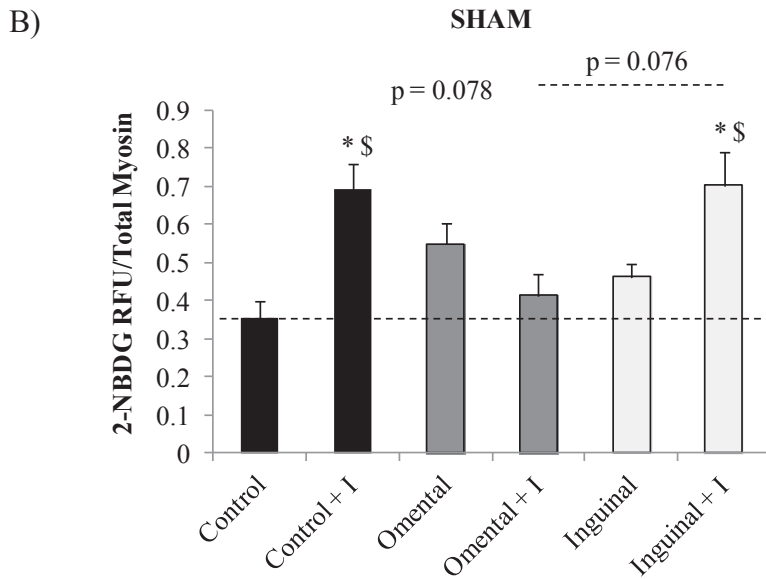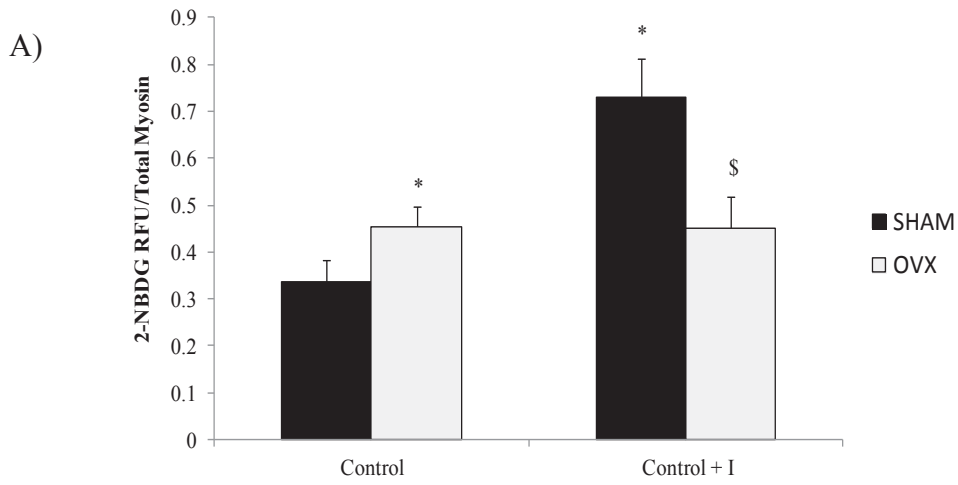
Figure 5.4

Figure 5.4 (A-C): Basal and insulin-induced (50 nM) uptake of the fluorescent glucose analog 2-NBDG in skeletal muscle fibers. Data are presented as relative fluorescence units (RFU) divided by total myosin protein content. $N = 5$/condition.

(A) The 2-NBDG response to insulin-stimulation was completely attenuated in OVX control fibers compared to SHAM control fibers.

* Indicates significantly different from SHAM control.

$ Indicates significantly different from SHAM control + I ($p \leq 0.05$).

(B) Insulin-induced 2-NBDG uptake by SHAM skeletal muscle fibers is inhibited by omental adipocyte co-culture, but not by inguinal adipocyte co-culture.

* Indicates significantly different from control.

$ Indicates significantly different from inguinal ($p \leq 0.05$).

(C) OVX fibers display impaired insulin-induced 2-NBDG uptake that was not altered by either omental or inguinal adipocyte co-culture.

Figure 5.5

A)

B)

C)
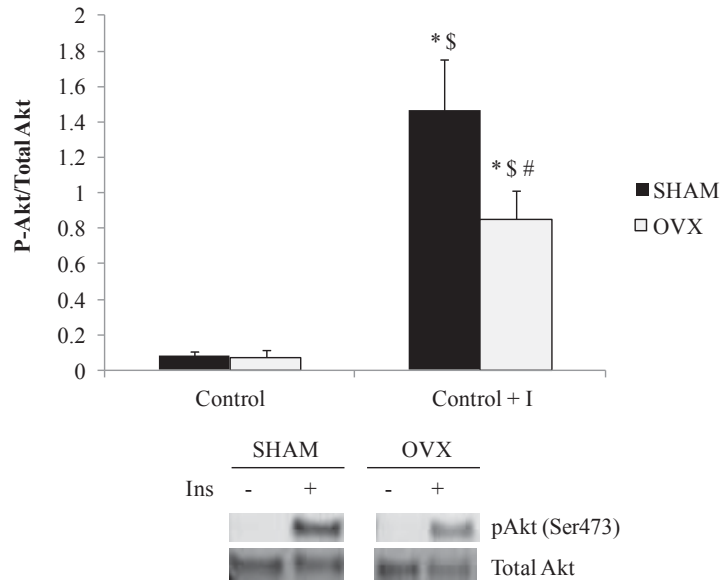
Figure 5.5 (A-C): Phosphorylation of Akt (Ser473) in skeletal muscle fibers under basal and insulin-stimulated conditions (50 nM).   Data are presented as phosphorylated Akt divided by total Akt. N = 10/condition.

(A) Akt phosphorylation in response to insulin-stimulation was significantly reduced in OVX control fibers compared to SHAM control fibers.

* Indicates significantly different from SHAM control

$ Indicates significantly different from OVX control

# Indicates significantly different from SHAM control + I ($p \leq 0.05$).

(B) In SHAM fibers, co-culture with both omental and inguinal adipocytes attenuates the phosphorylation of Akt in response to insulin to an equal extent.

* Indicates significantly different from respective basal condition.

$ Indicates significantly different from Control + I ($p \leq 0.05$).

(C) In OVX skeletal muscle fibers, neither omental nor inguinal adipocyte co-culture blunted the phosphorylation of Akt compared to the control condition.

Figure 5.6

A)

B)
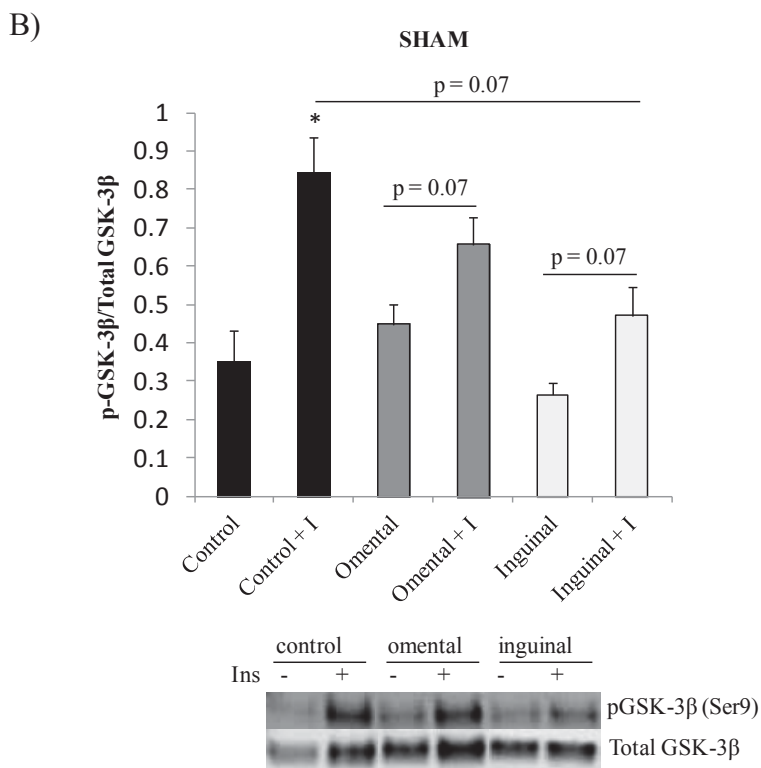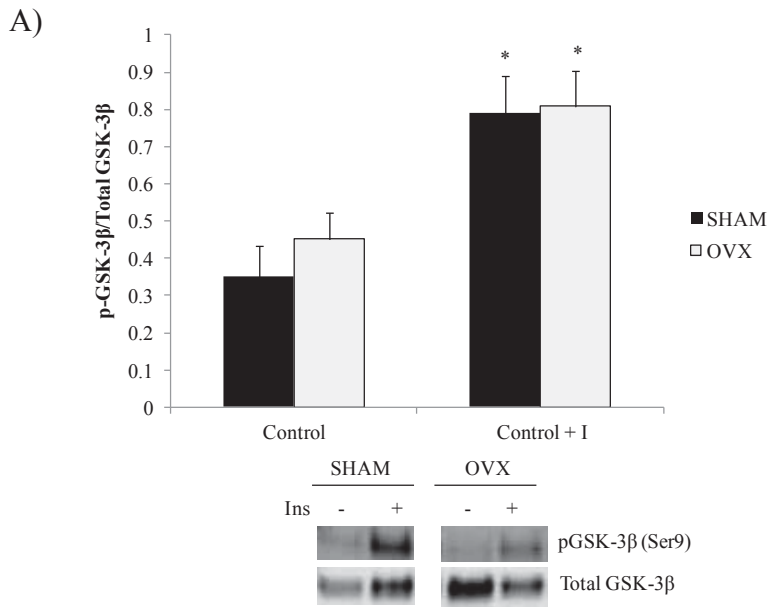
C)
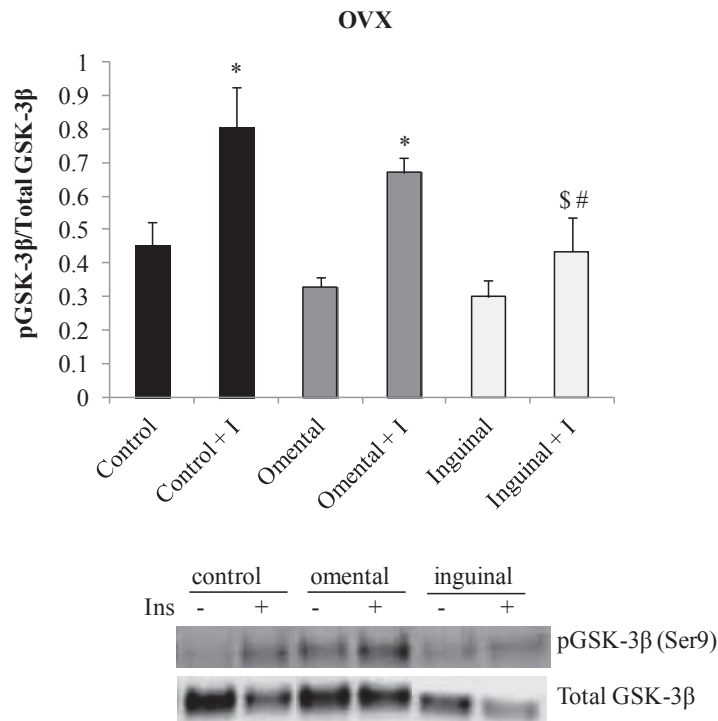
Figure 5.6 (A-C): Phosphorylation of GSK-3β (Ser9) in skeletal muscle fibers under basal and insulin-stimulated conditions (50 nM). Data are presented as phosphorylated GSK-3β divided by total GSK-3β. N = 10/condition.
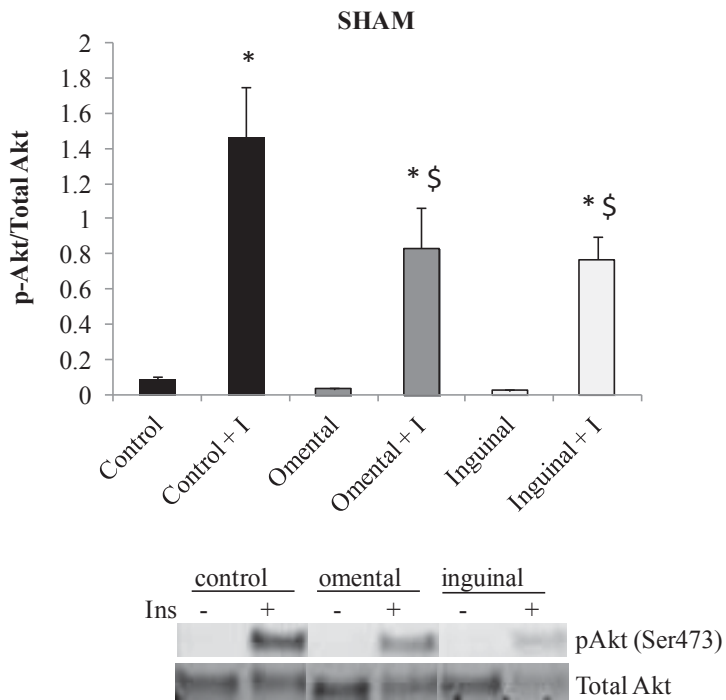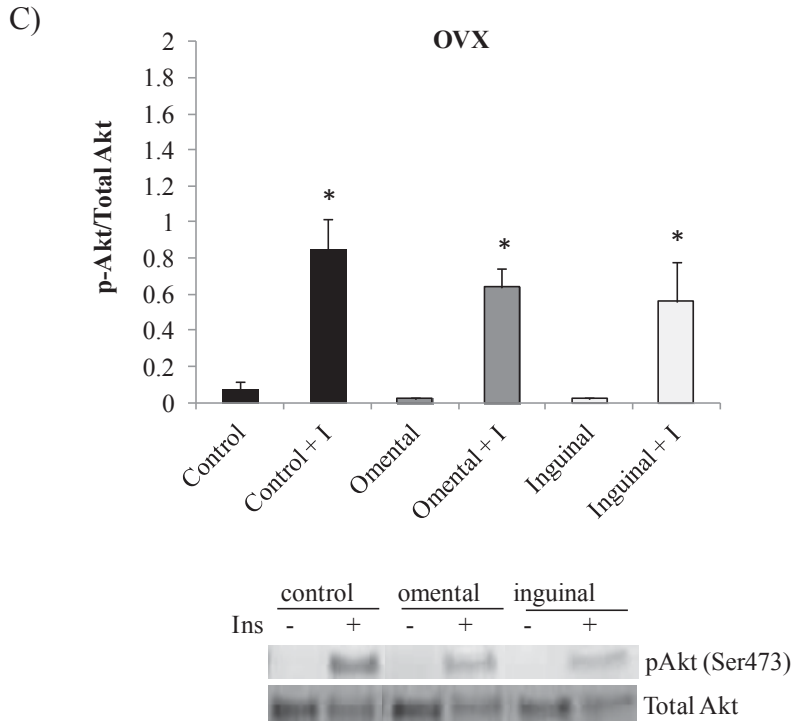(A) No difference in GSK-3β phosphorylation under basal conditions or in response to insulin stimulation was observed between SHAM and OVX control skeletal muscle fibers.
* Indicates significantly different from respective control condition ($p \leq 0.05$).
(B) In SHAM fibers, insulin stimulation increased GSK-3β phosphorylation in all conditions. The phosphorylation of GSK-3β in response to insulin was significantly reduced in fibers following inguinal adipocyte co-culture compared to control.
* Indicates significantly different from respective basal condition.
$ Indicates significantly different from Control + I ($p \leq 0.05$).
(C) Both control and omental co-culture fibers from OVX animals exhibited an increase in GSK-3β phosphorylation in response to insulin that was attenuated in fibers following inguinal adipocyte co-culture.
* Indicates significantly different from respective basal condition.
$ Indicates significantly different from Control + I.
# Indicates significantly different from Omental + I ($p \leq 0.05$).

Figure 5.7

A)

B)

C)
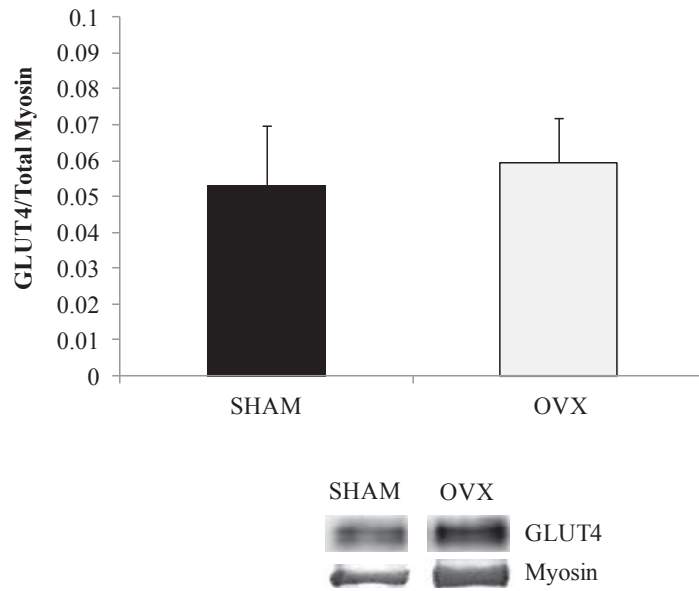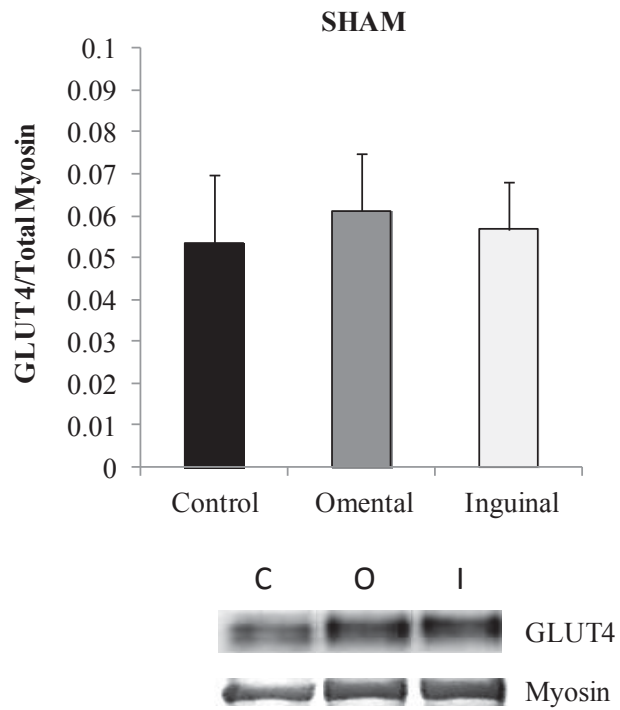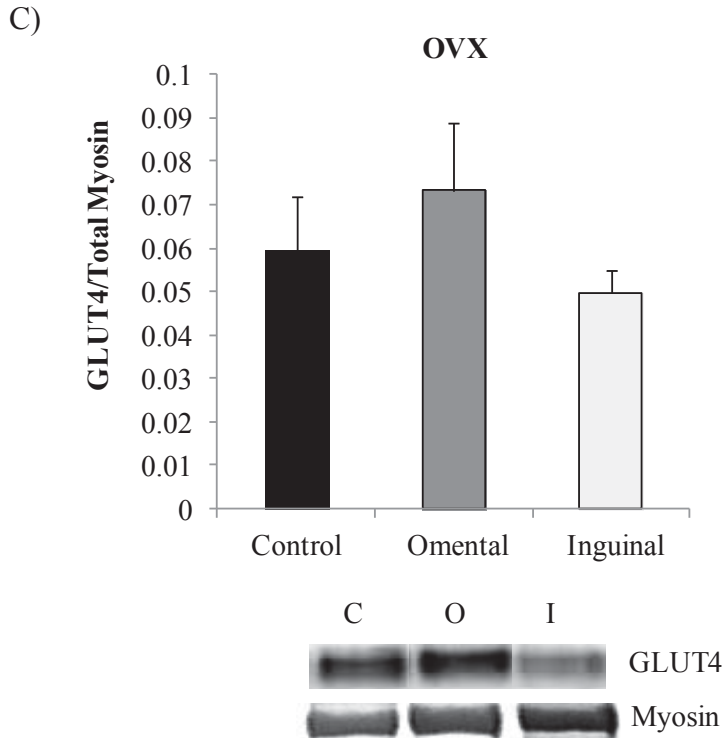
Figure 5.7 (A-C): GLUT4 protein content in skeletal muscle fibers. Data are presented as GLUT4 divided by total myosin content. GLUT4 protein content is not changed by insulin stimulation; therefore data is shown for the basal conditions only. N=10/condition.

(A) No difference in GLUT4 content was detected between SHAM and OVX control muscle fibers.

(B) GLUT4 content in SHAM skeletal muscle fibers is not altered by omental or inguinal adipocyte co-culture. For the representative blot shown below the figure, C = control, O = omental adipocyte co-culture, and I = inguinal adipocyte co-culture.

(C) GLUT4 content in OVX skeletal muscle fibers is not altered by omental or inguinal adipocyte co-culture. For the representative blot shown below the figure, C = control, O = omental adipocyte co-culture, and I = inguinal adipocyte co-culture.

Figure 5.8

B)

C)
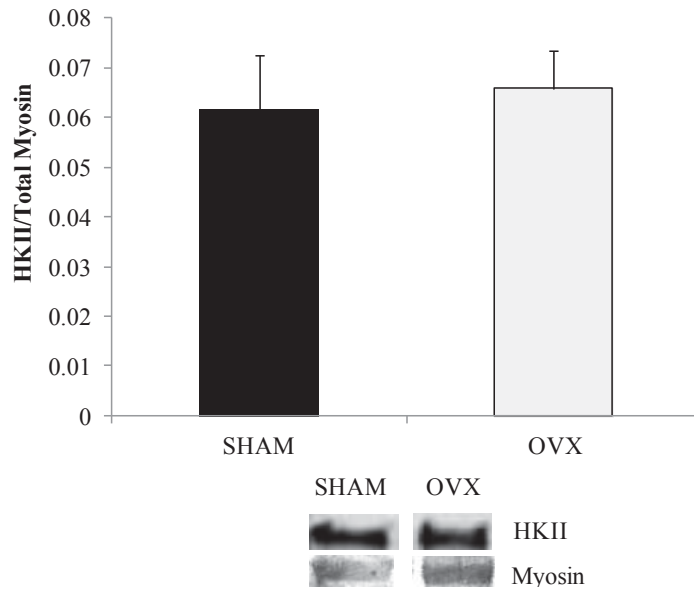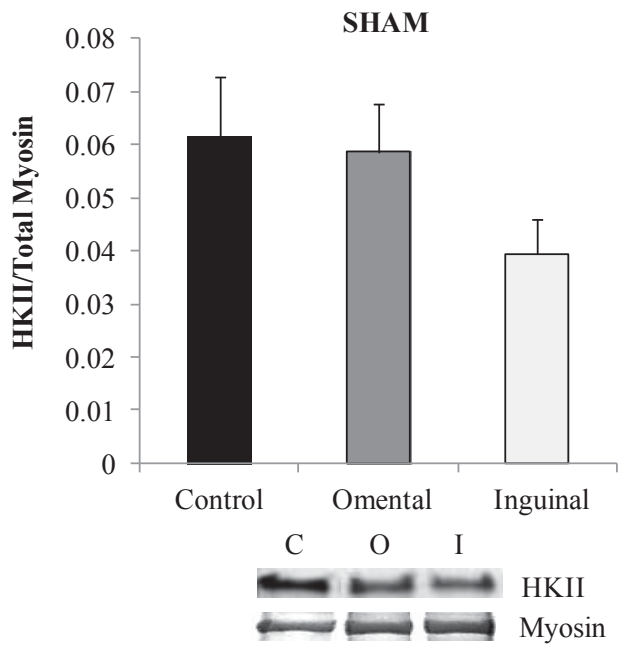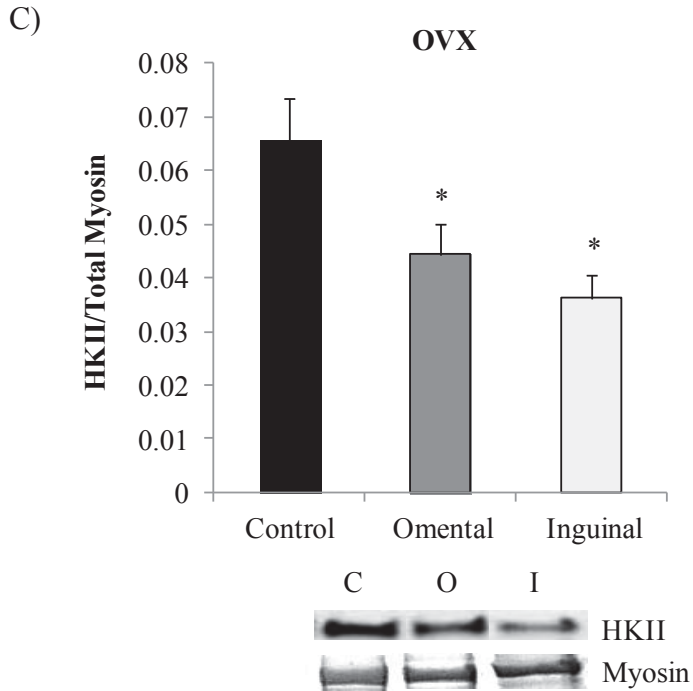
Figure 5.8 (A-C): HKII protein content in skeletal muscle fibers. Data are presented as HKII divided by total myosin content. HKII protein content is not changed by insulin stimulation; therefore data is shown for the basal conditions only. N=10/condition.
(A) No difference in HKII protein content was observed between SHAM and OVX control fibers.
(B) In SHAM skeletal muscle fibers, neither omental nor inguinal co-culture resulted in a significant change in HKII protein. For the representative blot shown below the figure, C = control, O = omental adipocyte co-culture, and I = inguinal adipocyte co-culture.
(C) In OVX skeletal muscle fibers, both omental and inguinal co-culture resulted in a significant reduction in HKII protein. For the representative blot shown below the figure, C = control, O = omental adipocyte co-culture, and I = inguinal adipocyte co-culture.
* Indicates significantly different from control ($p \leq 0.05$).

Figure 5.9

A)

B)

174

C)

OVX
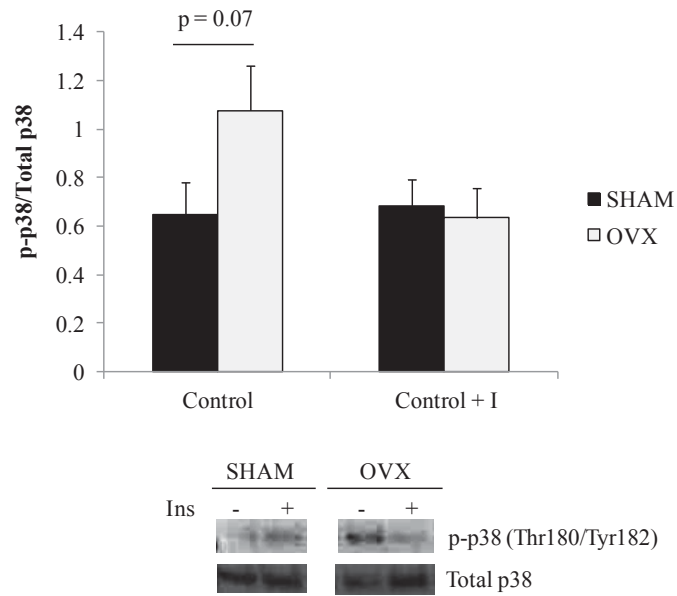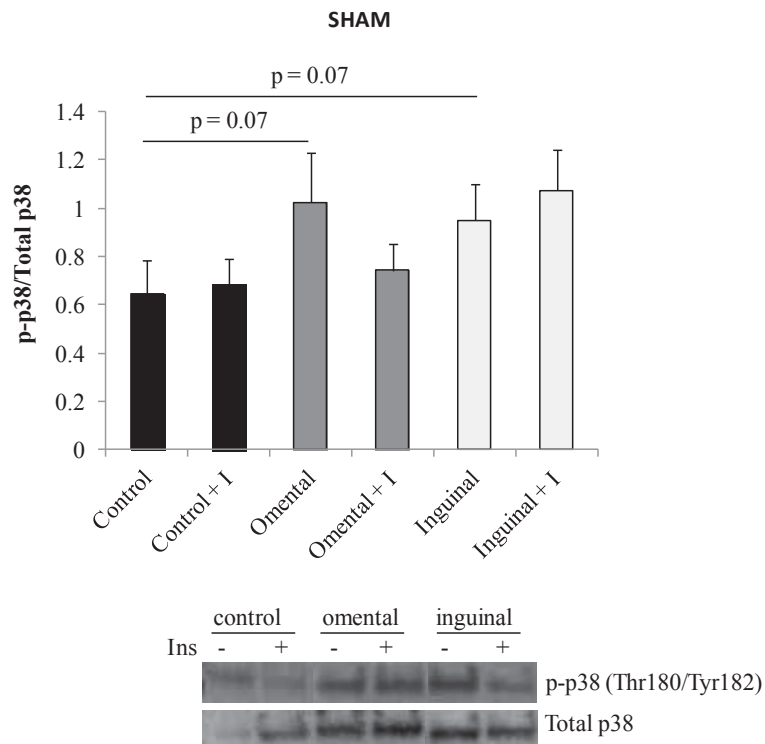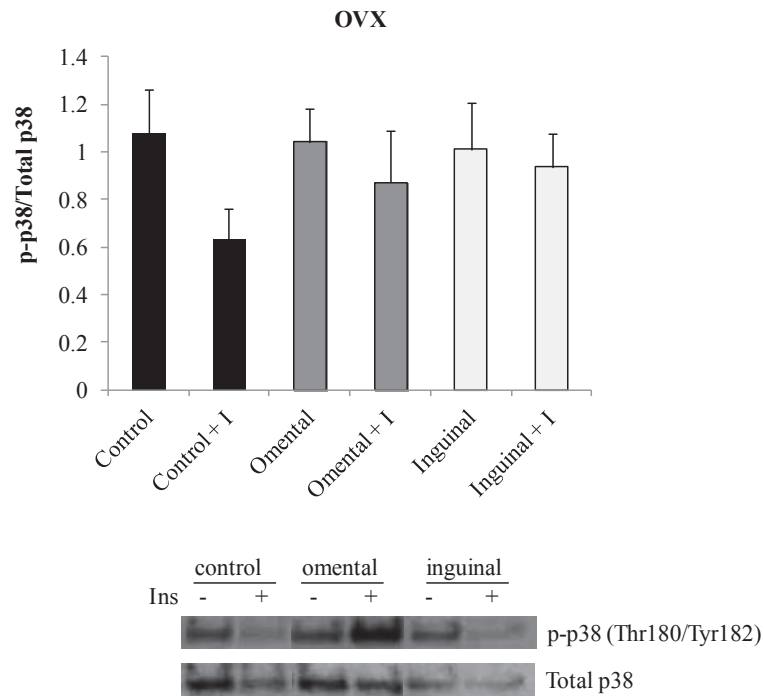
Figure 5.9 (A-C): Phosphorylation of p38 (Thr180/Tyr182) in skeletal muscle fibers under basal and insulin stimulated conditions (50 nM). Data are presented as phosphorylated p38 divided by total p38. N=10/condition.
(A) There was a tendency for phosphorylated p38 to be elevated in OVX control fibers compared to SHAM control fibers in the basal condition.
(B) In SHAM skeletal muscle fibers, no significant differences in phosphorylation of p38 were detected between conditions.
(C) In OVX skeletal muscle fibers, no significant differences in phosphorylation of p38 were detected between conditions.

Figure 5.10
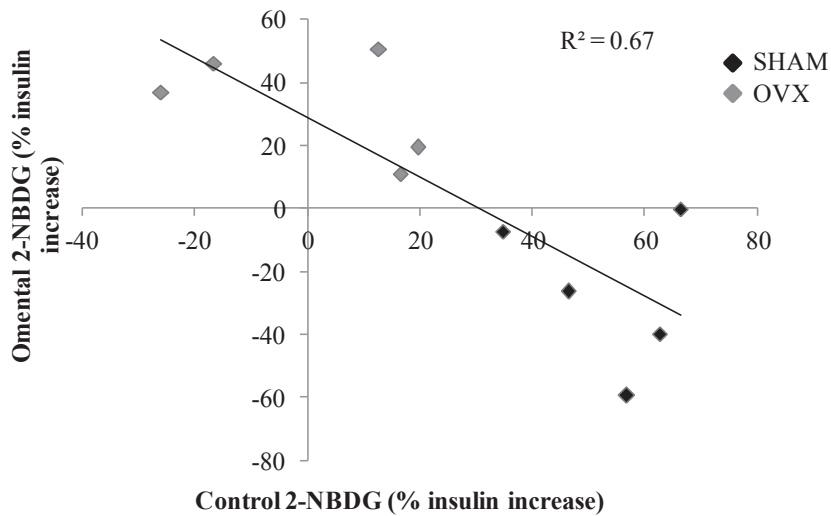
Figure 10: A moderate negative correlation was detected between control insulin-induced 2-NBDG uptake and insulin-induced 2-NBDG uptake following omental co-culture ($R^2 = 0.67$). The greater the insulin response to increase 2-NBDG uptake in control fibers, the worse the response following omental adipocyte co-culture. Light grey points indicate OVX while black points indicate SHAM.

Figure S1 (A/B)
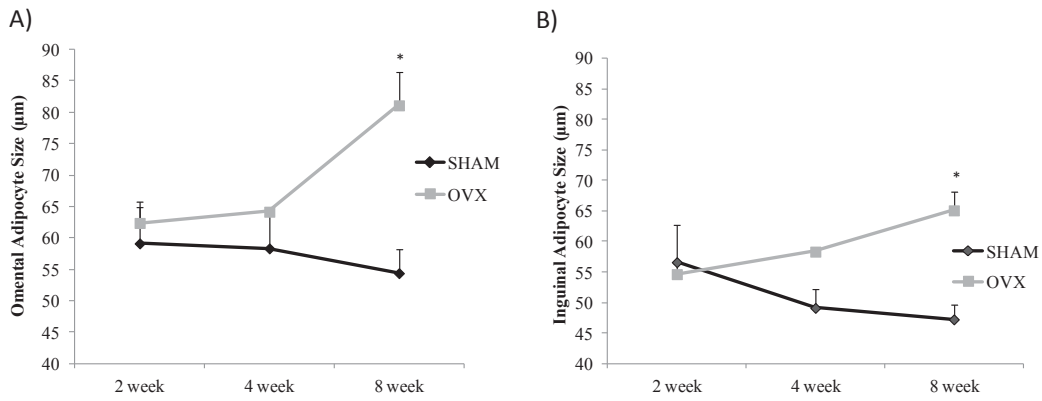
Figure S1 (A/B). Average omental (A) and inguinal (B) adipocyte size data from SHAM and OVX mice 2, 4, and 8 weeks following surgical ovariectomy or SHAM surgery. At the 8 week time point, both omental and inguinal adipocyte size was significantly greater in OVX animals compared to SHAM.
* Indicates significantly greater than SHAM ($p \leq 0.05$).

Figure S2 (A/B)

A)

B)
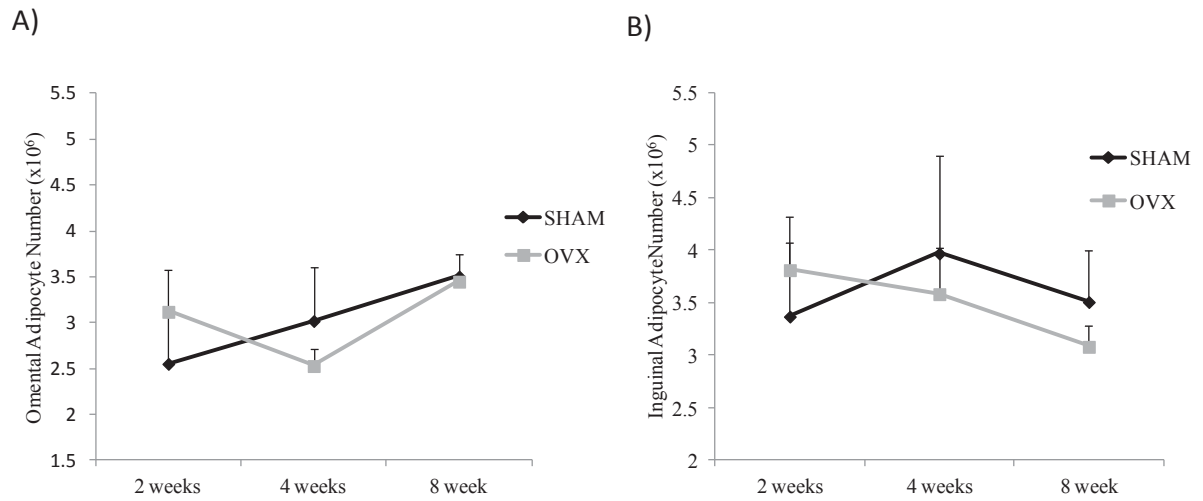
Figure S2 (A/B). No differences in omental (A) or inguinal (B) adipocyte number were detected between OVX and SHAM animals at any of the time-points. Black bars represent SHAM animals and grey bars represent OVX animals.

Chapter 6: Summary and Future Directions

Summary:

The studies contained within this dissertation have provided insight into alterations in metabolic regulation that occur under conditions of reduced ovarian hormone function. Specifically, the combined results of these three studies have demonstrated that ovarian hormone reduction results in significant visceral adiposity as a result of adipocyte hypertrophy, impaired lipolytic regulation of the adipocytes, and impaired skeletal muscle insulin responsiveness. Further, the data suggest that in the OVX animals there may development of lipotoxicity in the skeletal muscle, which is facilitated by lipid overflow from the dysfunctional adipocytes. In the first study a role for ovarian hormones in adipose tissue metabolism was demonstrated, as OVX was associated with impaired adipose tissue lipolytic regulation and elevated basal lipolysis compared to SHAM animals. In addition, many of the negative changes in adipose tissue lipolytic regulation and circulating metabolic parameters following OVX were completely attenuated by 17β-estradiol supplementation and partially attenuated by voluntary wheel running (Study #1). The data in study one suggested in OVX animals there was increased basal lipolysis coupled with a poor response to a drug that would be expected to induce lipolysis. Thus, in study two we addressed the ability of a physiological stimulus (i.e. acute exercise) to induce activation of lipolytic signaling in the SHAM and OVX mice. As expected, OVX mice exhibited impaired lipolytic activation during acute exercise, a state which should stimulate lipolysis. Specifically, in response to acute exercise adipose tissue HSL phosphorylation (Ser660) was higher than the control (sedentary) group in SHAM, but not in OVX animals. This acute exercise-

stimulated HSL phosphorylation was coupled with higher circulating glycerol levels in SHAM exercised compared to SHAM sedentary mice, but this acute exercise effect on glycerol levels was not observed for OVX animals (Study #2). The impact of OVX on adipose tissue lipolytic regulation demonstrated in Studies #1 and #2 supports a major role for adipose tissue in mediating the onset of metabolic diseases following ovarian hormone reduction. As adipose tissue phenotype is critical to whole body lipolytic regulation a third study was conducted to examine alterations in adipocyte size and number in mice following OVX. The adipose tissue expansion observed in OVX mice was determined to be mediated by increased adipocyte size, a change which may contribute to elevated basal lipolysis. Specifically, it is well documented that hypertrophic adipocytes are susceptible to lipid overflow, thus the observed adipocyte hypertrophy provides support that ectopic lipid deposition may occur when ovarian hormones levels are reduced. Further, we investigated the time-course of adipocyte alterations following OVX in both omental and inguinal adipose tissue depots. We found that OVX adipocyte size in omental and inguinal adipose tissue depots was significantly larger than SHAM 8 weeks following ovary removal. Determining the time-course of negative physiological changes, such as adipocyte hypertrophy, following OVX was critical for the next studies where we sought to examine the interaction between the adipocytes and skeletal muscle using a novel co-culture system. In isolated single skeletal muscle fibers, elevated lipid content, attenuated insulin signaling, and impaired insulin-induced glucose uptake were observed in fibers from OVX animals compared to SHAM. In OVX muscle fibers, co-culture did not further impair insulin-induced glucose uptake, while in SHAM fibers omental, but not inguinal co-culture attenuated glucose

180

uptake in response to insulin (Study #3). The findings of Study #3 suggest that the initial ectopic lipid deposition in skeletal muscle following OVX is lipotoxic, resulting in impaired insulin signal transduction and subsequent insulin-induced glucose uptake. Thus, this provides a direction for future investigation into the mechanisms which mediate the onset of insulin resistance in response to ovarian hormone dysfunction. The combined results of these studies have provided insight into changes in adipose tissue and skeletal muscle metabolic properties that may contribute to the onset of insulin resistance following a reduction in ovarian hormones (See Figure 6.1 below). These findings are of particular importance given the absence of a treatment for women with reduced ovarian hormones to prevent the onset of metabolic disease.

Limitations: One limitation to Studies #1 and #2 is that adipose tissue lipolysis was not directly measured; rather, glycerol levels were used as an indicator of lipolysis. However, while direct measurement would have been ideal, many other studies have utilized circulating glycerol levels to assess lipolysis (111, 128, 129, 137, 181, 238). Further, the first two studies measured content of lipolytic proteins in whole adipose tissue rather than isolated adipocytes. Thus, the possibility that macrophages and preadipocytes in the whole adipose tissue homogenate contributed to lipolytic protein content can't be ruled out, as both CGI-58 and ADRP in particular are observed in these cell types in addition to mature adipocytes. In addition, Study #1 and Study #2 investigated lipolytic regulation in whole adipose tissue, while Study #3 was conducted utilizing isolated adipocytes. In order to directly integrate the findings of the three

studies it would have been ideal for all to have been conducted utilizing isolated adipocytes.

For Study #3, the methods used to measure GLUT4 and HK are a potential limitation to the study. Particularly, we measured total content of GLUT4, rather than GLUT4 translocation. Reduced skeletal muscle GLUT4 translocation in rats following ovary removal has been reported by Rincon et al. (225). Thus it is possible that GLUT4 translocation, rather than total content, plays an important role in the attenuated insulin-induced glucose uptake in OVX skeletal muscle fibers and SHAM fibers following omental co-culture. Additionally, activity of HK is influenced by complex allosteric regulation, and thus total content of HK does not necessarily provide an indication of the functional consequences of OVX and adipocyte exposure. Lastly, the signaling data collected for Study #3 is all downstream of the insulin receptor, thus leaving open the possibility for reductions in insulin receptor sensitivity to be mediating the attenuation in insulin-induced glucose uptake observed in OVX skeletal muscle fibers and in SHAM fibers exposed to omental adipocytes.
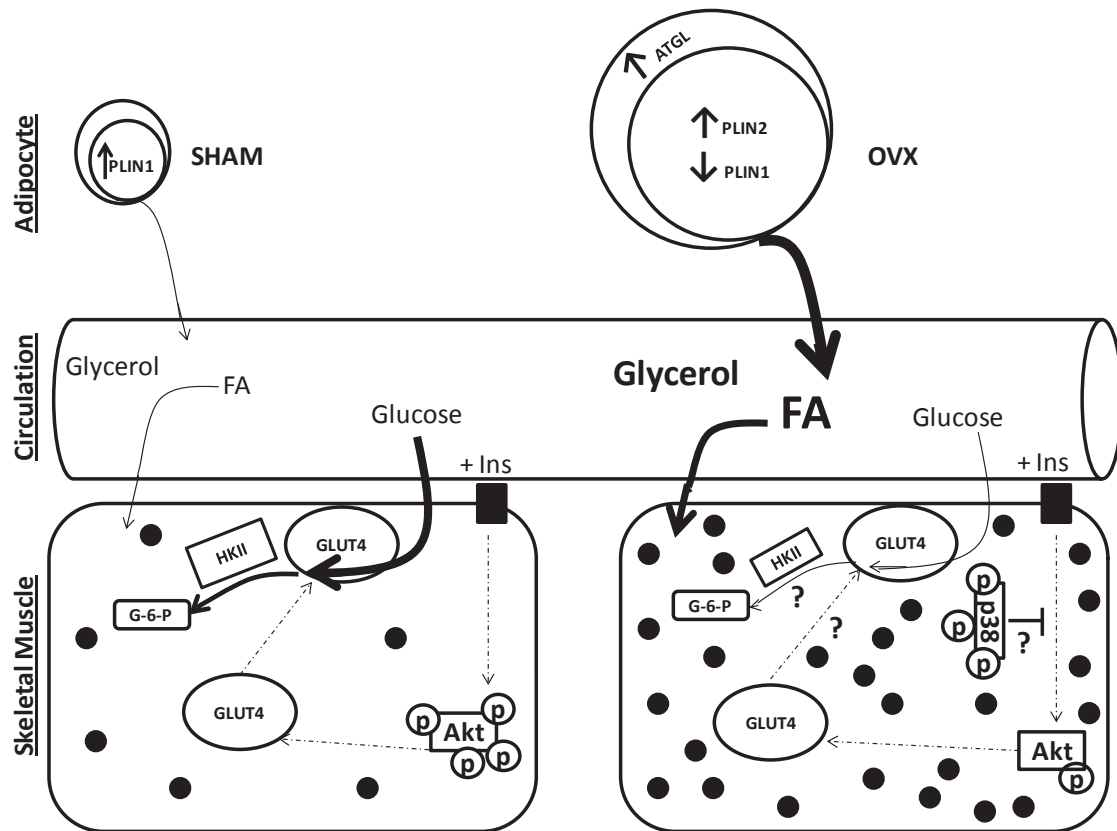
Figure 6.1. Physiological changes following OVX which contribute to skeletal muscle insulin resistance. Following ovariectomy, adipocyte expansion results in elevated adipose tissue ATGL content, coupled with changes in lipid droplet coat proteins, specifically an increase in PLIN2 and reduction in PLIN1. As adipocyte hypertrophy occurs, these changes in proteins which regulate lipolysis result in increased glycerol and fatty acid release from adipocytes into circulation as basal lipolytic rate is elevated. Ultimately, uptake of these fatty acids from circulation into skeletal muscle results in impaired insulin signal transduction and attenuated insulin-induced glucose uptake, facilitating the onset of insulin resistance.
PLIN1 = Perilipin, PLIN2 = adipose differentiation related protein, ATGL = adipose triglyceride lipase, GLUT4 = glucose transporter 4, FA = fatty acid; black circles indicate lipid droplets.

Future directions: Though these studies have provided novel insight into alterations in

adipose tissue and skeletal muscle which occur following OVX, additional questions

remain which require further investigation. Specifically, we have demonstrated that

adipose tissue expansion and adipocyte hypertrophy are associated with impaired insulin-

induced glucose uptake in skeletal muscle of OVX mice; however, it is unclear whether this association is driven by a direct effect of OVX on adipose tissue, skeletal muscle, or both. In addition, we and others have investigated a role for 17β-estradiol in mediating the metabolic changes which occur following OVX, however, the collective role of the multiple ovarian hormones which are altered by OVX has yet to be investigated. Further, we found lower insulin-induced skeletal muscle glucose uptake in fibers with high lipid content; however, the mechanisms which mediate the relationship between lipid content and insulin responsiveness remain to be determined. Lastly, depot-specific differences in the outcome of adipocyte co-culture on insulin-induced glucose uptake in SHAM fibers, and ovarian hormone status-specific differences in the outcome of co-culture on hexokinase content suggest that determination of the specific fatty acid species stored within adipocytes is critical.

Tissue specific effects of OVX – do changes in adipose tissue drive skeletal muscle insulin resistance? In multiple models of ovarian hormone dysfunction, adipose tissue expansion and insulin resistance have been reported. In our hands, ovariectomy of female mice results in expansion of omental and inguinal adipose tissue, as well as skeletal muscle lipid deposition that is coupled with impaired insulin signaling and insulin-induced glucose uptake. However, as the physiological systems within the body are complex, and ovarian hormones signal through receptors which are found in most tissues within the body, elucidation of mechanisms which are directly impacted by ovarian hormone reduction in the OVX model is extremely difficult. Specifically, it is unclear whether the onset of insulin resistance following OVX is due to changes in adipose tissue which then negatively impact skeletal muscle metabolism, to direct effects of ovarian hormone

184

reduction on skeletal muscle, or to a complex interplay between both tissues. Development of a tissue-specific estrogen receptor knock out is crucial in addressing the order of events which result in insulin resistance when ovarian hormones are reduced. For example, adipose tissue-specific knock out of the estrogen receptor may result in similar adipose tissue expansion, adipocyte hypertrophy, and elevated basal lipolysis to what we have observed in the OVX mouse. If these changes in adipocyte phenotype and function are paralleled by skeletal muscle lipid deposition and insulin resistance, it would implicate impaired estrogen action on adipose tissue as the primary factor contributing to the development of skeletal muscle insulin resistance when ovarian hormone dysfunction occurs.

Are the negative metabolic changes induced by OVX driven by reduced estrogens, or is there a complex interplay of multiple ovarian hormones that should be considered? While the use of a tissue-specific estrogen receptor knock out would prove useful in determining the direct consequences of estrogen reduction, the function of other hormones which are altered when ovarian function is compromised should be considered. Specifically, changes in follicle stimulating hormone (FSH), inhibin, and androstenedione levels occur in ovary compromised women and animal models with ovarian dysfunction. However, most studies have only investigated a role for the reduction in 17β-estradiol levels in the metabolic consequences associated with ovarian dysfunction. While these studies have provided insight, to completely understand the physiological consequences and to develop an intervention to prevent the onset of disease following ovarian dysfunction, the entire milieu of hormones which are influenced by ovarian status must be investigated. For example, it is possible that a change in the estrogen to androgen

ratio, rather than an effect of estrogen alone, is important in the regulation of adipose tissue following ovarian hormone reduction. The androgen receptor is highly expressed in preadipocytes in the visceral region, and may facilitate preferential deposition of fat in the visceral depot (i.e. omental) relative to subcutaneous depots (73, 74). It is therefore important to note that the androgen to estrogen ratio is elevated in post-menopause women relative to pre-menopausal women, with post-menopausal women exhibiting expansion of visceral adipose tissue (132). Particularly, the levels of free testosterone in post-menopausal women are highly correlated to visceral adipose tissue mass (132), further suggesting that hormonal factors other than estrogens should be considered in the study of metabolic changes in the ovary compromised state.

Does lipotoxicity mediate the effects of OVX and adipocyte exposure on skeletal muscle insulin responsiveness? In obese individuals, the capacity for oxidation of fatty acid (FA) in skeletal muscle is impaired. The reduced capacity for FA oxidation results in rerouting of FAs down other metabolic pathways, such as DAG and ceramide synthesis (131, 174). Build-up of DAG and ceramide has been implicated in the onset of insulin resistance in skeletal muscle by interfering with insulin signaling transduction (236). For instance, ceramide may inhibit activation of Akt (45), while DAG may activate protein kinase C (PKC) and nuclear factor kappa B (NF-κB) signaling, both of which interfere with IRS-1 activation (45, 131), thus impairing glucose uptake and contributing to the onset of obesity-induced insulin resistance. Here we have demonstrated an association between skeletal muscle lipid content and impaired insulin-induced glucose uptake; however, the mechanisms which mediate this association are yet to be determined. Further, DAG and

ceramide formation have not been investigated skeletal muscle following ovarian hormone reduction.

Lipid exposure has been shown to increase phosphorylation of p38, which may subsequently impair insulin signaling by facilitating IRS-1 serine phosphorylation (120). p38 has been implicated in lipotoxicity when ectopic lipid deposition in skeletal muscle is elevated in the sedentary state. It is thus of interest that we observed a tendency for greater p38 phosphorylation in OVX skeletal muscle fibers compared to SHAM, as well as a tendency for p38 to be elevated in SHAM fibers following adipocyte co-culture. To investigate a mechanistic role for p38 in attenuating insulin-induced glucose uptake it would be possible to utilize the same experimental design employed for Study #3, but with the addition of a p38 inhibitor. This would allow us to determine if activation of p38 in response to skeletal muscle lipid deposition is responsible for impaired glucose uptake. Specifically, inhibition should prevent the effect of omental adipocyte co-culture to attenuate insulin-induced glucose uptake in SHAM fibers, and may possibly reverse the impaired glucose uptake in response to insulin observed in OVX fibers.

Recently, treatment of primary human myotubes with a cAMP/PKA agonist concurrently with palmitate was reported to prevent the detrimental effects of palmitate exposure on substrate metabolism (256). Specifically, treatment with the cAMP/PKA agonist promoted complete lipid oxidation, as well as remodeling of lipid droplets for efficient storage of fatty acids. These findings support recent evidence that IMTG is not inherently lipotoxic; rather lipid-induced mitochondrial dysfunction which contributes to the build-up of other lipid-based products is responsible for the relationship between IMTG and insulin resistance. Thus, to investigate the role of lipotoxicity and

187

mitochondrial dysfunction in insulin responsiveness of OVX fibers and of SHAM fibers following omental adipocyte co-culture it would be interesting to employ the same co-culture model, with the addition of a cAMP/PKA agonist. Potentially, this cAMP/PKA agonist treatment could facilitate efficient storage and utilization of skeletal muscle lipid, thus preventing the rerouting of fatty acids toward DAG and ceramide synthesis, supporting the hypothesis that lipotoxicity mediates OVX and adipocyte co-culture induced impairments in insulin-induced glucose uptake.

Do depot- and ovarian hormone status-specific differences in adipocyte fatty acid composition exist which are critical in determining the impact of fatty acid exposure on skeletal muscle insulin responsiveness? Lastly, based on the results of Study #3, investigation of adipocyte fatty acid composition is of critical importance in determining OVX and adipocyte depot-specific responses observed in the co-culture model. Specifically, in SHAM skeletal muscle fibers, omental and inguinal adipocyte co-culture both impaired insulin signaling at the protein level, and resulted in skeletal muscle lipid deposition, but only omental co-culture impaired insulin-induced glucose uptake. And further, no differences in concentrations of known insulin-sensitizing adipokines were observed between omental and inguinal co-culture media. These findings strongly suggest a role for species of fatty acids that are found in larger quantities in adipocytes from one depot or another to impact the outcome of skeletal muscle lipid deposition on insulin-responsiveness. Further, skeletal muscle fiber HK protein content was lower following OVX, but not SHAM, adipocyte co-culture as compared to control fibers. Thus, it is also possible that changes in adipocyte fatty acid species occur in response to a

reduction in ovarian hormones, and that upon exposure, HK is sensitive to these fatty acids. Studies have reported depot-specific differences in fatty acid composition that may be altered in the obese state (91, 92). In particular, obese individuals present with elevated saturated fatty acids in omental adipose tissue compared to inguinal (91, 92). Together, our data and the current literature demonstrating depot- and obesity specific differences in fatty acid composition suggest that further investigation into depot and OVX specific adipocyte fatty acid composition of adipocytes is necessary.

Together, the findings presented within this dissertation, coupled with the future studies addressed above may provide insight into mechanisms which regulate metabolic tissue function and are altered by ovarian hormones. The elucidation of these mechanisms is critical such that an intervention may be developed to prevent the onset of disease in women experiencing ovarian hormone dysfunction.

Appendices

APPENDIX A:

Optimization of 2-NBDG
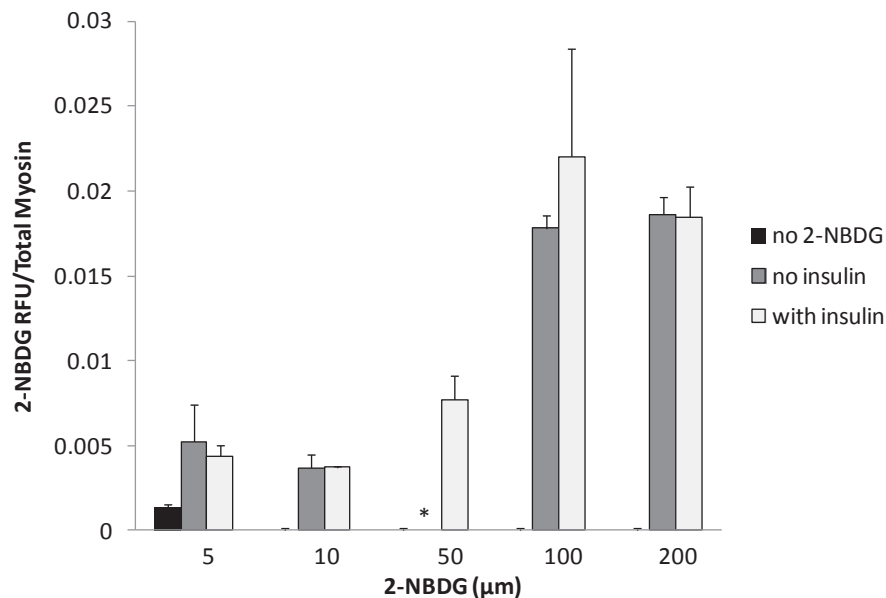
Figure A1. Optimization of 2-NBDG: dose response. N = 2 wells/condition. Insulin stimulation was with a 50 nm dose for 30 minutes to match the stimulation for the protein experiments. Insulin stimulated fibers were pretreated with insulin for 15 minutes prior to incubation with 2-NBDG plus insulin for 30 minutes (50 nm). Based on the literature, 5, 10, 50, 100, and 200 μm doses of 2-NBDG were tested, with the 50 μm dose previously reported in single muscle fibers studies. No insulin response was observed with the 5, 10, 100, and 200 μm doses.

* The samples without insulin for the 50 μm dose failed and are not included in the figure. Based on other preliminary experiments, the 50 μm dose was chosen for subsequent analyses as it was possible to detect an insulin response.
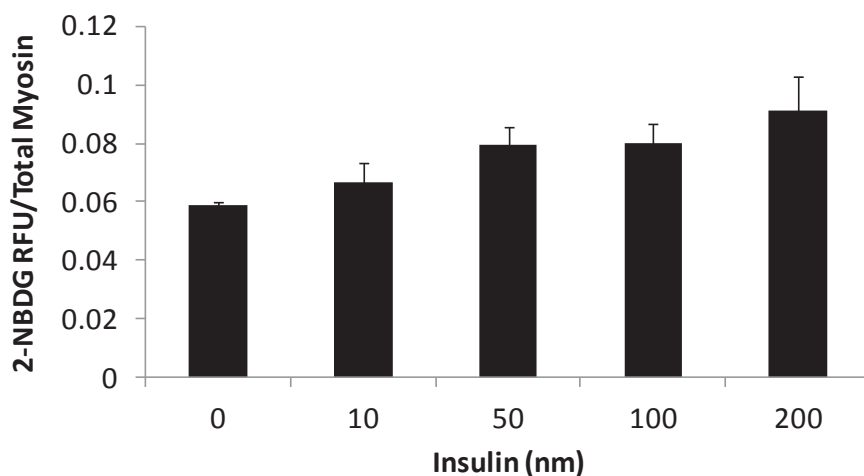
Figure A2. The effect of different insulin doses on 2-NBDG uptake was tested, with fibers exposed to either 0, 10, 50, 100, or 200 nm insulin. Fibers were pretreated with insulin for 15 minutes prior to incubation with 2-NBDG plus insulin for 30 minutes (50 nm). N = 3 wells/condition. Based on the ability to detect an insulin response, as well as on matching the insulin dose to that used for the protein analyses, a 50 nm insulin dose was selected for the 2-NBDG assay.
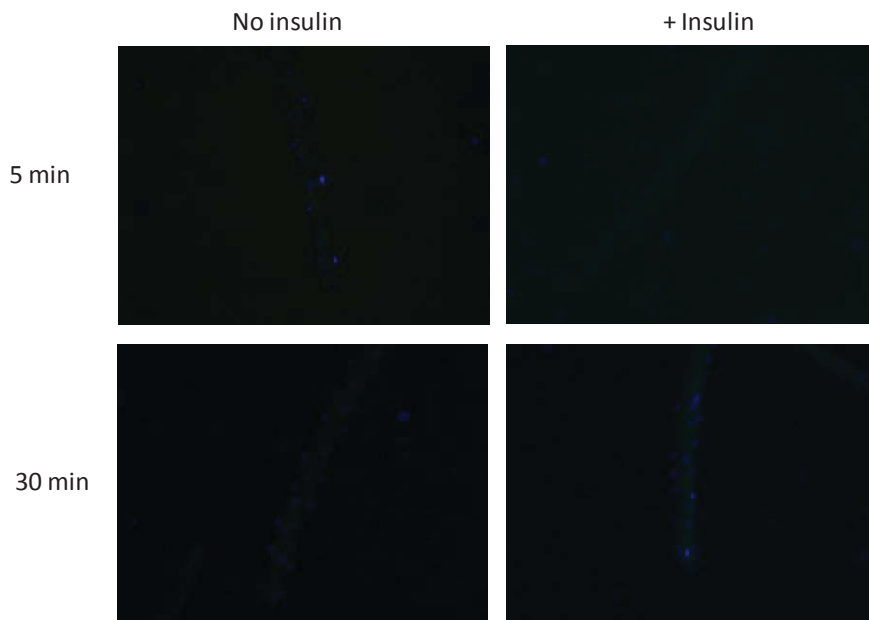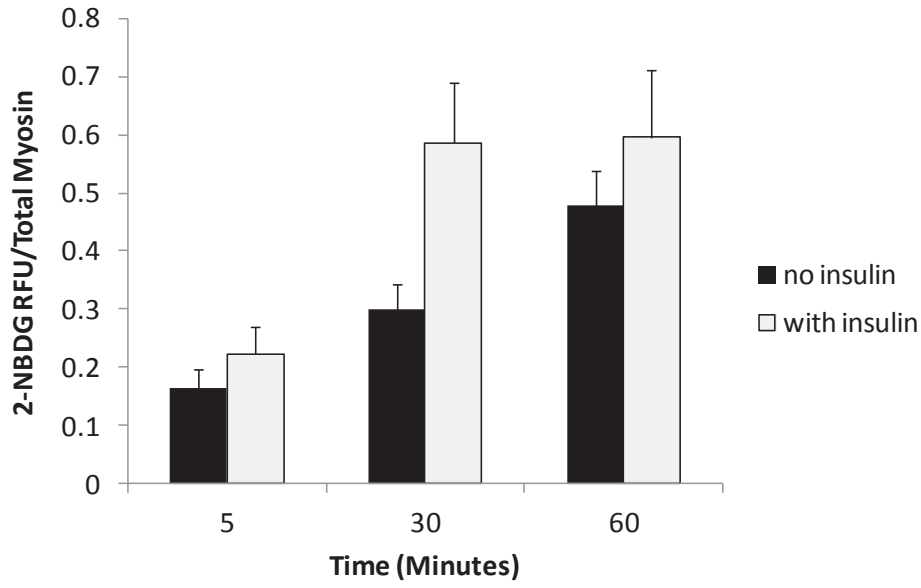
Figure A3. Time course of 2-NBDG uptake in skeletal muscle fibers. N = 8 wells/condition. Insulin stimulated fibers were pretreated with insulin for 15 minutes prior to incubation with 2-NBDG plus insulin for 30 minutes (50 nm).

(A) Basal and insulin stimulated 2-NBDG uptake were measured following 5, 30, and 60 minutes of incubation with 2-NBDG. The 30 minute time point was selected due to the ability to detect an insulin effect.

(B) The increase in 2-NBDG uptake in response to insulin was visually apparent at the 30 minute time point, but not at the 5 minute time point. The nuclei are shown in blue (DAPI), while 2-NBDG appears green.
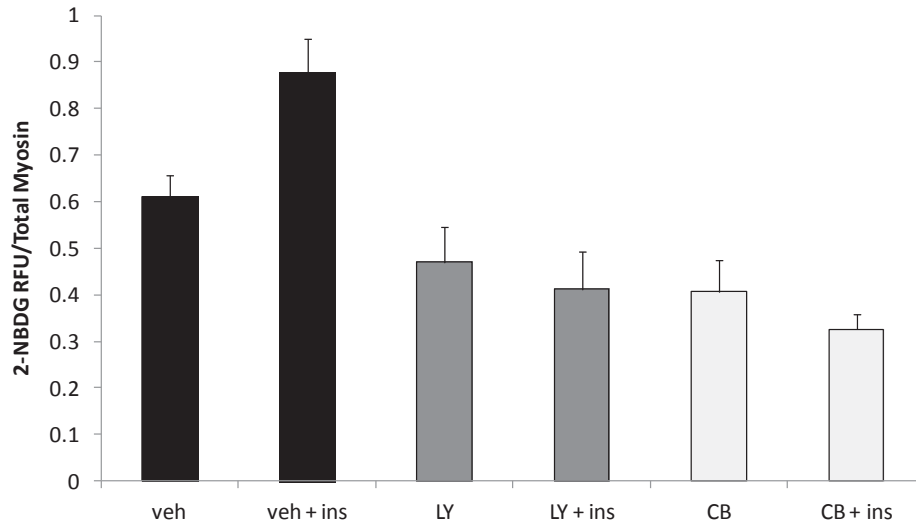
Figure A4. Treatment with both LY294002 and Cytochalasin B (CB) result in inhibition of insulin stimulated uptake of 2-NBDG in skeletal muscle fibers. N = 8 wells/condition. Insulin stimulated fibers were pretreated with insulin (50 nm) and either LY294002 (20 µM) or CB (25 µM) for 30 minutes prior to incubation with 2-NBDG plus insulin and inhibitor for an additional 30 minutes (50 nm).
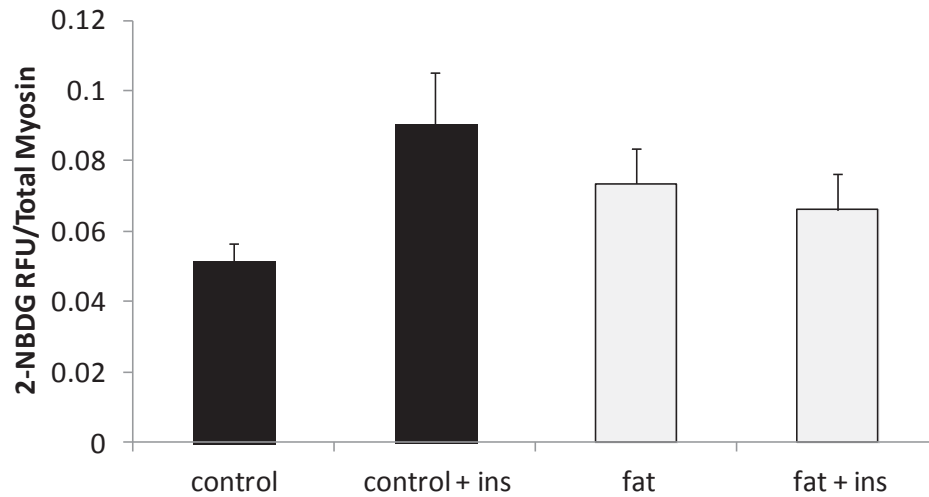
Figure A5. Fatty acid treatment attenuates insulin stimulated 2-NBDG uptake in skeletal muscle fibers. N = 8 wells/condition. Fibers were exposed to a mixture of 250 µM oleate plus 250 µM palmitate for 24 hours. Insulin stimulated fibers were pretreated with insulin for 30 minutes prior to incubation with 2-NBDG plus insulin for and additional 30 minutes (50 nm).

APPENDIX B:

Institutional animal care and use committee approval

Institutional Animal Care and Use Committee Approval

UNIVERSITY OF
MARYLAND

GRADUATE STUDIES AND RESEARCH
Institutional Animal Care & Use Committee

W. Ray Stricklin
IACUC Chair
wrstrick@umd.edu
Phone: (301)405-7044

June 17, 2010

Dr. Espen Spangenburg
Department: Kinesiology
University of Maryland
espen@umd.edu
Phone: (301)405-2450

Dr. Spangenburg,

  This letter is to inform you that on **June 17, 2010**, the members of the Institutional Animal Care & Use Committee (IACUC) reviewed and approved the protocol for:

The Role of Ovary in Metabolic Function

R-10-40

  Please note that an approved protocol is valid for three (3) years unless there is a change in the protocol. Thus, this protocol is valid until **June 17, 2013**. Federal laws indicate that protocols must be reviewed yearly. Thus, in order to keep your approved protocol active you **MUST** submit a protocol renewal/update by the first of the month of the anniversary of your approval (June 2011 & June 2012). All work extending beyond the approval date of the protocol must be submitted to the IACUC as a new protocol.

    Sincerely,

W. Ray Stricklin
Asst. Dean, College of Ag. & Natural Resources
Chair, IACUC

CC: Doug Powell, Amanda Underwood

IBC # _____

Application for
ANIMAL STUDY PROTOCOL – RESEARCH
University of Maryland, College Park, MD

Attention: Protocols are due to the IACUC Manager by the first of the month. The IACUC generally does not meet in August. Incorporate all protocol related information. For general instructions, see www.umdresearch.umd.edu/IACUC or click on Link.

Section A. Administrative Data: (Link)

1. Title of Project: The role of the ovary in metabolic function

2. Estimated Start Date: 6/1/2010   Estimated Completion Date: 05/31/2013

3. Type of Protocol. Complete each line.
    a. Initial submission [X] 3 Yr Renewal [] Modification [ ]
    b. Previous protocol number if 3 Yr renewal or Modification: NA [ ]
    c. Field Study: YES [ ]   NO [X]   If YES, attach required permits or provide
        documentation that permits are not required.
    d. Location of Research: College Park: YES [X] NO [ ]; Other-than UMD: YES [ ]
    NO [X]
    e. Location if research is conducted away from UMD: NA [X]
4. Principal Investigator.

 Name: Espen E Spangenburg, Ph.D.   Department: Kinesiology
UMD Address: 2134A SPH   Office phone: 5-2483   Lab phone: 5-4579
Fax: 5-5578   E-mail: espen@umd.edu   University Title: Assistant Professor

5. Key Personnel. List name, role*, university address, phone and e-mail.
    Lindsay Wohlers (GS) 2128 SPH Bldg kacampbe@umd.edu 301-405-4579
    Kathryn Campbell (GS) 2128 SPH Bldg lwohlers@umd.edu 301-405-4579

    * Indicate role of personnel as CO (co-investigator), CS (collaborating scientist), PD (post-doctoral)
    US (undergraduate student), GS (graduate student), T (technician).

    6.   Has or will this proposal be submitted through ORAA? YES [X] NO [ ]
    If applicable -
        a. ORAA Proposal ID number(s): unknown
        b. Title of associated proposal(s) or award(s): unknown not submitted yet
        c. Name of the PI on the proposal or award application: Espen E. Spangenburg
        d. Other key personnel supported under this proposal or award: [ ] NA

7. Funding for animal procurement and care: DRF and submitted grants
    (i.e. existing grant, pending grant, submitted grant, departmental, DRF, not yet determined,

1

199

not applicable)
Type of Grant (i.e. NIH, NSF, Other etc): not yet determined

Section B. Animal Requirements: (Link)

1. Animals. List species; age or weight at use; sex; strain, stock, common or scientific name; source; holding location (bldg) and total number.

   Species: Mouse
   Age at use: 2 months to 20 months
   Sex: Male and Female
   Strain: C57/BL6
     Stock:
   Common or Scientific Name: Mus musculus
   Source: Harlan
   Holding Location (bldg): CARF
   Total Number: 672

2. Description of Animal Usage.

   a) Approximate number of animals used each year: Detailed explanation appears below. Experiment 1 will be done over the course of 2 years. Experiment 2 will be completed in year 2 and experiment 3 in year 3.
   b) Approximate maximum number of animals on hand at any given time: ~130. This will only happen one time. Otherwise we anticipate less than 100 animals to be housed at CARF.
   c) Approximate maximum number of weeks any single animal may be housed: no more than 12 weeks

3. Number of animals by species that will be used in this study that are currently assigned to other protocols: none

4. Animal Accountability.
   a. Approximate number of rodent pups to be euthanized prior to weaning: NA [X]
   b. Approximate number of chicks to be used or euthanized immediately post-hatch: NA [X]

Section C. Transportation: (Link) NA [X]

Section D. Lay Summary: (Link)
State your study objectives and goals as they relate to the proposed use of animals. Write for nonspecialists and limit to 300 words.
       Loss of ovarian function in females is associated with the development of abdominal obesity, increased risk of type 2 diabetes, and the metabolic syndrome. Currently, we have poor understanding of how the ovary affects metabolic function of peripheral tissue. Therefore, the primary goal of this study is to delineate metabolic mechanisms that are altered when ovarian function is lost in female mice of various ages. In addition, a secondary goal will be to determine if physical activity can be used in a therapeutic sense to overcome the metabolic changes that occur with lost ovarian function.   Loss of ovarian function will be induced by either surgical ovariectomy or thoroughly weekly fulvestrant treatment. Further, two models of exercise will

2

200

performed using voluntary running wheels or a specifically designed rodent treadmill. The purpose of using the two models of exercise is to have an acute bout of exercise (treadmill) and exercise training (wheel running). Male mice will also measured to determine if any sex differences exist between the female mice that have undergone ovary ablation or fulvestrant treatment. It is expected that data obtained from these studies will improve our understanding of the influence of the ovary on mechanisms that regulate metabolic function of peripheral tissue and in addition provide additional data on the use of exercise as a therapeutic interventions for women who are experiencing loss of ovarian function.

Section E. Rationale for Animal Use: (Link)

1. Justify why animals are required over non-animal alternatives:

Due to the invasive nature of the protocol and the amount of tissue required human studies are not possible. One of the major tissues of interest in this study is the visceral fat pad, which cannot be obtained in humans without a highly specialized surgeon and an extremely invasive surgical procedure. Cell culture is also not an option since it is not possible to mimic age or exercise using cell culture models.

2. Justify appropriateness of species selected:

Mice are an appropriate species because we have shown in preliminary and published studies that using different means to disrupt the ovarian function in the mouse results in metabolic changes typically seen in humans that are post-menopausal or undergoing treatment for breast cancer. Other species of animals are not always suitable. For example, unlike the mouse, rats become hyperphagic with removal of the ovary which would add a cofounding element to our study design if we used the rat. In addition, mice are naturally strong runners in that will exercise for fairly long durations (5-10km/night) with no intervention, so mice are advantageous to our study design

3. Justify number of animals to be used:

We have determined in a priori power measure that the minimum number per group needed to maintain statistical power (0.80) for each experiment is 12 animals. For a complete breakdown of each group see section F (see below). We have broken down the whole proposal into three independent experiments for ease of reading. In experiment 1, we determine the effect of age (experiment 1) and ovary status on various biochemical based metabolic measures in adipose, liver, and skeletal muscle tissue. In addition, we will determine the effects of exercise across each age and treatment group. We will house the animals in cohorts, thus we will not have all the groups in CARF at once but instead do the study in smaller groups. In experiment 2, we determine the effect of ovary status on cellular and molecular mechanisms that regulate lipid metabolism in multiple tissues. In experiment 3, we will isolate primary cell lines from each group to determine the mechanistic function of the targets identified in experiments 1 and 2 on metabolic function in an ex vivo fashion. The total number of animals to be used is 672.

3

4. Justify duplicative research: NA [X]

Section F. Experimental Design and Animal Procedures:

1. Brief description of experimental design and animal procedures including summary table(s) of experimental groups and the number in each group: (Link)

Ovary dysfunction will be induced either through surgical removal of the ovaries or through weekly injections of fulvestrant. Ovariectomy is the most common model used to study the role of the ovary in women's health. All of the ovariectomy surgeries will be done at Harlan and the animals will then be shipped to UMD. Fulvestrant is an estrogen receptor antagonist that results in inhibition of estrogen receptors in peripheral tissue without ablation of the ovaries. It is approved for treatment of breast cancer in humans. Weekly injection of mice with fulvestrant results in increases in abdominal obesity and ovary dysfunction (see below for specifics on treatment protocol). The male mice are included as controls to determine if ovariectomy surgery or fulvestrant treatment causes the female mice to adopt a metabolic phenotype similar to male mice.

Exercise training will be accomplished through voluntary wheel running. Mice will run 5-10km/ night if exposed to a running wheel. We have 40 running wheels currently in CARF.

The acute exercise protocol will be done on a mouse specific treadmill. The animals will be placed on a treadmill and run at 15 m/min for 30 mins. This is an easy protocol for the mice and we do not anticipate any major issues. There is a mild electrical stimulus to encourage the animals to run. If we encounter a mouse that refuses to run (sits at the back of the treadmill for longer than 15-20 secs), we will remove it from the study. In our hands, we very rarely have mice that are not capable of running at this speed or duration. ==If the mice are removed from the study due to failure to run the mice will be euthanized as described in Section J.==

Three different experiments will be conducted to determine the metabolic effect of lost ovary function or estrogen receptor signaling on metabolic function of peripheral tissue. See table 1 for detail explanations (see below). We have divided the total number of animals into three distinct experiments. We need to do this because each experiment requires us to process the in completely different fashion. In experiment 1, we will perform GTT and ITT measures. In addition, we collect the necessary tissue and snap freeze the tissue. These tissues will be used for metabolomics and biochemical measures. In experiment 2, we collect the necessary tissue and snap freeze the tissue for cell signaling and gene expression measures. We are only planning to perform one age and one time point for these experiments until we can better establish our mechanistic targets. Once they are identified we will follow up in subsequent proposal to address the mechanisms across age and time. Finally, in experiment 3, we isolate the tissue from each group and isolate primary cell lines from the adipose tissue, liver tissue and skeletal muscle tissue. Using the targets we indentify in experiment 2, we will use these cultured cells to determine the critical nature of each target for the regulation of metabolic function. Due to the amount of tissue and completely different processing techniques required for each set of experiments, we will be required to repeat portions of the study three different times.

The summary table appears on the next page.

4

202

	Experiment 1		Experiment 2	Experiment 3	
	6 mo	18 mo	6 mo	6 mo	subtotal
Group 1- Control Female	12	12	12	12	48
Group 2- Control Female and Ovariectomy Surgery (2 weeks)	12	12			24
Group 2- Control Female and Ovariectomy Surgery (4 weeks)	12	12			24
Group 2- Control Female and Ovariectomy Surgery (8 weeks)	12	12	12	12	48
Group 3- Control Female and 2 weeks of Fulvestrant Treatment	12	12			24
Group 4- Control Female and 4 weeks of Fulvestrant Treatment	12	12			24
Group 5- Control Female and 8 weeks of Fulvestrant Treatment	12	12	12	12	48
Group 6- Control Male	12	12	12	12	48
Group 7- Exercised Female	12	12	12	12	48
Group 2- Chronic Exercise Female and Ovariectomy Surgery (2 weeks)	12	12			24
Group 2- Chronic Exercise Female and Ovariectomy Surgery (4 weeks)	12	12			24
Group 2- Chronic Exercise Female and Ovariectomy Surgery (8 weeks)	12	12	12	12	48
Group 9- Chronic Exercise Female and 2 weeks of Fulvestrant Treatment	12	12			24
Group 10- Chronic Exercise Female and 4 weeks of Fulvestrant Treatment	12	12			24
Group 11- Chronic Exercise Female and 8 weeks of Fulvestrant Treatment	12	12	12	12	48
Group 12- Acute Exercise Female and Ovariectomy Surgery	12	12	12	12	48
Group 13- Acute Exercise Female and 8 weeks of Fulvestrant Treatment	12	12	12	12	48
Group 14- Exercised Male	12	12	12	12	48
subtotal	216	216	120	120	
total					672

2. Administered substances other than aesthetics and analgesics. NA [ ]   (Link)
   a. List substance, dose or concentration, route, volume, frequency, site, and needle size.

Fulvestrant Treatment: Animals will be subjected to fulvestrant (Faslodex, Sigma) treatment will be intraperitoneal (IP) injected weekly at a dose of 10 mg/kg of body mass. The treatments will continue for 2, 4 or 8 weeks. IP injections will be administered using a sterile ½ inch 29 gauge needle and solutions will be sterilized before use. We have previously found that this dose is well tolerated in that mice show no outward symptoms of discomfort or stress. In addition, they eat and drink in normal fashion resulting in maintenance of their body weight during treatment.

Glucose Tolerance Test (GTT) Procedures: Circulating levels of blood glucose will be measured using a standard glucometer in a subset of animals from each group (n=7/group). We will remove food but maintain access to water 8-12 hours before the experiment. Prior to the start of the GTT the next morning, we will weigh the mice and nick the tail with a sterile scalpel blade at the very end to remove roughly 0.25 cm of the tail. A new sterile scalpel blade will be used for each mouse tested. Baseline blood glucose will be measured using a glucose meter (AlphaTRAK, Abbott Labs). A ~3 μL droplet is required for each measurement. Sterilized D-glucose (200 mg/ml, i.p.) warmed to 37°C will be injected at 2 mg/g body weight in normal saline. Blood glucose will be measured again at 30, 60, and 120 minutes by gentle massage of the tail and spotting the blood onto the glucometer strip. The first drop of blood is discarded to ensure accurate analysis of blood glucose. Mice are monitored throughout for excessive bleeding or other adverse conditions. If for

5

any reason an adverse reaction is detected the test will be discontinued and the campus veterinarian will be contacted. Following the final test, food is returned and mice are monitored for 2 hours to assure complete recovery. ==We will keep a written log of all times food is removed and returned to the animals.==

Insulin Tolerance Test (ITT) Procedures: Circulating levels of blood glucose will be measured using a standard glucometer in a subset of animals from each group (n=7/group). We will remove food for 6 hrs prior to experiment but <u>maintain access to water</u>. Prior to the start of the ITT the next morning, we will weigh the mice and nick the tail with a sterile scalpel blade at the very end to remove roughly 0.25 cm of the tail. A new sterile scalpel blade will be used for each mouse tested. Baseline blood glucose will be measured using a glucose meter (AlphaTRAK, Abbott Labs). A ~3 μL droplet is required for each measurement. Animals will then receive 0.75U/kg body weight (approximately 11 units) of bovine insulin (Sigma) via intraperitoneal injection. Intraperitoneal injections will be administered once using a sterile 1/2 inch 29 gauge needle. Blood glucose will be measured again at 30, 60, and 120 minutes by gentle massage of the tail and spotting the blood onto the glucometer strip. The first drop of blood is discarded to ensure accurate analysis of blood glucose. Mice are monitored throughout for excessive bleeding or other adverse conditions. If for any reason an adverse reaction is detected the test will be discontinued and the campus veterinarian will be contacted. Following the final test, food is returned and mice are monitored for 2 hours to assure complete recovery. ==We will keep a written log of all times food is removed and returned to the animals.==

    b. List and provide justification for any non-pharmaceutical grade substances including anesthetics, analgesic and injectable euthanasia solutions that will be used. NA [X]

All anesthetics (i.e. isoflurane) are pharmaceutical grade.

3. Blood collected from live animals. NA [ ]   (Link)

    a. List method, site, volume and frequency.

       Blood will be collected for glucose tolerance tests and insulin tolerance tests via tail snip. These tests require sampling of a single drop of blood over time following an intraperitoneal injection of glucose or insulin. See above response in #2 for specifics of testing procedures.

    b. Identify if terminal bleed. N/A

    c. Will animals be anesthetized (local or general) for blood collection? YES [ ] NO [X]
       If YES, add to table under Section H.
4. Describe methods of restraint: NA [X] (Link)

5. Survival surgery: NA [X] (Link) <u>All ovariectomy surgeries will be performed at Harlan and the animals will be shipped to UMD upon recovery from the surgery.</u>

    a. Describe the surgical procedure:

.

b. Describe aseptic methods:

.

c. List who will perform the surgery and their qualifications:

d. Describe post-operative care and who will provide it: We will monitor the animals and if we see any situations where the animal appears to sick, not eating/drinking, or stressed we will immediately contact the campus veterinarian.

e. Has major survival surgery been performed on any animal prior to being placed on this study? YES [X] NO [] If yes, justify: The ovariectomy model is the most commonly used animal model to replicate menopause in the women. It is well tolerated by the mice and will be performed by experts at Harlan before being shipped to UMD. We monitor the animals and if we detect any changes in food or water consumption we contact the campus veterinarian immediately.

f. Will more than one major survival surgery be performed on any animal while on this study? YES [ ] NO [X] If yes, justify:

6. Describe anticipated resultant effects: (Link)

The anticipated resultant effects of this study are that ovariectomy and fulvestrant treatments will result in peripheral metabolic alterations that increase visceral adipose tissue mass. The end results of fulvestrant treatment are anticipated to be similar to that ovariectomy, however, the underlying mechanisms may differ. We expect to find an upregulation of cellular or molecular mechanisms that regulate fat storage in the adipose, liver, and muscle tissue after ovariectomy and fulvestrant treatments. In addition, we expect that exercise training will prevent the accumulation of lipid by either inhibition of mechanisms that regulate lipid storage or by increasing the ability of the peripheral tissue to oxidize lipid. Finally, we anticipate that the acute exercise bouts will allow us to identify the signals that initiate the therapeutic events of exercise.

7. Describe experimental and humane endpoints: (Link) Include description of pain scoring, by whom, how often, intervention criteria and method to intervene.

All animals will be euthanized and specific tissues will be collected from the animal. None of the experiments will result in any pain or distress for the animal. If animal appears to be in pain, we will remove it from the study and contact the campus veterinarian.

8. Locations (Link)

Animal Procedure	Building(s)	Room(s)
Non-survival Surgery		
Survival Surgery		
Euthanasia	SPH	2128
Tissue Harvesting	SPH	2128
Behavior Testing		
Imaging		

7

205

Other Experimental Procedures: GTT and ITT			SPH	2128
Treadmill running			SPH	2128

Section G. Pain and Distress:

1. Categorize based on the most severe procedure to which they will be subjected. (Link)

Procedure	Species	Number of animals	Category I (Minimal, transient or no pain or distress)	Category II (Pain or distress relieved by appropriate means)	Category III (Pain or distress not relieved)
Tissue Collection	Mouse	672		X	
Tail Nicks	Mouse	186	X		
Fulvestrant	Mouse	168	X		

2. Literature Search for Alternatives to Painful or Distressful Procedures: (Link) Required for procedures under Category II and III to determine if other methods are available that could reduce or eliminate pain or distress.

   a. Sources used (at least 2): PubMed; Google Scholar

   b. Date search completed: 04/10/10

   c. Years covered: 1900-2010

   d. Key words used: anesthesia mice isoflurane safety

   e. Summary of the outcome of the search including a statement that no acceptable alternatives were found or why alternatives cannot be used:

We anesthetize all our animals (n=672 for the entire study) with isoflurane (induction 4-5%, maintenance 2-3%) and remove all of the necessary tissues (visceral fat, liver, skeletal muscle, and heart) while the animal is anesthetized. Other alternatives found include using injectable cocktails. These are less advantageous for us due to the accumulation of needles and a number of these drugs are regulated by the DEA, while isoflurane is not. In addition, by using isoflurane we can control the depth and reduce the handling of the mice to ensure lower stress levels. In addition, we do not use CO2 inhalation because a number of our experimental measures require blood flow to remain intact for as long as possible before the tissue is removed. Thus, no acceptable alternatives were found for our chosen form of anesthesia.

Section H. Anesthesia and Analgesia: (Link)

1. List agent, procedure requiring agent, dose, route, and frequency.

   Anesthesia will be performed by inhalation of 4-5% isoflurane induction. After the induction, the isoflurane is lowered 2-3%.

2. Provide details on fasting prior to anesthesia, methods of monitoring anesthesia, and care during anesthesia recovery if not mentioned in Section F: NA []

Food will be removed 4-5 hours prior to anesthesia. The animals will be initially induced in an induction box and then isoflurane exposure will be maintained by using a mouse specific nose cone. The level of induction will be monitored by reflex responses to toe pinches throughout the entire process of the tissue removal. No response to a toe pinch would indicate a sufficient level of induction, if the animal exhibits a toe pinch response we not perform any procedures until the animal reaches a suitable anesthetic plane.

Section I. Biological Materials for Use in Animals: (Link)

1. Will animals be exposed to any of the following materials? This information will help to prevent introductions of infectious agents to University animals.

Animal tissue, fluids or cells   YES [ ] NO [X]

2. If YES, explain:

3. Has the material been tested for murine pathogens? YES [ ]   NO [ ]

Section J. Animal Disposition and Euthanasia: (Link)

1. Will animals be euthanized? YES [X] NO [ ]

2. Method of euthanasia: NA [ ] List agent, dose, and route.

Animals will be anesthetized via inhalation of 4-5% isoflurane gas and maintained under 2-3% isoflurane. When animals have reached and appropriate plane of anesthesia (as determined by lack of toe pinch reflex), we will remove numerous tissues (heart, liver, skeletal muscle, brain, and adipose tissue) from the mice and snap freeze the tissues. It is important that we use anesthesia since we need the tissues to be blood flow intact.   Thus, the animal will be euthanized by exsanguinations, which is a necessity since we remove the heart and diaphragm for subsequent biochemical measures.

3. Method to ensure death: NA [ ]

The tissues to be removed following anesthetization include the heart and diaphragm, such that the animals will be euthanized through exsanguination. The animals will remain anesthetized throughout the entire procedure.

4. Justification for conditionally acceptable or unacceptable methods: NA [X]

5.   Method to dispose of euthanized animals: NA [ ]
   Final disposal of euthanized animals will be performed via incineration through CARF.

6. Final disposition of animals if not euthanasia: NA [X]

Section K. Hazardous Agents: (Link)

9

207

1. Identify all hazardous agents that will be administered to animals.

	Check all that apply	List agents & Registration Document # (if applicable)
Radionuclides		
Biological Agents		
Hazardous Chemicals		
Recombinant DNA including recombinant microorganisms and transgenic animals		

2. Study conducted at Animal Biosafety Level: NA [X]

3. Describe precautions and procedures: NA [X]

4. Has approval been obtained from the Division of Environmental Safety: Yes [ ]   No [ ]

5. Identify any agents administered and expected concentration/activity that will be expelled in animal waste: NA [X]

6. Identify any agents administered and expected concentrations/activity that will be in animal tissues when the animal is euthanized/disposed: NA [X]

Section L. Special Concerns or Requirements: (Link)   None [ ]

1. Describe deviations from standard housing and animal care: None [X]

2.   Describe special equipment requirements: None [ ]

Voluntary running wheels cages will be used in certain experiments. These cages have already been purchased by Dr. Spangenburg and used in previous studies approved by the UMD IACUC. The cages are already housed at CARF. The other equipment is in the Spangenburg lab.

3. Describe deviations from standard diet including amount and frequency: None [ ]

Prior to glucose tolerance testing and insulin tolerance testing food and bedding will be removed for 6-12 hours before the test. Upon completion of the test the food will be immediately returned to them.

4. Describe water restrictions: None [X]

5. Describe phenotypes and care of any animals which may be associated with morbidity or shortened lifespan: None [X]

6. Justify any deviations from the Guide for the Care and Use of Laboratory Animals. None

10

[X]

   7. Other: None [X]

Section M. Training: (Link) To be completed for each person named in this protocol including the PI.

Name: Espen E. Spangenburg, Ph. D.
Animal activities performed on this protocol: Will assist with tissue removal and oversee the experiments
Credentials: BS, MS, Ph. D.
Experience working with each species: since 1995
Experience with animal procedures listed above: greater than 10 years
Training the individual will receive: none
Year completed UMD PI/Animal User training: 2006

Name: Lindsay M. Wohlers
Animal activities performed on this protocol: Will monitor animals throughout the study, perform all injections and tissue removal
Credentials: BS, MS
Experience working with each species: since 2007
Experience with animal procedures listed above: 2007
Training the individual will receive: No new training is necessary
Year completed UMD PI/Animal User training: 2007

Name: Kathryn M. Campbell
Animal activities performed on this protocol: Will monitor animals throughout the study, perform all injections and tissue removal
Credentials: BS MS
Experience working with each species: 2008
Experience with animal procedures listed above: 2008
Training the individual will receive: No new training is necessary
Year completed UMD PI/Animal User training: 2008

Section N. Principal Investigator Certifications and Acknowledgments:

   1. I acknowledge responsibility for the conduct of these procedures and the care of these animals.
   2. I will conduct this work with animals in accordance with the protocol as approved by the IACUC and the campus animal care and use guidelines. I will obtain approval from the IACUC before initiating any changes in the protocol.

   3. I certify that I have determined that the research proposed herein is not unnecessarily duplicative of previously reported research.

   4. I certify that all individuals working on this proposal who have significant animal contact are participating in the Laboratory Animal Handler's Medical Surveillance Program.

   5. I will maintain appropriate animal records (e.g. census, health, veterinary care, surgery, diagnostic,

11

209

treatment, etc.)

6. For Category II and III proposals, I certify that I have reviewed the pertinent scientific literature, the sources and/or databases (2 or more) as noted in Section G, and have found no alternatives to any procedures described herein which may cause more than a momentary pain or distress whether it is relieved or not.

7. I certify that the individuals listed in Section A are authorized to conduct procedures involving animals under the proposal and have attended training. (Link) Training may include but not be limited to the biology, handling and care of the species, aseptic surgical techniques, research methods that limit the use of animals or minimize distress, proper use of anesthetics and analgesics, and procedures for reporting animal welfare concerns.

Principal Investigator: Signature_____ Date _____

Section O. Concurrences: Protocol number _____ (leave blank)   (Link)

O.1. Department Chair certification of approval of resources.

Name: _____ Signature: _____ Date: _____

O.2. Division of Environmental Safety Representative:
Required for studies utilizing hazardous agents.   Required prior to approval but not at submission.

Name: _____ Signature: _____ Date: _____

Name: _____ Signature: _____ Date: _____

O.3. Facility Manager or Veterinarian certification of resource capability:

Name: _____ Signature: _____ Date: _____

Facility: _____

Section P. Approval:

Certification of review and approval by the IACUC chairperson.

Name: _____ Signature: _____ Date: _____

ARAC Approved – October 8, 2008
Revised –

12

210

Literature Cited:

1.   Clinical Guidelines on the Identification, Evaluation, and Treatment of Overweight and Obesity in Adults--The Evidence Report. National Institutes of Health. *Obes Res* 6 Suppl 2: 51S-209S, 1998.
2.   State-specific incidence of diabetes among adults--participating states, 1995-1997 and 2005-2007. *MMWR Morb Mortal Wkly Rep* 57: 1169-1173, 2008.
3.   State-specific prevalence of obesity among adults--United States, 2007. *MMWR Morb Mortal Wkly Rep* 57: 765-768, 2008.
4.   Vital signs: state-specific obesity prevalence among adults --- United States, 2009. *MMWR Morb Mortal Wkly Rep* 59: 951-955.
5.   **Ackland JF and Schwartz NB.** Changes in serum immunoreactive inhibin and follicle-stimulating hormone during gonadal development in male and female rats. *Biol Reprod* 45: 295-300, 1991.
6.   **Adashi EY.** The climacteric ovary as a functional gonadotropin-driven androgen-producing gland. *Fertil Steril* 62: 20-27, 1994.
7.   **Alessi DR, Andjelkovic M, Caudwell B, Cron P, Morrice N, Cohen P, and Hemmings BA.** Mechanism of activation of protein kinase B by insulin and IGF-1. *Embo J* 15: 6541-6551, 1996.
8.   **Anthonsen MW, Ronnstrand L, Wernstedt C, Degerman E, and Holm C.** Identification of novel phosphorylation sites in hormone-sensitive lipase that are phosphorylated in response to isoproterenol and govern activation properties in vitro. *J Biol Chem* 273: 215-221, 1998.
9.   **Appt SE, Kaplan JR, Clarkson TB, Cline JM, Christian PJ, and Hoyer PB.** Destruction of primordial ovarian follicles in adult cynomolgus macaques after exposure to 4-vinylcyclohexene diepoxide: a nonhuman primate model of the menopausal transition. *Fertil Steril* 86: 1210-1216, 2006.
10.   **Archuleta TL, Lemieux AM, Saengsirisuwan V, Teachey MK, Lindborg KA, Kim JS, and Henriksen EJ.** Oxidant stress-induced loss of IRS-1 and IRS-2 proteins in rat skeletal muscle: role of p38 MAPK. *Free Radic Biol Med* 47: 1486-1493, 2009.
11.   **Arner P.** Differences in lipolysis between human subcutaneous and omental adipose tissues. *Ann Med* 27: 435-438, 1995.
12.   **Asterholm IW and Scherer PE.** Enhanced metabolic flexibility associated with elevated adiponectin levels. *Am J Pathol* 176: 1364-1376.
13.   **Attie AD and Scherer PE.** Adipocyte metabolism and obesity. *J Lipid Res* 50 Suppl: S395-399, 2009.
14.   **Babaei P, Mehdizadeh R, Ansar MM, and Damirchi A.** Effects of ovariectomy and estrogen replacement therapy on visceral adipose tissue and serum adiponectin levels in rats. *Menopause Int* 16: 100-104.
15.   **Backer JM, Myers MG, Jr., Shoelson SE, Chin DJ, Sun XJ, Miralpeix M, Hu P, Margolis B, Skolnik EY, Schlessinger J, and et al.** Phosphatidylinositol 3'-kinase is activated by association with IRS-1 during insulin stimulation. *Embo J* 11: 3469-3479, 1992.
16.   **Badin PM, Louche K, Mairal A, Liebisch G, Schmitz G, Rustan AC, Smith SR, Langin D, and Moro C.** Altered skeletal muscle lipase expression and activity contribute to insulin resistance in humans. *Diabetes* 60: 1734-1742.

17.   **Balla A, Danilovich N, Yang Y, and Sairam MR.** Dynamics of ovarian development in the FORKO immature mouse: structural and functional implications for ovarian reserve. *Biol Reprod* 69: 1281-1293, 2003.

18.   **Barros RP, Gabbi C, Morani A, Warner M, and Gustafsson JA.** Participation of ERalpha and ERbeta in glucose homeostasis in skeletal muscle and white adipose tissue. *Am J Physiol Endocrinol Metab* 297: E124-133, 2009.

19.   **Bartz R, Zehmer JK, Zhu M, Chen Y, Serrero G, Zhao Y, and Liu P.** Dynamic activity of lipid droplets: protein phosphorylation and GTP-mediated protein translocation. *J Proteome Res* 6: 3256-3265, 2007.

20.   **Bastard JP, Jardel C, Bruckert E, Blondy P, Capeau J, Laville M, Vidal H, and Hainque B.** Elevated levels of interleukin 6 are reduced in serum and subcutaneous adipose tissue of obese women after weight loss. *J Clin Endocrinol Metab* 85: 3338-3342, 2000.

21.   **Bastard JP, Maachi M, Lagathu C, Kim MJ, Caron M, Vidal H, Capeau J, and Feve B.** Recent advances in the relationship between obesity, inflammation, and insulin resistance. *Eur Cytokine Netw* 17: 4-12, 2006.

22.   **Beckett T, Tchernof A, and Toth MJ.** Effect of ovariectomy and estradiol replacement on skeletal muscle enzyme activity in female rats. *Metabolism* 51: 1397-1401, 2002.

23.   **Beckman M.** Menopause Mouse 10.1126/sageke.2002.32.nw112. *Sci Aging Knowl Environ* 2002: nw112-, 2002.

24.   **Berlan M, Lafontan M, and Dang Tran L.** [Adrenergic lipolysis in human fat cells: properties and physiological role of alpha-adrenergic receptors (author's transl)]. *J Physiol (Paris)* 76: 133-146, 1980.

25.   **Beylot M, Pinteur C, and Peroni O.** Expression of the adiponectin receptors AdipoR1 and AdipoR2 in lean rats and in obese Zucker rats. *Metabolism* 55: 396-401, 2006.

26.   **Bickel PE, Tansey JT, and Welte MA.** PAT proteins, an ancient family of lipid droplet proteins that regulate cellular lipid stores. *Biochim Biophys Acta* 1791: 419-440, 2009.

27.   **Bourgeois F, Alexiu A, and Lemonnier D.** Dietary-induced obesity: effect of dietary fats on adipose tissue cellularity in mice. *Br J Nutr* 49: 17-26, 1983.

28.   **Brasaemle DL.** Thematic review series: adipocyte biology. The perilipin family of structural lipid droplet proteins: stabilization of lipid droplets and control of lipolysis. *J Lipid Res* 48: 2547-2559, 2007.

29.   **Britt KL, Drummond AE, Cox VA, Dyson M, Wreford NG, Jones ME, Simpson ER, and Findlay JK.** An age-related ovarian phenotype in mice with targeted disruption of the Cyp 19 (aromatase) gene. *Endocrinology* 141: 2614-2623, 2000.

30.   **Brooks B, Arch JR, and Newsholme EA.** Effects of hormones on the rate of the triacylglycerol/fatty acid substrate cycle in adipocytes and epididymal fat pads. *FEBS Lett* 146: 327-330, 1982.

31.   **Brown M.** Skeletal muscle and bone: effect of sex steroids and aging. *Adv Physiol Educ* 32: 120-126, 2008.

32.   **Brozinick JT, Jr., Roberts BR, and Dohm GL.** Defective signaling through Akt-2 and -3 but not Akt-1 in insulin-resistant human skeletal muscle: potential role in insulin resistance. *Diabetes* 52: 935-941, 2003.

33.   **Bruce CR, Mertz VA, Heigenhauser GJ, and Dyck DJ.** The stimulatory effect of globular adiponectin on insulin-stimulated glucose uptake and fatty acid oxidation is impaired in skeletal muscle from obese subjects. *Diabetes* 54: 3154-3160, 2005.

34.   **Bruce CR, Thrush AB, Mertz VA, Bezaire V, Chabowski A, Heigenhauser GJ, and Dyck DJ.** Endurance training in obese humans improves glucose tolerance and mitochondrial fatty acid oxidation and alters muscle lipid content. *Am J Physiol Endocrinol Metab* 291: E99-E107, 2006.

35.   **Brussaard HE, Gevers Leuven JA, Frolich M, Kluft C, and Krans HM.** Short-term oestrogen replacement therapy improves insulin resistance, lipids and fibrinolysis in postmenopausal women with NIDDM. *Diabetologia* 40: 843-849, 1997.

36.   **Burns TW, Langley PE, Terry BE, Bylund DB, Hoffman BB, Tharp MD, Lefkowitz RJ, Garcia-Sainz JA, and Fain JN.** Pharmacological characterizations of adrenergic receptors in human adipocytes. *J Clin Invest* 67: 467-475, 1981.

37.   **Buzdar AU.** Advances in endocrine treatments for postmenopausal women with metastatic and early breast cancer. *Oncologist* 8: 335-341, 2003.

38.   **Campbell SE and Febbraio MA.** Effect of ovarian hormones on mitochondrial enzyme activity in the fat oxidation pathway of skeletal muscle. *Am J Physiol Endocrinol Metab* 281: E803-808, 2001.

39.   **Campbell SE, Mehan KA, Tunstall RJ, Febbraio MA, and Cameron-Smith D.** 17beta-estradiol upregulates the expression of peroxisome proliferator-activated receptor alpha and lipid oxidative genes in skeletal muscle. *J Mol Endocrinol* 31: 37-45, 2003.

40.   **Canoy D, Boekholdt SM, Wareham N, Luben R, Welch A, Bingham S, Buchan I, Day N, and Khaw KT.** Body fat distribution and risk of coronary heart disease in men and women in the European Prospective Investigation Into Cancer and Nutrition in Norfolk cohort: a population-based prospective study. *Circulation* 116: 2933-2943, 2007.

41.   **Carr MC.** The emergence of the metabolic syndrome with menopause. *J Clin Endocrinol Metab* 88: 2404-2411, 2003.

42.   **Chakrabarty K, Tauber JW, Sigel B, Bombeck CT, and Jeffay H.** Glycerokinase activity in human adipose tissue as related to obesity. *Int J Obes* 8: 609-622, 1984.

43.   **Chakraborty TR and Gore AC.** Aging-related changes in ovarian hormones, their receptors, and neuroendocrine function. *Exp Biol Med (Maywood)* 229: 977-987, 2004.

44.   **Chapados N, Collin P, Imbeault P, Corriveau P, and Lavoie JM.** Exercise training decreases in vitro stimulated lipolysis in a visceral (mesenteric) but not in the retroperitoneal fat depot of high-fat-fed rats. *Br J Nutr* 100: 518-525, 2008.

45.   **Chavez JA, Knotts TA, Wang LP, Li G, Dobrowsky RT, Florant GL, and Summers SA.** A role for ceramide, but not diacylglycerol, in the antagonism of insulin signal transduction by saturated fatty acids. *J Biol Chem* 278: 10297-10303, 2003.

46.   **Cicero AF, Magni P, Lentini P, Ruscica M, Dozio E, Strollo F, and Borghi C.** Sex hormones and adipokines in healthy pre-menopausal, post-menopausal and elderly women, and in age-matched men: data from the Brisighella Heart study. *J Endocrinol Invest* 34: e158-162.

47.   **Clegg DJ, Riedy CA, Smith KA, Benoit SC, and Woods SC.** Differential sensitivity to central leptin and insulin in male and female rats. *Diabetes* 52: 682-687, 2003.

48.   **Clifford GM, Londos C, Kraemer FB, Vernon RG, and Yeaman SJ.** Translocation of hormone-sensitive lipase and perilipin upon lipolytic stimulation of rat adipocytes. *J Biol Chem* 275: 5011-5015, 2000.

49.   **Coen PM, Dube JJ, Amati F, Stefanovic-Racic M, Ferrell RE, Toledo FG, and Goodpaster BH.** Insulin resistance is associated with higher intramyocellular triglycerides in type I but not type II myocytes concomitant with higher ceramide content. *Diabetes* 59: 80-88.

50.   **Colditz GA, Willett WC, Stampfer MJ, Manson JE, Hennekens CH, Arky RA, and Speizer FE.** Weight as a risk factor for clinical diabetes in women. *Am J Epidemiol* 132: 501-513, 1990.

51.   **Coleman RA and Lee DP.** Enzymes of triacylglycerol synthesis and their regulation. *Prog Lipid Res* 43: 134-176, 2004.

52.   **Combs TP, Pajvani UB, Berg AH, Lin Y, Jelicks LA, Laplante M, Nawrocki AR, Rajala MW, Parlow AF, Cheeseboro L, Ding YY, Russell RG, Lindemann D, Hartley A, Baker GR, Obici S, Deshaies Y, Ludgate M, Rossetti L, and Scherer PE.** A transgenic mouse with a deletion in the collagenous domain of adiponectin displays elevated circulating adiponectin and improved insulin sensitivity. *Endocrinology* 145: 367-383, 2004.

53.   **Cross DA, Alessi DR, Cohen P, Andjelkovich M, and Hemmings BA.** Inhibition of glycogen synthase kinase-3 by insulin mediated by protein kinase B. *Nature* 378: 785-789, 1995.

54.   **Cuendet GS, Loten EG, Jeanrenaud B, and Renold AE.** Decreased basal, noninsulin-stimulated glucose uptake and metabolism by skeletal soleus muscle isolated from obese-hyperglycemic (ob/ob) mice. *J Clin Invest* 58: 1078-1088, 1976.

55.   **Cusi KJ, Pratipanawatr T, Koval J, Printz R, Ardehali H, Granner DK, Defronzo RA, and Mandarino LJ.** Exercise increases hexokinase II mRNA, but not activity in obesity and type 2 diabetes. *Metabolism* 50: 602-606, 2001.

56.   **Danilovich N, Babu PS, Xing W, Gerdes M, Krishnamurthy H, and Sairam MR.** Estrogen deficiency, obesity, and skeletal abnormalities in follicle-stimulating hormone receptor knockout (FORKO) female mice. *Endocrinology* 141: 4295-4308, 2000.

57.   **Danilovich N, Harada N, Sairam MR, and Maysinger D.** Age-related neurodegenerative changes in the central nervous system of estrogen-deficient follitropin receptor knockout mice. *Exp Neurol* 183: 559-572, 2003.

58.   **Danilovich N, Javeshghani D, Xing W, and Sairam MR.** Endocrine alterations and signaling changes associated with declining ovarian function and advanced biological aging in follicle-stimulating hormone receptor haploinsufficient mice. *Biol Reprod* 67: 370-378, 2002.

59.   **Danilovich N, Roy I, and Sairam MR.** Emergence of uterine pathology during accelerated biological aging in FSH receptor-haploinsufficient mice. *Endocrinology* 143: 3618-3627, 2002.

60.   **Danilovich N, Roy I, and Sairam MR.** Ovarian pathology and high incidence of sex cord tumors in follitropin receptor knockout (FORKO) mice. *Endocrinology* 142: 3673-3684, 2001.

61.   **Danilovich N and Sairam MR.** Haploinsufficiency of the follicle-stimulating hormone receptor accelerates oocyte loss inducing early reproductive senescence and biological aging in mice. *Biol Reprod* 67: 361-369, 2002.

62.   **Danilovich N, Sairam MR, and Maysinger D.** The menopausal mouse: a new neural paradigm of a distressing human condition. *Neuroreport* 14: 1617-1622, 2003.

63.   **DeFronzo RA, Gunnarsson R, Bjorkman O, Olsson M, and Wahren J.** Effects of insulin on peripheral and splanchnic glucose metabolism in noninsulin-dependent (type II) diabetes mellitus. *J Clin Invest* 76: 149-155, 1985.

64.   **DeFronzo RA, Jacot E, Jequier E, Maeder E, Wahren J, and Felber JP.** The effect of insulin on the disposal of intravenous glucose. Results from indirect calorimetry and hepatic and femoral venous catheterization. *Diabetes* 30: 1000-1007, 1981.

65.   **DeFronzo RA and Tripathy D.** Skeletal muscle insulin resistance is the primary defect in type 2 diabetes. *Diabetes Care* 32 Suppl 2: S157-163, 2009.

66.   **Demark-Wahnefried W, Hars V, Conaway MR, Havlin K, Rimer BK, McElveen G, and Winer EP.** Reduced rates of metabolism and decreased physical activity in breast cancer patients receiving adjuvant chemotherapy. *Am J Clin Nutr* 65: 1495-1501, 1997.

67.   **Demark-Wahnefried W, Rimer BK, and Winer EP.** Weight gain in women diagnosed with breast cancer. *J Am Diet Assoc* 97: 519-526, 529; quiz 527-518, 1997.

68.   **D'Eon TM, Souza SC, Aronovitz M, Obin MS, Fried SK, and Greenberg AS.** Estrogen regulation of adiposity and fuel partitioning. Evidence of genomic and non-genomic regulation of lipogenic and oxidative pathways. *J Biol Chem* 280: 35983-35991, 2005.

69.   **Despres JP, Nadeau A, Tremblay A, Ferland M, Moorjani S, Lupien PJ, Theriault G, Pinault S, and Bouchard C.** Role of deep abdominal fat in the association between regional adipose tissue distribution and glucose tolerance in obese women. *Diabetes* 38: 304-309, 1989.

70.   **Diamond-Stanic MK, Marchionne EM, Teachey MK, Durazo DE, Kim JS, and Henriksen EJ.** Critical role of the transient activation of p38 MAPK in the etiology of skeletal muscle insulin resistance induced by low-level in vitro oxidant stress. *Biochem Biophys Res Commun* 405: 439-444.

71.   **Dierich A, Sairam MR, Monaco L, Fimia GM, Gansmuller A, LeMeur M, and Sassone-Corsi P.** Impairing follicle-stimulating hormone (FSH) signaling in vivo: targeted disruption of the FSH receptor leads to aberrant gametogenesis and hormonal imbalance. *Proc Natl Acad Sci U S A* 95: 13612-13617, 1998.

72.   **Dieudonne MN, Leneveu MC, Giudicelli Y, and Pecquery R.** Evidence for functional estrogen receptors alpha and beta in human adipose cells: regional specificities and regulation by estrogens. *Am J Physiol Cell Physiol* 286: C655-661, 2004.

73.   **Dieudonne MN, Pecquery R, Boumediene A, Leneveu MC, and Giudicelli Y.** Androgen receptors in human preadipocytes and adipocytes: regional specificities and regulation by sex steroids. *Am J Physiol* 274: C1645-1652, 1998.

74.   **Dieudonne MN, Pecquery R, Leneveu MC, Jaubert AM, and Giudicelli Y.** Androgen receptors in cultured rat adipose precursor cells during proliferation and

differentiation: regional specificities and regulation by testosterone. *Endocrine* 3: 537-541, 1995.

75. **Dube JJ, Amati F, Toledo FG, Stefanovic-Racic M, Rossi A, Coen P, and Goodpaster BH.** Effects of weight loss and exercise on insulin resistance, and intramyocellular triacylglycerol, diacylglycerol and ceramide. *Diabetologia* 54: 1147-1156.

76. **Dubnov-Raz G, Pines A, and Berry EM.** Diet and lifestyle in managing postmenopausal obesity. *Climacteric* 10 Suppl 2: 38-41, 2007.

77. **Duncan RE, Ahmadian M, Jaworski K, Sarkadi-Nagy E, and Sul HS.** Regulation of lipolysis in adipocytes. *Annu Rev Nutr* 27: 79-101, 2007.

78. **Eckel RH, Grundy SM, and Zimmet PZ.** The metabolic syndrome. *Lancet* 365: 1415-1428, 2005.

79. **Egan JJ, Greenberg AS, Chang MK, Wek SA, Moos MC, Jr., and Londos C.** Mechanism of hormone-stimulated lipolysis in adipocytes: translocation of hormone-sensitive lipase to the lipid storage droplet. *Proc Natl Acad Sci U S A* 89: 8537-8541, 1992.

80. **Emery EM, Schmid TL, Kahn HS, and Filozof PP.** A review of the association between abdominal fat distribution, health outcome measures, and modifiable risk factors. *Am J Health Promot* 7: 342-353, 1993.

81. **Fain JN, Madan AK, Hiler ML, Cheema P, and Bahouth SW.** Comparison of the release of adipokines by adipose tissue, adipose tissue matrix, and adipocytes from visceral and subcutaneous abdominal adipose tissues of obese humans. *Endocrinology* 145: 2273-2282, 2004.

82. **Famulla S, Lamers D, Hartwig S, Passlack W, Horrighs A, Cramer A, Lehr S, Sell H, and Eckel J.** Pigment epithelium-derived factor (PEDF) is one of the most abundant proteins secreted by human adipocytes and induces insulin resistance and inflammatory signaling in muscle and fat cells. *Int J Obes (Lond)* 35: 762-772.

83. **Ferrara CM, Lynch NA, Nicklas BJ, Ryan AS, and Berman DM.** Differences in adipose tissue metabolism between postmenopausal and perimenopausal women. *J Clin Endocrinol Metab* 87: 4166-4170, 2002.

84. **Franck N, Stenkula KG, Ost A, Lindstrom T, Stralfors P, and Nystrom FH.** Insulin-induced GLUT4 translocation to the plasma membrane is blunted in large compared with small primary fat cells isolated from the same individual. *Diabetologia* 50: 1716-1722, 2007.

85. **Frangioudakis G and Cooney GJ.** Acute elevation of circulating fatty acids impairs downstream insulin signalling in rat skeletal muscle in vivo independent of effects on stress signalling. *J Endocrinol* 197: 277-285, 2008.

86. **Fredrikson G, Tornqvist H, and Belfrage P.** Hormone-sensitive lipase and monoacylglycerol lipase are both required for complete degradation of adipocyte triacylglycerol. *Biochim Biophys Acta* 876: 288-293, 1986.

87. **Fueger PT, Lee-Young RS, Shearer J, Bracy DP, Heikkinen S, Laakso M, Rottman JN, and Wasserman DH.** Phosphorylation barriers to skeletal and cardiac muscle glucose uptakes in high-fat fed mice: studies in mice with a 50% reduction of hexokinase II. *Diabetes* 56: 2476-2484, 2007.

88.   **Fujioka S, Matsuzawa Y, Tokunaga K, and Tarui S.** Contribution of intra-abdominal fat accumulation to the impairment of glucose and lipid metabolism in human obesity. *Metabolism* 36: 54-59, 1987.

89.   **Gaidhu MP, Anthony NM, Patel P, Hawke TJ, and Ceddia RB.** Dysregulation of lipolysis and lipid metabolism in visceral and subcutaneous adipocytes by high-fat diet: role of ATGL, HSL, and AMPK. *Am J Physiol Cell Physiol* 298: C961-971.

90.   **Gambacciani M, Ciaponi M, Cappagli B, De Simone L, Orlandi R, and Genazzani AR.** Prospective evaluation of body weight and body fat distribution in early postmenopausal women with and without hormonal replacement therapy. *Maturitas* 39: 125-132, 2001.

91.   **Garaulet M, Hernandez-Morante JJ, Lujan J, Tebar FJ, and Zamora S.** Relationship between fat cell size and number and fatty acid composition in adipose tissue from different fat depots in overweight/obese humans. *Int J Obes (Lond)* 30: 899-905, 2006.

92.   **Garaulet M, Perez-Llamas F, Perez-Ayala M, Martinez P, de Medina FS, Tebar FJ, and Zamora S.** Site-specific differences in the fatty acid composition of abdominal adipose tissue in an obese population from a Mediterranean area: relation with dietary fatty acids, plasma lipid profile, serum insulin, and central obesity. *Am J Clin Nutr* 74: 585-591, 2001.

93.   **Garton AJ and Yeaman SJ.** Identification and role of the basal phosphorylation site on hormone-sensitive lipase. *Eur J Biochem* 191: 245-250, 1990.

94.   **Geiger PC, Hancock C, Wright DC, Han DH, and Holloszy JO.** IL-6 increases muscle insulin sensitivity only at superphysiological levels. *Am J Physiol Endocrinol Metab* 292: E1842-1846, 2007.

95.   **Giles ED, Jackman MR, Johnson GC, Schedin PJ, Houser JL, and MacLean PS.** Effect of the estrous cycle and surgical ovariectomy on energy balance, fuel utilization, and physical activity in lean and obese female rats. *Am J Physiol Regul Integr Comp Physiol* 299: R1634-1642.

96.   **Gonzalez E and McGraw TE.** Insulin signaling diverges into Akt-dependent and -independent signals to regulate the recruitment/docking and the fusion of GLUT4 vesicles to the plasma membrane. *Mol Biol Cell* 17: 4484-4493, 2006.

97.   **Goodpaster BH and Brown NF.** Skeletal muscle lipid and its association with insulin resistance: what is the role for exercise? *Exerc Sport Sci Rev* 33: 150-154, 2005.

98.   **Goodpaster BH, He J, Watkins S, and Kelley DE.** Skeletal muscle lipid content and insulin resistance: evidence for a paradox in endurance-trained athletes. *J Clin Endocrinol Metab* 86: 5755-5761, 2001.

99.   **Goodpaster BH, Krishnaswami S, Resnick H, Kelley DE, Haggerty C, Harris TB, Schwartz AV, Kritchevsky S, and Newman AB.** Association between regional adipose tissue distribution and both type 2 diabetes and impaired glucose tolerance in elderly men and women. *Diabetes Care* 26: 372-379, 2003.

100.   **Goodyear LJ, Giorgino F, Sherman LA, Carey J, Smith RJ, and Dohm GL.** Insulin receptor phosphorylation, insulin receptor substrate-1 phosphorylation, and phosphatidylinositol 3-kinase activity are decreased in intact skeletal muscle strips from obese subjects. *J Clin Invest* 95: 2195-2204, 1995.

101. **Gorres BK, Bomhoff GL, Gupte AA, and Geiger PC.** Altered estrogen receptor expression in skeletal muscle and adipose tissue of female rats fed a high-fat diet. *J Appl Physiol*.

102. **Gorres BK, Bomhoff GL, Morris JK, and Geiger PC.** In vivo stimulation of oestrogen receptor alpha increases insulin-stimulated skeletal muscle glucose uptake. *J Physiol* 589: 2041-2054.

103. **Gorzek JF, Hendrickson KC, Forstner JP, Rixen JL, Moran AL, and Lowe DA.** Estradiol and tamoxifen reverse ovariectomy-induced physical inactivity in mice. *Med Sci Sports Exerc* 39: 248-256, 2007.

104. **Gower BA, Nagy TR, Goran MI, Toth MJ, and Poehlman ET.** Fat distribution and plasma lipid-lipoprotein concentrations in pre- and postmenopausal women. *Int J Obes Relat Metab Disord* 22: 605-611, 1998.

105. **Granneman JG, Moore HP, Krishnamoorthy R, and Rathod M.** Perilipin controls lipolysis by regulating the interactions of AB-hydrolase containing 5 (Abhd5) and adipose triglyceride lipase (Atgl). *J Biol Chem* 284: 34538-34544, 2009.

106. **Gray JM and Wade GN.** Food intake, body weight, and adiposity in female rats: actions and interactions of progestins and antiestrogens. *Am J Physiol* 240: E474-481, 1981.

107. **Greenberg AS, Egan JJ, Wek SA, Garty NB, Blanchette-Mackie EJ, and Londos C.** Perilipin, a major hormonally regulated adipocyte-specific phosphoprotein associated with the periphery of lipid storage droplets. *J Biol Chem* 266: 11341-11346, 1991.

108. **Greenberg AS, Shen WJ, Muliro K, Patel S, Souza SC, Roth RA, and Kraemer FB.** Stimulation of lipolysis and hormone-sensitive lipase via the extracellular signal-regulated kinase pathway. *J Biol Chem* 276: 45456-45461, 2001.

109. **Gross DN, Miyoshi H, Hosaka T, Zhang HH, Pino EC, Souza S, Obin M, Greenberg AS, and Pilch PF.** Dynamics of lipid droplet-associated proteins during hormonally stimulated lipolysis in engineered adipocytes: stabilization and lipid droplet binding of adipocyte differentiation-related protein/adipophilin. *Mol Endocrinol* 20: 459-466, 2006.

110. **Grossbard L and Schimke RT.** Multiple hexokinases of rat tissues. Purification and comparison of soluble forms. *J Biol Chem* 241: 3546-3560, 1966.

111. **Haemmerle G, Lass A, Zimmermann R, Gorkiewicz G, Meyer C, Rozman J, Heldmaier G, Maier R, Theussl C, Eder S, Kratky D, Wagner EF, Klingenspor M, Hoefler G, and Zechner R.** Defective lipolysis and altered energy metabolism in mice lacking adipose triglyceride lipase. *Science* 312: 734-737, 2006.

112. **Haemmerle G, Zimmermann R, Hayn M, Theussl C, Waeg G, Wagner E, Sattler W, Magin TM, Wagner EF, and Zechner R.** Hormone-sensitive lipase deficiency in mice causes diglyceride accumulation in adipose tissue, muscle, and testis. *J Biol Chem* 277: 4806-4815, 2002.

113. **Hajer GR, van Haeften TW, and Visseren FL.** Adipose tissue dysfunction in obesity, diabetes, and vascular diseases. *Eur Heart J* 29: 2959-2971, 2008.

114. **Hammarstedt A, Sopasakis VR, Gogg S, Jansson PA, and Smith U.** Improved insulin sensitivity and adipose tissue dysregulation after short-term treatment with pioglitazone in non-diabetic, insulin-resistant subjects. *Diabetologia* 48: 96-104, 2005.

115.   **Hansen PA, McCarthy TJ, Pasia EN, Spina RJ, and Gulve EA.** Effects of ovariectomy and exercise training on muscle GLUT-4 content and glucose metabolism in rats. *J Appl Physiol* 80: 1605-1611, 1996.

116.   **Hassanein M, Weidow B, Koehler E, Bakane N, Garbett S, Shyr Y, and Quaranta V.** Development of high-throughput quantitative assays for glucose uptake in cancer cell lines. *Mol Imaging Biol* 13: 840-852.

117.   **Haugaard SB, Mu H, Vaag A, and Madsbad S.** Intramyocellular triglyceride content in man, influence of sex, obesity and glycaemic control. *Eur J Endocrinol* 161: 57-64, 2009.

118.   **Heine PA, Taylor JA, Iwamoto GA, Lubahn DB, and Cooke PS.** Increased adipose tissue in male and female estrogen receptor-alpha knockout mice. *Proc Natl Acad Sci U S A* 97: 12729-12734, 2000.

119.   **Helge JW, Stallknecht B, Pedersen BK, Galbo H, Kiens B, and Richter EA.** The effect of graded exercise on IL-6 release and glucose uptake in human skeletal muscle. *J Physiol* 546: 299-305, 2003.

120.   **Herschkovitz A, Liu YF, Ilan E, Ronen D, Boura-Halfon S, and Zick Y.** Common inhibitory serine sites phosphorylated by IRS-1 kinases, triggered by insulin and inducers of insulin resistance. *J Biol Chem* 282: 18018-18027, 2007.

121.   **Hevener A, Reichart D, Janez A, and Olefsky J.** Female rats do not exhibit free fatty acid-induced insulin resistance. *Diabetes* 51: 1907-1912, 2002.

122.   **Hillgartner FB, Salati LM, and Goodridge AG.** Physiological and molecular mechanisms involved in nutritional regulation of fatty acid synthesis. *Physiol Rev* 75: 47-76, 1995.

123.   **Hoffstedt J, Arner P, Hellers G, and Lonnqvist F.** Variation in adrenergic regulation of lipolysis between omental and subcutaneous adipocytes from obese and non-obese men. *J Lipid Res* 38: 795-804, 1997.

124.   **Hoffstedt J, Wahrenberg H, Thorne A, and Lonnqvist F.** The metabolic syndrome is related to beta 3-adrenoceptor sensitivity in visceral adipose tissue. *Diabetologia* 39: 838-844, 1996.

125.   **Howard BV, Kuller L, Langer R, Manson JE, Allen C, Assaf A, Cochrane BB, Larson JC, Lasser N, Rainford M, Van Horn L, Stefanick ML, and Trevisan M.** Risk of cardiovascular disease by hysterectomy status, with and without oophorectomy: the Women's Health Initiative Observational Study. *Circulation* 111: 1462-1470, 2005.

126.   **Huang SH, Shen WJ, Yeo HL, and Wang SM.** Signaling pathway of magnolol-stimulated lipolysis in sterol ester-loaded 3T3-L1 preadipocyes. *J Cell Biochem* 91: 1021-1029, 2004.

127.   **Hue L and Taegtmeyer H.** The Randle cycle revisited: a new head for an old hat. *Am J Physiol Endocrinol Metab* 297: E578-591, 2009.

128.   **Huijsman E, van de Par C, Economou C, van der Poel C, Lynch GS, Schoiswohl G, Haemmerle G, Zechner R, and Watt MJ.** Adipose triacylglycerol lipase deletion alters whole body energy metabolism and impairs exercise performance in mice. *Am J Physiol Endocrinol Metab* 297: E505-513, 2009.

129.   **Hurley BF, Nemeth PM, Martin WH, 3rd, Hagberg JM, Dalsky GP, and Holloszy JO.** Muscle triglyceride utilization during exercise: effect of training. *J Appl Physiol* 60: 562-567, 1986.

130. **Ishikawa K, Takahashi K, Bujo H, Hashimoto N, Yagui K, and Saito Y.** Subcutaneous fat modulates insulin sensitivity in mice by regulating TNF-alpha expression in visceral fat. *Horm Metab Res* 38: 631-638, 2006.

131. **Itani SI, Ruderman NB, Schmieder F, and Boden G.** Lipid-induced insulin resistance in human muscle is associated with changes in diacylglycerol, protein kinase C, and IkappaB-alpha. *Diabetes* 51: 2005-2011, 2002.

132. **Janssen I, Powell LH, Kazlauskaite R, and Dugan SA.** Testosterone and visceral fat in midlife women: the Study of Women's Health Across the Nation (SWAN) fat patterning study. *Obesity (Silver Spring)* 18: 604-610.

133. **Jenkins CM, Mancuso DJ, Yan W, Sims HF, Gibson B, and Gross RW.** Identification, cloning, expression, and purification of three novel human calcium-independent phospholipase A2 family members possessing triacylglycerol lipase and acylglycerol transacylase activities. *J Biol Chem* 279: 48968-48975, 2004.

134. **Jensen LB, Vestergaard P, Hermann AP, Gram J, Eiken P, Abrahamsen B, Brot C, Kolthoff N, Sorensen OH, Beck-Nielsen H, Nielsen SP, Charles P, and Mosekilde L.** Hormone replacement therapy dissociates fat mass and bone mass, and tends to reduce weight gain in early postmenopausal women: a randomized controlled 5-year clinical trial of the Danish Osteoporosis Prevention Study. *J Bone Miner Res* 18: 333-342, 2003.

135. **Jeong S and Yoon M.** Swimming's prevention of ovariectomy-induced obesity through activation of skeletal-muscle PPARalpha. *Int J Sport Nutr Exerc Metab* 22: 1-10.

136. **Jin X, Zimmers TA, Perez EA, Pierce RH, Zhang Z, and Koniaris LG.** Paradoxical effects of short- and long-term interleukin-6 exposure on liver injury and repair. *Hepatology* 43: 474-484, 2006.

137. **Jocken JW, Langin D, Smit E, Saris WH, Valle C, Hul GB, Holm C, Arner P, and Blaak EE.** Adipose triglyceride lipase and hormone-sensitive lipase protein expression is decreased in the obese insulin-resistant state. *J Clin Endocrinol Metab* 92: 2292-2299, 2007.

138. **Jones ME, Thorburn AW, Britt KL, Hewitt KN, Misso ML, Wreford NG, Proietto J, Oz OK, Leury BJ, Robertson KM, Yao S, and Simpson ER.** Aromatase-deficient (ArKO) mice accumulate excess adipose tissue. *J Steroid Biochem Mol Biol* 79: 3-9, 2001.

139. **Kamei N, Tobe K, Suzuki R, Ohsugi M, Watanabe T, Kubota N, Ohtsuka-Kowatari N, Kumagai K, Sakamoto K, Kobayashi M, Yamauchi T, Ueki K, Oishi Y, Nishimura S, Manabe I, Hashimoto H, Ohnishi Y, Ogata H, Tokuyama K, Tsunoda M, Ide T, Murakami K, Nagai R, and Kadowaki T.** Overexpression of monocyte chemoattractant protein-1 in adipose tissues causes macrophage recruitment and insulin resistance. *J Biol Chem* 281: 26602-26614, 2006.

140. **Kaneko S, Iida RH, Suga T, Fukui T, Morito M, and Yamane A.** Changes in triacylglycerol-accumulated fiber type, fiber type composition, and biogenesis in the mitochondria of the soleus muscle in obese rats. *Anat Rec (Hoboken)* 294: 1904-1912.

141. **Katzen HM and Schimke RT.** Multiple forms of hexokinase in the rat: tissue distribution, age dependency, and properties. *Proc Natl Acad Sci U S A* 54: 1218-1225, 1965.

142.	**Keck M, Romero-Aleshire MJ, Cai Q, Hoyer PB, and Brooks HL.** Hormonal status affects the progression of STZ-induced diabetes and diabetic renal damage in the VCD mouse model of menopause. *Am J Physiol Renal Physiol* 293: F193-199, 2007.

143.	**Keller C, Keller P, Marshal S, and Pedersen BK.** IL-6 gene expression in human adipose tissue in response to exercise--effect of carbohydrate ingestion. *J Physiol* 550: 927-931, 2003.

144.	**Kelley DE, Goodpaster B, Wing RR, and Simoneau JA.** Skeletal muscle fatty acid metabolism in association with insulin resistance, obesity, and weight loss. *Am J Physiol* 277: E1130-1141, 1999.

145.	**Kern PA, Ranganathan S, Li C, Wood L, and Ranganathan G.** Adipose tissue tumor necrosis factor and interleukin-6 expression in human obesity and insulin resistance. *Am J Physiol Endocrinol Metab* 280: E745-751, 2001.

146.	**Kim BS, Cha HN, Kim YW, Kim JY, Dan JM, and Park SY.** Inhibition of lipid infusion-induced skeletal muscle insulin resistance by cotreatment with tempol and glutathione in mice. *J Pharmacol Sci* 110: 370-380, 2009.

147.	**Kim JY, van de Wall E, Laplante M, Azzara A, Trujillo ME, Hofmann SM, Schraw T, Durand JL, Li H, Li G, Jelicks LA, Mehler MF, Hui DY, Deshaies Y, Shulman GI, Schwartz GJ, and Scherer PE.** Obesity-associated improvements in metabolic profile through expansion of adipose tissue. *J Clin Invest* 117: 2621-2637, 2007.

148.	**Kim TH, Choi SE, Ha ES, Jung JG, Han SJ, Kim HJ, Kim DJ, Kang Y, and Lee KW.** IL-6 induction of TLR-4 gene expression via STAT3 has an effect on insulin resistance in human skeletal muscle. *Acta Diabetol*.

149.	**Klein NA, Houmard BS, Hansen KR, Woodruff TK, Sluss PM, Bremner WJ, and Soules MR.** Age-related analysis of inhibin A, inhibin B, and activin a relative to the intercycle monotropic follicle-stimulating hormone rise in normal ovulatory women. *J Clin Endocrinol Metab* 89: 2977-2981, 2004.

150.	**Klip A, Li G, and Logan WJ.** Induction of sugar uptake response to insulin by serum depletion in fusing L6 myoblasts. *Am J Physiol* 247: E291-296, 1984.

151.	**Klover PJ, Clementi AH, and Mooney RA.** Interleukin-6 depletion selectively improves hepatic insulin action in obesity. *Endocrinology* 146: 3417-3427, 2005.

152.	**Klover PJ, Zimmers TA, Koniaris LG, and Mooney RA.** Chronic exposure to interleukin-6 causes hepatic insulin resistance in mice. *Diabetes* 52: 2784-2789, 2003.

153.	**Koistinen HA, Chibalin AV, and Zierath JR.** Aberrant p38 mitogen-activated protein kinase signalling in skeletal muscle from Type 2 diabetic patients. *Diabetologia* 46: 1324-1328, 2003.

154.	**Koonen DP, Sung MM, Kao CK, Dolinsky VW, Koves TR, Ilkayeva O, Jacobs RL, Vance DE, Light PE, Muoio DM, Febbraio M, and Dyck JR.** Alterations in skeletal muscle fatty acid handling predisposes middle-aged mice to diet-induced insulin resistance. *Diabetes* 59: 1366-1375.

155.	**Koster A, Stenholm S, Alley DE, Kim LJ, Simonsick EM, Kanaya AM, Visser M, Houston DK, Nicklas BJ, Tylavsky FA, Satterfield S, Goodpaster BH, Ferrucci L, and Harris TB.** Body fat distribution and inflammation among obese older adults with and without metabolic syndrome. *Obesity (Silver Spring)* 18: 2354-2361.

156.   **Koumanov F, Richardson JD, Murrow BA, and Holman GD.** AS160 phosphotyrosine-binding domain constructs inhibit insulin-stimulated GLUT4 vesicle fusion with the plasma membrane. *J Biol Chem* 286: 16574-16582.

157.   **Kovalik JP, Slentz D, Stevens RD, Kraus WE, Houmard JA, Nicoll JB, Lea-Currie YR, Everingham K, Kien CL, Buehrer BM, and Muoio DM.** Metabolic remodeling of human skeletal myocytes by cocultured adipocytes depends on the lipolytic state of the system. *Diabetes* 60: 1882-1893.

158.   **Koves TR, Ussher JR, Noland RC, Slentz D, Mosedale M, Ilkayeva O, Bain J, Stevens R, Dyck JR, Newgard CB, Lopaschuk GD, and Muoio DM.** Mitochondrial overload and incomplete fatty acid oxidation contribute to skeletal muscle insulin resistance. *Cell Metab* 7: 45-56, 2008.

159.   **Kramer HF, Witczak CA, Taylor EB, Fujii N, Hirshman MF, and Goodyear LJ.** AS160 regulates insulin- and contraction-stimulated glucose uptake in mouse skeletal muscle. *J Biol Chem* 281: 31478-31485, 2006.

160.   **Krssak M, Falk Petersen K, Dresner A, DiPietro L, Vogel SM, Rothman DL, Roden M, and Shulman GI.** Intramyocellular lipid concentrations are correlated with insulin sensitivity in humans: a 1H NMR spectroscopy study. *Diabetologia* 42: 113-116, 1999.

161.   **Kuiper GG, Carlsson B, Grandien K, Enmark E, Haggblad J, Nilsson S, and Gustafsson JA.** Comparison of the ligand binding specificity and transcript tissue distribution of estrogen receptors alpha and beta. *Endocrinology* 138: 863-870, 1997.

162.   **Kusminski CM, Shetty S, Orci L, Unger RH, and Scherer PE.** Diabetes and apoptosis: lipotoxicity. *Apoptosis* 14: 1484-1495, 2009.

163.   **Lafontan M and Berlan M.** Evidence for the alpha 2 nature of the alpha-adrenergic receptor inhibiting lipolysis in human fat cells. *Eur J Pharmacol* 66: 87-93, 1980.

164.   **Landau IT and Zucker I.** Estrogenic regulation of body weight in the female rat. *Horm Behav* 7: 29-39, 1976.

165.   **Lanner JT, Bruton JD, Assefaw-Redda Y, Andronache Z, Zhang SJ, Severa D, Zhang ZB, Melzer W, Zhang SL, Katz A, and Westerblad H.** Knockdown of TRPC3 with siRNA coupled to carbon nanotubes results in decreased insulin-mediated glucose uptake in adult skeletal muscle cells. *Faseb J* 23: 1728-1738, 2009.

166.   **Lanner JT, Katz A, Tavi P, Sandstrom ME, Zhang SJ, Wretman C, James S, Fauconnier J, Lannergren J, Bruton JD, and Westerblad H.** The role of Ca2+ influx for insulin-mediated glucose uptake in skeletal muscle. *Diabetes* 55: 2077-2083, 2006.

167.   **Lass A, Zimmermann R, Haemmerle G, Riederer M, Schoiswohl G, Schweiger M, Kienesberger P, Strauss JG, Gorkiewicz G, and Zechner R.** Adipose triglyceride lipase-mediated lipolysis of cellular fat stores is activated by CGI-58 and defective in Chanarin-Dorfman Syndrome. *Cell Metab* 3: 309-319, 2006.

168.   **Latour MG, Shinoda M, and Lavoie JM.** Metabolic effects of physical training in ovariectomized and hyperestrogenic rats. *J Appl Physiol* 90: 235-241, 2001.

169.   **Laudenslager ML, Wilkinson CW, Carlisle HJ, and Hammel HT.** Energy balance in ovariectomized rats with and without estrogen replacement. *Am J Physiol* 238: R400-405, 1980.

170.   **Laughlin GA, Barrett-Connor E, Kritz-Silverstein D, and von Muhlen D.** Hysterectomy, oophorectomy, and endogenous sex hormone levels in older women: the Rancho Bernardo Study. *J Clin Endocrinol Metab* 85: 645-651, 2000.

171.   **Laughlin MH, Simpson T, Sexton WL, Brown OR, Smith JK, and Korthuis RJ.** Skeletal muscle oxidative capacity, antioxidant enzymes, and exercise training. *J Appl Physiol* 68: 2337-2343, 1990.

172.   **Lauritzen HP, Galbo H, Brandauer J, Goodyear LJ, and Ploug T.** Large GLUT4 vesicles are stationary while locally and reversibly depleted during transient insulin stimulation of skeletal muscle of living mice: imaging analysis of GLUT4-enhanced green fluorescent protein vesicle dynamics. *Diabetes* 57: 315-324, 2008.

173.   **Lee CG, Carr MC, Murdoch SJ, Mitchell E, Woods NF, Wener MH, Chandler WL, Boyko EJ, and Brunzell JD.** Adipokines, inflammation, and visceral adiposity across the menopausal transition: a prospective study. *J Clin Endocrinol Metab* 94: 1104-1110, 2009.

174.   **Lee JS, Pinnamaneni SK, Eo SJ, Cho IH, Pyo JH, Kim CK, Sinclair AJ, Febbraio MA, and Watt MJ.** Saturated, but not n-6 polyunsaturated, fatty acids induce insulin resistance: role of intramuscular accumulation of lipid metabolites. *J Appl Physiol* 100: 1467-1474, 2006.

175.   **Leite RD, Prestes J, Bernardes CF, Shiguemoto GE, Pereira GB, Duarte JO, Domingos MM, Baldissera V, and de Andrade Perez SE.** Effects of ovariectomy and resistance training on lipid content in skeletal muscle, liver, and heart; fat depots; and lipid profile. *Appl Physiol Nutr Metab* 34: 1079-1086, 2009.

176.   **Lew EA and Garfinkel L.** Variations in mortality by weight among 750,000 men and women. *J Chronic Dis* 32: 563-576, 1979.

177.   **Lewin TM, Granger DA, Kim JH, and Coleman RA.** Regulation of mitochondrial sn-glycerol-3-phosphate acyltransferase activity: response to feeding status is unique in various rat tissues and is discordant with protein expression. *Arch Biochem Biophys* 396: 119-127, 2001.

178.   **Ley CJ, Lees B, and Stevenson JC.** Sex- and menopause-associated changes in body-fat distribution. *Am J Clin Nutr* 55: 950-954, 1992.

179.   **Li G, Barrett EJ, Barrett MO, Cao W, and Liu Z.** Tumor necrosis factor-alpha induces insulin resistance in endothelial cells via a p38 mitogen-activated protein kinase-dependent pathway. *Endocrinology* 148: 3356-3363, 2007.

180.   **Libinaki R, Heffernan M, Jiang WJ, Ogru E, Ignjatovic V, Gianello R, Trickey L, Taylor M, and Ng F.** Effects of genetic and diet-induced obesity on lipid metabolism. *IUBMB Life* 48: 109-113, 1999.

181.   **Lonnqvist F, Nyberg B, Wahrenberg H, and Arner P.** Catecholamine-induced lipolysis in adipose tissue of the elderly. *J Clin Invest* 85: 1614-1621, 1990.

182.   **Lonnqvist F, Thorne A, Large V, and Arner P.** Sex differences in visceral fat lipolysis and metabolic complications of obesity. *Arterioscler Thromb Vasc Biol* 17: 1472-1480, 1997.

183.   **Lovejoy JC.** The menopause and obesity. *Prim Care* 30: 317-325, 2003.

184.   **Lovering RM, Michaelson L, and Ward CW.** Malformed mdx myofibers have normal cytoskeletal architecture yet altered EC coupling and stress-induced Ca2+ signaling. *Am J Physiol Cell Physiol* 297: C571-580, 2009.

185.   **Luisi S, Florio P, Reis FM, and Petraglia F.** Inhibins in female and male reproductive physiology: role in gametogenesis, conception, implantation and early pregnancy. *Hum Reprod Update* 11: 123-135, 2005.

186.   **MacGillivray MH, Morishima A, Conte F, Grumbach M, and Smith EP.** Pediatric endocrinology update: an overview. The essential roles of estrogens in pubertal growth, epiphyseal fusion and bone turnover: lessons from mutations in the genes for aromatase and the estrogen receptor. *Horm Res* 49 Suppl 1: 2-8, 1998.

187.   **Mackrell JG and Cartee GD.** A novel method to measure glucose uptake and Myosin heavy chain isoform expression of single fibers from rat skeletal muscle. *Diabetes* 61: 995-1003.

188.   **Malide D.** Application of immunocytochemistry and immunofluorescence techniques to adipose tissue and cell cultures. *Methods Mol Biol* 456: 285-297, 2008.

189.   **Maroulis GB and Abraham GE.** Ovarian and adrenal contributions to peripheral steroid levels in postmenopausal women. *Obstet Gynecol* 48: 150-154, 1976.

190.   **Mauriege P, Galitzky J, Berlan M, and Lafontan M.** Heterogeneous distribution of beta and alpha-2 adrenoceptor binding sites in human fat cells from various fat deposits: functional consequences. *Eur J Clin Invest* 17: 156-165, 1987.

191.   **Mayer LP, Devine PJ, Dyer CA, and Hoyer PB.** The follicle-deplete mouse ovary produces androgen. *Biol Reprod* 71: 130-138, 2004.

192.   **McCormick KM, Burns KL, Piccone CM, Gosselin LE, and Brazeau GA.** Effects of ovariectomy and estrogen on skeletal muscle function in growing rats. *J Muscle Res Cell Motil* 25: 21-27, 2004.

193.   **Minokoshi Y and Kahn BB.** Role of AMP-activated protein kinase in leptin-induced fatty acid oxidation in muscle. *Biochem Soc Trans* 31: 196-201, 2003.

194.   **Miyoshi H, Souza SC, Zhang HH, Strissel KJ, Christoffolete MA, Kovsan J, Rudich A, Kraemer FB, Bianco AC, Obin MS, and Greenberg AS.** Perilipin promotes hormone-sensitive lipase-mediated adipocyte lipolysis via phosphorylation-dependent and -independent mechanisms. *J Biol Chem* 281: 15837-15844, 2006.

195.   **Mohamed-Ali V, Goodrick S, Rawesh A, Katz DR, Miles JM, Yudkin JS, Klein S, and Coppack SW.** Subcutaneous adipose tissue releases interleukin-6, but not tumor necrosis factor-alpha, in vivo. *J Clin Endocrinol Metab* 82: 4196-4200, 1997.

196.   **Moran AL, Nelson SA, Landisch RM, Warren GL, and Lowe DA.** Estradiol replacement reverses ovariectomy-induced muscle contractile and myosin dysfunction in mature female mice. *J Appl Physiol* 102: 1387-1393, 2007.

197.   **Moro C, Galgani JE, Luu L, Pasarica M, Mairal A, Bajpeyi S, Schmitz G, Langin D, Liebisch G, and Smith SR.** Influence of gender, obesity, and muscle lipase activity on intramyocellular lipids in sedentary individuals. *J Clin Endocrinol Metab* 94: 3440-3447, 2009.

198.   **Muhammad FS, Goode AK, Kock ND, Arifin EA, Cline JM, Adams MR, Hoyer PB, Christian PJ, Isom S, Kaplan JR, and Appt SE.** Effects of 4-vinylcyclohexene diepoxide on peripubertal and adult Sprague-Dawley rats: ovarian, clinical, and pathologic outcomes. *Comp Med* 59: 46-59, 2009.

199.   **Muoio DM.** Intramuscular triacylglycerol and insulin resistance: guilty as charged or wrongly accused? *Biochim Biophys Acta* 1801: 281-288.

200.   **Muoio DM, Dohm GL, Fiedorek FT, Jr., Tapscott EB, and Coleman RA.** Leptin directly alters lipid partitioning in skeletal muscle. *Diabetes* 46: 1360-1363, 1997.

201.   **Muoio DM and Koves TR.** Skeletal muscle adaptation to fatty acid depends on coordinated actions of the PPARs and PGC1 alpha: implications for metabolic disease. *Appl Physiol Nutr Metab* 32: 874-883, 2007.

202.   **Muoio DM and Lynis Dohm G.** Peripheral metabolic actions of leptin. *Best Pract Res Clin Endocrinol Metab* 16: 653-666, 2002.

203.   **Muttukrishna S, Sharma S, Barlow DH, Ledger W, Groome N, and Sathanandan M.** Serum inhibins, estradiol, progesterone and FSH in surgical menopause: a demonstration of ovarian pituitary feedback loop in women. *Hum Reprod* 17: 2535-2539, 2002.

204.   **Nedungadi TP and Clegg DJ.** Sexual dimorphism in body fat distribution and risk for cardiovascular diseases. *J Cardiovasc Transl Res* 2: 321-327, 2009.

205.   **Nicklas BJ, Penninx BW, Cesari M, Kritchevsky SB, Newman AB, Kanaya AM, Pahor M, Jingzhong D, and Harris TB.** Association of visceral adipose tissue with incident myocardial infarction in older men and women: the Health, Aging and Body Composition Study. *Am J Epidemiol* 160: 741-749, 2004.

206.   **Nicklas BJ, Rogus EM, Colman EG, and Goldberg AP.** Visceral adiposity, increased adipocyte lipolysis, and metabolic dysfunction in obese postmenopausal women. *Am J Physiol* 270: E72-78, 1996.

207.   **O'Connell J, Lynch L, Cawood TJ, Kwasnik A, Nolan N, Geoghegan J, McCormick A, O'Farrelly C, and O'Shea D.** The relationship of omental and subcutaneous adipocyte size to metabolic disease in severe obesity. *PLoS One* 5: e9997.

208.   **Okazaki H, Osuga J, Tamura Y, Yahagi N, Tomita S, Shionoiri F, Iizuka Y, Ohashi K, Harada K, Kimura S, Gotoda T, Shimano H, Yamada N, and Ishibashi S.** Lipolysis in the absence of hormone-sensitive lipase: evidence for a common mechanism regulating distinct lipases. *Diabetes* 51: 3368-3375, 2002.

209.   **Osuga J, Ishibashi S, Oka T, Yagyu H, Tozawa R, Fujimoto A, Shionoiri F, Yahagi N, Kraemer FB, Tsutsumi O, and Yamada N.** Targeted disruption of hormone-sensitive lipase results in male sterility and adipocyte hypertrophy, but not in obesity. *Proc Natl Acad Sci U S A* 97: 787-792, 2000.

210.   **Panotopoulos G, Raison J, Ruiz JC, Guy-Grand B, and Basdevant A.** Weight gain at the time of menopause. *Hum Reprod* 12 Suppl 1: 126-133, 1997.

211.   **Paquette A, Shinoda M, Rabasa Lhoret R, Prud'homme D, and Lavoie JM.** Time course of liver lipid infiltration in ovariectomized rats: impact of a high-fat diet. *Maturitas* 58: 182-190, 2007.

212.   **Park SM, Park CH, Wha JD, and Choi SB.** A high carbohydrate diet induces insulin resistance through decreased glucose utilization in ovariectomized rats. *Korean J Intern Med* 19: 87-92, 2004.

213.   **Park YW, Zhu S, Palaniappan L, Heshka S, Carnethon MR, and Heymsfield SB.** The metabolic syndrome: prevalence and associated risk factor findings in the US population from the Third National Health and Nutrition Examination Survey, 1988-1994. *Arch Intern Med* 163: 427-436, 2003.

214.   **Peacock A, Alvi NS, and Mushtaq T.** Period problems: disorders of menstruation in adolescents. *Arch Dis Child* 97: 554-560.

215.   **Pelleymounter MA, Baker MB, and McCaleb M.** Does estradiol mediate leptin's effects on adiposity and body weight? *Am J Physiol* 276: E955-963, 1999.

216.   **Perez-Perez R, Ortega-Delgado FJ, Garcia-Santos E, Lopez JA, Camafeita E, Ricart W, Fernandez-Real JM, and Peral B.** Differential proteomics of omental and subcutaneous adipose tissue reflects their unalike biochemical and metabolic properties. *J Proteome Res* 8: 1682-1693, 2009.

217.   **Phillips SA, Ciaraldi TP, Oh DK, Savu MK, and Henry RR.** Adiponectin secretion and response to pioglitazone is depot dependent in cultured human adipose tissue. *Am J Physiol Endocrinol Metab* 295: E842-850, 2008.

218.   **Plomgaard P, Bouzakri K, Krogh-Madsen R, Mittendorfer B, Zierath JR, and Pedersen BK.** Tumor necrosis factor-alpha induces skeletal muscle insulin resistance in healthy human subjects via inhibition of Akt substrate 160 phosphorylation. *Diabetes* 54: 2939-2945, 2005.

219.   **Pouliot MC, Despres JP, Nadeau A, Moorjani S, Prud'Homme D, Lupien PJ, Tremblay A, and Bouchard C.** Visceral obesity in men. Associations with glucose tolerance, plasma insulin, and lipoprotein levels. *Diabetes* 41: 826-834, 1992.

220.   **Prasannarong M, Vichaiwong K, and Saengsirisuwan V.** Calorie restriction prevents the development of insulin resistance and impaired insulin signaling in skeletal muscle of ovariectomized rats. *Biochim Biophys Acta* 1822: 1051-1061.

221.   **Randle PJ, Garland PB, Hales CN, and Newsholme EA.** The glucose fatty-acid cycle. Its role in insulin sensitivity and the metabolic disturbances of diabetes mellitus. *Lancet* 1: 785-789, 1963.

222.   **Reid CM, Dart AM, Dewar EM, and Jennings GL.** Interactions between the effects of exercise and weight loss on risk factors, cardiovascular haemodynamics and left ventricular structure in overweight subjects. *J Hypertens* 12: 291-301, 1994.

223.   **Reynisdottir S, Langin D, Carlstrom K, Holm C, Rossner S, and Arner P.** Effects of weight reduction on the regulation of lipolysis in adipocytes of women with upper-body obesity. *Clin Sci (Lond)* 89: 421-429, 1995.

224.   **Ribas V, Nguyen MT, Henstridge DC, Nguyen AK, Beaven SW, Watt MJ, and Hevener AL.** Impaired oxidative metabolism and inflammation are associated with insulin resistance in ERalpha-deficient mice. *Am J Physiol Endocrinol Metab* 298: E304-319.

225.   **Rincon J, Holmang A, Wahlstrom EO, Lonnroth P, Bjorntorp P, Zierath JR, and Wallberg-Henriksson H.** Mechanisms behind insulin resistance in rat skeletal muscle after oophorectomy and additional testosterone treatment. *Diabetes* 45: 615-621, 1996.

226.   **Roca-Rivada A, Alonso J, Al-Massadi O, Castelao C, Peinado JR, Seoane LM, Casanueva FF, and Pardo M.** Secretome analysis of rat adipose tissues shows location-specific roles for each depot type. *J Proteomics* 74: 1068-1079.

227.   **Rodbell M.** Metabolism of Isolated Fat Cells. I. Effects of Hormones on Glucose Metabolism and Lipolysis. *J Biol Chem* 239: 375-380, 1964.

228.   **Rogers NH, Perfield JW, 2nd, Strissel KJ, Obin MS, and Greenberg AS.** Reduced energy expenditure and increased inflammation are early events in the development of ovariectomy-induced obesity. *Endocrinology* 150: 2161-2168, 2009.

229.   **Romanatto T, Roman EA, Arruda AP, Denis RG, Solon C, Milanski M, Moraes JC, Bonfleur ML, Degasperi GR, Picardi PK, Hirabara S, Boschero AC, Curi R, and Velloso LA.** Deletion of tumor necrosis factor-alpha receptor 1 (TNFR1)

protects against diet-induced obesity by means of increased thermogenesis. *J Biol Chem* 284: 36213-36222, 2009.

230.   **Rosano GM, Vitale C, Marazzi G, and Volterrani M.** Menopause and cardiovascular disease: the evidence. *Climacteric* 10 Suppl 1: 19-24, 2007.

231.   **Rosano GM, Vitale C, and Tulli A.** Managing cardiovascular risk in menopausal women. *Climacteric* 9 Suppl 1: 19-27, 2006.

232.   **Ryden M, Jocken J, van Harmelen V, Dicker A, Hoffstedt J, Wiren M, Blomqvist L, Mairal A, Langin D, Blaak E, and Arner P.** Comparative studies of the role of hormone-sensitive lipase and adipose triglyceride lipase in human fat cell lipolysis. *Am J Physiol Endocrinol Metab* 292: E1847-1855, 2007.

233.   **Saengsirisuwan V, Pongseeda S, Prasannarong M, Vichaiwong K, and Toskulkao C.** Modulation of insulin resistance in ovariectomized rats by endurance exercise training and estrogen replacement. *Metabolism* 58: 38-47, 2009.

234.   **Saha PK, Kojima H, Martinez-Botas J, Sunehag AL, and Chan L.** Metabolic adaptations in the absence of perilipin: increased beta-oxidation and decreased hepatic glucose production associated with peripheral insulin resistance but normal glucose tolerance in perilipin-null mice. *J Biol Chem* 279: 35150-35158, 2004.

235.   **Sakai T, Sakaue H, Nakamura T, Okada M, Matsuki Y, Watanabe E, Hiramatsu R, Nakayama K, Nakayama KI, and Kasuga M.** Skp2 controls adipocyte proliferation during the development of obesity. *J Biol Chem* 282: 2038-2046, 2007.

236.   **Savage DB, Petersen KF, and Shulman GI.** Disordered lipid metabolism and the pathogenesis of insulin resistance. *Physiol Rev* 87: 507-520, 2007.

237.   **Schneider JG, Tompkins C, Blumenthal RS, and Mora S.** The metabolic syndrome in women. *Cardiol Rev* 14: 286-291, 2006.

238.   **Schoiswohl G, Schweiger M, Schreiber R, Gorkiewicz G, Preiss-Landl K, Taschler U, Zierler KA, Radner FP, Eichmann TO, Kienesberger PC, Eder S, Lass A, Haemmerle G, Alsted TJ, Kiens B, Hoefler G, Zechner R, and Zimmermann R.** Adipose triglyceride lipase plays a key role in the supply of the working muscle with fatty acids. *J Lipid Res* 51: 490-499.

239.   **Schweiger M, Schreiber R, Haemmerle G, Lass A, Fledelius C, Jacobsen P, Tornqvist H, Zechner R, and Zimmermann R.** Adipose triglyceride lipase and hormone-sensitive lipase are the major enzymes in adipose tissue triacylglycerol catabolism. *J Biol Chem* 281: 40236-40241, 2006.

240.   **Sell H, Dietze-Schroeder D, Kaiser U, and Eckel J.** Monocyte chemotactic protein-1 is a potential player in the negative cross-talk between adipose tissue and skeletal muscle. *Endocrinology* 147: 2458-2467, 2006.

241.   **Sell H, Laurencikiene J, Taube A, Eckardt K, Cramer A, Horrighs A, Arner P, and Eckel J.** Chemerin is a novel adipocyte-derived factor inducing insulin resistance in primary human skeletal muscle cells. *Diabetes* 58: 2731-2740, 2009.

242.   **Senn JJ, Klover PJ, Nowak IA, Zimmers TA, Koniaris LG, Furlanetto RW, and Mooney RA.** Suppressor of cytokine signaling-3 (SOCS-3), a potential mediator of interleukin-6-dependent insulin resistance in hepatocytes. *J Biol Chem* 278: 13740-13746, 2003.

243.   **Shen WJ, Patel S, Miyoshi H, Greenberg AS, and Kraemer FB.** Functional interaction of hormone-sensitive lipase and perilipin in lipolysis. *J Lipid Res* 50: 2306-2313, 2009.

244.	**Sherk VD, Malone SP, Bemben MG, Knehans AW, Palmer IJ, and Bemben DA.** Leptin, fat mass, and bone mineral density in healthy pre- and postmenopausal women. *J Clin Densitom* 14: 321-325.

245.	**Shinoda M, Latour MG, and Lavoie JM.** Effects of physical training on body composition and organ weights in ovariectomized and hyperestrogenic rats. *Int J Obes Relat Metab Disord* 26: 335-343, 2002.

246.	**Shulman GI, Rothman DL, Jue T, Stein P, DeFronzo RA, and Shulman RG.** Quantitation of muscle glycogen synthesis in normal subjects and subjects with non-insulin-dependent diabetes by 13C nuclear magnetic resonance spectroscopy. *N Engl J Med* 322: 223-228, 1990.

247.	**Simpson ER, Mahendroo MS, Means GD, Kilgore MW, Hinshelwood MM, Graham-Lorence S, Amarneh B, Ito Y, Fisher CR, Michael MD, and et al.** Aromatase cytochrome P450, the enzyme responsible for estrogen biosynthesis. *Endocr Rev* 15: 342-355, 1994.

248.	**Sitnick M, Foley AM, Brown M, and Spangenburg EE.** Ovariectomy prevents the recovery of atrophied gastrocnemius skeletal muscle mass. *J Appl Physiol* 100: 286-293, 2006.

249.	**Solinas G, Summermatter S, Mainieri D, Gubler M, Pirola L, Wymann MP, Rusconi S, Montani JP, Seydoux J, and Dulloo AG.** The direct effect of leptin on skeletal muscle thermogenesis is mediated by substrate cycling between de novo lipogenesis and lipid oxidation. *FEBS Lett* 577: 539-544, 2004.

250.	**Somwar R, Kim DY, Sweeney G, Huang C, Niu W, Lador C, Ramlal T, and Klip A.** GLUT4 translocation precedes the stimulation of glucose uptake by insulin in muscle cells: potential activation of GLUT4 via p38 mitogen-activated protein kinase. *Biochem J* 359: 639-649, 2001.

251.	**Song G, Ouyang G, and Bao S.** The activation of Akt/PKB signaling pathway and cell survival. *J Cell Mol Med* 9: 59-71, 2005.

252.	**Souza MR, Diniz Mde F, Medeiros-Filho JE, and Araujo MS.** Metabolic syndrome and risk factors for non-alcoholic fatty liver disease. *Arq Gastroenterol* 49: 89-96.

253.	**Souza SC, Palmer HJ, Kang YH, Yamamoto MT, Muliro KV, Paulson KE, and Greenberg AS.** TNF-alpha induction of lipolysis is mediated through activation of the extracellular signal related kinase pathway in 3T3-L1 adipocytes. *J Cell Biochem* 89: 1077-1086, 2003.

254.	**Spangenburg EE, Le Roith D, Ward CW, and Bodine SC.** A functional insulin-like growth factor receptor is not necessary for load-induced skeletal muscle hypertrophy. *J Physiol* 586: 283-291, 2008.

255.	**Spangenburg EE, Pratt SJ, Wohlers LM, and Lovering RM.** Use of BODIPY (493/503) to visualize intramuscular lipid droplets in skeletal muscle. *J Biomed Biotechnol* 2011: 598358.

256.	**Sparks LM, Moro C, Ukropcova B, Bajpeyi S, Civitarese AE, Hulver MW, Thoresen GH, Rustan AC, and Smith SR.** Remodeling lipid metabolism and improving insulin responsiveness in human primary myotubes. *PLoS One* 6: e21068.

257.	**Stefan N, Kantartzis K, Machann J, Schick F, Thamer C, Rittig K, Balletshofer B, Machicao F, Fritsche A, and Haring HU.** Identification and

characterization of metabolically benign obesity in humans. *Arch Intern Med* 168: 1609-1616, 2008.

258.   **Steinberg GR, Kemp BE, and Watt MJ.** Adipocyte triglyceride lipase expression in human obesity. *Am J Physiol Endocrinol Metab* 293: E958-964, 2007.

259.   **Steinberg GR, Michell BJ, van Denderen BJ, Watt MJ, Carey AL, Fam BC, Andrikopoulos S, Proietto J, Gorgun CZ, Carling D, Hotamisligil GS, Febbraio MA, Kay TW, and Kemp BE.** Tumor necrosis factor alpha-induced skeletal muscle insulin resistance involves suppression of AMP-kinase signaling. *Cell Metab* 4: 465-474, 2006.

260.   **Stern JS, Hirsch J, Drewnowski A, Sullivan AC, Johnson PR, and Cohn CK.** Glycerol kinase activity in adipose tissue of obese rats and mice: effects of diet composition. *J Nutr* 113: 714-720, 1983.

261.   **Stewart JM and Blakely JA.** Long chain fatty acids inhibit and medium chain fatty acids activate mammalian cardiac hexokinase. *Biochim Biophys Acta* 1484: 278-286, 2000.

262.   **Strawford A, Antelo F, Christiansen M, and Hellerstein MK.** Adipose tissue triglyceride turnover, de novo lipogenesis, and cell proliferation in humans measured with 2H2O. *Am J Physiol Endocrinol Metab* 286: E577-588, 2004.

263.   **Stubbins RE, Najjar K, Holcomb VB, Hong J, and Nunez NP.** Oestrogen alters adipocyte biology and protects female mice from adipocyte inflammation and insulin resistance. *Diabetes Obes Metab* 14: 58-66.

264.   **Subramanian V, Rothenberg A, Gomez C, Cohen AW, Garcia A, Bhattacharyya S, Shapiro L, Dolios G, Wang R, Lisanti MP, and Brasaemle DL.** Perilipin A mediates the reversible binding of CGI-58 to lipid droplets in 3T3-L1 adipocytes. *J Biol Chem* 279: 42062-42071, 2004.

265.   **Sutherland C, Leighton IA, and Cohen P.** Inactivation of glycogen synthase kinase-3 beta by phosphorylation: new kinase connections in insulin and growth-factor signalling. *Biochem J* 296 (Pt 1): 15-19, 1993.

266.   **Suzuki R, Tobe K, Aoyama M, Sakamoto K, Ohsugi M, Kamei N, Nemoto S, Inoue A, Ito Y, Uchida S, Hara K, Yamauchi T, Kubota N, Terauchi Y, and Kadowaki T.** Expression of DGAT2 in white adipose tissue is regulated by central leptin action. *J Biol Chem* 280: 3331-3337, 2005.

267.   **Takeda K, Toda K, Saibara T, Nakagawa M, Saika K, Onishi T, Sugiura T, and Shizuta Y.** Progressive development of insulin resistance phenotype in male mice with complete aromatase (CYP19) deficiency. *J Endocrinol* 176: 237-246, 2003.

268.   **Tansey JT, Huml AM, Vogt R, Davis KE, Jones JM, Fraser KA, Brasaemle DL, Kimmel AR, and Londos C.** Functional studies on native and mutated forms of perilipins. A role in protein kinase A-mediated lipolysis of triacylglycerols. *J Biol Chem* 278: 8401-8406, 2003.

269.   **Tansey JT, Sztalryd C, Gruia-Gray J, Roush DL, Zee JV, Gavrilova O, Reitman ML, Deng CX, Li C, Kimmel AR, and Londos C.** Perilipin ablation results in a lean mouse with aberrant adipocyte lipolysis, enhanced leptin production, and resistance to diet-induced obesity. *Proc Natl Acad Sci U S A* 98: 6494-6499, 2001.

270.   **Taylor WM, Goldrick RB, and Ishikawa T.** Glycerokinase in rat and human adipose tissue: response to hormonal and dietary stimuli. *Horm Metab Res* 11: 280-284, 1979.

271.   **Tchernof A, Belanger C, Morisset AS, Richard C, Mailloux J, Laberge P, and Dupont P.** Regional differences in adipose tissue metabolism in women: minor effect of obesity and body fat distribution. *Diabetes* 55: 1353-1360, 2006.

272.   **Tchernof A, Desmeules A, Richard C, Laberge P, Daris M, Mailloux J, Rheaume C, and Dupont P.** Ovarian hormone status and abdominal visceral adipose tissue metabolism. *J Clin Endocrinol Metab* 89: 3425-3430, 2004.

273.   **Thompson AL and Cooney GJ.** Acyl-CoA inhibition of hexokinase in rat and human skeletal muscle is a potential mechanism of lipid-induced insulin resistance. *Diabetes* 49: 1761-1765, 2000.

274.   **Tomas E, Tsao TS, Saha AK, Murrey HE, Zhang Cc C, Itani SI, Lodish HF, and Ruderman NB.** Enhanced muscle fat oxidation and glucose transport by ACRP30 globular domain: acetyl-CoA carboxylase inhibition and AMP-activated protein kinase activation. *Proc Natl Acad Sci U S A* 99: 16309-16313, 2002.

275.   **Tonelli J, Li W, Kishore P, Pajvani UB, Kwon E, Weaver C, Scherer PE, and Hawkins M.** Mechanisms of early insulin-sensitizing effects of thiazolidinediones in type 2 diabetes. *Diabetes* 53: 1621-1629, 2004.

276.   **Trayhurn P, Bing C, and Wood IS.** Adipose tissue and adipokines--energy regulation from the human perspective. *J Nutr* 136: 1935S-1939S, 2006.

277.   **Treloar AE.** Menstrual cyclicity and the pre-menopause. *Maturitas* 3: 249-264, 1981.

278.   **Unger RH.** Lipid overload and overflow: metabolic trauma and the metabolic syndrome. *Trends Endocrinol Metab* 14: 398-403, 2003.

279.   **Unger RH.** Lipotoxicity in the pathogenesis of obesity-dependent NIDDM. Genetic and clinical implications. *Diabetes* 44: 863-870, 1995.

280.   **Van Kempen TA, Milner TA, and Waters EM.** Accelerated ovarian failure: a novel, chemically induced animal model of menopause. *Brain Res* 1379: 176-187.

281.   **Van Pelt RE, Gozansky WS, Hickner RC, Schwartz RS, and Kohrt WM.** Acute modulation of adipose tissue lipolysis by intravenous estrogens. *Obesity (Silver Spring)* 14: 2163-2172, 2006.

282.   **Villena JA, Roy S, Sarkadi-Nagy E, Kim KH, and Sul HS.** Desnutrin, an adipocyte gene encoding a novel patatin domain-containing protein, is induced by fasting and glucocorticoids: ectopic expression of desnutrin increases triglyceride hydrolysis. *J Biol Chem* 279: 47066-47075, 2004.

283.   **Vozarova B, Weyer C, Hanson K, Tataranni PA, Bogardus C, and Pratley RE.** Circulating interleukin-6 in relation to adiposity, insulin action, and insulin secretion. *Obes Res* 9: 414-417, 2001.

284.   **Wajchenberg BL.** Subcutaneous and visceral adipose tissue: their relation to the metabolic syndrome. *Endocr Rev* 21: 697-738, 2000.

285.   **Wang SP, Laurin N, Himms-Hagen J, Rudnicki MA, Levy E, Robert MF, Pan L, Oligny L, and Mitchell GA.** The adipose tissue phenotype of hormone-sensitive lipase deficiency in mice. *Obes Res* 9: 119-128, 2001.

286.   **Wasserman DH, Kang L, Ayala JE, Fueger PT, and Lee-Young RS.** The physiological regulation of glucose flux into muscle in vivo. *J Exp Biol* 214: 254-262.

287.   **Watt MJ.** Storing up trouble: does accumulation of intramyocellular triglyceride protect skeletal muscle from insulin resistance? *Clin Exp Pharmacol Physiol* 36: 5-11, 2009.

288.   **Watt MJ.** Triglyceride lipases alter fuel metabolism and mitochondrial gene expression. *Appl Physiol Nutr Metab* 34: 340-347, 2009.
289.   **Watt MJ, Holmes AG, Pinnamaneni SK, Garnham AP, Steinberg GR, Kemp BE, and Febbraio MA.** Regulation of HSL serine phosphorylation in skeletal muscle and adipose tissue. *Am J Physiol Endocrinol Metab* 290: E500-508, 2006.
290.   **Watt MJ and Steinberg GR.** Regulation and function of triacylglycerol lipases in cellular metabolism. *Biochem J* 414: 313-325, 2008.
291.   **Weigert C, Hennige AM, Brodbeck K, Haring HU, and Schleicher ED.** Interleukin-6 acts as insulin sensitizer on glycogen synthesis in human skeletal muscle cells by phosphorylation of Ser473 of Akt. *Am J Physiol Endocrinol Metab* 289: E251-257, 2005.
292.   **Wiest R, Moleda L, Farkas S, Scherer M, Kopp A, Wonckhaus U, Buchler C, Scholmerich J, and Schaffler A.** Splanchnic concentrations and postprandial release of visceral adipokines. *Metabolism* 59: 664-670.
293.   **Wise PM, Smith MJ, Dubal DB, Wilson ME, Krajnak KM, and Rosewell KL.** Neuroendocrine influences and repercussions of the menopause. *Endocr Rev* 20: 243-248, 1999.
294.   **Witczak CA, Sharoff CG, and Goodyear LJ.** AMP-activated protein kinase in skeletal muscle: from structure and localization to its role as a master regulator of cellular metabolism. *Cell Mol Life Sci* 65: 3737-3755, 2008.
295.   **Witte MM, Resuehr D, Chandler AR, Mehle AK, and Overton JM.** Female mice and rats exhibit species-specific metabolic and behavioral responses to ovariectomy. *Gen Comp Endocrinol* 166: 520-528.
296.   **Wohlers LM, Jackson KC, and Spangenburg EE.** Lipolytic signaling in response to acute exercise is altered in female mice following ovariectomy. *J Cell Biochem* 112: 3675-3684.
297.   **Wohlers LM and Spangenburg EE.** 17beta-estradiol supplementation attenuates ovariectomy-induced increases in ATGL signaling and reduced perilipin expression in visceral adipose tissue. *J Cell Biochem* 110: 420-427.
298.   **Wohlers LM, Sweeney SM, Ward CW, Lovering RM, and Spangenburg EE.** Changes in contraction-induced phosphorylation of AMP-activated protein kinase and mitogen-activated protein kinases in skeletal muscle after ovariectomy. *J Cell Biochem* 107: 171-178, 2009.
299.   **Wright LE, Christian PJ, Rivera Z, Van Alstine WG, Funk JL, Bouxsein ML, and Hoyer PB.** Comparison of skeletal effects of ovariectomy versus chemically induced ovarian failure in mice. *J Bone Miner Res* 23: 1296-1303, 2008.
300.   **Yamada K, Saito M, Matsuoka H, and Inagaki N.** A real-time method of imaging glucose uptake in single, living mammalian cells. *Nat Protoc* 2: 753-762, 2007.
301.   **Yamauchi T, Hara K, Kubota N, Terauchi Y, Tobe K, Froguel P, Nagai R, and Kadowaki T.** Dual roles of adiponectin/Acrp30 in vivo as an anti-diabetic and anti-atherogenic adipokine. *Curr Drug Targets Immune Endocr Metabol Disord* 3: 243-254, 2003.
302.   **Yang YK, Chen M, Clements RH, Abrams GA, Aprahamian CJ, and Harmon CM.** Human mesenteric adipose tissue plays unique role versus subcutaneous and omental fat in obesity related diabetes. *Cell Physiol Biochem* 22: 531-538, 2008.

303.   **Yokota T, Oritani K, Takahashi I, Ishikawa J, Matsuyama A, Ouchi N, Kihara S, Funahashi T, Tenner AJ, Tomiyama Y, and Matsuzawa Y.** Adiponectin, a new member of the family of soluble defense collagens, negatively regulates the growth of myelomonocytic progenitors and the functions of macrophages. *Blood* 96: 1723-1732, 2000.

304.   **Yusuf S, Hawken S, Ounpuu S, Bautista L, Franzosi MG, Commerford P, Lang CC, Rumboldt Z, Onen CL, Lisheng L, Tanomsup S, Wangai P, Jr., Razak F, Sharma AM, and Anand SS.** Obesity and the risk of myocardial infarction in 27,000 participants from 52 countries: a case-control study. *Lancet* 366: 1640-1649, 2005.

305.   **Zhai W, Xu C, Ling Y, Liu S, Deng J, Qi Y, Londos C, and Xu G.** Increased lipolysis in adipose tissues is associated with elevation of systemic free fatty acids and insulin resistance in perilipin null mice. *Horm Metab Res* 42: 247-253.

306.   **Zhang W and Liu HT.** MAPK signal pathways in the regulation of cell proliferation in mammalian cells. *Cell Res* 12: 9-18, 2002.

307.   **Zheng CF and Guan KL.** Cytoplasmic localization of the mitogen-activated protein kinase activator MEK. *J Biol Chem* 269: 19947-19952, 1994.

308.   **Zimmermann R, Strauss JG, Haemmerle G, Schoiswohl G, Birner-Gruenberger R, Riederer M, Lass A, Neuberger G, Eisenhaber F, Hermetter A, and Zechner R.** Fat mobilization in adipose tissue is promoted by adipose triglyceride lipase. *Science* 306: 1383-1386, 2004.

309.   **Zisman A, Peroni OD, Abel ED, Michael MD, Mauvais-Jarvis F, Lowell BB, Wojtaszewski JF, Hirshman MF, Virkamaki A, Goodyear LJ, Kahn CR, and Kahn BB.** Targeted disruption of the glucose transporter 4 selectively in muscle causes insulin resistance and glucose intolerance. *Nat Med* 6: 924-928, 2000.

310.   **Zou C, Wang Y, and Shen Z.** 2-NBDG as a fluorescent indicator for direct glucose uptake measurement. *J Biochem Biophys Methods* 64: 207-215, 2005.

311.   **Zurlo F, Larson K, Bogardus C, and Ravussin E.** Skeletal muscle metabolism is a major determinant of resting energy expenditure. *J Clin Invest* 86: 1423-1427, 1990.